Bench Scale Thin Film Composite Hollow Fiber Membranes for Post-Combustion Carbon Dioxide Capture

Final Scientific/Technical Report

Reporting Period Start Date: 10/1/2011

Reporting Period End Date: 12/31/2014

Paul Glaser, Dhaval Bhandari, Kristi Narang, Pat McCloskey, Surinder Singh, Balajee Ananthasayanam, Paul Howson, Julia Lee, Ron Wroczynski

GE Global Research

1 Research Circle, Niskayuna, NY 12309

Frederick F. Stewart, Christopher J. Orme, John R. Klaehn, Joshua S. McNally

Idaho National Laboratory

P.O. Box 1625

Idaho Falls, ID 83415-2208

Dr. Ali Rownaghi, Dr. Liu (Lucy) Lu, and Prof. William Koros, Roberto C. Goizueta Chair

Georgia Institute of Technology

School of Chemical and Biomolecular Engineering

778 Atlantic Dr. NW

Atlanta, Georgia 30332

Vijay Sethi

Western Research Institute
3474 N. 3rd Street
Laramie, WY 82072

Date Report Issued: April 2015

DE-FE0007514

Acknowledgment

"The material described in the report is based upon work supported by the Department of Energy National Energy Technology Laboratory (DOE-DOE-NETL) under award number DE-FE0007514."

Disclaimer

Abstract

GE Global Research, Idaho National Laboratory (INL), Georgia Institute of Technology (Georgia Tech), and Western Research Institute (WRI) proposed to develop high performance thin film polymer composite hollow fiber membranes and advanced processes for economical post-combustion carbon dioxide (CO2) capture from pulverized coal flue gas at temperatures typical of existing flue gas cleanup processes.

The project sought to develop and then optimize new gas separations membrane systems at the bench scale, including tuning the properties of a novel polyphosphazene polymer in a coating solution and fabricating highly engineered porous hollow fiber supports. The project also sought to define the processes needed to coat the fiber support to manufacture composite hollow fiber membranes with high performance, ultra-thin separation layers. Physical, chemical, and mechanical stability of the materials (individual and composite) towards coal flue gas components was considered via exposure and performance tests. Preliminary design, technoeconomic, and economic feasibility analyses were conducted to evaluate the overall performance and impact of the process on the cost of electricity (COE) for a coal-fired plant including capture technologies

At the onset of the project, Membranes based on coupling a novel selective material polyphosphazene with an engineered hollow fiber support was found to have the potential to capture greater than 90% of the CO2 in flue gas with less than 35% increase in COE, which would achieve the DOE-targeted performance criteria.

While lab-scale results for the polyphosphazene materials were very promising, and the material was incorporated into hollow-fiber modules, difficulties were encountered relating to the performance of these membrane systems over time. Performance, as measured by both flux of and selectivity for CO_2 over other flue gas constituents was found to deteriorate over time, suggesting a system that was more dynamic than initially hypothesized. These phenomena are believed to be associated with the physical and mechanical properties of the separation material, rather than chemical degradation by flue gas or one of its constituents.

Strategies to improve the composite systems via alternate chemistries and processing techniques were only partially successful in creating a more robust system, but the research provided critical insight into the barriers to engineering sophisticated composite systems for gas separation. Promising concepts, including a re-engineering of the separation material with interpenetrating polymer networks were identified which may prove useful to future efforts in this field.

Table of Contents

Executive Summary

GE Global Research, Idaho National Laboratory (INL), Georgia Institute of Technology (Georgia Tech), and Western Research Institute (WRI) proposed to develop high performance thin-film polymer composite hollow fiber membranes and improved processes for economical post-combustion carbon dioxide (CO_2) capture from pulverized coal flue gas at temperatures typical of existing flue gas cleanup processes.

The project sought to optimize novel membrane systems at the bench scale, including tuning the properties of a novel poly(phosphazene) material and fabricating highly engineered porous hollow fiber supports. The project also investigated processes for coating the fiber support to manufacture ultra-thin, defect-free composite hollow fiber membranes. Physical, chemical, and mechanical stability of the materials (individual and composite) towards coal flue gas components were be evaluated using exposure and performance tests. Module design, technical, and economic feasibility analyses were be conducted to evaluate the overall performance and impact of the process on the cost of electricity (COE).

Initial studies showed that membranes based on coupling novel selective materials (with an engineered hollow fiber support have the potential to capture greater than 90% of the CO2 in flue gas with less than 35% increase in COE, which would achieve the DOE performance criteria.

The project demonstrated, however, that the polyphosphazene materials chosen for the project were not as amenable to incorporation into a robust engineered hollow fiber system as hoped. The performance of targeted systems was found to be both sensitive to preparation parameters and variable over time.

Significant insights into the nature of these materials as well as promising alternative strategies were developed during the program, including promising initial results for an Interpenetrating polymer network (IPN) formulation, which could lead to greatly improved robustness in future systems.

Introduction

Project overview

Due to increasing concerns about global warming in recent years, a substantial interest exists in reducing greenhouse gas emissions like carbon dioxide (CO_2) from large industrial point sources. In this context, post-combustion CO_2 capture from flue gas has become a primary research and development focus. Currently, the most commonly employed technology is solvent capture of CO_2 using monoethanolamine (MEA).(Favre 2007) Amine absorption, when applied to CO_2 capture from flue gas, could cause a 50–90% increase in cost of electricity (COE) for 90% CO_2 removal.(Figueroa, Fout et al. 2008; Black 2010) Analysis at GE Global Research estimates that CO_2 capture by this process will increase COE by 80%. The breakdown of this cost is presented in Figure 1

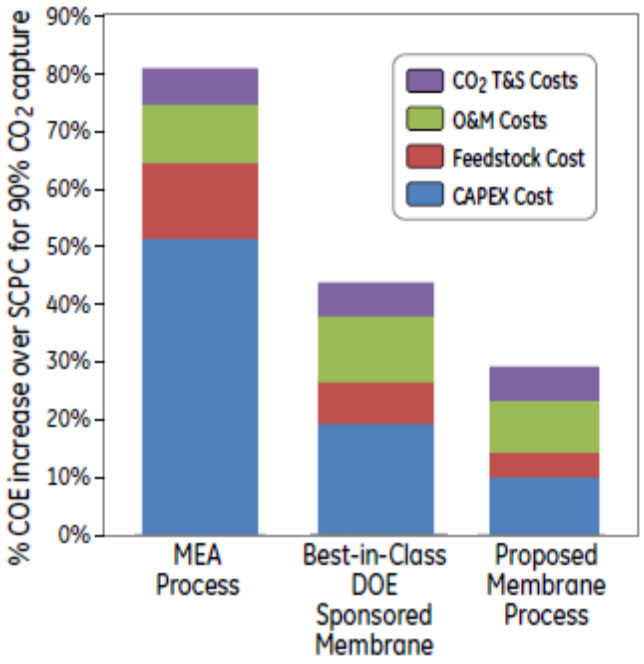

Figure 1. Waterfall plot comparison of COE for CO_2 capture using the MEA process, best-in-class DOE sponsored membrane process and the proposed membrane process applied to a supercritical pulverized coal plant

As shown in Figure 1, the largest driver for this increase is the capital expenditure, which alone accounts for more than 50% of the increase in COE. This cost expenditure includes the contribution of the separation equipment and modifications required to maintain the net plant power despite efficiency loss created by the capture process. Efficiency is lost by the thermal load needed to heat the CO_2 stripper, which uses steam that is redirected from steam turbines. Efficiency is also lost to mechanical loads required for CO_2 compression, flue gas handling, and auxiliary loads. Operating a larger power plant is necessary to achieve the same net power, thus the plant will consume more coal and increases the fuel cost.

In addition to the large increase in COE, another major criticism of amine-based CO_2 capture is that it approximately doubles the power plant water demand due to the cooling tower makeup water necessary to continuously cool the absorber fluid. In addition to the large increase in COE, another major criticism of amine-based CO_2 capture is that it approximately doubles the power plant water demand due to the cooling tower makeup water necessary to continuously cool the absorber fluid. Finally, because amine absorption is a mature technology, achieving significant improvements is a serious challenge.

Polymeric membrane-based CO_2 capture technologies are seen as a potentially promising alternative to existing liquid sorbent-based options. Although originally dismissed without analysis by several groups as uneconomical, membrane technology is gaining support in the broader scientific community.(Favre 2007) However, membranes that are designed with appropriate material and process benefits for economical post-combustion carbon capture applications are still in an early developmental or pilot stage.

Membrane processes for CO_2 capture have the potential to impact both COE (by reducing parasitic loads and operating costs) and the additional water demand (by eliminating the need to continuously cool the solvent stream). Since early concepts were devised, increased viability has come from advances in system designs for post-combustion capture of CO_2 from pulverized coal power plants. For example, operating membranes with vacuum permeate rather than with greatly compressed flue gas decreases overall cost despite larger membrane area requirements and the higher cost of vacuum equipment.(Favre 2007)

Under DOE-DOE-NETL sponsorship, Membrane Technology and Research Inc. has developed a best-in-class membrane material—Polaris™. Polaris™ is a thin film composite membrane in a spiral wound configuration with reported CO_2 permeance around 1000 GPU (estimated, permeability = 100 Barrer, based on 0.1 μm thick selective layer) and a CO_2 /N_2 selectivity approaching 50, as shown in Figure 2 (Merkel, Lin et al. 2010). Several process configurations have been proposed that increase the partial pressure driving force at the membrane and reduce the required membrane area by recycling (including exhaust gas recycling of CO_2 to the boiler).

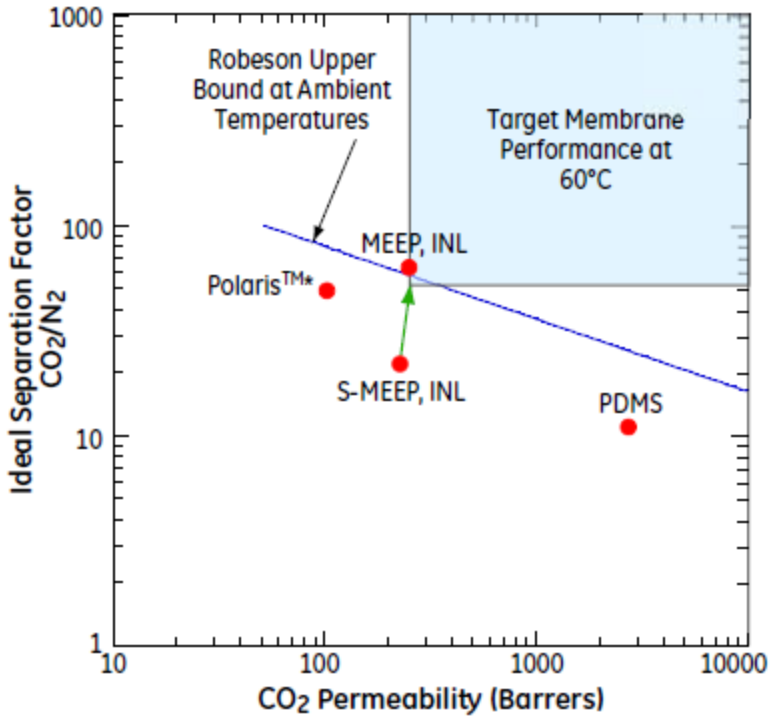

Figure 2. Permeability-selectivity plot for the CO_2 /N_2 gas pair at ambient temperature and the target membrane performance at 60°C (S-MEEP: stabilized MEEP). (*Permeability of Polaris™ is estimated based on a selective layer thickness of 100 nm)

Significant advancements are necessary to drive the performance further into the favorable region plotted in Figure 2 . Advances are required in 1) membrane materials—higher CO_2 permeance with improved CO_2 selectivity, longer membrane lifetime, and less susceptibility to fouling; 2) membrane modules—higher packing density and improved economics with easier scalability; and 3) process configurations to lower energy penalties.

Improvements in these three aspects of membrane technology required a strong team. The project brought together partners with critical knowledge and capabilities in the areas of polymer materials and processing (Idaho National Laboratory [INL]), polymeric membrane fabrication and scalable coating technologies (GE Global Research and Georgia Institute of Technology [Georgia Tech]), expertise in system modeling (GE Global Research), and bench scale coal flue gas test systems (Western Research Institute [WRI]). The project utilized novel polyphosphazene polymeric materials for economical and scalable composite hollow fiber membrane modules capable of efficiently separating CO_2 from coal flue gas.

Novel commercial polyphosphazene materials

The choice of an appropriate selective membrane layer is a crucial aspect of defining an effective CO_2 separation membrane. Novel poly(phosphazene) materials developed by INL were selected for this work. Polyphosphazenes are a unique family of rubbery polymers consisting of alternating phosphorus and nitrogen in the polymer backbone. Work conducted at INL on very low glass transition temperature phosphazenes with systematic loading of ethylene oxide pendant groups, specifically 2-(methoxyethoxy)ethanol (MEE), has demonstrated very

high values of CO_2 permeability (P=250 barrer) and CO_2/N_2 ideal gas selectivity (S CO_2 /N_2=62.5). In fact, as shown in Figure 2, Robeson used these values in a 2008 publication to establish the theoretical upper bound for membrane performance for this gas pair.(Robeson 2008)

Pure 2-(2-methoxyethoxy) ethanol phosphazene (MEEP), despite its superior CO_2 separation performance and CO_2 permeability, required stabilization to maintain mechanical integrity. With the addition of 4-methoxyphenol and 2-allylphenol in different ratios, the stabilization and mechanical properties of the MEEP were significantly improved. Polyphosphazenes with different loadings of pendant groups were synthesized in the project. (Stewart, Harrup et al. 2000)The desired properties of the downselected polymer was a trade-off between various physical factors such as a) solubility of the polymer in a solvent benign to the hollow fiber support, b) improved physical handling, c) high molecular weight to reduce infiltration and performance factors of d) high CO_2 permeance, e) high CO_2 /N_2 selectivity, and f) long term membrane stability. Additionally, simple free radical cross-linking mechanism in terms of ozone crosslinking or thermal crosslinking was also desired for scale-up and optimization of the polymer. The presence of fly ash and other particulate matter in the coal flue gas feed streams can significantly degrade membrane performance due to fouling. Advantageously, the polyphosphazene material properties could be modified to create non-adhering membrane surfaces. This can improve membrane cleanability by enabling, for example, a simple water wash to remove foulants. Stabilized polyphosphazene are also thermally robust. They exhibit no mass losses until 250–350 °C, which is significantly above typical membrane operating temperatures (60°C). Further, they are resistant to degradation by acid gases (NOx, SOx) and H2S present in flue gas. Treatment of MEEP with aromatic cross-linking moieties improves mechanical and chemical stability of the membrane while maintaining solubility in ethanol. However, the added aromatic content can increase the glass transition temperature of the polymer, which leads to a lower CO_2 permeability and a lower CO_2 /N_2 selectivity, so it must be added judiciously. (Orme, Klaehn et al. 2004)

Engineered hollow fiber support structure

Rubbery materials typically do not have suitable properties for fabrication into monolithic membranes with the desired asymmetric morphology. Therefore, the project goal was to support the polyphosphazene material onto a highly porous support with engineered surface porosity. The support polymer should be commercially available, easily processable with high mechanical and chemical stability, and compatible with the selective layer.

Hollow fiber membranes provide the optimum geometry for high production rates and ease of module formation while providing high surface area and membrane packing density compared to flat sheets. In fact, most of the commercial gas separation membranes are formed into hollow fiber modules with fewer than 20% being formed into spiral wound modules (Baker 2002) By pursuing the innovative coating approaches described below, it is expected that the proposed membranes will cost about $15–20/m2, which is much lower than the cost for spiral wound membrane modules.

Composite hollow fiber membranes can be manufactured by either: (a) simultaneous co-extrusion of the selective and support polymer layers, or (b) casting the selective layer on a

pre-existing porous support. The co-extrusion approach works well when both the selective and support layers are glassy polymers and form compatible asymmetric layers. The rubbery selective layer makes the co-extrusion approach difficult due to defect formation in the selective layer and problems associated with achieving efficient phase separation in the coagulation bath. Even if efforts are made to create a selective layer primarily by vaporization of the volatile solvent in the air gap, a dense layer will be obtained with low permeance. This can also cause slow phase separation of the support layer, making the support layer less porous.

The second approach has been implemented by continuous dip and spray coating onto porous supports, and by batch-coating pre-formed hollow fiber bundles or modules. (Cabasso and Lundy 1986; Murphy 1988; Puri 1989) However, it is difficult to form ultra-thin (~0.1 µm), defect-free coatings onto porous supports. Further, the coating solution can penetrate the highly porous substrate, leading to material loses and poor performance.

Rubbery coatings have been applied as "caulking layers" to glassy membrane materials to create ultra-thin layers. The technique has been highly successful primarily due to the small pore sizes (<1 nm) and low porosity (<10 ppm area fraction) in conventional glassy polymer skins. In the proposed approach however, the permeance and selectivity of the membrane will be controlled by the rubbery coating layer rather than by the glassy support layer. Thus, to enable the creation of an ultra-thin selective layer, it is necessary to fabricate a highly porous support with engineered pore-sizes and surface porosity.

In this project multiple approaches were taken to fabricate the hollow fiber supports. GE Global Research and Georgia Tech spent the first budget period in screening through different materials for hollow fiber support fabrication.

Polydimethylsiloxane (PDMS) was used as the rubbery intermediate layer polymer for the proposed work. PDMS is roughly 10 times more permeable than the polyphosphazene selective layer as shown in the Robeson's plot in Figure 2 and will create minimum hindrance to gas transport through the selective phosphazene layer. Typical polymer coils have sizes greater than 200–400Å, depending on molecular weight, which can be easily tuned to create ultrathin defect free selective layers. The highly permeable intermediate layer will not hinder the phase separation of the support layer. Further, the intermediate layer with controlled surface porosity will prevent intrusion of selective layer coating solution, which is often problematic in conventional coating processes. The support and intermediate polymer layers have little or no solubility in the coating solvent (e.g., ethanol), which enables compatibility of these materials in the coating process. The proposed approach is thus expected to enable ultra-thin defect-free composite hollow fiber membranes that are effective for CO_2 capture from flue gas.

Task 2: Polyphosphazene polymer and coating solution development

Overview

While it has been demonstrated that phosphazene materials give high transport and separation performance in mixed gas laboratory experiments, it is the goal of this task to characterize and optimize separation performance on actual coal flue gas and modify the

material into easily processable coating solutions. This task will be performed through a number of subtasks that will ultimately lead to optimized materials and recommendations.

Phosphazenes are hybrid organic-inorganic polymers that gain functionality through backbone substitution processes. The backbone consists of alternating phosphorus and nitrogen atoms. Organic substituents are attached at phosphorus to create functional materials. These materials have many advantages including thermal stability (decomposition temperature > 250 °C), good film forming characteristics, good solubility in a variety of solvents, and near infinite adjustability for specific gas separation performance.

The synthesis of these polymers differs from traditional organic polymers where a monomer is formed and then polymerized. In phosphazenes, the backbone is formed initially, followed by nucleophilic substitution with organic pendant groups. In this work, commercially available hexachlorocyclotriphosphazene was polymerized under vacuum at 250 °C to yield poly(bis-chlorophosphazene), Figure 3.

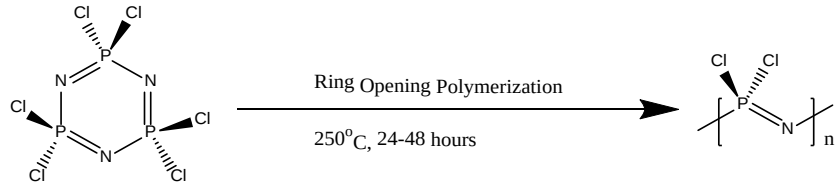

Figure 3. Ring opening polymerization of Hexachlorocyclotriphosphazene yielding poly(bis-chlorophosphazene).

Poly(bis-chlorophosphazene), a clear, colorless rubber, is hydrolytically unstable and will degrade in the presence of water due to the lability of the P-Cl bond. Stabilization of the backbone is performed by nucleophilic substitution of chlorine using organic nucleophiles through O, N, or a carbanion, Figure 4. The most common linkage is through O, which tends to be robust and impart into the polymers good chemical and thermal stability. (Gleria and De Jaeger 2005)

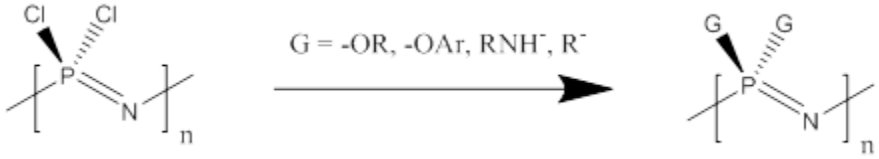

Figure 4. Stabilization of the P-N backbone through nucleophilic substitution.

A series of polyphosphazenes were developed and reported by INL using three differing pendant groups, each with their own function, Figure 5.(Orme, Harrup et al. 2001) This initial INL report discussed polymers substituted with 2-allylphenol (2-AP), 4-methoxyphenol (4-MEOP), and 2-(2-methoxyethoxy)ethanol (MEE), where the aromatic components were used to dimensionally stabilize the polymers. These stabilizers play distinctive roles in the control of mechanical properties. 2-AP contains an easily activated allylic moiety that provides a handle for free-radical induced cross-linking. 4-MEOP improves aspects of the physical properties such as creep and gives the material a higher tensile strength. It also can influence surface behaviors such as tackiness. MEE, as the majority component, provides ethanol solubility and a depressed glass transition temperature (Tg).

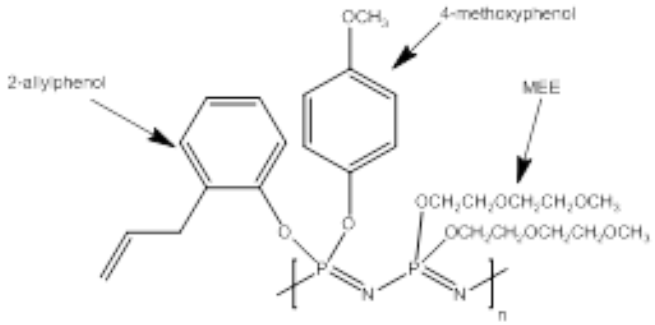

Figure 5. Generalized structure of the phosphazene heteropolymer.

Cross-linking in these polymers has been accomplished using several methods including chemical (Orme, Harrup et al. 2001), and UV (Allcock 1994), gamma (Allcock, Gebura et al. 1988), and electron beam irradiation. (Stewart, Harrup et al. 2000)Cross-linking occurs through homolytic bond cleavage of the allylic methylene C-H bond. The resulting free-radical is stabilized by the alkene and phenol ring. It is critical that the lifetime of the free radical be long enough to allow for C-C bond formation with another free radical. With this requirement, it becomes imperative that the casting solution facilitate both the formation of a defect-free membrane and ensure adequate dispersal of a free-radical initiator, which is required to accomplish rapid and facile polymer cross-linking.

Synthesis of these stabilized MEE-containing phosphazene (X%-MEEP) polymers is performed by initial substitution of poly(bis-chlorophosphazene) (PNCl2) with the aromatic components (2-AP and 4-MEOP), where X refers to the percentage of MEE loading. The attachment chemistry of the pendant groups is monitored by P-31 Nuclear Magnetic Resonance (NMR) spectroscopy. Once the phenolics are attached, an excess of MEE is added to the reaction to ensure removal of the remaining chlorines from the polymer backbone. It is critical to remove all chlorine from the backbone because they are reactive to water, which will degrade the polymer and lessen the lifetime of the membrane.

Methods for determining the permeability and ideal gas selectivity of phosphazene membranes have been reported in several articles. (Allcock, Nelson et al. 1993; Peterson, Stone et al. 1993; Peterson, Stone et al. 1995; Orme, Klaehn et al. 2004) In 2001, the initial report on 100% MEEP and stabilized MEEP with various percentages of MEE was reported on cross-linked membranes. (Orme, Harrup et al. 2001) CO_2 permeability was found to increase as a function of the MEE content in the polymer ultimately leading to 100% MEEP, which had the highest permeance at approximately 2500 GPU (Permeability = 250 Barrers) with a selectivity of 62.5 at 30 °C. It should be noted that Robeson used these data in his 2008 paper to establish the theoretical upper bound in membrane performance for this gas pair. (Robeson 2008)

The dimensional stability of the materials containing 2-AP could be improved by thermally cross-links between the 2-AP moieties. However, in order to cross-link the 100% MEE polymer, which is actually a high viscosity liquid and that contains no 2-AP groups, UV irradiation was used. The UV irradiation can activate C-H bonds associated with polyether chains (MEE). However, only partial stability was imparted due to long term creep (vide infra). Therefore, these membranes were cross-linked just prior to analysis.

An exciting aspect of this work was that the trend observed for CO_2 was not noted for permanent gases, such as N_2. From Figure 6, it can be seen that the highest levels of permeability and separation factor were derived from the highest MEE containing phosphazenes, which represent 100% MEEP and dimensionally stabilized 74% MEEP. Please note that with only this pair under consideration, the 100% MEEP was superior to the 74% MEEP in terms of both permeability and selectivity, suggesting that the MEE loading must be kept as high as possible. This presented a challenge in maintaining high levels of MEE loading to maintain high permeance and selectivity while also achieving suitable dimensional stability.

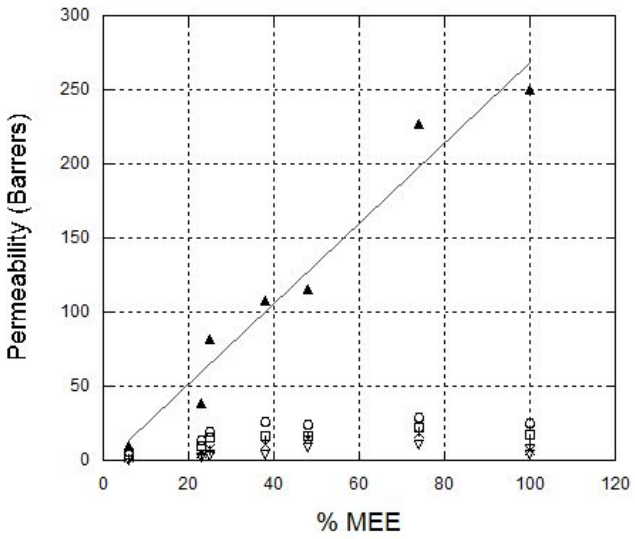

Figure 6. Permeabilities of MEEP Containing Phosphazenes for Selected Gases. (Hydrogen (○), Helium (□), Nitrogen (∇), Oxygen (×), Methane (+), and Carbon Dioxide (▲).

The 2001 report (Orme, Harrup et al. 2001) suggested that CO_2 permeability was largely due to solubility interactions between the polymer and the permeant gas. Specifically, it was proposed that the MEE chains acted to increase the solubility component of transport through chemical affinity. A refinement of this work was reported in 2006 where the chemical affinity aspect between MEE and CO_2 was downplayed. (Orme, Klaehn et al. 2006) The relative polarity of the pendant group was not found to be a significant factor in CO_2 permeability, rather a simple correlation between Tg and CO_2 permeability was observed. This suggests diffusivity, rather than solubility, has a major influence on transport and further supports the project goal of maintaining high MEE content on the polymer.

The Fox relationship, equation 1, describes a net Tg for intimately mixed organic copolymers. The Tg of a copolymer can be calculated as a function of the Tgs for each individual component. However, this relationship is only valid for amorphous systems with little to no phase separation. This equation was successfully applied to phosphazenes in a previous report. (Beres, Schneider et al. 1979)

$$1/Tg = (W1/Tg1) + (W2/Tg2) \qquad \text{Eq. 1}$$

The variables W1 and W2 are the weight percentages of each homopolymer matrix and Tg1 and Tg2 are the corresponding Tg values for the homopolymers. In cases where the heat capacities of the individual monomers are similar, Equation 1 may be simplified to:

$$Tg = M1Tg1 + M2Tg2 \qquad \text{Eq. 2}$$

where M1 and M2 are the percentages of each monomer in the copolymer. This relationship was applied with a high degree of correlation to phosphazene heteropolymers with random distribution of pendant groups. (Stewart, Harrup et al. 2000) Extension of this relationship to MEE containing polymers is shown graphically in Figure 7. Tg is seen as a function of the MEE loading. Thus, further impetus is provided to keep MEE loadings high, thus depressing Tg and maximizing both CO_2 permeability and CO_2 /N_2 selectivity. The ability to tailor the phosphazene to the specific needs of this gas separation provides additional justification for the selection of phosphazenes for this application.

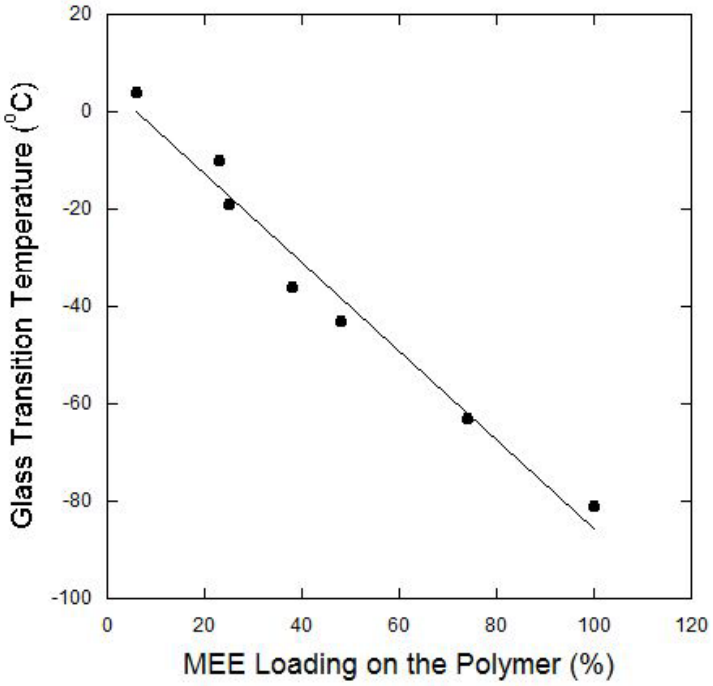

Figure 7. Correlation between Tg and MEE loading.

Down-selection of MEEP material with 2-allyl and 4-methoxy side groups.

As shown from the literature, the use of 2-AP, 4-MEOP, and MEE as pendant groups served to give the properties needed to act as a hollow fiber selective layer. Care must be taken to control the amount of 2-AP, the crosslinking moiety, added to the polymer. The allyl group tends to be reactive and excessive loading can lead to premature cross-linking, resulting in material insolubility. Thus, the loading of this group was kept below 10 %.

Synthesis roadmap of different MEEP materials (different loadings)

Three differing loadings of MEE were explored in this work, whose derived data was combined with that from the literature to select a specific "recipe" for coating development. For 45 % and 80 % MEEP polymers, 4-MEOP was used to make up the difference between the 2-AP and MEE loadings, Table 1. For 95% MEEP, 4-MEOP was not included. This polymer represented a cross-linkable variant of 100% MEEP and was synthesized with the goal of dimensionally stabilizing the polymer only through cross-linking.

Table 1. Targeted MEEP polymer compositions.

Polymer	%MEE	% 4-MEOP	% 2-AP
45% MEEP	45	49	6
80% MEEP	82	13	5
95% MEEP	95	0	5

45% MEEP and 80% MEEP were synthesized in a multi-step process, Figure 8. The aromatic components, 2-AP (step 1) and 4-MEOP (step 2), can be added to the polymer backbone sequentially or concurrently. We found that combining steps 1 and 2 together was the best method and it saved time. Step 3 was then performed using a 100% excess of MEE to ensure complete removal of all remaining chlorines. A detailed synthetic procedure for 80 % MEEP is shown in Appendix A

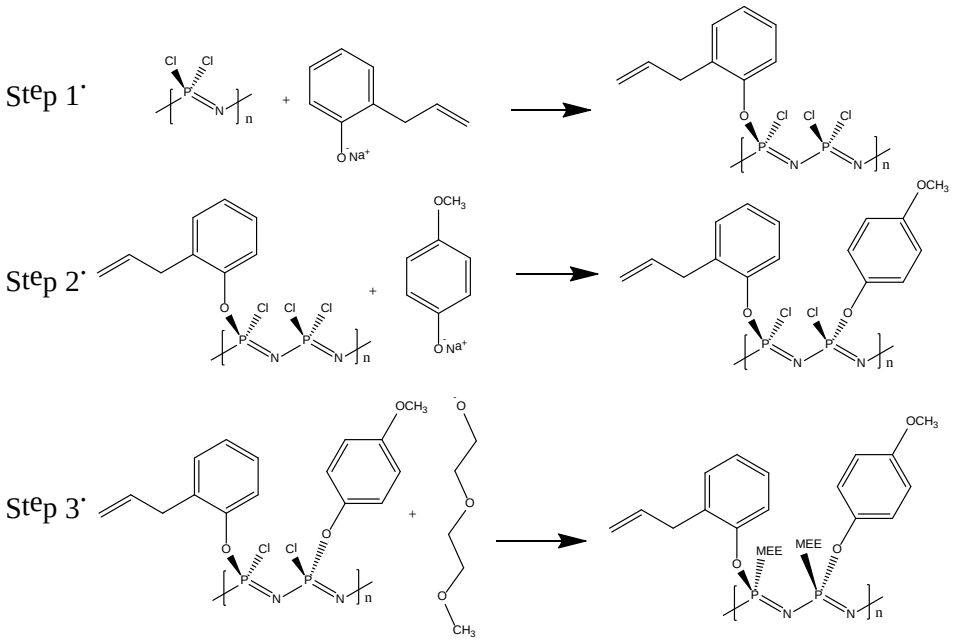

Figure 8. Generalized roadmap for synthesis if MEE/4-MEOP/2-AP substituted polyphosphazenes.

Progress of the chemical synthesis is followed by P-31 NMR analysis of aliquots removed from the reaction vessel. An example of the data obtained for a batch of 80 % MEEP is shown in Figure 9. Individual peaks in the spectra directly correlate to structure. Observed is the loss of the peak associated with PNCl2, and the creation of peaks that are associated with substitution with the three pendant groups. For example, in a typical synthesis, PNCl2 is added to a mixture of the aromatic nucleophiles. After 2 hours, a broad envelope is observed between -14 and -21 ppm, which corresponds to the various possible substitutions (PNCl(2-AP), PNCl(4-MEOP); PN(2-

AP)(4-MEOP), PN(2-AP)2, PN(4-MEOP)2). It should be noted that PNCl2 is indicated at -18 ppm as a relatively sharp peak. After 18 hours reaction time, the P-31 spectrum is largely unchanged suggesting that this aspect of the reaction was complete. MEE was then added and after 45 minutes, P-31 NMR spectroscopy revealed a very different spectrum, with a broad envelope between -11 and -14 ppm, which represents phosphorus substituted with one MEE and one aromatic group; and another at -8 ppm, which corresponds to PN(MEE)2. Spectra taken at five and seven hours reveal sharper resolution and higher signal to noise ratio, both of which are indicative of reaction completion. The breadth of the peaks is attributed to 1) two differing aromatic groups (4-MEOP and 2-AP) that are slightly different from an NMR perspective, and 2) neighboring group effects.

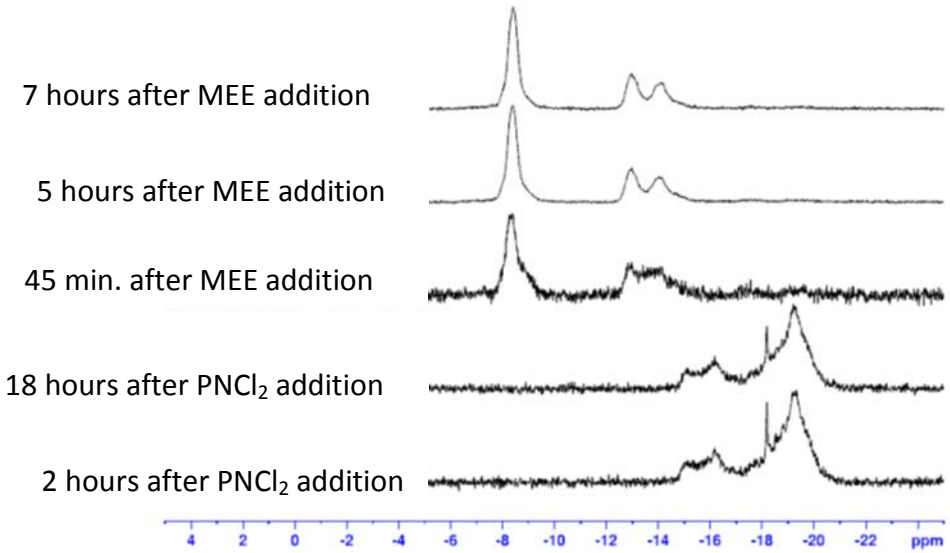

Figure 9. NMR data for the various synthetic stages for a batch of 80 % MEEP.

Polymer purification.

Purification of the polymer product is critical to minimizing batch to batch variation in both gas transport behavior and physical properties. In general, polymeric phosphazenes are purified by precipitation of polymer solutions into non-solvents. This method was successfully employed in this project. Upon completion of the substitution reactions, the tetrahydrofuran (THF) solution contains the polymer (whose precursor polymer was delivered to the reaction with toluene), excess nucleophile (MEE, sodium salt), sodium chloride (a byproduct of the substitution reaction), and trace phenols. Removal of the contaminants is accomplished by precipitation of the polymer solution into a solvent that will dissolve the contaminants and not the polymer. The first precipitation of the mother liquor was into hexane, which solubilized trace phenols, MEE, and the reaction solvent mixture (THF and toluene). The precipitated polymer was physically removed and re-dissolved in THF. It was then precipitated into water, upon which it may or may not precipitate. Isolation of the polymer from this solution was performed by heating the solution to ~70°C, where precipitation is completed, while solubilizing

any water soluble contaminants, such as salts and MEE. 80% MEEP is a polymer that is less water soluble at 70°C than at ambient temperature. This behavior, lower critical solution temperature (LCST), is not uncommon for hydrophilic phosphazenes (Allcock and Dudley 1996; Harrup and Stewart 2000) and is an effective way to purify these materials.

Once recovered from the water solution, the polymer was rigorously dried and then dissolved into THF. At this point, the THF solution was centrifuged to remove trace amounts of salts that were trapped in the polymer when it precipitated during the LCST step. Clarified THF solutions were precipitated into hexane to yield the final polymer that was then dried. Refined syntheses gave approximately 70 % yield of usable material. A precise purification method is shown in Appendix A. Batch-wise polymer yields are shown in Appendix B.

45% MEEP was purified using a similar procedure; however precipitations were from THF into: 1) hexane; 2) water twice; and 3) hexane. Due to the reduced MEE content, this polymer showed little affinity for water and clearly separated from an aqueous bath. 95% MEEP, on the other hand, was soluble in water and was only collected from solution using the LCST procedure.

Characterization of 80% MEEP.

NMR spectroscopy was used to determine speciation of the backbone. Specifically, proton NMR spectra were taken so that the peaks could be integrated to determine the loading of each pendant group. An example of proton NMR data is shown in Figure 10. Three regions, denoted as A, B, and C were marked for integration. Region A corresponds to aromatic protons of both 2-AP and 4-MEOP. Region B is the peak attributed to protons on the allylic chain of 2-AP. Region C contains MEE protons plus the methyl of group of 4-MEOP. Percentages of each pendant group were determined by calculating the area/H ratio for 2-AP. Since B consists of only one molecule, it was then used to deconvolute region A by subtracting the area attributable to 2-AP from the protons of 4-MEOP. Once the area/H ratio was determined for 4-MEOP, the area attributed to the methyl group of 4-MEOP is subtracted from region C to yield the area/H ratio for MEE. With the three ratios, the mole fraction/percentage of each pendant group was determined from the total. A tabulation of the data from each batch is shown in Appendix B.

P-31 NMR spectroscopy was used to verify complete substitution of the polymer backbone. For the final product, a “finger print” was generated that included peaks attributable to the substitution patterns that are possible with random distribution of three differing pendant groups. Also, it should be noted that adjacent phosphorus atoms (and their substitution patterns) will influence the signals, generally through broadening. An example of the P-31 NMR spectrum obtained from 80% MEEP is shown in Figure 11. Additional NMR support is provided by carbon-13 NMR, Figure 12, which allows for the direct characterization of the carbon-containing pendant groups. Peaks are consistent with the three pendant groups.

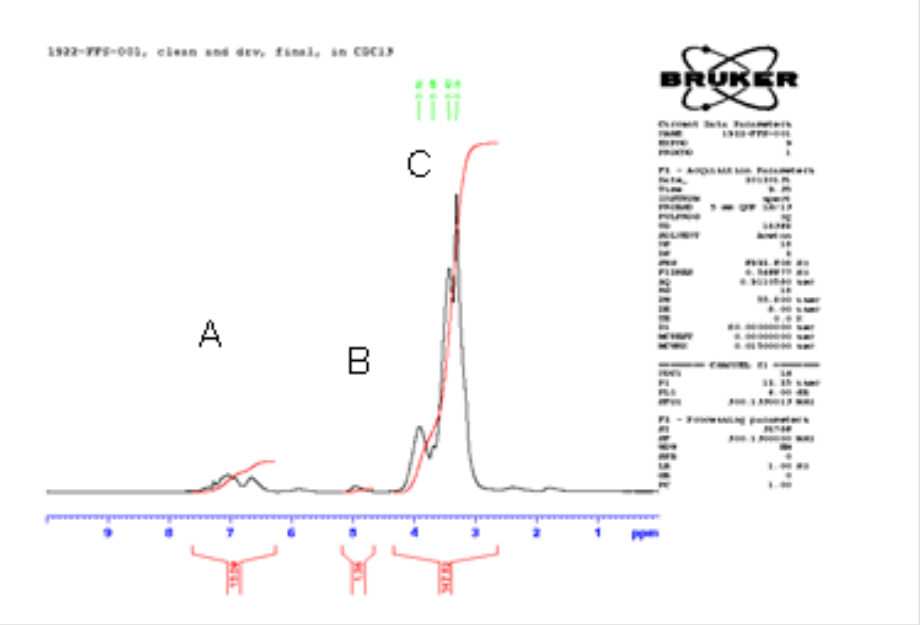

Figure 10 Representative proton NMR spectrum for 80 % MEEP

.

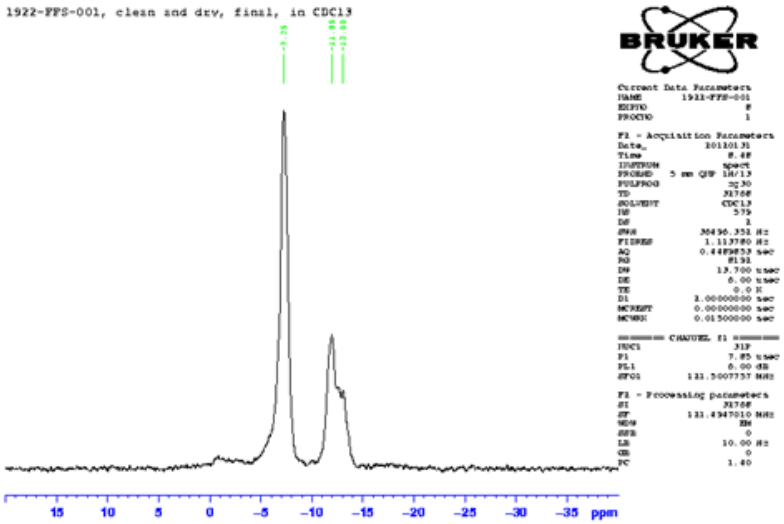

Figure 11. Representative P-31 NMR spectrum of 80% MEEP.

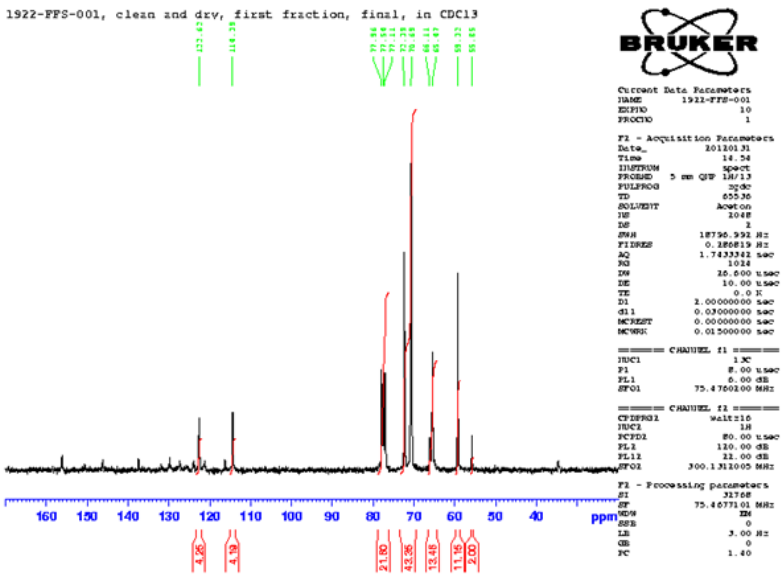

Figure 12. Representative spectrum carbon-13 NMR spectrum of 80% MEEP.

Thermal analysis consists of a variety of analytical techniques that probe material properties as a function of temperature. Two methods were chosen to support this project: Differential Scanning Calorimetry (DSC) and Thermogravimetric Analysis (TGA). DSC measures heat flow into and out of a sample as a function of temperature. This technique can measure physical properties such as melting point and crystalline transformations. A temperature range of -75°C to 200 °C was used to study morphological behaviors. For a batch of 80% MEEP, an endothermic transition was noted at -66 °C, Figure. This feature was assigned to a Tg. Compared to many polymers, this Tg is low, which is attributed to the inherent flexibility of the phosphazene backbone plus the flexibility of the MEE chains. Glass transition data for the various batches synthesized during the project are shown in Appendix C. Some slight variation in batches is noted, which is a reflection of the small differences in pendant groups' speciation between batches.

One of the critical advantages of phosphazenes is their relatively high onset temperatures for decomposition. TGA was used to probe thermal stability. In general, little mass loss as a function of temperature is seen until approximately 280 °C, Figure 14. At temperatures higher than 280 °C, rapid mass loss is evident, which is attributed to loss of MEE pendant groups since polyether chains are less thermally stable than aromatic moieties. TGA experiments were not conducted on every batch since it was not expected that any batch-to-batch variation would yield polymers with insufficient stability in the temperature range of interest to this project (30-60 °C).

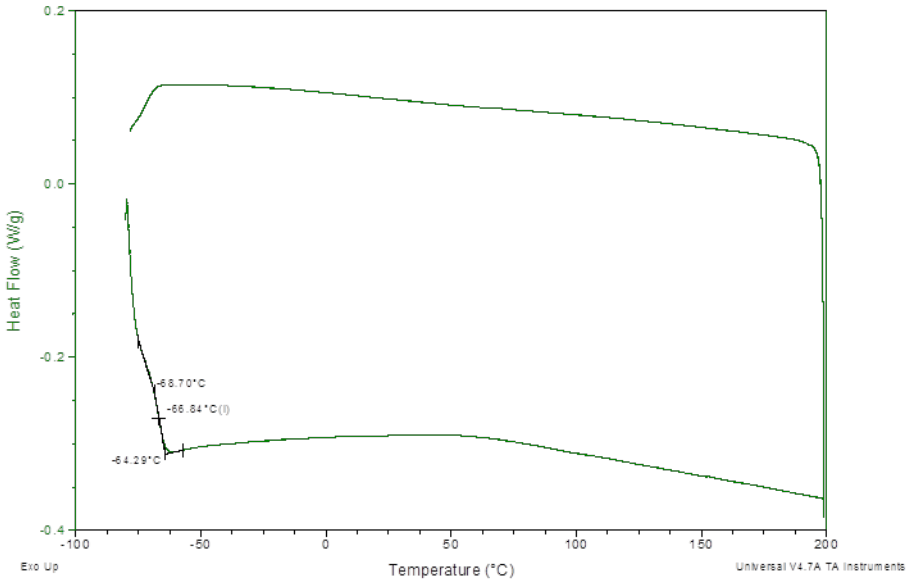

Figure 13. DSC thermogram for 80% MEEP.

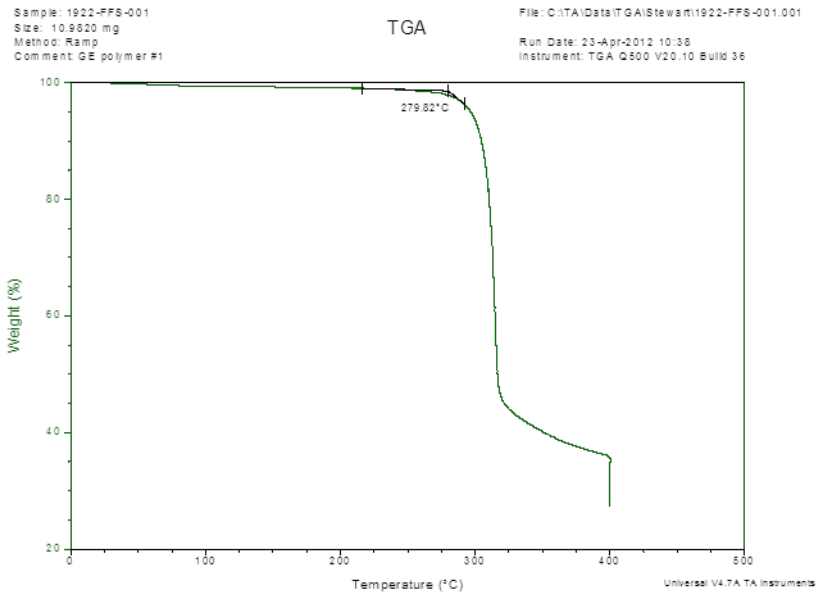

Figure 14. Representative TGA data for 80 % MEEP.

Molecular weight analysis was performed on several batches with less than satisfactory results. Samples were sent to an external laboratory for analysis and the resulting data showed molecular weights in the 104-105 Dalton range. This is substantially lower than expected. With MEE containing polymers, molecular weights measured by reverse phase Gel Permeation Chromatography will read an order of magnitude or two too low if the eluting solvent is pure THF. It is recommended that tetra-n-butyl ammonium bromide should be added at 0.1 % to give proper molecular weight data. The vendor was not capable of adjusting the eluting solvent. Rather than finding another vendor, it became apparent the polymer solution viscosity was a

more important measure needed for hollow fiber coating, so the characterization effort was re-focused in that direction. Further, observation of flow became another important consideration on product quality. Some variation was seen from batch to batch and synthetic procedures were revised to obtain a non-flowing solid.

Pure gas permeability is another characterization technique applied to the membranes, Table 2. In these experiments, CO_2 and N_2 permeabilities were determined. Ideal separation factors (α) were determined as a function of the permeabilities, Equation 3.

$$\alpha = p(CO_2)/p(N_2) \qquad \text{Eq 3.}$$

In a pure gas analysis, a barometric method is employed, where a membrane is mounted in a cell and known calibrated volumes are attached on both sides of the membrane and then drawn down in pressure using a vacuum pump. The feed side is then charged with a known pressure (typically 30 psi) of the analyte gas and the pressure is monitored on the permeate side as a function of time. Generally, there is a time lag associated with the gas achieving steady state transport and this is characterized by a permeate-side non-linear pressure-time response. Once steady state has been achieved, the response is linear where the slope corresponds to permeability.

Initial characterization attempts were performed on cross-linked membranes, Table 2. However, it became apparent that the precise cross-linking protocol for the hollow fiber membranes had not been established and that it would be better to benchmark batch performance on uncross-linked membranes. This change is reflected in the permeability data for the individual batches provided in Appendix C .From this we were able to establish performance baseline criteria from which to measure batch quality. We found that polymers generating CO_2 permeability of 450-500 Barrers and CO_2 /N_2 ideal gas selectivities of 30-40 were acceptable for follow-on hollow fiber membrane development.

Table 2. Pure gas permeability data for three differing MEEP compositions as a function of temperature.

Polymer	**Temperature**	N_2 **(Barrers)**	CO_2 **(Barrers)**	CO_2 /N_2
80 % MEEP	30 °C	6.9	202.6	29.6
80 % MEEP	60 °C	12.9	252.0	19.6
45 % MEEP	30 °C	12.5	155.9	12.5
45 % MEEP	60 °C	23.2	264.1	11.4
95 % MEEP	30 °C	10.2	375	36

Characterization of 45% and 95% MEEP.

Similar chemical characterization tools used for 80% MEEP were applied to 45 % MEEP. In the composition of this polymer, the reduced MEE was made up using 4-MEOP. The P-31 and proton NMR spectra clearly reflect this chemistry. The major P-31 peak at -8 ppm, corresponding to PN(MEE)2 is greatly reduced in intensity, Appendix D. Replacing this peak is the broad peak between -12 and -15 ppm, which corresponds to phosphorus atoms substituted with one MEE and one aromatic, which is expected because of the lower amount of MEE and the higher aromatic content of this polymer. Integration of the proton NMR spectrum revealed the speciation of each pendant group, Table 1 and was calculated as described for 80% MEEP, Appendix D

DSC revealed a single transition attributed to the Tg. Reducing the MEE content and increasing the 4-MEOP would be expected to increase the Tg, and that was what was seen with a Tg at approximately -44 °C, Appendix D. Many of the bulk physical properties were much better than those seen in 80% MEEP. More robust films were formed from this formulation that exhibited no creep. For this polymer, the need for cross-linking is substantially less. Furthermore, surface tackiness was substantially less. These improvements in physical properties are a direct result of the increased amount of 4-MEOP on the polymer backbone.

NMR data for 95% MEEP is shown in Appendix D. The proton NMR spectrum is dominated by peaks assigned to the MEE pendant groups. The small amount of 2-AP (5%) is also seen, but with much less intensity due to the lower content. This polymer also showed a much simpler P-31 spectrum with one major peak attributable to PN(MEE)2; although there is a much smaller peak at -14 ppm due to the 2-AP content. Consistent with the role of MEE in depressing Tg, 95% had the lowest at <-80 °C. An exact measurement was not possible on our equipment due to an insufficient instrumental temperature range.

Membranes for gas analysis were prepared by casting followed by heat-induced cross-linking, Table 2. The 30 °C experiments for the three polymers show that the highest permeability and selectivity was given by 95 % MEEP. This is consistent with the findings from our 2006 report. (Orme, Klaehn et al. 2006) The lowest performance was the 45 % MEEP, especially in terms of selectivity. At 60 °C, permeabilities were generally higher, as expected; however this came with a loss in selectivity. In terms of utility, although the 95% MEEP offered superior performance, it was too physically unstable to form a durable membrane. It exhibited an unacceptable amount of creep that prevents its use in this application.

Solubility of MEEP materials.

One of the goals of the project was to develop durable coating materials that could be applied using less hazardous solvents such as ethanol. Solubility data for the three MEEP polymers is shown in Table 3. The most significant impact on solubility was demonstrated for water where reducing the MEE content reduced solubility. It should be noted that THF is the best solvent for these polymers.

Table 3. Targeted MEEP polymer compositions.

Polymer	Water	Ethanol	THF
45% MEEP	Insoluble	Soluble	Soluble
80% MEEP	Slightly soluble	Soluble	Soluble
95% MEEP	Soluble	Soluble	Soluble

Chemical and physical characterization

Working with GE Global Research and WRI, INL worked to adjust the polymer cross-linking properties. INL worked with GE Global Research to define other necessary properties for coating compatibility. These targets were based on the preliminary technical and economic study from Task 6 completed by GE Global Research, coating application on individual hollow fiber supports produced in Task 3 and flat sheet membrane performance testing in coal flue gas in Task 5.

It was expected that during the optimization process, adjustments in cross-link density would be necessary to achieve both acceptable gas transport performance and mechanical properties. In this subtask, the amount of 2-allylphenol was optimized by carefully varying the loading to provide effective cross-linking. Further, the effect of cross-linking on performance was assessed.

Various efforts to crosslink MEEP material.

Building on the literature data, synthetic efforts were begun with an 80% MEEP formulation with 8% 2-AP. 0.25 mole scale reactions gave polymer materials in about 40 % yield that were studied as flat sheet membranes. In these initial efforts, casting solutions were formed in THF with benzoyl peroxide (BP) as a cross-link initiator. BP undergoes homolytic bond cleavage at approximately 105 °C to yield short-lived free radicals, which then activate the allylic methylene groups of 2-AP to initiate the carbon-carbon bond forming process. Temperatures as high as 130 °C for 10 minutes were employed to ensure initiation of the cross-linking event, which required heating of the membrane to at least the initiator's decomposition point. Gas permeability measurements yielded widely ranging CO_2 permeability data, but all of it consistently low, which we attributed to effects on the polymer induced by the cross-linking process.

A study on a similarly cross-linked (2% BP, 130 °C, 10 minutes) membrane was conducted where the relationships between temperature and both CO_2 permeability and CO_2 /N_2 ideal selectivity were determined. This data, taken above ambient temperature, was compared with literature data reported by the Way group (Jha, Mason et al. 2006) taken at sub-ambient temperature, Figure 15. The CO_2 /N_2 ideal gas selectivities correspond well, suggesting that cross-linking conditions and density may not influence membrane selectivity to a great degree. However, the permeability data does not correlate with the elevated temperature data set, which exhibited less permeability than would be expected. This data suggests that a careful consideration for cross-linking chemistry and conditions is necessary to both stabilize the membrane and provide maximum performance.

Alternate methods to increase dimensional stability and cross-link density of 80 % MEEP were explored, Table. First, AIBN was studied as an initiator. Although the literature data suggested the use of BP, it is not soluble in ethanol, a preferred casting solvent. AIBN, with an initiation temperature of 102 °C, exhibited more solubility in ethanol. A second method was the inclusion of tetraethylene glycol diacrylate (TEGDA). TEGDA is a highly reactive species that cross-links polymers in the presence of a free radical initiator. A final method was to mix 80 % MEEP with another phosphazene, poly[bis-phenoxyphosphazene] with 1% 2-AP (PPOP), and then cross-link the structure to prevent phase separation. Mixing can result in an interpenetrating network (IPN) of both polymers randomly distributed within the membrane if the two polymers are mutually miscible.

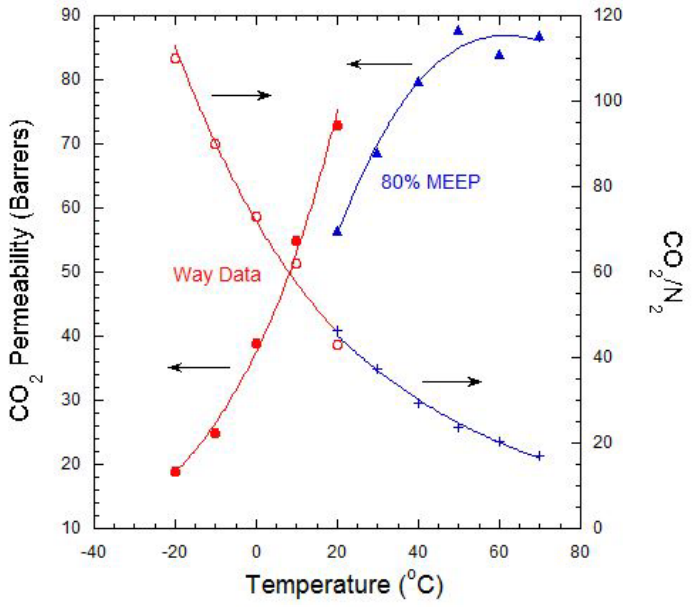

Figure 15. 80% MEEP membrane performance as a function of temperature.

AIBN was added to the membrane similarly to the method employed for BP. Upon evaporation of the solvent, the membrane was incrementally heated first to 95 °C, then to 110 °C, and finally to 120 °C. At each step, surface tackiness was detected, prompting the temperature elevation. The resulting membrane was then characterized for CO_2 , N_2, and O2 permeability. O_2 was added because phosphazenes exhibit a characteristic $O2/N_2$ ideal selectivity of ~2. Less than two suggests membrane failure (tear, pinhole, etc.). At 30 °C, performance was good with CO_2 ideal selectivity at 33.6. Experiments were also conducted at 60 °C to characterize the performance and also to accelerate any dimensional changes to which the membrane may be susceptible. At 60 °C, both CO_2 permeability and CO_2 /N_2 selectivity decrease, which was not expected. Typically, permeability increases with temperature. The $O2/N_2$ selectivity of 1.6 reveals that the membrane lost dimensional stability and suffered a partial failure. This data also suggests that the AIBN may not have generated enough cross-links to provide a durable film.

Two experiments were conducted with the TEGDA additive. The first, using a titania support for the membrane gave low permeability and selectivity data; although the $O2/N_2$ selectivity suggested that the membrane retained integrity at 30 °C. However, some creep was evident at 60 °C but the membrane exhibited little tackiness. Use of a PDMS support gave similar transport data with slightly higher CO_2 permeability; however the surface was somewhat tacky and creep was evident at the higher temperature. This approach was abandoned due to the low performance and poor mechanical integrity of the membranes.

The IPN approach yielded membranes with excellent non-adhesive surface characteristics. At 30 °C, CO_2 permeability was nearly 300 Barrers with a selectivity of 33, which is similar to pure 80 % MEEP membranes without cross-linking. Increasing the temperature to 60 °C increased CO_2 permeability to above 400 Barrers while the ideal selectivity for CO_2 /N_2

was reduced to 19. It also should be noted that the mechanical integrity of the polymers was good with $O2/N_2$ selectivities > 2.

Table 4. Alternate cross-linking protocols and results.

Polymer, Support Material and Casting Solvent	Cross-linking protocol	Qualitative Properties	Temp (°C)	P(CO_2) (Barrers)	O_2/N_2	CO_2/N_2
80% MEEP Titania (0.1 µm) THF	AIBN (1 %), 0 min at 95 °C, 110 °C, then 120 °C	Some tackiness	30	264.4	33.6	22.3
			60	142.3	19.3	11.6
80% MEEP Titania (0.1 µm) Ethanol	Tetraethylene glycol diacrylate/Benzoyl peroxide (1 % each, 120 °C, 10 min)	Not tacky	30	98.6	16.7	22
			60	72	11.1	11.8
80% MEEP PDMS Dense film (250 µm thick) Ethanol	Tetraethylene glycol diacrylate/Benzoyl peroxide (1 % each , 120 °C, 10 min)	Some tackiness and creep	30	116.9	17.7	22.1
			60	129.8	9.8	11.8
80% MEEP and PPOP Titania (0.1 µm) THF	Benzoyl peroxide (1%, 130 °C for 10 min)	Hard Surface, no tackiness or creep	30	279.4	33.1	22.3
			60	406.7	19.8	22

Also investigated were polymer mixtures with other polymers and/or fillers to enhance stability and performance, Table 5. Polyethylene glycol of 400 Dalton molecular weight (PEG-400) was found to act as a plasticizer and create largely impermeable membranes. Addition of higher molecular weight 100,000 Dalton polyethylene oxide (PEO) into the casting solution resulted in membranes that were not tacky to the touch. Permeability and selectivity were comparable to neat 80 % MEEP membranes, both at 30 °C and 60 °C; however it was decided that these membranes were excessively hydrophilic and would not remain stable in the presence of water.

Carbosil, which acts as an inert filler material, was suspended in the membrane. This was accomplished through addition of the Carbosil into the casting solution and then forming the membrane similarly to that of 80 % MEEP. No clear determination of Carbosil loading across the membrane was performed; however the surface was influenced by the material in that tackiness was reduced. Permeability and selectivity of this membrane was generally lower than expected, Table 5 . To address this, DER was added to the formulation. DER is an epoxide terminated PEO that potentially could participate in the cross-linking chemistry. The result of this addition was a significant loss in permeability, which was consistent with the previous PEG-

400 result that suggested that small organics make poor additives to 80 % MEEP. Thus, this avenue was not investigated further.

Table 5. Performance of 80 % MEEP membranes mixed with selected agents.

Polymer Blend	Cross-linking	Solvent	Film characteristics	Temp (°C)	P(CO_2) (Barrers)	CO_2 /N_2
80 % MEEP/PEG 400 (80/20)	Benzoyl peroxide, 130 °C	THF	Tacky	30	28	8
80 % MEEP/100K PEO (80/20)	none	water	No tackiness	30	546	34
				60	756	20
80 % MEEP/0.45 µm Carbosil	Benzoyl peroxide, 130 °C	THF	No tackiness	30	217	28.1
				60	306	18.8
80% MEEP/0.45 µm Carbosil / DER	Benzoyl peroxide, 130 °C	THF	No tackiness	30	36	28
				60	48	17

Effect of support pore size on performance.

Adapting the poly(phosphazene) selective layer coating process to hollow fibers requires, among other things, an appreciation of the effect of support pore size on membrane performance. To determine the relationship between transport performance and support pore size, a series of membranes were formed as flat sheets using four differing ceramic type supports with pore diameters ranging from 0.005 µm to 0.5 µm. For these four supports, membranes were cast from THF solution using BP as the initiator. Permeation behavior was measured at 30°C and 60 °C for CO_2 , N_2, and O2, Table 6. Although the CO_2 permeability data indicated some variability, selectivity for both gas pairs, in general, decreased as pore size increased. The data seems to suggest that pore penetration by the selective layer does occur and can be minimized by reducing the pore size of the support layer.

Effect of cross-linking time, initiator, temperature, long term testing

With the limited amount of available information concerning the use of AIBN to cross-link 80% MEEP, some fundamental studies were conducted where we probed the effect of cross-linking time and temperature, and casting solution concentration on gas permeability. CO_2 permeability was measured on membranes cross-linked using AIBN (2 weight % with respect to the polymer) and cast from ethanol at 70 °C, 110 °C, and 130 °C as a function of cross-linking time, Figure 16. A clear trend of drastically reduced permeabilities is observed. The data suggests that cross-linking temperature is not a significant determining factor for performance. However, time does appear to influence performance. From this data, it can be proposed that the performance loss is due to polymer creep and insufficient cross-linking. CO_2 /N_2 ideal selectivity was largely maintained (ranging from 26 to 33 with no clear trend) in these experiments which suggests that defect structures, such as holes, were not formed during cross-linking. A plausible explanation would be that the cross-linking process in this set of experiments did not preclude annealing, or the re-ordering of the polymer chains in the

membrane that squeezes out fractional free volume and results in a denser less permeable membrane. Complete data sets are located in Appendix E.

Table 6. Performance data for 80 % MEEP membrane cast onto various pore size ceramic supports.

Polymer Support Material and Casting Solvent	**Cross-linking**	**Temperature (°C)**	**P(CO_2) (Barrers)**	CO_2 /N_2	**O_2/N_2**
Titania (0.005 µm)/THF	Benzoyl peroxide (2%, 130 °C for 10 min)	30	68.6	37.3	2.3
		60	84.1	20.0	2.0
Titania (0.1 µm)/THF	Benzoyl peroxide (1%, 130 °C for 10 min)	30	92.3	25.9	2.2
		60	130.6	15.9	1.9
Whatman Alumina (0.2 µm)/THF	Benzoyl peroxide (1%, 130 °C for 10 min)	30	154.2	23.2	1.8
		60	229.2	14.3	1.9
Titania (0.5 µm)/THF	Benzoyl peroxide (1%, 130 °C for 10 min)	30	85.9	7.9	0.9
		60	108.8	8.2	1.4

Since the cross-linking time and temperature studies revealed that gas selectivity is largely conserved, it was desired to determine whether it would be maintained over a long term test. A 200 hour performance test was conducted on an 80 % MEEP cross-linked membrane. In this test, selectivity was monitored initially at 30 °C and then the temperature was raised to 60 °C for a longer period of time. Although there is appreciable scatter in the data, no trend of selectivity loss could be identified, as shown in **Figure 17**.

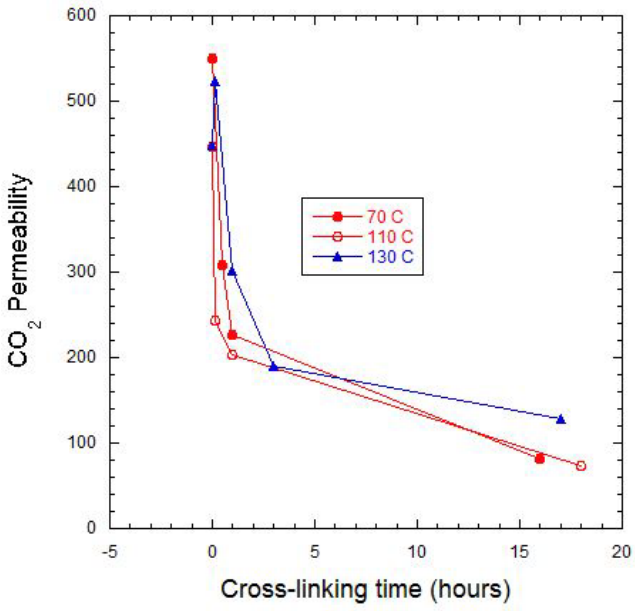

Figure 16. CO_2 permeability as a function of cross-linking time and temperature.

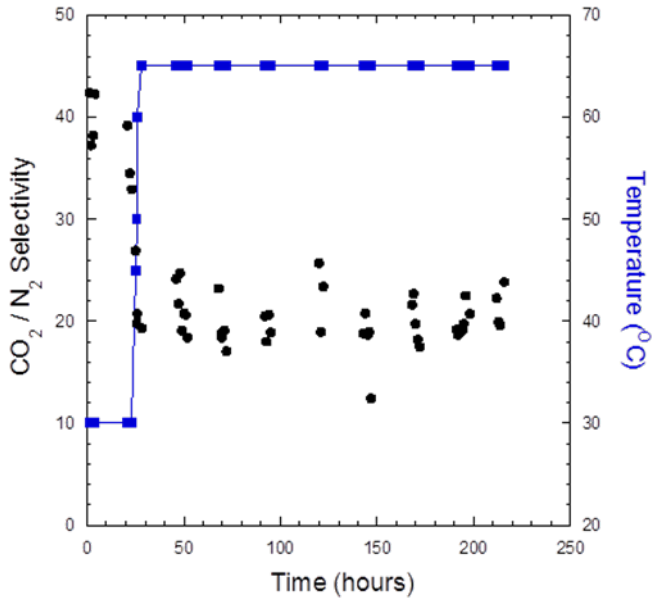

Figure 17. 200 hour performance test for 80 % MEEP as a function of temperature.

Task 2.3: Optimize polyphosphazene stabilization (INL)

INL worked to improve robustness by optimizing polyphosphazene stabilization to achieve refined membrane performance goals proposed in Task 6. Working with GE Global Research and Georgia Tech, INL identified critical solution properties affecting both the in situ batch process and dip coating continuous process. INL adjusted the polymer coating to assure

that the composite hollow fiber membranes meet the performance targets, which represented the go/no-go decision point at the end of Q6.

The goal of this subtask was to incorporate an amount of a fluorinated stabilizer into the membrane. Fluorinated systems discourage surface adhesion and change the properties of the membrane that will lead to less buildup of particulate matter at the membrane surface. These additives can be included into the polymer using either of two methods. First is simple mixing. During the membrane casting process, a fluorinated modifier can be added into the casting solution. Once cast, the membrane should have the additive randomly distributed throughout. This method does have a disadvantage in that the additive would be expected to leach out over time, thus negatively influencing the membrane's durability. The second method involves direct bonding of the fluorinated additive to the polymer backbone, which is done in the same method used to form the polymer with other pendant groups. Using this method gives membranes where the fluorinated component cannot leach. For this reason, this second route was chosen because the application requires long term chemical stability of the membrane.

Two differing fluorinated pendant groups were used: 2,2,2-trifluoroethanol (TFE) and 2,2,3,3,4,4,5,5-octafluoropentanol (OFP), structures are shown in Figure 16. While both compounds add fluorine to the polymers, they impact physical properties differently. The shorter chain TFE tends to increase Tg, thus decreasing rubberiness, as compared to MEE. The longer five carbon chain OFP will "self-plasticize" the phosphazene, thus serving to decreasing Tg in a manner similar to that of MEE.

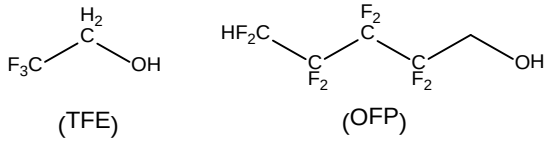

Figure 18. Chemical structures for TFE and OFP.

Two polymer compositions were selected that took advantage of the properties imparted by these pendant groups. In the first polymer, TFE was added in place of 4-MEOP due to the fact that these two pendant groups have a similar influence on Tg. Thus the targeted polymer composition was 60 % MEE, 32 % TFE, and 8 % 2-AP. This polymer was synthesized with a two-step addition process similar to that of 80 % MEEP. 2-AP and TFE were attached to the backbone in the first addition step, followed by MEE, which was added in a 100% excess to ensure complete removal of all chlorine from the polymer backbone. NMR data was found to be consistent with the proposed structure, Appendix F Thermal analysis revealed a weak Tg transition at -66 °C and an onset of decomposition at 245 °C, Appendix F

The second polymer was formed using OFP that is similar to MEE in its ability to lower Tg. Instead of completely replacing a pendant group, as was done with the TFE polymer, MEE content was lowered by 5% to account for the OFP content. Thus, the polymer contained four pendant groups, rather than three with the following speciation: 75 % MEE, 12 % 4-MEOP, 8 % 2-AP, and 5 % OFP. The structural assignment for this new polymer was supported by multinuclear NMR spectroscopy, Appendix G. DSC revealed a Tg at -70 °C, which is consistent

with the 80 % MEEP. Additionally, TGA showed that this polymer began decomposition at 236 °C, which is almost 50 °C lower than 80 % MEEP, which was both unexpected and undesired. Complete data is shown in Appendix G

Membranes were formed by solution casting and cross-linked with either BP or AIBN. Both methods applied to both polymers gave membranes that displayed some tackiness. The TFE polymer yielded dimensionally stable membranes, as shown in the $O2/N_2$ ideal gas selectivities measured at 30 °C and 60 °C, Table 7. Gas permeability data on flat sheet membranes formed from OFP and TFE phosphazenes.. However, the CO_2 /N_2 selectivities are lower than those seen for 80 % MEEP. Interestingly, the CO_2 permeability decreased upon raising the temperature to 60 °C, which is evidence of flow into the pores of the support. The OFP polymer provided a membrane with poor dimensional stability as shown by the low $O2/N_2$ selectivities. Further, the CO_2 permeabilities and selectivities were low. Thus, the addition of a fluorinated pendant group did not provide better surface properties and did not give better transport properties than 80 % MEEP. The polymers were not pursued for further development.

Table 7. Gas permeability data on flat sheet membranes formed from OFP and TFE phosphazenes.

Polymer	**Support and cross-linking**	**Temperature (^{o}C)**	CO_2 **perm. (Barrers)**	CO_2 /N_2	**O_2/N_2**
TFE	AIBN (1 %, in THF, 130 ^{o}C, 10 min)	30	196.1	24.2	2.2
		60	169.5	13.3	2.1
OFP	Benzoyl peroxide (1 %, in THF, 130 °C, 10 min)	30	40.1	8.7	1.1
		60	53.3	10.3	1.6

Efforts and issues with poly(phosphazene) scaleup

Polymer syntheses in the initial tasks of this project were performed at the 0.25 mole scale, which corresponded to approximately 29 grams of $PNCl_2$ per batch. The procedures and material handling associated with this scale were well-understood by the INL team and is described in the literature. The initial preparations gave a target pendant group composition of 80 % MEE, 12 % 4-MEOP, and 8 % 2-AP with yields ranging from 40-50 %, with respect to the starting amount of PNCl2. To meet the needs of the project, both the synthetic scale and the yield needed to be increased.

Doubling of the scale up to 0.5 moles was accomplished; however modifications to the synthetic procedure were required. At this scale, yields were exceedingly low due to a large amount of material that became intractably insoluble during purification. These portions, which became insoluble, were presumed to be due to premature polymer cross-linking. There were two immediate remedies for this behavior: 1) increase the amount of solvent volume used during synthesis; and 2) slightly reduce the 2-AP percentage on the polymer. The former route was not considered because of the limitations placed on the activity within the laboratory. Thus, the latter route was followed where the targeted speciation was changed to 80 % MEE,

15 % 4-MEOP, and 5 % 2-AP. Other small improvements in polymer collection during purification, along with the reduction in 2-AP, gave higher yields of subsequent batches. Yields of each of the 18 batches synthesized in the project are shown in Appendix B.

Casting of 80 % MEEP onto PDMS dense film supports

Since it became clear that an effective method for forming the hollow fiber support entailed fiber extrusion followed by coating with poly(dimethylsiloxane) (PDMS) prior to application of the phosphazene, it became necessary to characterize flat sheet 80 % MEEP membranes cast onto PDMS support layers. Initially, thin PDMS membranes (50 µm) were used; however solution casting the phosphazene from ethanol proved problematic as the ethanol would penetrate the PDMS and cause some dimensional instability, yielding wrinkled membranes that could not be effectively smoothed so that they could be mounted into a membrane test cell.

Use of 250 µm PDMS resulted in a successfully formed membrane. The thicker PDMS was more resistant to deformation during 80 % MEEP membrane casting. Three separate membranes were prepared that varied by cross-linking: 1) no cross-linking; 2) cross-linked with 2 % AIBN at 70°C for 8 hours; and 3) same cross-linking conditions for 24 hours. Pure gas permeability measurements were conducting using O_2, N_2, and CO_2 as the analyte gases. Ideal O_2/N_2 selectivities, Table 8, ranged between 2.1 and 2.2, suggesting defect free membranes were formed for all three preparations. CO_2 permeabilities and CO_2 /N_2 selectivities were determined for the bulk composites. Interestingly, the permeabilities and selectivities were not influenced by the cross-linking process. The loss in CO_2 permeability upon heat curing seen for 80 % MEEP membranes cast on porous ceramic supports was not observed in these PDMS composites.

The permeabilities measured in this experiment represent performance of a composite membrane. To assess the performance of the selective layer alone, the known performance of PDMS was used to deconvolute the performance of the 80 % MEEP, as shown in Table 8. Calculated CO_2 permeability of the selective layer in the absence of cross-linking was nearly 500 Barrers, which corresponds well to the 80 % MEEP without cross-linking cast onto ceramic supports. Upon cross-linking, the performance was undiminished, which suggests a synergistic effect between the two polymer layers that serves to stabilize the 80 % MEEP. Having this synergistic effect also apply to the hollow fiber membrane geometry would be advantageous to this project.

Interpenetrating Network Strategy.

From Task 2, a successful method to obtain a membrane with a non-tacky surface was to blend the 80 % MEEP with another polymer with non-tacky behavior, forming an interpenetrating network (IPN). An additional driver for exploring this method is the heat-related aging that is seen in pure phosphazene materials. In an IPN, it is thought that the more flexible, lower Tg polymer is prevented from rearranging into a denser and less permeable morphology by becoming entrained in a less flexible polymer.

Table 8. Gas permeability data (measured and calculated) for 80 % MEEP PDMS composite membranes as a function of cross-linking time at 70 °C.

Exp. #	MEEP thickness	cross-linking	Permeability measurement	P(N_2) (Barrers)	P(O_2) (Barrers)	P(CO_2) (Barrers)	O_2/N_2	CO_2/N_2
1	24 um	none	bulk composite	10	21.2	169.7	2.1	17.0
			calculated for just the selective layer	17.2	35.5	491.4	2.1	28.6
2	24 um	8 hours at 70 °C	bulk composite	9.3	20.1	167.6	2.2	18.0
			calculated for just the selective layer	15.2	32.5	474.3	2.1	31.2
3	24 um	24 hours at 70 °C	bulk composite	9.1	20	168.0	2.2	18.5
			calculated for just the selective layer	14.6	32.2	477.3	2.2	32.7

This strategy was studied in more depth. IPN membranes were cast similarly to that of pure 80 % MEEP membranes. The choice of the polymer to be mixed with the 80 % MEEP was critical to the desired outcome. The two polymers were added to a mutual solvent, typically THF, and mixed together and then cast onto a support. Upon drying the membrane could be cross-linked to provide additional stability; however cross-linking was not necessary to yield a durable membrane at least over the short term.

Three IPN formulations, Table 9, were synthesized where the relative ratios of the two polymers were varied to cover a range of compositions. DSC analysis of IPN 2, Figure 19, shows endothermic transitions associated with crystalline rearrangements. 80 % MEEP is not crystalline and does not show crystalline thermal behavior; however PPOP is a well-known semi-crystalline polymer. (Orme, Klaehn et al. 2004) It would be reasonable to propose that the crystallinity in PPOP would be disrupted by intimate mixing with the 80 % MEEP. However, the observation of the transitions in the DSC suggests that some portion of crystallinity remains. The degree of remaining crystallinity was not quantified.

Table 9. Composition of IPN membrane.

Membrane	80 % MEEP (Weight Percent)	PPOP (Weight Percent)
IPN 1	30	70
IPN 2	50	50
IPN 3	70	30

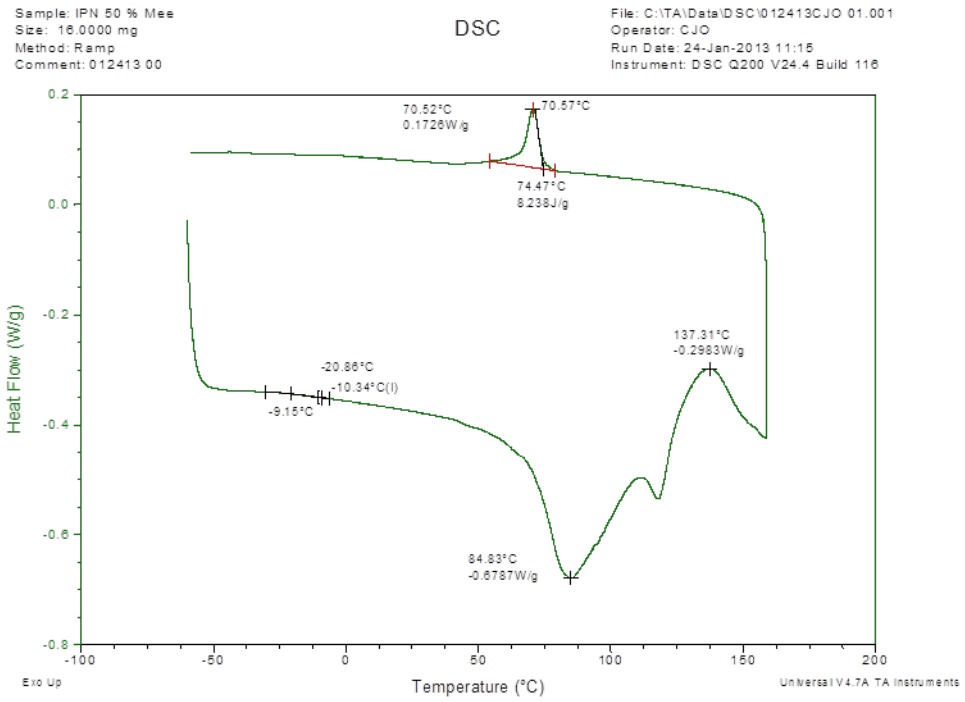

Figure 19. DSC plot of IPN 2.

Gas separation performance results

Pure gas experiments were conducted on the three IPN formulations plus the pure (100%) IPN constituents (PPOP and 80 % MEEP), Table 10. In this series at 30 °C, permeability and selectivity were found to increase as the weight percent of 80 % MEEP was increased, which is somewhat unusual because modifications that increase permeability tend to decrease selectivity, and vice-versa. It should be noted that this series was formed by cross-linking, thus the lower data obtained for the pure 80 % MEEP membrane. If the 80 % MEEP membrane were not cross-linked, its data would be expected to correlate well with the 70% (80 % MEEP) IPN.

Increasing the temperature to 60 °C resulted in the expected increase in permeability and decrease in selectivity. The highest CO_2 permeability at this temperature was IPN 3, with the highest amount of 80 % MEEP, which was measured at 661.6 Barrers. However the effect of heating on selectivity was significant with a drop from 35.8 to 20.4 over this temperature range. Although the selectivity of IPN 3 was not that much different from pure 80 % MEEP, the much lower CO_2 permeability for the cross-linked 80 % MEEP suggests that the IPN strategy has significant value in dimensionally stabilizing the MEEP polymer in the place of utilizing only thermal cross-linking.

Table 10. Gas transport data for 100 % PPOP, IPNs 1-3 and 80 % MEEP at 30 °C and 60 °C.

Membrane	Temperature	CO_2 Permeability	CO_2 /N_2 Selectivity
100% PPOP	30	12.2	23.1
	60	42.4	15.1
IPN 1 30 % (80 % MEEP) / 70 % PPOP	30	125.6	23.7
	60	249.5	16.3
IPN 2 50 % (80 % MEEP) / 50 % PPOP	30	279.4	33.1
	60	406.7	19.8
IPN 3 70 % (80 % MEEP) / 30 % PPOP	30	458.6	35.8
	60	661.6	20.4
100 % (80% MEEP)	30	90.8	29.3
	60	145.9	21.8

Figure 20 is a permeability-selectivity plot that allows for comparative assessment of IPN performance. Ideally, improvement in membrane performance includes increases in both the permeability of the selected permeant and the selectivity of the membrane for the permeant over other gases. This has been expressed by Lloyd Robeson (Robeson, 2008) as a log-log plot of selectivity vs. permeability. This plot graphically describes the trade off in performance in terms of an upper bound, which represents a theoretical upper limit of performance. Moving towards the upper bound can be considered improved performance. The plot shows the performance target for the project at 30 °C, 80 % MEEP data, and literature data for 48 % and 74 % MEEP. IPN data plotted against these data indicate that enhanced permeability and selectivity result from using the IPN strategy. The highest MEE containing IPN 3 exhibits the best performance. IPN performance data at 60 °C shows the typical trade-off with a loss in selectivity and an increase in permeability.

Long term test results

A 90 hour test of IPN 3 was performed at 65 °C. In this experiment, conducted over 90 hours, CO_2 permeability averaged 402 Barrers, while the CO_2 /N_2 selectivity was approximately 13, Figure 21. It should be noted that this experiment was conducted using different cross-linking conditions (130 °C, 10 min, and AIBN initiator) than those in Table 10 (110 °C, 10 min, 1% BP initiator). The data is substantially lower than shown in Table 10 at 60 °C which suggests that the IPN method may not be immune from the loss in performance induced by cross-linking.

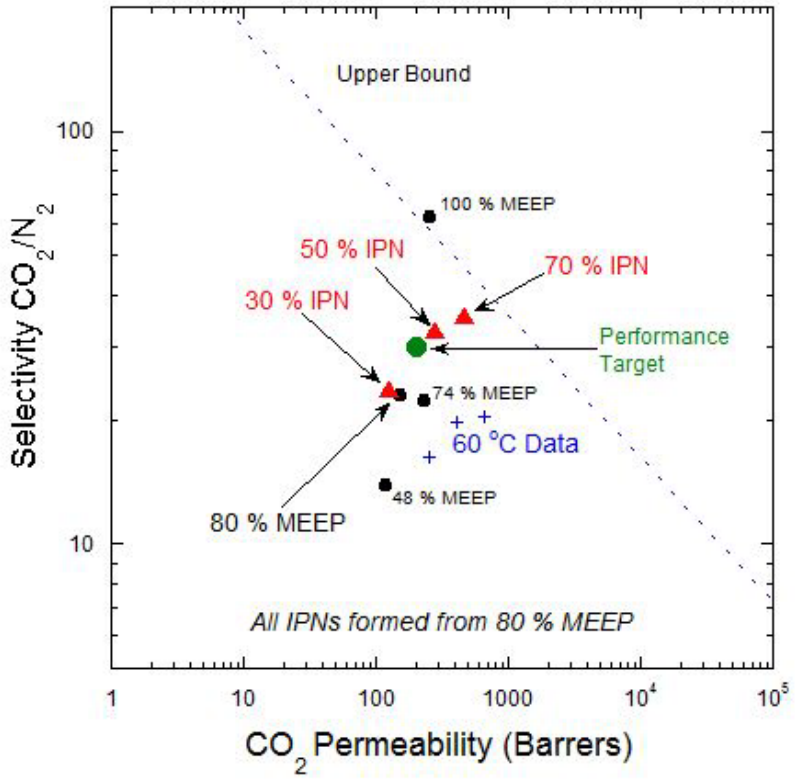

Figure 20. Permeability-selectivity plot for selected phosphazene membrane.

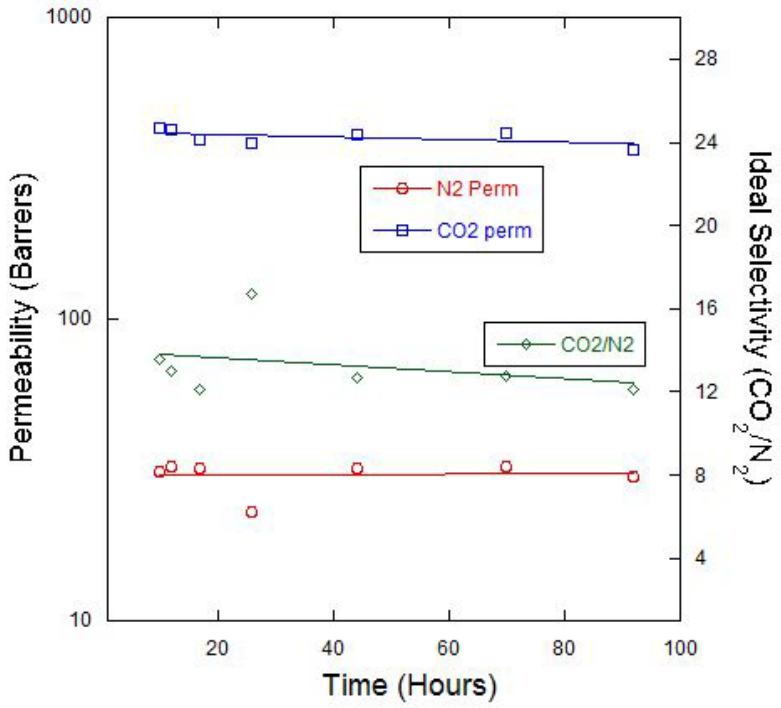

Figure 21. 90 hour test of IPN 3 at 65 °C.

Performance vs. temperature

A multi-day experiment was conducted to determine the durability of cross-linked IPN 3 (130 °C, 10 minutes, AIBN initiator) under thermal stress. In this experiment, Figure 22.data was collected over four days using a mixed gas experimental method. In a mixed gas experiment, the membrane was interrogated with a mixture of CO_2 , N_2, and water. Feed and permeant compositions were determined using gas chromatography.

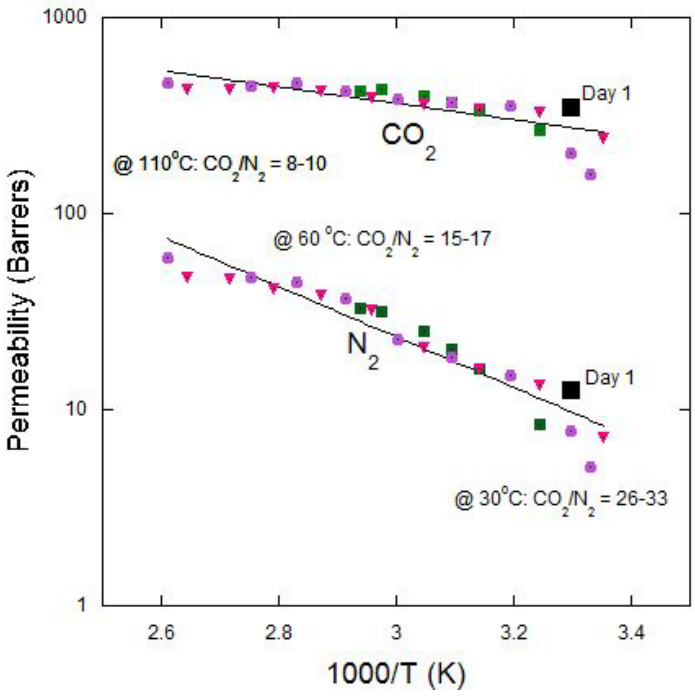

Figure 22. Multi-day membrane performance as a function of temperature.

On day 1, data was acquired only at 30 °C, as shown in the plot as black squares. For the subsequent days, the temperature was ramped upward and permeabilities were measured. All of the data was then superimposed to reveal Arrhenius type behavior. Selectivities were found to be self-consistent at each temperature. At 30 °C, they ranged from 26-33. Increasing the temperature increased permeability; however the selectivity was reduced. At 60°C and 110 °C, the selectivities for CO_2 /N_2 were 15-17, and 8-10, respectively.

Figure 23 shows the water permeation data as a function of temperature with CO_2 included for comparison. Water, being both smaller than CO_2 and more condensable, exhibits much higher permeability. There is a significant degree of scatter in the data, which is attributed to unwanted condensation in the system and anomalies in the gas chromatographic analysis. Regardless of the scatter, the trend is that water is significantly more permeable through IPN 3 than CO_2 . Separation factors ranged from 4-7 at 25°C-30 °C to 3-4 at > 100 °C. The complete data set is located in Appendix H.

The reproducibility of the performance as the temperature was raised and lowered multiple times suggested a stable membrane morphology induced by the IPN structure. Furthermore, no membrane degradation was observed at 110 °C, which indicates that the structure would be stable at the desired operating temperature of 60 °C and would have a built-in safety margin should the membrane be exposed to a temperature excursion.

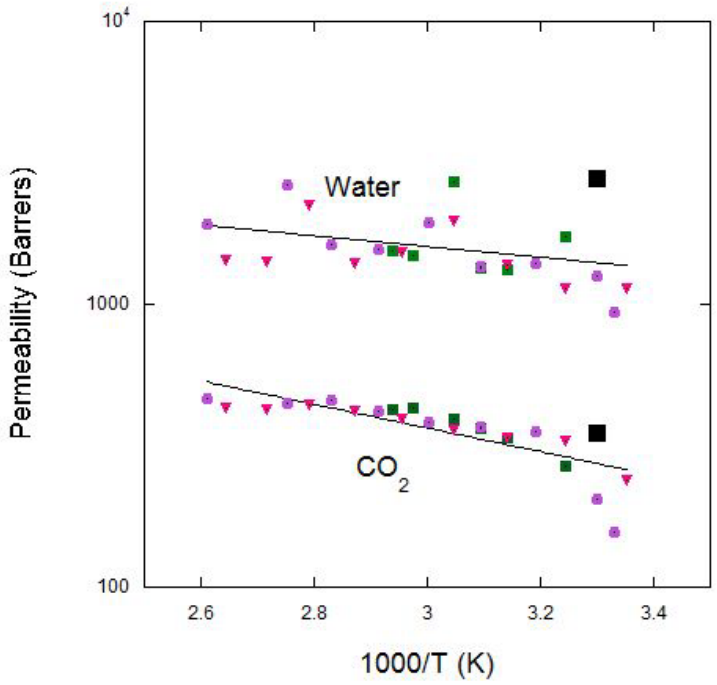

Figure 23. CO_2 and water permeability as a function of temperature through IPN 3.

Conclusions: Polyphosphazene polymer and coating solution development

Using flat sheet membranes, the INL team was able to reproducibly measure consistent membrane performance from batch to batch. INL determined intrinsic permeability and selectivity for 80 % MEEP and used that as a quality control measure. Prior to cross-linking, the CO_2 permeability was approximately 450-500 Barrers with a selectivity over N_2 that ranged from 34-37 at 30 °C. Conducting the transport measurements at 60 °C increased permeability; however at the expense of selectivity, which was reduced to 20-25. In the process of moving this technology closer to deployment, several important aspects were identified that needed optimization. Dimensional stability was a characteristic that was particularly challenging. Further, surface tackiness was another important consideration that needed remedy. Also, we identified that interfacial behavior between layers can influence both the stability and performance of these composite membranes.

Stabilization of phosphazene polymers that give the highest performance for CO_2 permeability and CO_2 /N_2 selectivity is not a trivial exercise. Creep is the largest factor that had to be addressed. Creep is defined as flow of the polymer. In this instance, creep can be embodied as flow into the pores of its supporting substrate. As the pores are filled by a flowing polymer, the effective membrane thickness becomes the coating thickness plus the pore depth, which can often be significant. Permeability is a function of selective layer thickness, assuming that the principal resistance to permeation is due to the selective layer. Thus, permeabilities can fall drastically as the selective layer flows and fills pores. This may have been an issue during cross-linking of pure 80 % MEEP. Using a thermally induced cross-linking process, approximately 50 % of the intrinsic permeability of 80 % MEEP was lost. Attempts were made

to understand this phenomenon and it was attributed to a degree of polymer creep plus potential annealing effects that create a denser, and therefore less permeable, structure.

Another important consideration that was addressed in this project was surface properties. For the flue-gas application, fly ash is an expected component. 80 % MEEP tends to be tacky and encourages adhesion to particulate matter to the surface, which will ultimately lead to membrane fouling and a reduction in performance. Several methods were explored to eliminate surface adhesion. Addition of fluorinated pendant groups was not found to remedy the surface tackiness. A marginal degree of success was found through cross-linking. The best method was the addition of either a high molecular weight polymer (PPOP or 100K PEO) or a solid material, such as Carbosil. In both cases, the surface behavior was dramatically improved. In fact, PPOP, which formed an IPN, gave a hard smooth surface that was considerably more durable than any of the membranes formed using other methods.

The importance of the nature of the support and the potential for interactions between selective and support layers was evident in the research. The bulk of the data available to INL prior to this work were from membranes cast onto one specific support. As other supports were considered, the team was able to study the dependence of pore size on permeability. It was concluded that > 0.2 μm pores encouraged polymer creep. Likewise, the smallest pore size supports discouraged polymer infiltration The casting of 80 % MEEP directly onto films of dense PDMS was also explored. We were encouraged by the observation that cross-linking of the phosphazene on PDMS composite did not show the characteristic loss in permeability seen with porous supports. However, we did identify that the PDMS did influence the performance of the resulting asymmetric membrane and the data suggested that it is critical to keep the PDMS layer as thin as possible.

Recommendations and path forward

Three alternate pathways seem feasible to develop 80 % MEEP materials into durable and reliably performing membranes. First, the cross-link density must be increased. During cross-linking, there is loss of performance that occurs, which is attributed to creep. Increasing the cross-link density, accomplished by increasing the 2-AP content on the polymers, would serve to position cross-linkable groups in closer proximity to each other, thus obtaining cross-links more rapidly. It is expected that the cross-link chemistry should result in large increases in molecular weight with a corresponding loss in the ability to creep. Accelerating the apparent reaction rate would mean forming the desired stabilized structure before the polymer has time to creep. However, caution must be exercised in increasing the 2-AP loading. In this project, loading had to be reduced due to premature activation of the allyl group that lowered product yield. This behavior may have a dependence on concentration, where increases in 2-AP loading must be met with increased dilution of the synthetic reaction solution. Increased reaction concentrations may encourage premature cross-linking.

The second route is to explore more energetic means of cross-linking the 80 % MEEP. Work reported by INL and others have suggested that UV, gamma, and electron beam irradiation will rapidly cross-link polyphosphazenes without heating. Application of these methods would eliminate the driving force for creep, which is heat, and result in rapid cross-link chemistry with higher cross-link densities. An unpublished study at INL suggested that electron

beam irradiation can achieve high cross-link densities without affecting gas transport performance.

Thirdly, the IPN chemistry needs to be fully developed. In this project, promising results were obtained on flat sheet membranes. However, the best results were obtained on membranes that were solution cast from THF, which is a hazardous solvent and can have deleterious effects on many materials. Even though the 80 % MEEP was successfully designed to be soluble in "green" solvents, the current IPN formulation requires a polymer that is more hydrophobic. Hydrophobic polymers tend to be insoluble in desired solvents such as water and ethanol. This limitation needs to be overcome.

Publications and educational opportunities

The project team has one manuscript that is currently being written. In this paper, we will describe the stabilization of 80 % MEEP with cross-linking and through formation of IPN structures. This paper will be submitted to Journal of Membrane Science in 2015. Also, the team brought in a post-doctoral fellow to perform the 80 % synthesis and characterization experiments. This activity served to broaden his background in phosphazene synthesis and allowed him to learn about membrane separations and transport mechanisms.

Journal articles

Christopher J. Orme, Frederick F. Stewart, John R. Klaehn, Joshua S. McNally, "Formation of stabilized polyphosphazene membranes for CO_2 /N_2 flue gas separation", Manuscript in Preparation, to be submitted to Journal of Membrane Science

Presentations

Christopher J. Orme, Frederick F. Stewart and John R. Klaehn, "Gas Permeability of Tailored Phosphazene Polymer Blends", Presented at the 23rd North American Membrane Society Meeting, Boise, ID, June 2013

Task 3: Fabricate Hollow Fiber Support Layer

Hollow fiber support fabrication at GE

Appropriate support geometry and material characteristics were significant aspects of this project. Hollow fibers provide the optimum geometry for high production rates and ease of module formation while providing high surface area and membrane packing density compared to flat sheets. The criteria for the support polymers included commercially availability, processability, high mechanical and chemical stability, ability to operate with existing flue gas clean up conditions (20-60 °C), and high porosity while still having an asymmetric structure to minimize intrusion of the intermediate polymer coating layer.

An analysis of the gas transport, mechanical, and economic constraints for the membrane was performed to determine microstructural and performance targets for the hollow fiber support layer. The key membrane performance parameters, relevant physical

constraints, and resulting (measurable) intermediate layer performance targets are listed in **Error! Reference source not found.**.

Table 11.Membrane Performance Parameters, Physical Constraints, and Intermediate Layer Performance Targets.

Parameter	Physical Constraint/Rationale	Target (measurable)
Selectivity	It is desired that the support layer does not offer any selectivity and just provides high permeance for all the gases. No selectivity or Knudsen selectivity is desired.	CO_2 /N_2 selectivity =1 or Knudsen.
	Best way to check is through gas permeance measurements	
Pore size	Low surface roughness to allow coating of continuous 100 nm polymer layer	Intermediate layer RMS roughness < 30 nm
	Pore size smaller than solvated polymer coil size to avoid infiltration during coating	Intermediate layer pore size < 30 nm
Stability	Chemical compatibility with flue gas components at realistic operating temperatures and pressures	Stability and performance measured under 100 h testing under realistic flue gas conditions
	No delamination or thermal stress-driven cracking of polymer layers due to CTE mismatch	*Determined by any selectivity loss during the*
Economics	Finalized membrane module cost to be lower than state of the art membranes	Cost of composite hollow fiber membrane < Cost of state of the art membranes
Pore size & pore density	Minimize infiltration of polymer layer during processing. Maximize permeance of intermediate layer. Since the pores are small, the pore density should be high around 10-20% to allow for high permeance	Measureable through SEM or pore size analysis < 30 nm >5 nm
Thickness	200-400 µm > 1 µm	Low pressure operation so no fear of fiber burst or collapse. Thickness should be kept low, but sufficient that the fiber can withstand pressure.
Failure pressure	> 2.5 to 25 MPa	The fiber should be able to withstand enough pressure differential across to not deform or elongate. It must be compatible with intermediate or selective layer. The failure and elongation pressure is also important in designing the hollow fiber coater rig
Compatibility with seals	TBD	Maintain module performance and stability through hermetic and thermo-mechanically stable junctions at end seals
Solubility		Solubility of the polymer should be good in solvents typical for fiber spinning, but should be benign to solvents suitable for hollow fiber spinning

Selectivity

Analysis of the CO_2 removal system indicated that the membrane CO_2 /N_2 selectivity should be >30 to achieve meaningful benefits in energy efficiency. As discussed above in Task 2 , laboratory mixed gas selectivities of the polyphosphazene material approach this target. However, in order to realize the full potential of the material, the composite membrane structure must be constructed so that the polymer layer controls the transport through the composite structure. Consequently, the permeance of the intermediate layer and support must exceed that of the polymer layer.

The numerical target for the support/intermediate layer permeance was derived from the assumption that the polymer layer has a CO_2 permeability of approximately 200 Barrer and a target thickness of 0.1 µm, resulting in an upper bound on the permeance of about 2000 GPU. For the selectivity of a composite membrane to exceed 90% that of the polymer layer alone, the permeance of the intermediate layer and support should be greater than 20,000 GPU.

The support/intermediate layer must also be free of pinhole defects, which allow flow to bypass the selective layer. For this project, defects were defined to be pores larger than about 50 nm, which was about half the target thickness of the polymer selective layer. In the limit where 1% of the total flow through the membrane passes through defects as non-selective viscous flow, the selectivity of the composite membrane selectivity will still approach about 90% of the polymer layer alone.

Permeance

Gas transport through a multilayer structure is controlled by the least permeable layer. In an ideal structure, the permeance of the polymer layer should be as high as possible, but still about an order of magnitude less than the permeance of the intermediate layer and support to ensure high selectivity. One simple way to increase the permeance of the polymer layer is to make the membrane as thin as possible.

To accommodate an ultrathin polymer layer, the support and intermediate layer must have low surface roughness, and sufficiently small pore sizes to prevent infiltration of the polymer during deposition. In a liquid-based coating process, the surface roughness should be at most half the target thickness of the polymer coating. For a 100 nm thick polymer coating, this means the RMS roughness should be less than about 50 nm. With a 200 Barrer CO_2 permeability obtained by the polyphosphazene membrane, and a best case thickness of 100 nm for the selective layer a permeance of 2000 GPU is to be expected. Since it is desired that the permeance of support layer be an order of magnitude higher than the selective layer, it is desired that the support layer permeance be around 20,000 GPU or higher.

The pore size of the support/intermediate layer should be sufficiently small to prevent infiltration of the polymer during coating. The numerical target will vary because the hydrodynamic size of the solvated polymer depends on the polymer chain length, the quality of the solvent, degree of aggregation, and presence of ternary components such as binders. As a starting point, a nominal pore size of about 30 nm, as determined by experimental observation was used in support/intermediate layer development.

Stability

The chemistry and microstructure of the support/intermediate layer must exhibit chemical and mechanical stability of the membrane under realistic operating conditions. Flue gas produced from the combustion of coal contains a number of components that may react with the polymer or intermediate layers, such as water vapor, SOx, NO, fly-ash, Hg, various metals1.

Membranes under realistic operating conditions will also be subject to vibration and thermal cycling, which can lead to mechanical failure. Longitudinal thermal gradients in the membrane reactor were also expected. A more detailed mechanical analysis of the membrane module is needed to determine specific criteria for the adhesion strength requirement and allowable CTE mismatch between the intermediate layer and the other layers of the membrane structure.

Economics

The overall economic constraint for the membrane is that the cost of increase in electricity due to a CO_2 capture system must be competitive with the conventional technology. The overall economics will be strongly influenced by the permeance of the membrane, as that parameter sets the required area. High permeance membranes have allowable costs, due to the lower area requirement. Corresponding targets for the microstructure of the intermediate layer are derived from the performance targets, and were summarized in Table I.

Pore size, thickness and porosity

The permeance of the support/intermediate layer is a function of the pore size (distribution), thickness of the layer, and total porosity. The interrelationship of microstructural factors is relatively easy to explain in qualitative terms – larger pore sizes, thinner layers, and higher total porosity lead to higher permeances.

It is difficult to obtain a quantitative relationship between these factors, because of the need to incorporate assumptions about the mechanism of transport and interconnectivity between pores. In this project, the primary metric for the optimization of the intermediate layer was the direct measurement of permeance. Direct imaging of the microstructure using electron microscopy provided secondary information to guide the adjustment of the processing conditions. For example, if the measured permeance was too low, but imaging revealed layers with acceptable pore sizes, with thickness in excess of 100 µm, the process was adjusted to favor decreased thickness.

Bounds on the nominal pore size of the intermediate layer arise from two competing physical effects. As discussed above, the upper bound is necessary to minimize the infiltration of polymer into the intermediate layer. The lower bound is needed to ensure the intermediate layer does not contribute a limiting resistance to overall gas transport through the integrated membrane structure.

Adhesion, stress and elongation requirements

Table 12lists the microstructural targets for the support layer. The adhesion requirement arises from the risk of delamination or buckling of the intermediate and coating

layer when the membrane sustains a pressure gradient. As seen schematically in Figure 24, the intermediate layer bridges the pores of the support structure. In cases where the intermediate layer is downstream of the feed, there is a risk the intermediate layer can delaminate from the support due to the pressure gradient.

Table 12. Support layer microstructural targets.

Parameter	Target (measurable)	Rationale
Pore size	< 30 nm >5 nm	Minimize infiltration of polymer layer during processing. Maximize permeance of intermediate layer
Thickness	<100 µm > 1 µm	Minimize cracks during drying & delamination risks Minimize defects due to incomplete coverage of support
Adhesion	> 2.5 to 25 MPa	Sustain pressure gradient due to bridging of support pores (assumes applied pressure gradient of 10 bar)
Compatibility with seals	TBD	Maintain module performance and stability through hermetic and thermo-mechanically stable junctions at end seals

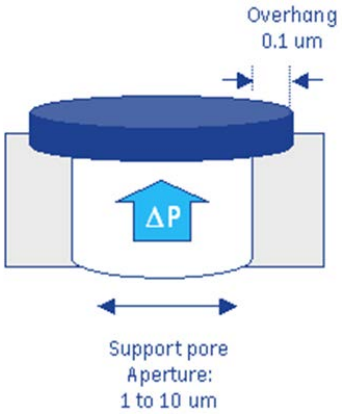

Figure 24. Schematic of idealized pressure gradient-driven mechanical failure modes for the intermediate layer.

A rough estimate of the adhesion strength can be obtained by idealizing the support pores as circular windows with diameters ranging from 1 to 10 µm. Assuming the intermediate layer overlaps the window with a uniform ring of 100 nm, the adhesion strength requirement is roughly 25 times that of the applied pressure gradient. For example, a pressure gradient of 10 bars implies adhesion strengths of order 2.5 to 25 MPa. Also, it is desired that the support and intermediate layer can handle the mechanical wear and tear and are strong enough to survive the coating conditions.

Compatibility with seals and the coating material

One additional constraint identified was the need for hermetic and thermo-mechanically stable junctions between the membrane and end seals. The end seals are typically of epoxy. Since this project involves ambient to 60 C temperature and pressures in the range of vacuum to 60 psig, there is not a lot of problem in providing a good seal with epoxy. This interface presents integration challenges because the support layer and the intermediate and

coating layers must form hermetic junctions to eliminate paths for bypass of gas. In addition, if the seal-intermediate layer interface comprises materials with different coefficients of thermal expansion, long-term mechanical failure is a risk.

Over the course of the project three different hollow fiber support materials were evaluated: microporous polyethersulfone (PES), polyamide-imide (Torlon® ®) and cellulose acetate (CA). It was found that after post-treatment with the interface layer the PES fibers showed decreased permeabilities. Since the PES fibers were too impermeable, the decision was made to move forward with the Torlon® and CA fibers which both showed high permeability. Subsequently, the CA fibers were found to have poor resistance to some of the casting solvents (e.g., ethanol) and therefore, Torlon® was the focus of the later studies.

In hollow fiber membrane/support creation it is desired to choose a one-phase dope composition in close proximity to the binodal curve to ensure rapid phase separation and high porosity of the membrane. Figure 25 shows the schematic representation of a binodal curve used to determine the core layer spin dope composition.

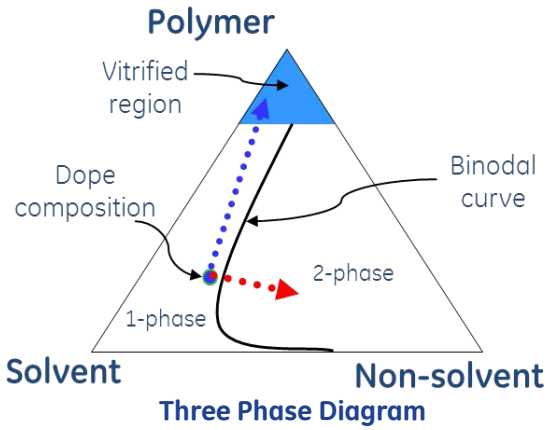

Figure 25. Schematic representation of a binodal curve used to determine core layer spin dope composition.

In the cloud point technique to determine the binodal curve, one-phase dopes in small quantities (15 ml) were made with varying amounts of polymer(CA or PES)/solvent(NMP or THF)/non-solvent(water)/additive(PVP). These dope samples were then visually observed as shown in Figure 26 to determine a 1-phase solution (transparent and homogenous), a cloudy solution (translucent) indicating the onset of phase separation and a 2-phase solution (non-homogenous and phase separated). The 'cloudy' dope solution composition was defined as the practical binodal point.

A one-phase dope composition in close proximity to the cloud point having appropriate viscosity (determined by viscosity measurements) was selected for scale–up (500 mL dope mixtures). From the cloud point experiments and observations during the fiber spinning process, various sets of core layer dope compositions were developed as described in Table 13.

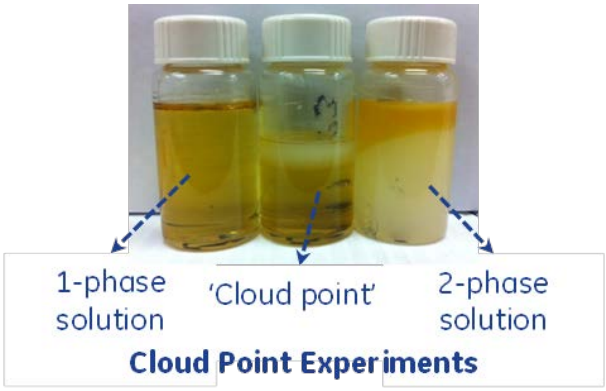

Figure 26. Cloud point experimental study to determine PES spin dope composition.

Table 13. Summary of core layer spin dope compositions (units in wt. %)

Dope ID	CA or PES	NMP	THF	Water	PVP
CA-Gen-1	20	68	-	9	3
CA-Gen-2	20	65	-	10	5
PES-Gen-1	33	53.1	5.9	3	5
PES-Gen-2	26	61.5	-	2	10.5

PDMS intermediate layer spin dope solution requirements were different than the core layer. The PDMS solution should be stable with low viscosity during the hollow fiber extrusion from the nozzle and rapidly cure (Zipcone®) or phase separate (Sibrid®) with the core layer in the water coagulation bath. Table 14 provides a summary of the sheath dope solutions used.

Table 14. Summary of sheath layer spin dope compositions (units in wt. %).

Dope ID	Polymer	Hexane	NMP
Zipcone® -Gen-1	100	-	-
Zipcone®-Gen-2	50	50	-
Sibrid®-Gen-1	15	-	75

A mixture of solvent and non-solvent, referred to as the bore fluid (or internal coagulant) was also prepared by adding measured quantities of solvent and non-solvent. (Table 15)

Table 15. Summary of bore fluid compositions (units in wt%).

Bore Fluid	NMP	Water
For PES dopes (Gen-1 & Gen-2)	75	25
For CA dopes (Gen-1 & Gen-2)	70	30

Viscosity measurements

Viscosity of Gen-1 CA and PES core dopes was measured to augment the observations from the cloud point technique. TA instruments rheometer, Model ARG2 fitted with a cone-plate fixture at a sweep rate from 0.01 s-1 to 10 s-1 was used. The dope viscosity was measured at 25, 40 and 50 °C respectively. The viscosity measured at low shear rates (0.01 s-1) can be used to approximate the dope viscosity in the binodal diagram, while the viscosity at high shear rate (10 s-1), can be approximated as the dope viscosity at the nozzle annulus during the fiber spinning process. Typically, pure polymer hollow fiber membrane spin dopes had a viscosity of ≈ 100-500 Pa.s.

Single and dual layer hollow fiber membrane fabrication procedure

For spin dope preparation, measured amount of solvents (THF or NMP), followed by non-solvents (DI water) and then additive (PVP) were added to a 1000 mL glass jar. The solution was then sonicated in an ultra-sonication bath till complete dissolution of the additive was observed. The desired quantity of the polymer was then added and the dope vessel was sealed and put on a roller at room temperature (dopes w/o THF) or heated to 40 to 50 °C (dopes w/ THF) with the help of an IR lamp, until complete polymer dissolution and dope uniformity was observed. The core and sheath dopes were then poured into syringe pumps for spinning and kept undisturbed for about 12 h to ensure complete degassing of the dope solution. Hollow fiber membranes were made by the dry jet-wet quench solution spinning technique. Figure 1 shows a schematic representation of the fiber spinning apparatus. Figure 28 shows the photograph of the triple orifice nozzle and the 20X magnified view of the nozzle annulus.

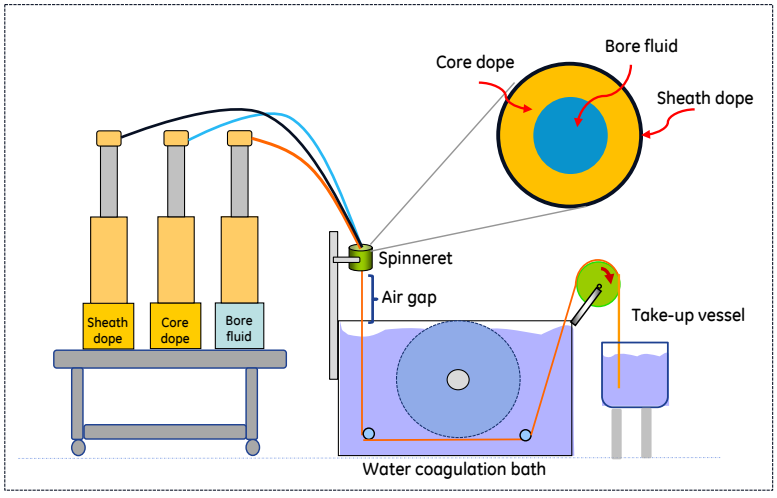

Figure 27. Schematic representation of the hollow fiber fabrication setup.

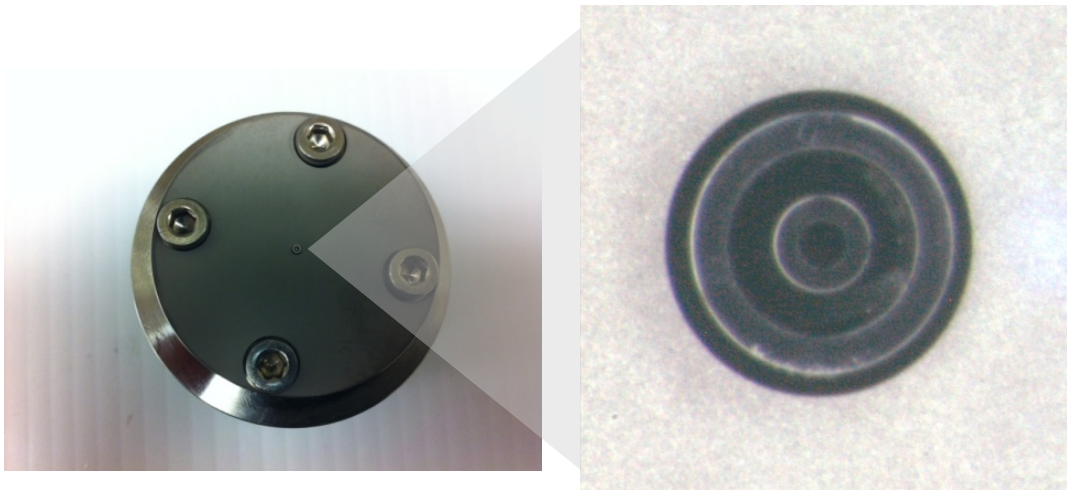

Figure 28. Photograph of the triple orifice nozzle and the 20X magnified view of the nozzle annulus.

Table 16 summarizes the various spinning parameters used in the project with their typical range. The core dope flow rate was varied between 180-600 mL/hr., while, the bore layer flow rate was varied between 1:3 to 1:2 times the core flow rate and the sheath flow rate was varied between 1:30 to 1:10 times the core flow rate. For dual-layer fiber fabrication all three fluids were extruded simultaneously, while for single-layer fiber fabrication only the core dope and bore fluid were extruded. The core and sheath dopes were filtered through 40 µm mesh size in-line filters to remove any insoluble particles in the spin dope before entering the nozzle channels. Spinning temperature (nozzle, pumps and transfer lines temperature) between 25 °C and 40 °C were studied. The extruded nascent fiber then passed through an adjustable air gap (dry jet) varied between 5-15 cm before entering the external coagulant or quench bath (wet quench) where it phase separates and vitrifies. DI water was used as an environmentally friendly and easily available quench bath (1 m deep) medium. A rotating water wheel located in the coagulation bath was used to maintain uniform mixing and bath temperature. Quench bath temperatures of 40 °C and 50 °C were studied.

The fiber then passed under two Teflon guides located in the coagulation bath followed by a guide wheel and then collected by a free-fall mechanism into a collection bath filled with DI water. In cases where the fiber had sufficient strength the fibers were collected onto a take-up drum partially submerged in DI water. The take-up drum speed could be varied between 5-60 m/min. Once collected, each state was allowed to soak in the collection bath for about 15 min to allow complete phase separation and vitrification. Fibers spun under identical conditions (called a spin state) were then wound manually onto a rotating take-up drum with a circumference of 75 cm. The fibers from the same spin state were then removed from the take-up drum as individual strands and tied together. In the case of direct collection on the take-up drum, the fibers were directly cut as individual strands. By manipulating various spinning parameters, several spin states were collected.

The fibers were soaked in de-ionized (DI) water for up to 5-7 days changing with fresh DI water daily. The water present in the fiber sub-structure was then solvent exchanged by immersion of spin states for 30 minutes each in two batches of fresh methanol. To remove the residual methanol the fibers were exposed to N_2 at room temperature for 2 days, followed by

drying under N_2 at 80 °C for 2 days in a custom made drying oven followed by storage for further characterization.

Table 16. Spinning conditions for hollow fiber support fabrication.

Dope (Core)	
Pump temperature	40 °C (CA/PES Gen-1), 35 °C (CA Gen-2), 25 °C (PES Gen-2)
In-line temperature	40 °C (CA/PES Gen-1), 35 °C (CA Gen-2), 25 °C (PES Gen-2)
Flow rate	180-600 mL/h (preferably 300 mL/h)
Dope (Sheath)	
Pump temperature	25 °C (CA/PES Gen-1 and Gen-2)
In-line temperature	25 °C (CA/PES Gen-1 and Gen-2)
Flow rate	1:30 to 1:10 – sheath flow:core ratio (preferably 1:20)
Bore fluid	
Temperature	Room temperature
Flow rate	1:3 to 1:2 – bore flow:core flow ratio (preferably 1:3)
Nozzle temperature	40 °C (CA/PES Gen-1), 35 °C (CA Gen-2), 25 °C (PES Gen-2)
Air temperature	Room temperature (≈ 25 °C)
Air-gap	10-15 cm
Quench bath	
Media	DI water
Depth	1 m
Temperature, T_{quench}	40 °C (CA/PES Gen-1) and 50 °C (CA/PES Gen-2)
Take-up rate	Free-fall

Characterization

The as-spun hollow fiber supports were evaluated by SEM-EDX analysis and gas permeation analysis. The main criteria for evaluating these initial fibers was by (i) the quality of the fiber (roundness, structural uniformity, concentricity) and (ii) whether the PDMS intermediate layer was successfully and continuously applied to the outer diameter of the fiber without infiltration into the core layer.

The Gen-1 dopes selected by cloud point measurements were found to have a low shear viscosity in the range of 100-500 Pa.s as shown in Figure 29. The CA dope was found to be slightly shear thinning while the PES dope had a Newtonian behavior. The dope viscosities were found to reduce with higher temperature, as expected.

CA and PES Gen-1 core dopes (Table 13), Zipcone®-Gen-1 sheath solution (Table 14) and the CA and PES dope bore fluids (Table 15) were utilized for the fabrication of Gen-1 hollow fiber supports. Single-layer CA and PES hollow fibers were fabricated using the spin dope formulation and process conditions mentioned earlier in Table 16**Error! Reference source not found.**. Both the CA and PES single-layer hollow fiber supports were found to have a desired round, concentric structure with a relatively smooth outer surface as shown in Figure 30 and Figure 31**Error! Reference source not found.**. A dense, thin skin-layer was observed on the hollow fiber supports which were undesirable as this could lead to lower permeance. Macrovoids were observed in both CA and PES hollow fibers. Macrovoids can reduce the

mechanical strength of the fiber causing it to burst or collapse at high trans-membrane pressures. Macrovoids can be reduced or eliminated by increasing the dope viscosity which delays the diffusion of solvent into the polymer-lean phase during phase separation in the coagulant bath causing the growth of macrovoids.

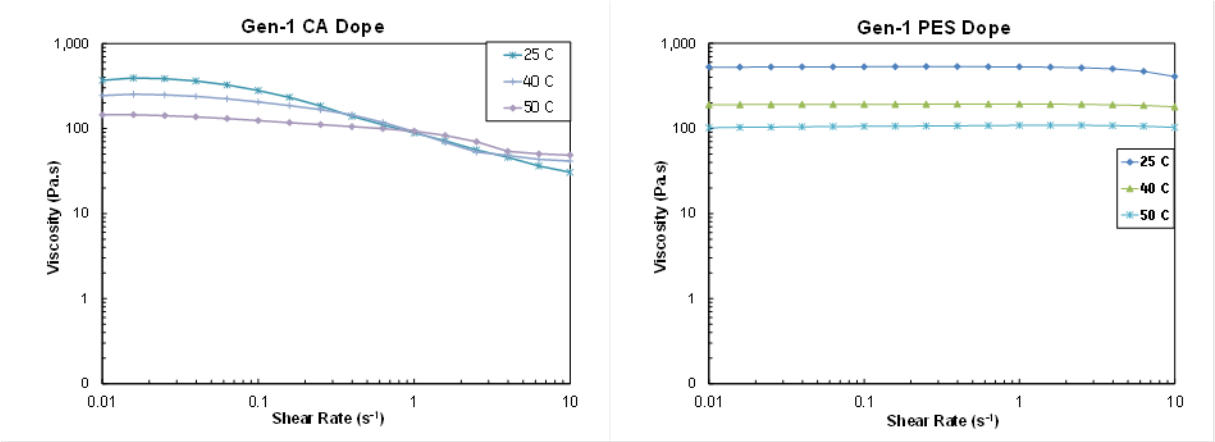

Figure 29. Viscosity measurements for Gen-1 CA and PES core dopes.

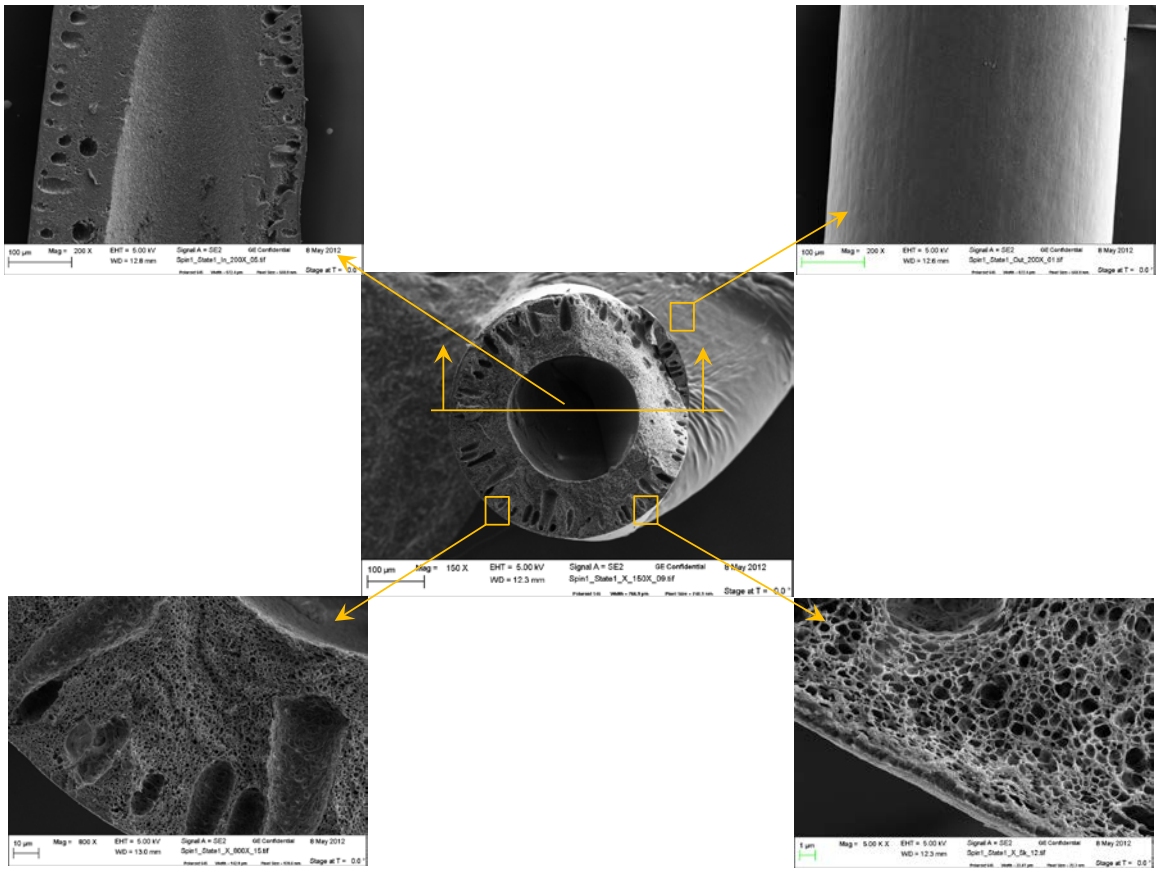

Figure 30. Single-layer CA-Gen-1 hollow fiber supports .

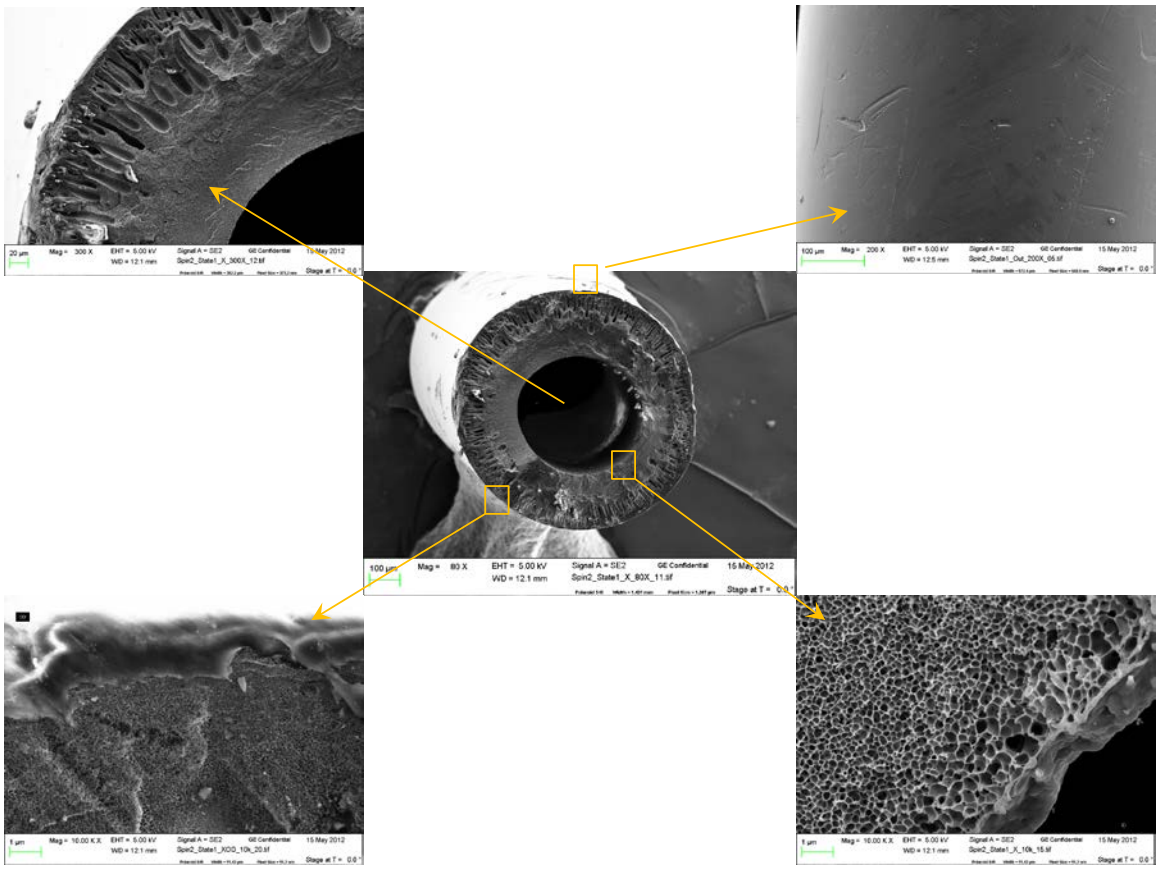

Figure 31. Single-layer PES-Gen-1 hollow fiber supports.

Upon introduction of the Zipcone®-Gen-1 sheath solution along with the core dope and the bore fluid, the nascent fiber strand was found to break easily due to slow curing of the PDMS oligomer solution in the water coagulation bath. The fiber strand could not be threaded through the guide rolls due to the stickiness due to the uncured PDMS sheath solution. To eliminate this problem, single layer fibers were first threaded through and collected and upon reaching a stable extrusion rate, the sheath solution flow was started. A low sheath solution flow rate was desired to obtain thin coating on the core layer, providing a relative ease of curing without affecting the core layer morphology.

Low sheath flow rates, however led to pulsing issues leading to frequent fiber breaks and non-uniform coverage of the fibers (globules vs. uniform coverage) as shown in Figure 32 for CA/PDMS fibers and Figure 33for PES/PDMS fibers. Fiber core layer morphology was distorted upon introduction of the sheath layer in these first runs (Figure 32 and Figure 33) due to premature curing of the PDMS solution in the nozzle sheath annulus upon exposure to moisture for prolonged period during the run. On a positive note, these first runs demonstrated that a well adhered PDMS coating with minimum infiltration could be obtained for both CA and PES hollow fiber supports.

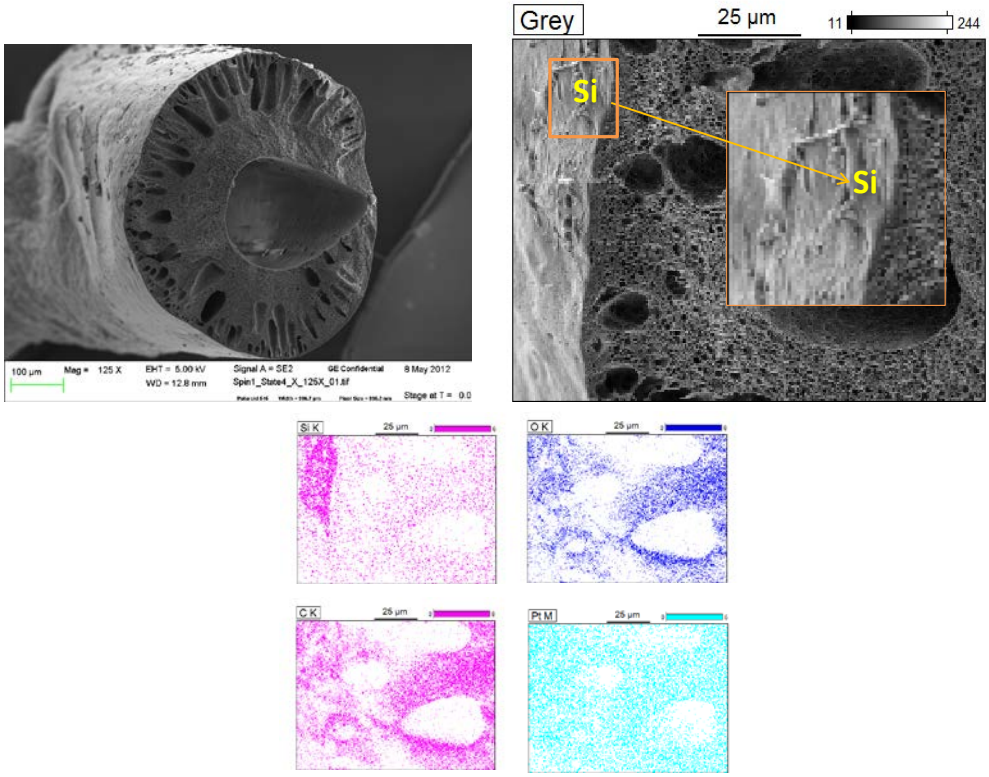

Figure 32. Dual-layer CA-Gen-1/Zipcone®-Gen-1 hollow fiber supports. A thin, layer of PDMS can be observed on the sheath layer with minimum infiltration into the core layer. Fiber morphology was distorted due to premature curing of the PDMS solution in the nozzle

Moisture cure PDMS was found to be difficult to clean from the syringe pump barrel, supply lines and the nozzle annulus using conventional PDMS solvents like heptane or hexane. Upon discussions with silicone experts at GE, a 10 % KOH solution in isopropyl alcohol (IPA) was found to be effective for cleaning the surfaces exposed to PDMS.

In the following runs, appropriate care was taken to prevent premature curing of the PDMS solution by continuously running the sheath flow once started. Improved CA/PDMS and PES/PDMS hollow fiber supports were obtained as shown in Figure 34 and Figure 35.

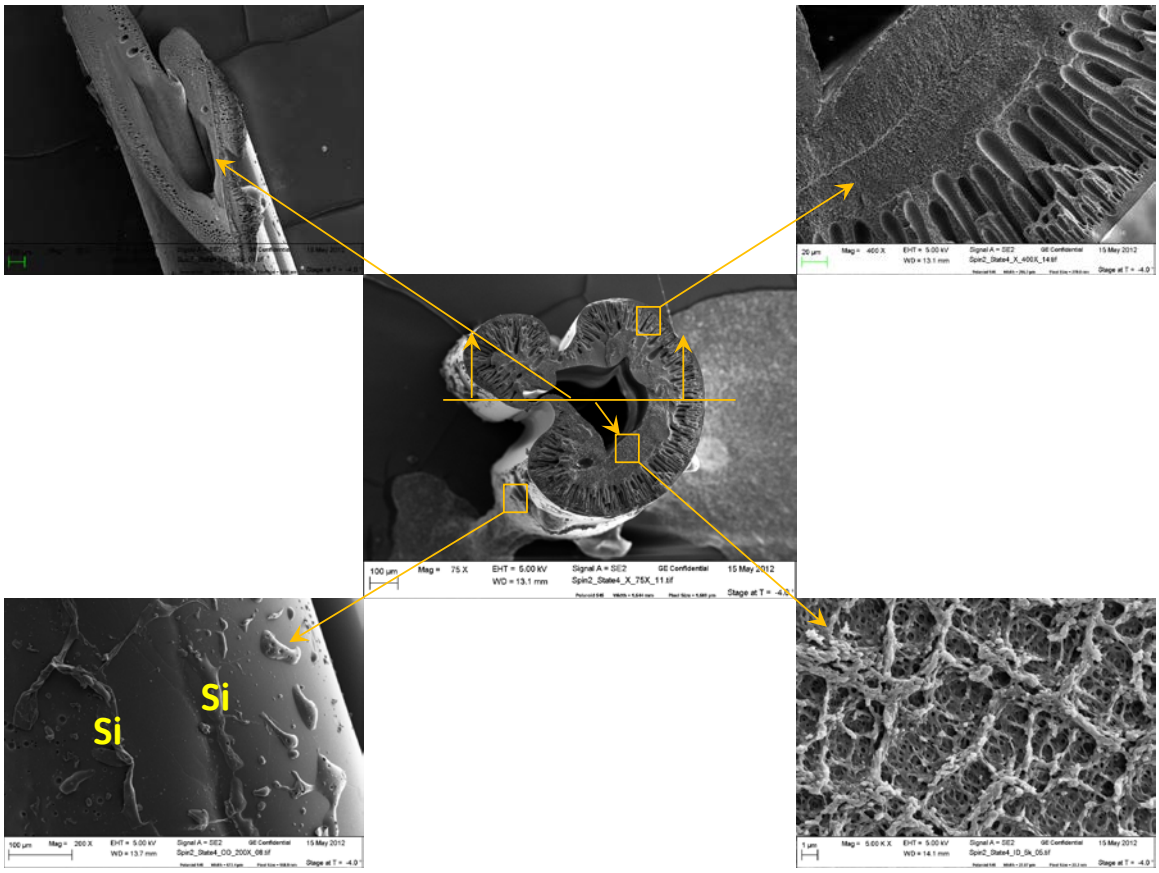

Figure 33. Dual-layer PES-Gen-1/Zipcone®-Gen-1 hollow fiber supports. A thin, layer of PDMS can be observed on the sheath layer. Fiber morphology was distorted due to pre-mature curing of the PDMS solution in the nozzle sheath annulus.

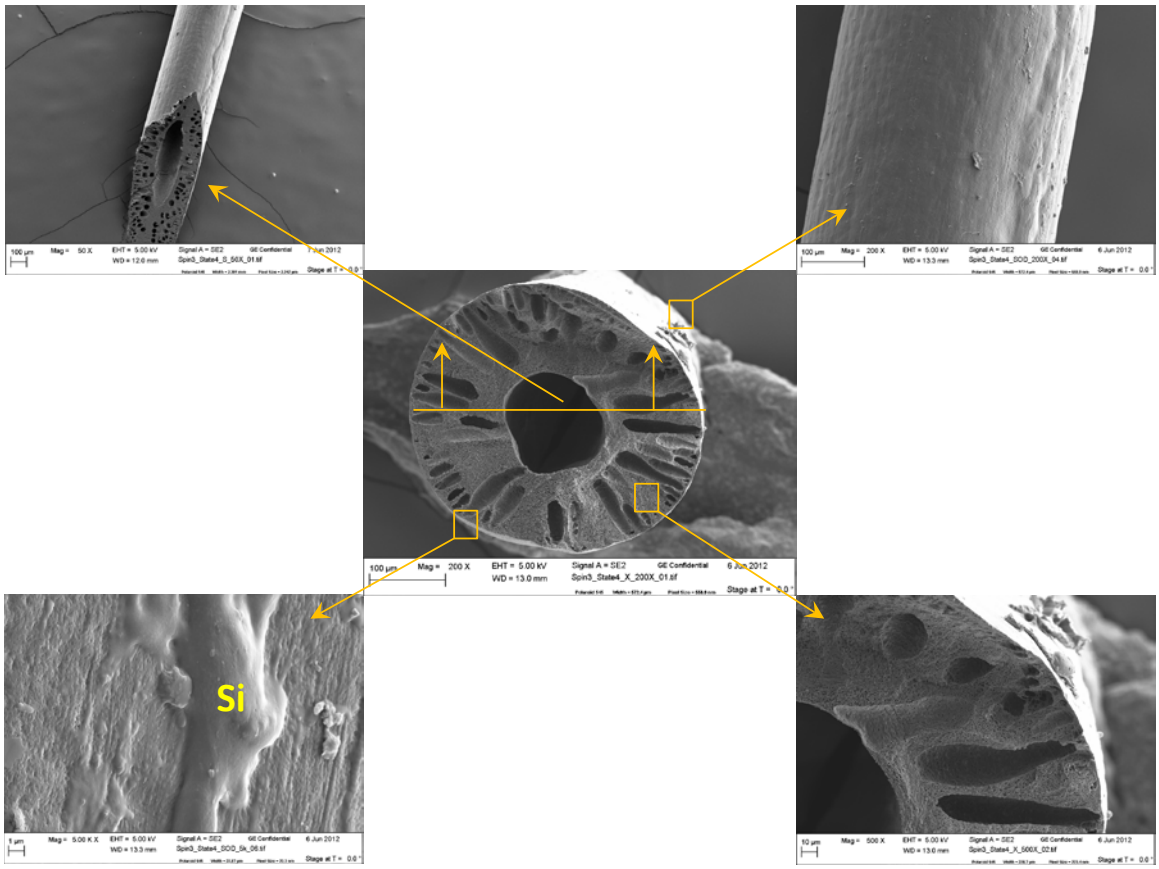

Figure 34. Improved dual-layer CA-Gen-1/Zipcone®-Gen-1 hollow fiber supports. A thin, non-uniform layer of PDMS can be observed on the sheath layer. Minimum infiltration into the core layer was observed.

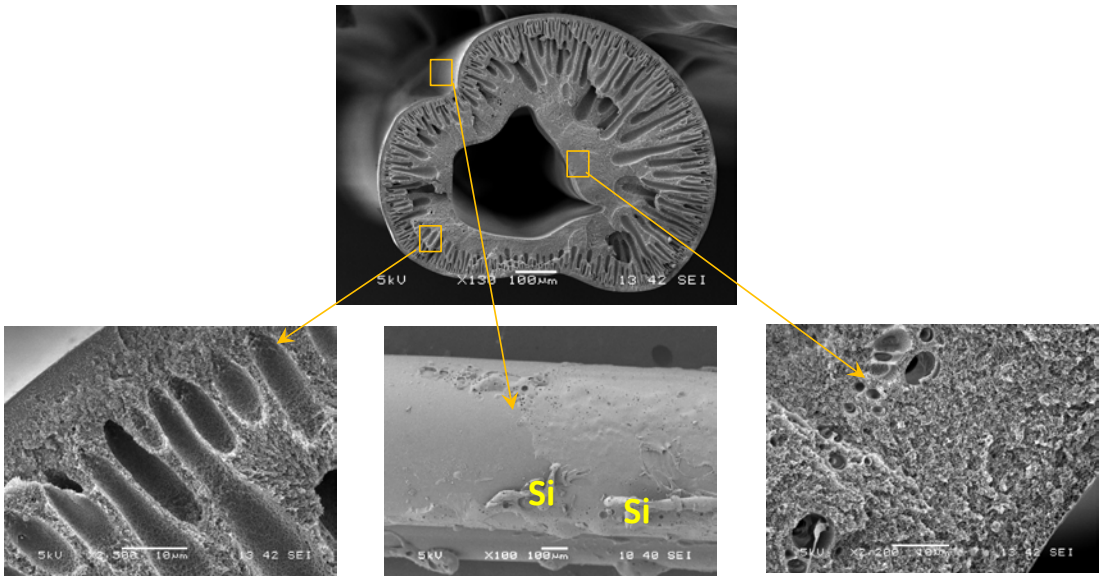

Figure 35. Improved dual-layer PES-Gen-1/Zipcone®-Gen-1 hollow fiber supports. A non-uniform layer of PDMS can be observed on the sheath layer. Minimum infiltration into the core layer was observed.

Several challenges still exist in the creation of optimized dual-layer hollow fiber supports i.e. macrovoids were still present in the core layer, PDMS coverage was not uniform and continuous, and the core layer appeared to be less porous as observed in the SEM images and confirmed by gas permeation studies (described in later sections). Hence, both the CA and PES core layer dope compositions were modified (Gen-2, Table 13) by increasing the pore former (PVP) content, eliminating the volatile solvent (THF), increasing the non-solvent (water) content and by reducing the polymer content (CA or PES) to bring the one-phase spin dope closer to the binodal curve enabling faster phase separation in the water coagulation bath eventually leading to a porous structure. The as received Zipcone® solution (Gen-1) was diluted with hexane (Gen-2, Table 14) to further reduce its viscosity to enable uniform coverage or reduction in pulsing of the sheath solution at low sheath flow rates (1:30 to 1:10 times the core flow rate). As an alternative to the moisture/air curable PDMS solution a 15 wt.% thermoplastic Silicone-polyimide block co-polymer (Sibrid®) in NMP was also explored. Gen-2 fiber supports had been successfully created by using CA or PES Gen-2 core dopes (Table 13), Zipcone® Gen-2 and Sibrid® Gen-1 dopes (Table 14), bore fluids and process conditions as summarized in Table 16.

Gen-2 fibers from both PES and CA were obtained but then PES was not selected since the overall permeance from the PES fiber was not good. CA-PDMS fibers were further refined and the process conditions were improved to improve the concentricity and coverage of the hollow fibers. Even with the best of controls the PDMS coverage on the fibers was not very good. Based on SEM and EDX analysis a definitive conclusion could not be drawn whether the PDMS coating layer was present or not.

Hollow fiber spinning process and support material at Georgia Tech

Torlon®® 4000T-HV polyamide-imide (PAI) supplied by Solvay Advanced Polymers was used as the polymer. PAI can form inter- and intra-chain hydrogen bonding due to the presence of amide groups, which enhances its swelling resistance. The reported glass transition temperature (Tg) of this polymer is 273 °C. The polymer dope composition for spinning was determined at Georgia Tech by the cloud-point technique (described earlier). De-ionized (DI) water was added as a non-solvent in the fiber dope, while NMP, Laboratory grade, Fisher Scientific was selected as a spinning solvent due to its strong solvent power, low volatility and good water miscibility. PVP (MW 1300K Sigma Aldrich) was utilized as a pore former. PVP was dried at 80 °C for 24 h while Torlon® was dried at 110 °C for 24 h both under vacuum to remove sorbed water vapor.

To achieve the goal of low membrane production cost and high membrane productivity, Georgia Tech optimized the spinning parameters, including line temperatures, bore fluid, spinneret temperature, quench bath temperature and air-gap and identified a robust process window to produce permeable Torlon® hollow fibers with engineered surface porosity. Relationships were developed between process parameters (including polymer dope compositions and spinning parameters) and performance established for bare hollow fiber membranes. The permeability to N_2, CO_2 and He gases were carried out at 35 °C and about 30 psig to establish a baseline performance of hollow fiber supports. In addition, surface

morphology including skin layer, substructure and internal and outer surface of Torlon® hollow fibers were characterized by using SEM.

Single layer Torlon® hollow fiber spinning (conventional process) at Georgia Tech

PAI hollow fiber supports were spun using a dry-jet, wet-quench process based on a known phase inversion process. During the fabrication process, three parameters control the morphology of the hollow fibers to a great extent: composition of the polymer dope, composition of the bore liquid, and air gap conditions. Other parameters, such as composition and temperature of the quenching bath, spinning speed, and post-treatment, are important as well. Using a non-volatile solvent (NMP) and non-solvent (water) and pore formers (PVP) in the dope composition, different air gaps conditions (0.5 ; 3 and 10 cm) were applied in order to control the membrane morphology.

Fibers spun under identical conditions (spin state) were removed from the take-up drum, tied and soaked in de-ionized (DI) water for 7 days with daily fresh DI-water changes to remove the residual NMP. This procedure was used for high molecular weight (Mw ~1300 K) PVP involved fiber, which were soaked in DI-water for a week to ensure complete removal of the water-soluble PVP. The water present in the fiber sub-structure was then solvent exchanged by immersion of the spin states for 1 h each in three batches of fresh methanol (to remove excess water) followed by three batches of fresh hexane (to replace excess methanol). This standard solvent exchange process is critical to prevent the pore structure from collapsing under capillary forces. After a 2 h air drying step, the PAI fibers were dried at 180 °C for 72 h to completely remove any residual NMP.

The inner surface morphology was mostly determined by the composition of the bore liquid (i.e., NMP: water was 88:12: w/w%). The sheath surface morphology was adjusted by different quench bath temperatures, i.e., 45, 55 and 65 °C.

Effect of Quench Bath Temperature on the Membrane Characteristics and Performance

Figure 36 show SEM images of the cross section (bore side, middle and sheath side) of a hollow fiber membrane prepared from a PAI dope solution (25% Torlon®®: 63% NMP: 5% water: 7% PVP) via phase separation techniques at variable quench bath temperatures (45, 55 and 65°C). The SEM images of the bore side showed that the change of the pore size with quench temperature was not very significant. This is attributed to the fact that, the bore side is controlled by the bore fluid temperature, which was kept at the dope solution temperature (i.e., 50 C) throughout the process. On the other hand, the SEM images of the sheath side demonstrated that, at low quenching bath temperature (i.e., 45°C) the outer regime of the polymer presumably phase separated more slowly due to slower diffusional exchange with the quench bath. In any case, porous skin layers were formed at all temperatures, based on transport properties discussed later. Such structures cause the mass transfer resistance to increase, as indicated by low CO_2 , N_2 and He permeances at 45 °C (See Table 17). Raising the bath temperature requires precise control to guarantee high reproducibility. In addition, gas transport properties of fibers were similar at 55° and 65 °C, therefore, we continued spinning at the optimum quench bath temperature of 55 °C.

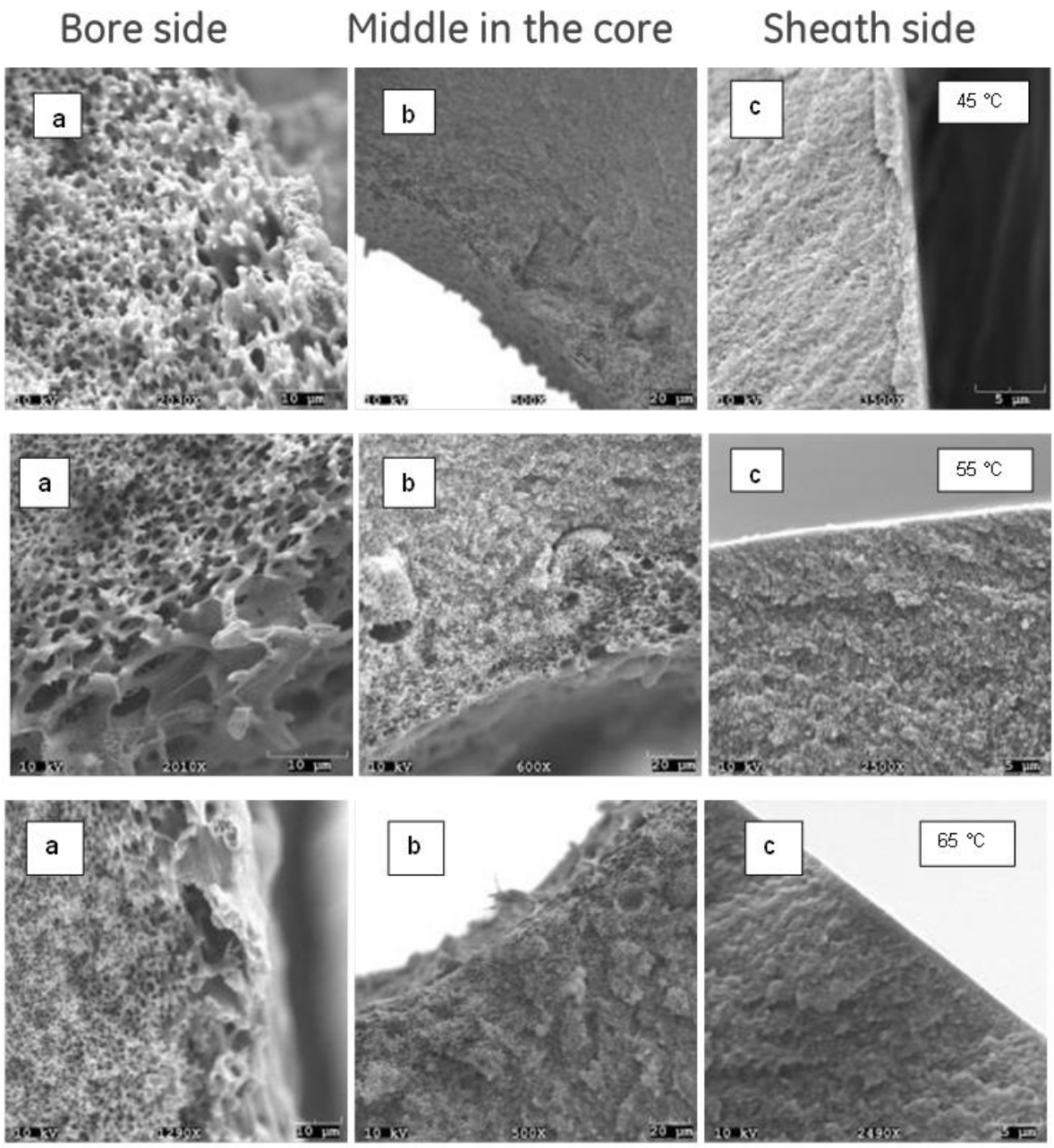

Figure 36. Permeation data for Torlon®® hollow fibers spun at different quench bath temperatures, i.e., 45, 55 and 65 °C (Test at 35 °C and 30 psig).

Table 17. Permeation data for Torlon® hollow fibers spun at different quench bath temperatures, i.e., 45, 55 and 65 °C (Test at 35 °C and 30 psig).

Module	Quenching bath temperature/ °C	Selectivity		CO_2 (P/l) (GPU)	N_2 (P/l) (GPU)	He (P/l) (GPU)
		CO_2/N_2	He/N_2			
ARS2-117-St.1	45	0.90	2.27	5657	6281	14274
ARS2-120-St.4	55	0.92	2.05	16374	17883	36674
ARS2-123-St.7	65	0.90	2.09	15671	17424	36448

Effect of Air Gap Height on Gas Transport and CO_2 /N_2 Selectivity for Fibers Spun from PAI Dope

The polymer dope composition for our initial hollow fibers was; PAI (25 wt%): NMP (63 wt%); water (5 wt%), PVP (7 wt%). The corresponding spinning conditions for polymer used a spinneret temperature of 50 °C with quench bath temperature of 55 °C, a draw ratio of 2.0 and air gaps of 0.5, 5 and 10 cm.

Figure 37(a) show SEM images of the cross-section and sheath (surface) for neat PAI fibers spun at air gap of 0.5 cm. The pore size becomes smaller towards the outer regime. The Torlon® hollow fiber supports exhibited permeance (GPU) to CO_2 , N_2 and He of about 16000, 17000, and 30000, respectively at 0.5 cm air-gap (Table 18). Higher air-gaps densify the polymer chains on the outer regime of the fibers, where pore cells are generally smaller than those in inward regimes, thereby resulting in a dense regime. Moreover, a higher air-gap also leads to undesirable gas transport properties. With this in mind, both air-gap and quench bath temperatures were adjusted to engineer both gas transport and separation processes.

All samples showed the tendency for the pore size to become larger towards the bore side. This trend is likely due to the fact that the bore fluid is comprised mainly of NMP, thus decreasing the phase separation rate at the interior regime of the polymer. On the other hand, the outer regime of the polymer presumably phase separated quickly due to a high driving force of water from the quench bath. The SEM images demonstrate that pore cells of PAI fibers spun with higher air-gaps were smaller, which is undesirable for producing high porosity hollow fiber supports applications even though they formed porous skin layers (See Figure 2c). Such structures may cause the mass transfer resistance to increase, as indicated by low CO_2 , N_2 and He permeance (See Table 18). Interestingly, a lower air-gap (~0.5 cm) produced open pore cells in the middle regime of the core with an approximate size of 200 nm (See Figure 2a) resulting in high permeance for CO_2 , N_2 and He with a low CO_2 /N_2 and He/N_2 selectivity (See Table 18). However, PAI fibers associated with a medium air-gap (5 cm) showed smaller pore cells (See Figure 2b).

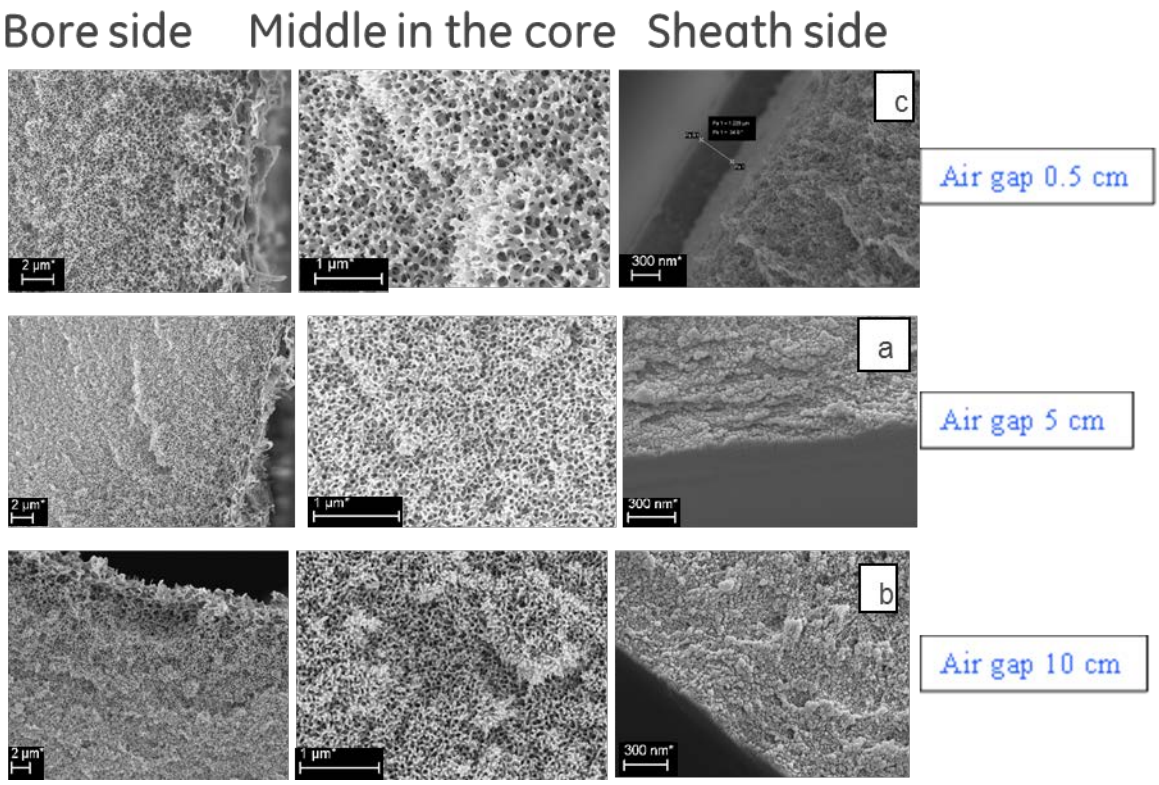

Figure 37. SEM images of the cross-section and sheath of a fiber spun from PAI dope at different air-gap conditions.

Table 18. Gas transport properties, P/l, and $\alpha CO_2 / N_2$ of Torlon® hollow fibers membrane at different air gaps height (Test at 35 °C and 30 psig)

Air-gap (cm)	$\alpha CO_2 / N_2$	α_{He}/N_2	CO_2 (P/l) (GPU)	N_2 (P/l) (GPU)	He (P/l) (GPU)
0.5	0.87	2.25	15407	17602	40006
5	0.9	2.24	6446	7172	16043
10	0.84	2.23	1800	2142	4783

The results from the pure gas permeation tests are shown in Table 2. Each of the listed values is the average of two separate modules with 15 cm2 of active surface area per module. There were some distinguishable differences between fibers spun from similar PAI dope composition when examined under SEM and tested for gas transport properties. Table 2 shows the CO_2 / N_2 and He/N_2 selectivity and CO_2 , N_2 and He permeances, respectively, at different air gaps height. From these results, it is obvious that increasing the air gap leads to lower permeances, although, all fibers exhibit Knudsen selectivities when permeated with gas. Larger air gaps allow more time for mass transfer to occur, resulting in thicker skins which have fewer defects.

A Single Layer Hollow Fiber Spinning with a Triple-Orifice Spinneret (recent development process)

A triple orifice annular die (spinneret) was used for spinning of hollow fiber membranes with a high surface porosity. The residence time of the nascent fiber in the air gap between the spinneret and the coagulant bath creates a denser sheath layer. Considering the general rules of diffusion induced phase separation, a low polymer concentration is desirable at the outer layer to obtain a highly interconnected open-porous structure. Therefore, by using NMP and water with the similar concentration of bore fluid as the sheath fluid solution at the outside orifice of the spinneret, a highly porous surface can be obtained. A dope solution was co-extruded with a sheath solution and a bore fluid through a triple orifice spinneret simultaneously out of the spinneret, passing through different air gaps of 0.5, 5 and 10 cm and immersed in a water bath at 55 °C temperature. The bore and sheath solutions were a mixture of NMP and water with a weight ratio of 88:12 while the dope solution was 100% NMP. The composition of the core dope (polymer/solvent/non-solvent) and the sheath solution (solvent/non-solvent) can be abruptly changed by non-solvent invasion to shift to the two-phase region, thereby generating a porous hollow fiber membrane. The experimental setup is depicted in Figure 38.

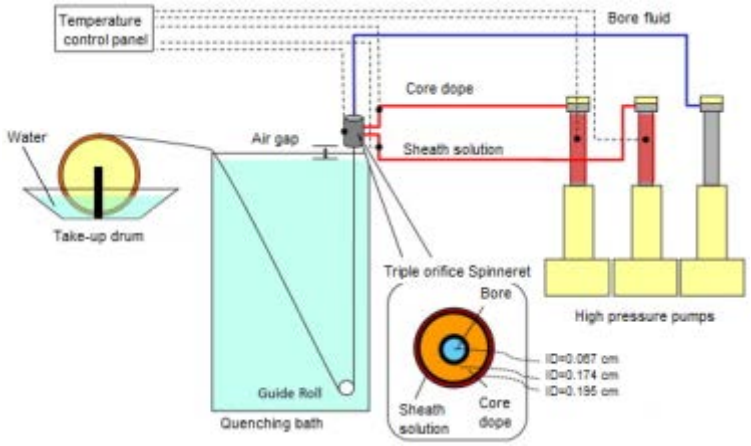

Figure 38. Georgia Tech new spinning apparatus

Effect of Sheath Side Fluid on Structure and Permeation Properties of Membranes

The spinning process and conditions used to produce these fibers were similar to the conventional process (as explained above), except for the elimination of the skin layer. We used a 1/3 fluid ratio of NMP/water solvent with the same concentration of bore fluid as the sheath side fluid. When NMP/water (88:12, w:w) was used in the outer orifice, an extremely open surface with a lacy structure was obtained, as can be seen in Figure 39. We reasoned that the polymer concentration at the outer layer was diluted by NMP and became probably low enough to pass the binodal curve close to the critical point, forming an open, loose structure. Increasing the air-gap from 0.5 cm to 10 cm, therefore enhancing the solvency, resulted in a much open surface structure as shown in SEM image (See Figure 39). The results indicated that unlike the conventional spinning process, a less open surface was obtained using a solution of NMP/water at the lowest air-gap (i.e., 0.5 cm). The morphology was confirmed by the cross-

section and outer surface of various structures seen in Figure 39. Below the top layer, the membrane prepared from NMP/water as the sheath fluid solution in the outer orifice shows a more symmetric porous and interconnected structure layer. In the top layer, a very porous skin of about 10 to 20 µm consists of opened cells. Table 3 shows that the permeation properties correspond fairly well to the observed morphology.

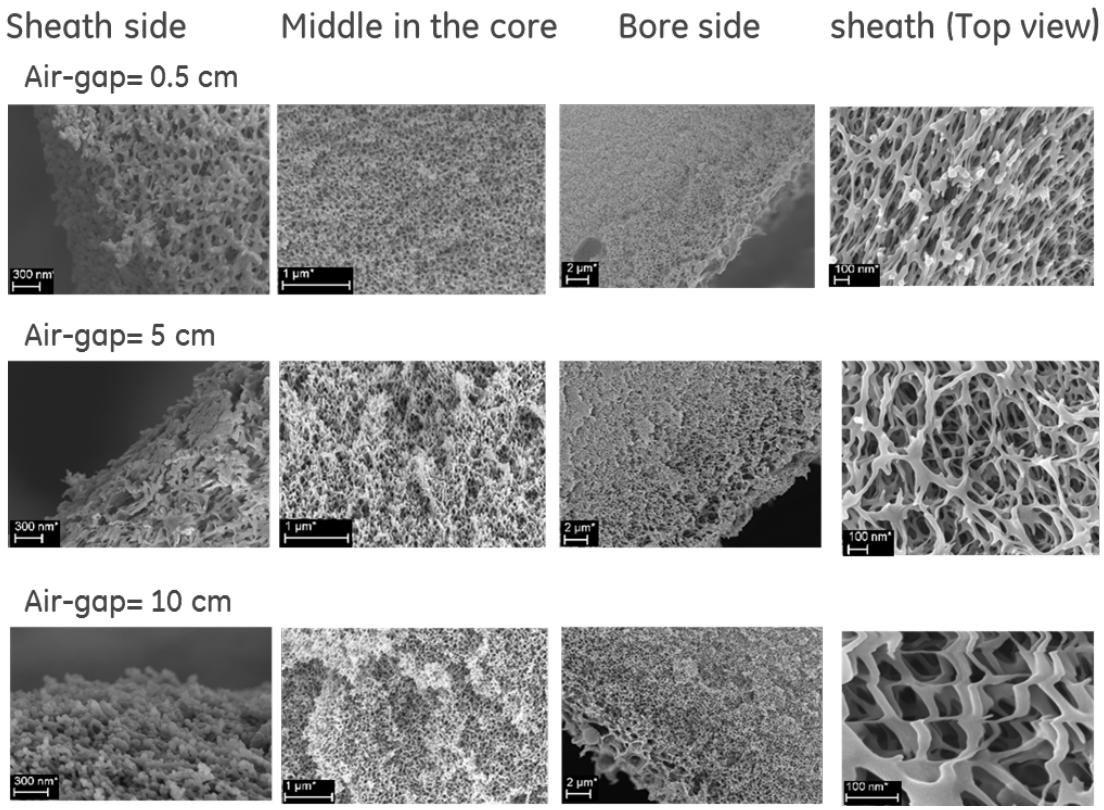

Figure 39. SEM images of the cross-section of the hollow fibers spun with a sheath fluid from the outside orifice channel

The gas permeation properties indicate that the membrane using NMP/water as the external fluid at the lower air gap shows the highest resistance, therefore the lowest gas permeability (See Table 19). However, this flux is significantly higher than in the conventional process (about 2X) . Slightly higher fluxes are obtained for the membrane spun at higher air-gap (i.e., 5 cm). Further improvement of the flux can be achieved by using the NMP/water as the external fluid at highest air-gap (i.e., 10 cm) that forms a far more opened cell. The pore size was bigger and significantly higher gas permeability (Table 19) was obtained. However, this may not be desirable for coating due to the higher surface porosity with pores ranging from 10 to 200 nm in diameter.

Table 19. Gas transport properties, P/l, and $\alpha CO_2 / N_2$ of Torlon® hollow fibers membrane at different air gaps height- developed new spinning process (Test at 35 °C and 30 psig).

Air-gap (cm)	$\alpha CO_2 / N_2$	α_{He}/N_2	CO_2 (P/l) (GPU)	N_2 (P/l) (GPU)	He (P/l) (GPU)
0.5	0.93	1.73	33069	35691	61571
5	0.82	1.85	35739	43459	80593
10	0.82	1.96	51955	63278	124175

To our knowledge, no hollow fiber exists from pure dope polymer with these significant gas transport properties. According to the proposed concept, a highly porous surface can be obtained using NMP/water as the sheath fluid and Figure 39 indeed confirms this. The whole surface consists of a lacy interconnected porous structure and an extremely low mass transport resistance of the outside skin was expected. This lacy structure was an indication of a rather low polymer concentration at the outer layer before phase separation occurs. Again, NMP dilutes the polymer dope solution at the top layer during the short period of contact, which results in a loose structure.

Georgia Tech. used various approaches to engineer the outer surface of Torlon® hollow fibers with different pore sizes by (i) eliminating solvent exchange, (ii) post-treating the outside of Torlon® hollow fibers by using 1,8-Diazabicyclo[5.4.0]undec-7-ene, (DBU)[1] , (iii) using different solvents with various surface densities. The reason for solvent exchange after spinning is to replace a high surface tension solvent with a low surface tension solvent to avoid pore collapse due to the capillary force. Traditionally this is done using methanol and then hexane. We investigated eliminating the solvent exchange process completely and also investigated the effects of stopping after the methanol step, by eliminating exchange with hexane. These process modifications should allow tighter pores be to obtained in the outer regime of the Torlon® hollow fibers. The first approach was unsuccessful since no or very small permeance was observed on the final Torlon® hollow fibers. All of the pores on the outside of Torlon® fibers collapsed due to the capillary force of wet fibers in the presence of air. Table 20 shows permeance results for fibers treated by this method. The original Torlon® fibers showed about 15000 GPU and 17000 GPU permeance to CO_2 and N_2, respectively. SEM images of fiber showing a skin layer and transition layer. SEM images have been confirmed that the most pores collapsed only in the outer regime (Figure 40). A dense skin layer was observed that increased resistance of the substrate and decreased permeate flow of the membrane.

[1] DBU is a chemical compound and belongs to the class of amidine compounds. It is used as a non-nucleophilic base in methanol and heptane.

Table 20. Permeation results of full solvent exchange (R12a) and without solvent exchange(12a-WOSE) fibers.

Before post-treatment			Selectivity		CO_2	N_2	He
Module	#F	dpore nm	CO_2/N_2	He/N_2	(P/l) (GPU)	(P/l) (GPU)	(P/l) (GPU)
AR-23-S3-R12a	1	18.1	0.92	1.88	15897	17213	32439
AR-33-S3-R12a-WOSE	2	-	0.6	3.13	0.89	1.5	4.7
AR-34-S3-R12a-WOSE	1	-	0.44	3.5	0.54	1.2	4.3

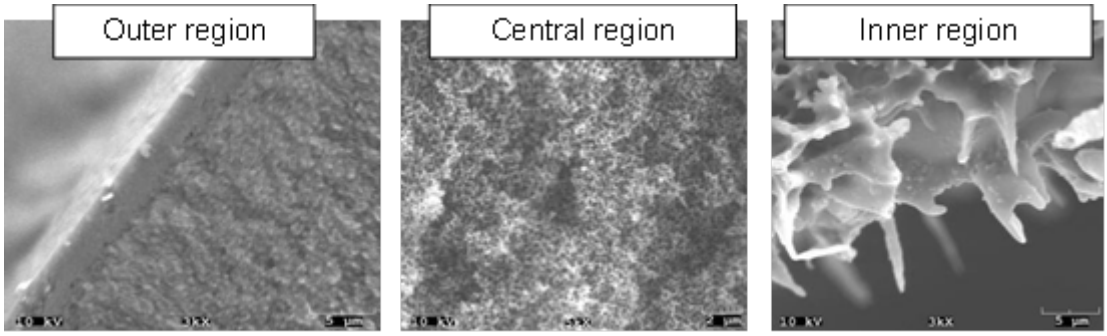

Figure 40. Cross-section SEM Images of as spun hollow fibers without solvent exchange.

The gas test results (Table 21) showed that the second approach involving a swelling solution was milder compared to the first approach. However, permeance to CO_2 , N_2 and He were still significantly reduced for the Torlon® hollow fibers treated with 10% DBU solution. SEM images confirmed that the pores collapsed only in the outer regime, and this process might be able to be developed either by using a lower concentration of BDU solution or treatment time and temperature.

Table 21. Permeation results of fibers after post-treatment with BDU solutions.

Module	POSTTREATMENT COND.	Selectivity		CO_2	N_2	He
	TEM. TIME	CO_2/N_2	He/N_2	(P/l) (GPU)	(P/l) (GPU)	(P/l) (GPU)
AR-57-S1-ST1-MeOH+Hex	10% BDU in heptane, 70 °C, 2h	0.85	2.02	745	880	1777
AR-57-S1-ST1-MeOH+Hex	10% BDU in Methanol 50 °C, 2h	0.59	4.12	6	10	43

In any case, the test results and SEM images show that the skin layer thickness increased by either avoiding solvent exchange using hexane as a solvent, or by treatment of the outer skin with a DBU solution. Due to time constraints, we decided that these approaches offered no advantage over the ones we have used in in the past (using methanol, and or combination of methanol and hexane), so we did not pursue them further in this study.

Georgia Tech also tested permeation and pore size characteristics of porous cellulose acetate and poly ether sulfone (PES) hollow fibers made from different spin states and provided by GE. We made two modules with single and dual fibers from each spin state fiber. Most of GE fibers showed high permeance to CO_2 /N_2. However, selectivity was less than unity in the coated state. Cellulose acetate (CA) fibers showed higher permeance for CO_2 and N_2. The permeation results are listed in Table 22. Based on the permeation results, we have identified spin 5, state 9 and 12 as the best fibers.

Table 22. Permeation results of porous CA and PES hollow fibers from GE spinning studies..

		Selectivity		CO_2	N_2	He
				(P/l)	(P/l)	(P/l)
Module	#F	CO_2 /N_2	He/N_2	(GPU)	(GPU)	(GPU)
AR-46-S5-ST.1	2	0.92	1.65	7639	8285	13677
AR-47-S5-ST.2	2	0.81	1.90	4683	5798	11013
AR-48-S5-ST.5	2	0.92	1.00	70	76	76
AR-49-S5-ST.7	2	0.92	1.53	6818	7412	11376
AR-50-S5-ST.9	2	0.84	1.66	13050	15543	25786
AR-51-S5-ST.11	2	0.86	1.61	7671	8952	14376
AR-52-S5-ST.12	2	0.88	2.33	7715	8773	20460
AR-53-S6-ST1	2	0.65	3.86	0.6	0.9	3
AR-54-S6-ST5	2	0.96	1.63	3871	4025	6581
AR-55-S6-ST6	2	0.99	1.42	944	957	1358
AR-56-S6-ST11	2	0.74	1.08	40	54	58

As noted above, based on the results of the permeation study, the solvent exchanged Torlon® hollow fibers with either methanol and hexane or only methanol as well as porous cellulose acetate were selected as highly preamble asymmetric hollow fiber supports for further coating studies. Selectivity was less than one for all fibers, consistent with our goals, since a defect-free Torlon® or CA support was desired for our subsequent composite casting work.

Based on the extensive optimization studies at Georgia Tech, a spin dope composition of Torlon®/NMP/Water/PVP – 25/63/5/7 wt. % and a bore fluid composition of NMP/Water-88/12 wt. % were down-selected for scale-up at GE. Spinning process conditions (Table 23) were found to give high permeance HF supports (CO_2 permeance ≈20,000-30,000 GPU), high porosity sub-structure with small surface pores (20-40 nm) to enable intermediate/selective layer coating without infiltration into the sub-structure. Figure 41 below shows the SEM images of the Georgia Tech fabricated hollow fiber supports.

Table 23. Spinning conditions for engineered Torlon®® hollow fiber support fabrication.

Dope (Core)	
Pump temperature	50 °C
In-line temperature	50 °C
Flow rate	180-600 mL/h (preferably 300 mL/h)
Bore fluid	
Temperature	Room temperature
Flow rate	1:3 to 1:2 – bore flow:core flow ratio (preferably 1:3)
Nozzle temperature	50 °C
Air temperature	Room temperature (≈ 25 °C)
Air-gap	0-3 cm (preferably 0.5 cm)
Quench bath	
Media	DI water
Depth	1 m
Temperature, T_{quench}	55-65 °C (Preferably 55 °C)
Take-up drum rate	2-10 m/min (preferably 4.2 m/min)

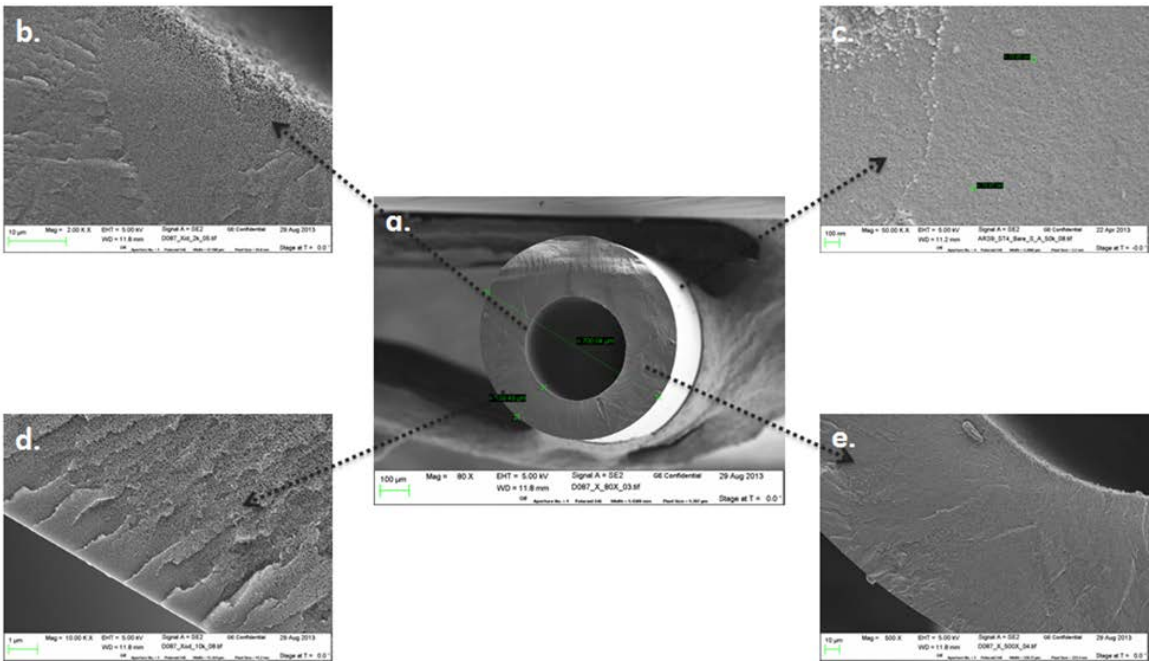

Figure 41. SEM images of the Georgia Tech hollow fiber support a. cross-section view of the hollow fiber support, b. cross-section view showing porosity close to the lumen, c. top-down view showing 20-40 nm surface pores, d. cross-section view showing asymmetric.

Torlon® hollow fiber supports were fabricated at GE utilizing the dope compositions and process conditions specified by Georgia Tech. The GE hollow fiber spinning process is described in earlier sections. For fabrication of membrane mini-modules in Budget Period-1, HF supports

spun under identical conditions were removed from the take-up drum, cut into 1m long strands, tied together and solvent exchanged. However, to enable continuous roll-to-roll coating of HF supports, the 20-50 m continuous strand was kept intact on a polypropylene take-up drum and solvent exchanged. The solvent exchange protocol developed by Georgia Tech was followed for both strands and spools. The fibers were soaked in DI-Water for 7 days to ensure complete removal of residual solvent (NMP), Torlon® oligomer debris and water-soluble additive (PVP). The DI-water was changed every day to allow improved mass transfer. The water present in the fiber sub-structure was then solvent exchanged by immersion of the spin states for 3 h each in fresh methanol (to remove excess water) followed by soaking for 3 h in fresh hexane (to replace excess methanol). Both methanol and hexane are non-solvents for Torlon® and were not expected to cause any changes in the fiber morphology. The solvent exchange process was critical to remove high surface tension liquids from the fiber pores and prevent pore structure collapse under capillary forces during fiber drying. The fiber supports were then left in a fume hood to air dry at room temperature followed by drying at 120 °C for 24-72 h to completely remove any residual solvents/non-solvents. The solvent exchanged fiber supports were then characterized by SEM and gas permeation analysis to determine the morphology and gas transport properties.

Hollow fiber supports utilizing the dope composition, spinning process conditions and solvent exchange protocol described above were fabricated. Dope preparation and processing conditions were replicated with ease during the scale-up. However, challenges were encountered during solvent exchange of the hollow fiber spools. Fiber strands were also collected with spinning process conditions identical to hollow fiber spools. Hollow fiber strands were solvent exchanged by soaking each spin state individually in 1 m long, 2.5 cm diameter solvent exchange tubes to prevent curling and entanglement of the fibers as shown in Figure 42.

Figure 42. Extruded hollow fiber supports in a solvent exchange tube filled with DI water

A new protocol had to be developed for solvent exchange of hollow fiber spools. Initially, the spools were kept fully submerged in the solvent exchange fluids as shown in Figure 43. The process was found to work well during solvent exchange with water.

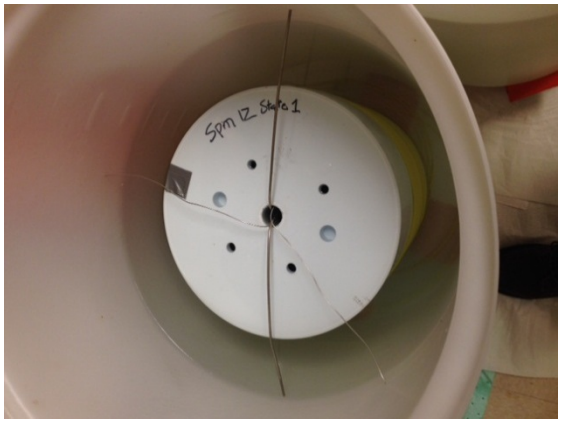

Figure 43. Hollow fiber spool fully submerged in a solvent exchange fluid (water in this case) during the solvent exchange process.

However, during solvent exchange with methanol and hexane the fibers showed a small degree of swelling upon exposure to the fluids causing the fibers to slide-off from the winder-drum causing fiber entanglement. An alternate strategy was then developed to keep the fiber spools in a horizontal position during methanol and hexane solvent exchange. The fiber spool was kept partially submerged in the solvent exchange fluid bath and hand rotated intermittently to keep the fibers wet. The modified process is shown in Figure 44. Following the solvent exchange, the fiber spools were left in a fume hood to air dry followed by drying at 120 °C for 24-72 hours to fully dry as shown in Figure 45.

Figure 44. Fiber spools being solvent exchanged with methanol and hexane with a horizontal orientation.

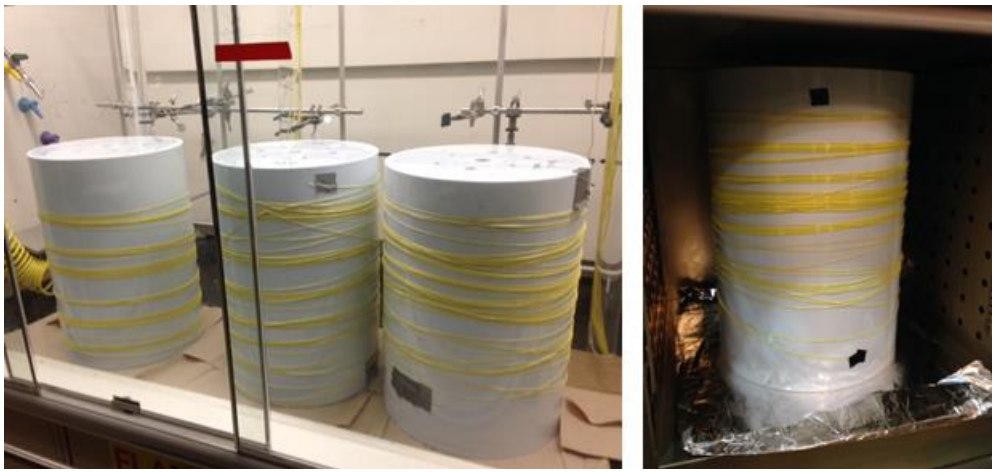

Figure 45. Hollow fiber spools in (left to right) a. fume hood for air drying and b. in an oven for drying at 120 °C.

Hollow fiber strands fabricated at GE showed an overall permeance ≈20,000 GPU, similar to results obtained at Georgia Tech. However; hollow fiber spools showed an overall permeance of < 10 GPU. The permeation test conditions were Δp = 30 psid, T=60 °C with a feed gas composition of CO_2 /N_2/O2 – 17/78/5 vol. %. Since the strands and the spools were fabricated from the same spin dope and were collected under the same process conditions, the only difference in processing was the solvent exchange process. Several improvements were made to the spool solvent exchange process to improve mass transfer, prevent premature drying during the solvent exchange process, and reduce the stress on the fiber surface pores. During subsequent fiber spinning trials, the hollow fiber spools were carefully unwound from the winder-drum and collected as continuous lassos. It was hypothesized that this would reduce the stress on the fiber surface pores during the solvent exchange process. Collection of fiber lassos also reduced the overall volume of fluids required during solvent exchange. Since the fibers were already unwound the orientation of the winder-drum during the solvent exchange process was irrelevant. The solvent exchange process with water was modified to allow continuous recirculation of warm DI water (40 °C) to improve the rate of mass transfer. The modified solvent exchange process using fiber lassos is shown in Figure 46.

Incomplete leaching of solvents (NMP) and pore former additive (PVP) due to poor mass transfer in stagnant water exchange could cause blockage of surface pores. The first three days of water exchange, Figure 47, showed that continuous recirculation was indeed helpful with the color change of the water in the first two days indicating the possible leaching out of residual solvent (NMP), Torlon® oligomer debris, and water-soluble additive (PVP). No such color change was observed during stagnant water exchange (Figure 43). The changes were found to improve the overall gas permeance by one order of magnitude to < 100 GPU.

While every effort was taken to follow the fiber spinning conditions specified by Georgia Tech, the hollow fiber support permeance was found most sensitive to the air-gap followed by the take-up rate as reported by Georgia Tech. The effect of variation of air-gap (0.5 cm and 3 cm) and take-up rate (4.2 m/min and 8.4 m/min) is summarized in Table 24.

Figure 46. Modified solvent exchange process using fiber lassos with continuous recirculation of warm (40 °C) DI water.

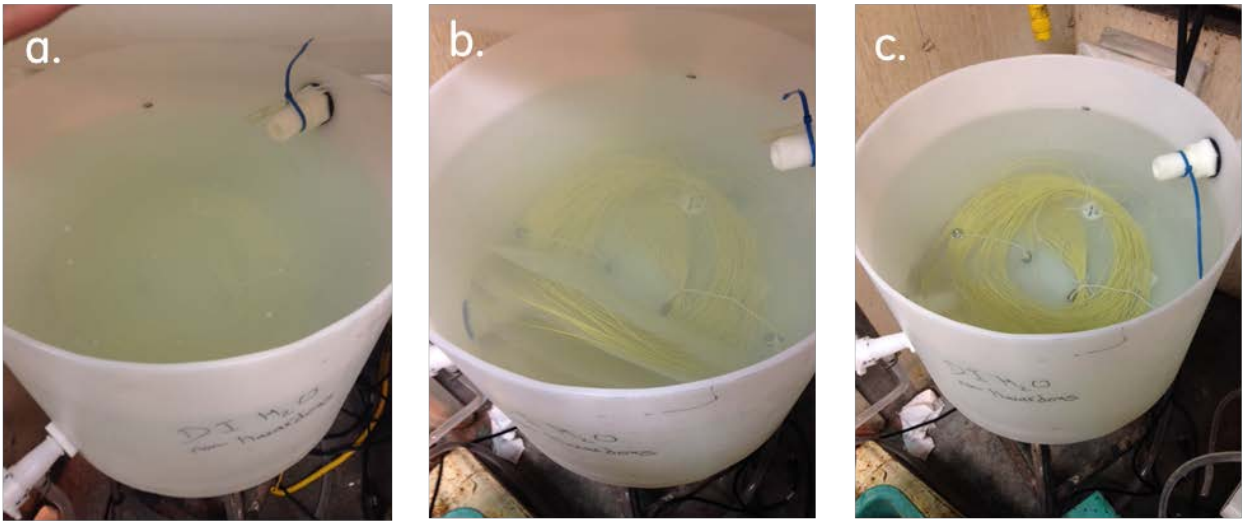

Figure 47. Leaching of possible oligomer and additive (PVP) from the fiber lassos during solvent exchange process. Days 1-2-3 (left to right) are shown for comparison.

Table 24. The effect of variation of air-gap (0.5 cm and 3 cm) and take-up rate (4.2 m/min and 8.4 m/min) on gas permeance of Torlon® hollow fiber supports.

Core	Core Line	Bore Fluid	In-Line	Spinneret Assembly	Air Gap	Take-Up	Quench Bath	Permeance (GPU)	
ml/hr	T (°C)	ml/hr	T (°C)	T (°C)	cm	m/min	T (°C)	CO_2	N_2
600	50	200	50	50	0.5	4.2	55	16,000	18,000
600	50	200	50	50	0.5	8.5	55	12,000	13,000
600	50	200	50	50	3	8.5	55	1,100	1,700
600	50	200	50	50	3	4.2	55	7,000	8,500

Even after modifications in the solvent exchange protocol and tight control on the fiber spinning parameters, the fiber lasso/spool permeance continued to remain two orders of magnitude lower than the hollow fiber strands fabricated by Georgia Tech. Figure 48 shows the SEM images of the Torlon® hollow fiber support fabricated at GE as a continuous spool/lasso. The SEM images reveal the morphology of the hollow fiber support spools to be similar to the Georgia Tech hollow fiber support strands with porous, macrovoid free cross-section and surface pores in the 20-40 nm range

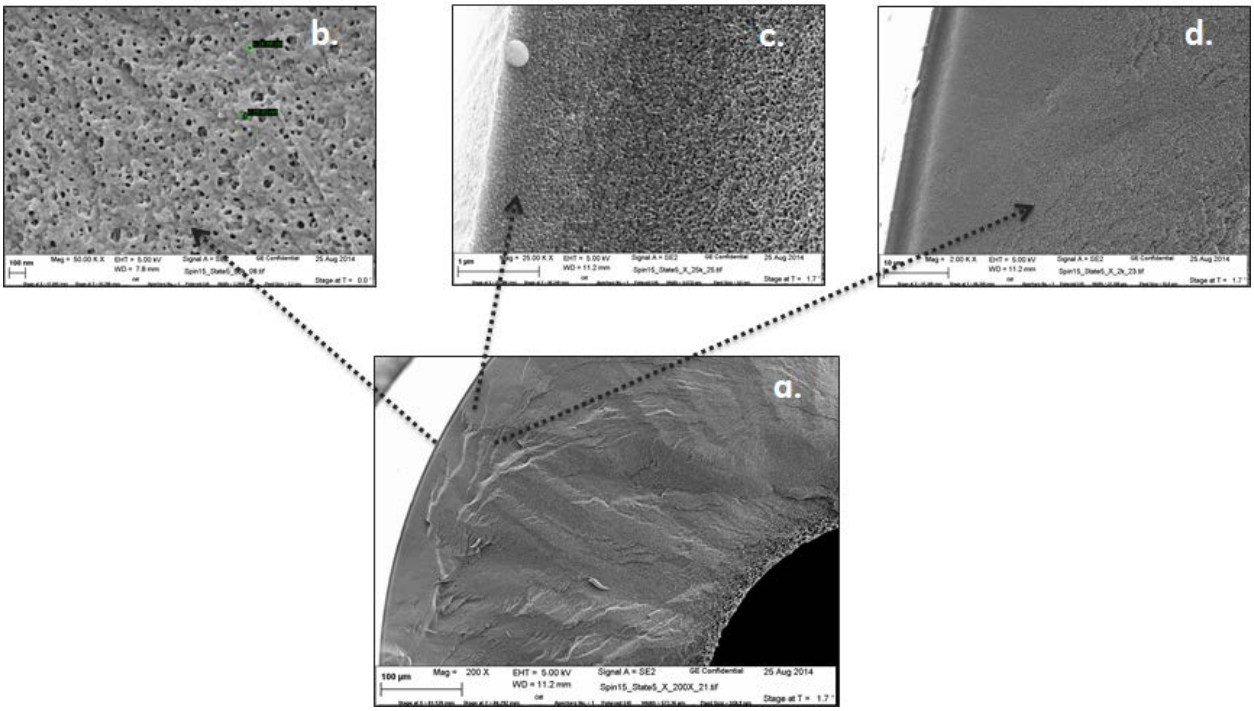

Figure 48. SEM images of the Torlon®® hollow fiber support fabricated at GE as a continuous spool/lasso a. cross-section view of the hollow fiber support, b. top-down view showing uniformly distributed 20-40 nm surface pores, c. cross-section view showing asymmetric structure, and d. cross-section view showing macrovoid free morphology.

A detailed evaluation of the polymer drying protocol, spin dope preparation, fiber fabrication and solvent exchange process was conducted. It was decided to further evaluate the Torlon® polymer batches used by GE and Georgia Tech. GE utilized a 2.2 lb batch for the first

three scale-up runs (Spin 12-14) followed by a 55 lb batch for the fourth run (Spin 15). Hydrogen-Nuclear Magnetic Resonance (1H-NMR) studies were done to identify presence of any impurities and varying extent of imidization in the polymer batches which could lead to variations in the final hollow fiber morphology. 1H-NMR indicated the batches to be almost identical indicating similar levels of imidization and no presence of external impurities in the polymer. Figure 49 shows the 1H-NMR results of the different Torlon®® batches and the chemical structure of Torlon®. Gel Permeation chromatography (GPC) conducted with NMP as the solvent showed molecular weight of the Georgia Tech batch to be roughly 10% higher than the two GE batches (Table 25).

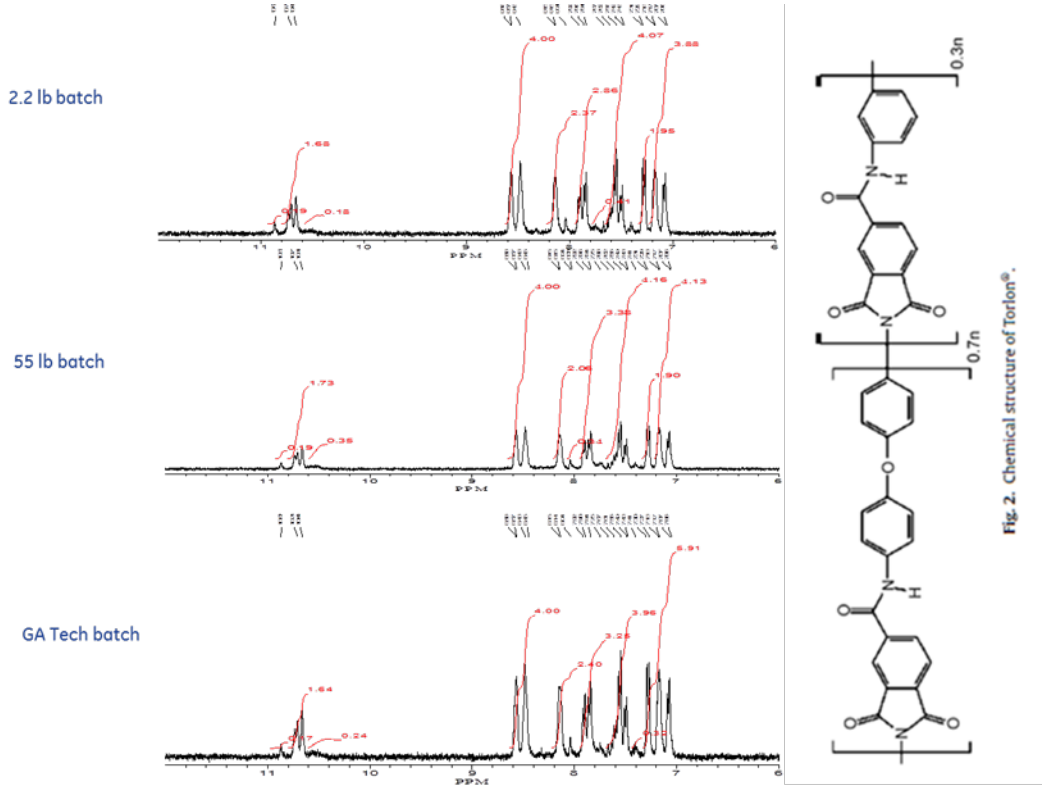

Figure 49. H-NMR results of various batches of Torlon®-4000-THV grade received from Solvay Advanced Polymer (1) 2.2 lb trial batch (2) 55 lb large batch (3) Georgia Tech batch. Also, shown is the chemical structure of Torlon® polyamide-imide.

Table 25. GPC results of the various batches of Torlon®-4000-THV grade received from Solvay Advanced Polymer (1) 2.2 lb trial batch (2) 55 lb large batch (3) Georgia Tech batch.

GPC measurements - NMP solvent			
Batch ID	Sample	Mw(k)	Mw/Mn
134600034A	2.2 lb batch	100.5	2.67
144600084A	55 lb batch	101.5	2.68
	Georgia Tech batch	113.4	2.69

Additionally, Torlon®/NMP 25/75 wt.% solutions were created and the solution viscosity was measured at 50 °C to mimic the dope solution and the fiber spinning temperature

respectively. The viscosity results were found to be contradictory to the GPC results indicating that the 55 lb GE batch had the highest viscosity and correspondingly a higher molecular weight (Table 26). Further characterization is required to elucidate any differences between the batches.

Table 26. Viscosity measurement results of the various batches of Torlon®-4000-THV grade received from Solvay Advanced Polymer (1) 2.2 lb trial batch (2) 55 lb large batch (3) Georgia Tech batch

Viscosity measurements, 6 RPM, 50 °C		
Batch ID	Sample	Viscosity (Pa.sec)
134600034A	2.2 lb batch	22.6
144600084A	55 lb batch	69
	Georgia Tech batch	55.8

While the characterization studies were being conducted, a spin dope (spin 17) was prepared utilizing the Georgia Tech Torlon® batch since it had been used multiple times to fabricate high permeance hollow fiber supports at Georgia Tech. The polymer/additive drying protocol, spin dope preparation, fiber fabrication and lasso solvent exchange protocols developed earlier were followed. As seen with the previously reported result, the fibers that went through solvent exchange as 2 m strands again showed a significantly higher gas permeance than the fibers that were solvent exchanged as a 30 m lasso (Table 27).

Table 27. Gas permeance performance of Torlon® hollow fiber supports from Spin 17 in strand and lasso form.

Core	Core Line	Bore Fluid	In-Line	Spinneret Assembly	Air Gap	Take-Up	Quench Bath	Mixed Gas Permeance (GPU)	
ml/hr	T (°C)	ml/hr	T (°C)	T (°C)	cm	m/min	T (°C)	Strand	Lasso
300	50	100	50	50	0.5	4.2	55	2,667	137
180	50	60	50	50	0.5	4	55	4,139	5
300	50	100	50	50	0.5	4.2	60	3,052	74
180	50	60	50	50	0.5	4	60	6,433	19
300	50	100	50	50	0.5	4.2	65	6,054	600
~600	50	200	50	50	0.5	8.4	65	5,602	212

Based on this result, the low permeance of the Torlon® hollow fiber membranes is believed to be related to the nature of the solvent exchange process rather than the dope formulation or fiber spinning conditions.

Task 4: Fabricate Composite Coated Hollow Membranes

Deposition of a thin intermediate/selective layer onto engineered porous hollow fiber supports to form defect-free composite hollow fiber membranes is the key enabler of the technology. The coating process needs to be economical, scalable, and minimize coating solution losses. GE and Georgia Tech worked in parallel to delineate both batch and continuous coating processes. GE pursued the continuous dip coating process, with a focus on scaling up the intermediate (PDMS) and selective (polyphosphazene) coating layers by leveraging its experience in coating ultra-thin film selective layers on flat sheet reverse osmosis membranes for water purification applications. The process comprised passing the spun hollow fiber support substrate at fixed tension and fixed speed into the intermediate layer (PDMS) or selective layer (polyphosphazene) coating solutions. The coating solution was evaporated in an oven by a controlled drying step resulting in a uniform, defect-free coating. The advantages of a continuous process over a batch process are scalability, improved control of coating properties and reduced fiber agglomeration. The batch process developed by Georgia Tech is most suitable for fabrication of mini-modules and also defect-repair of the coated layers in a composite hollow fiber membrane module. The schematic representation of the proposed continuous coating process is shown in Figure 50.

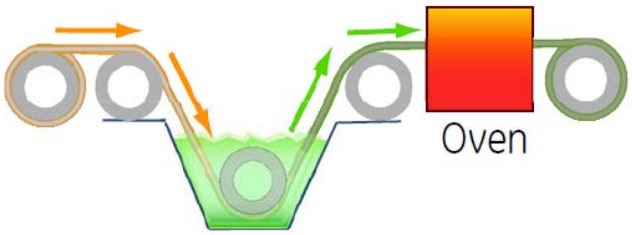

Figure 50. Schematic representation of the continuous coating setup.

Continuous Hollow Fiber Coating Line

A continuous hollow fiber coating rig was designed and constructed to allow continuous roll-to-roll coating of hollow fiber supports. Computer aided-design (CAD) representation of the coating rig is shown in Figure 51, Figure 52, and Figure 53show the front and the back view of the constructed hollow fiber coating line.

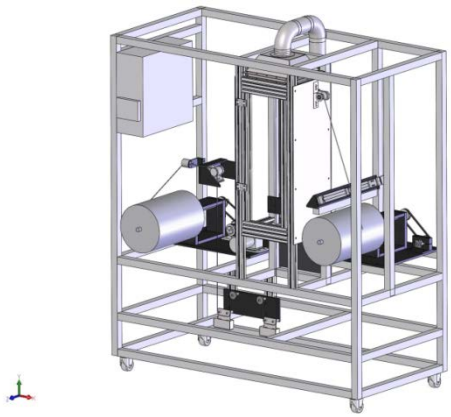

Figure 51. Computer aided-design (CAD) of the hollow fiber coating line.

Figure 52. Front view of the continuous hollow fiber coating line.

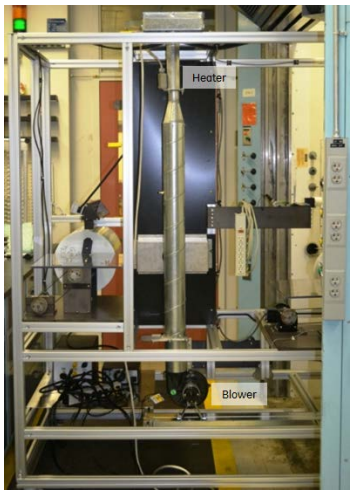

Figure 53. Back view of the continuous hollow fiber coating line.

20-50 m of continuous hollow fiber support strand on a winder-drum was inserted on the unwinder side for coating. The fiber winder drums were made of solvent resistant polypropylene with 12" diameter X 18" length. The hollow fibers were then threaded through the system, making sure to string through appropriate pulleys, linear guides, and rollers onto the re-winder drum so the hollow fiber strand traveled freely and at the proper tension without breakage. The hollow fiber re-winder speed could be adjusted between 0.1-10 m/min, with the re-winder acting as the master control, and the unwinder in slave configuration. The unwinder drum tension could be adjusted between 0-226 grams using a tensiometer. Typically, the tension exerted by a strung hollow fiber strand was between 30-40 grams. The unwound fiber would first pass through a conical guide cup to orient the fiber in a single direction. The hollow fiber strand would then be directed towards the coating baths via low friction, stainless steel pulleys. Two coating baths could be utilized with each bath having a capacity of 200 mL of solution. The coating baths could be arranged to allow various configurations such as a) two coating solutions, b) pre-coating solvent followed by coating solution, and c) coating solution followed by a non-solvent. The coating baths were kept partially covered to prevent evaporation of the coating solvents (hexane in case of PDMS, ethanol in case of polyphosphazene).

The coated fiber would then travel directly to bottom of the fiber drying oven through an adjustable slit. The drying oven was designed as a forced air convection oven, by utilizing a blower providing air flow velocity between 0-150 feet/min or air flow rate inside the oven of 0-20 ft3/min controlled by a 0-30 Vdc power supply. The air velocity could be monitored using an anemometer. An in-line heater downstream to the blower was used to heat the air going into the oven. Temperatures of up to 80 °C could be obtained inside the oven using the in-line heater. Higher temperatures up to 145 °C could be achieved inside the oven utilizing six heat pads located in the oven. Desired set point temperature could be achieved by controlling the voltage supplied to the heat pads using Variacs. The hot air supply line to the oven was insulated using fiberglass insulation, while the oven walls were insulated utilizing 2" thick melamine insulation. An electrostatic filter was utilized at the air entrance of the oven to allow uniform distribution and also prevent dust particles from entering the oven which might get

sucked-in through the air blower. The direction of fiber traverse was counter-current to the hot air flow for improved mass and heat transfer and better drying. The oven had a plexiglass door in the front to allow easy viewing of the fiber coating operation. The residence time of the fiber strand in the oven could be varied between 1-45 min by having 1,3, or 5 fiber bends/winds inside the oven to allow complete removal of the coating solvent, while also allowing thermal crosslinking of the intermediate (PDMS) or coating layer (polyphosphazene) polymer.

The dried/cross-linked fiber would then exit from the top right end of the fiber oven. The fiber strand would then pass through a slide jogger and onto the re-winder. The slide jogger speed could be adjusted to allow uniformly spaced re-winding of the coated fibers without overlap. The coated fibers could then be cut along the re-winder axis to create multiple 1m long individual fiber strands for making modules or the continuous coated fiber spool could be used for further coating and processing.

Because of the difficulties in preparing long continuous runs of hollow fibers with adequate permeability to serve as porous supports, the coating apparatus described here was not used to prepare high-performing separation membranes after initial coating validation (*vida infra*) was completed.

Intermediate PDMS layer

Polydimethylsiloxane (PDMS) is extensively used in various applications due to its low glass transition temperature (Tg = -123 °C), as well as its adequate thermal, chemical and oxidative stability. These properties are useful in preparing the silicone rubber membrane, and the PDMS should be cross-linked to stabilize it against flow into the support. A crosslinkable polydimethylsiloxane formulation (PDMS, SYLGARD® 184) available from Dow Corning was used to create the intermediate layer. Hexane was chosen as the diluting solvent for the partial PDMS crosslinking. Hexane was chosen since it is a non-solvent for the Torlon® hollow fiber support, and has a high vapor pressure/low boiling point which is highly beneficial during the continuous roll-to-roll fiber coating process enabling rapid drying. SYLGARD® 184 is two-part Pt catalyzed addition cure providing PDMS films with good mechanical strength, which can be cured with mild heat (the reaction chemistry shown below in Figure 54). Part A is a vinyl terminated pre-polymer with Part B being the cross-linker.

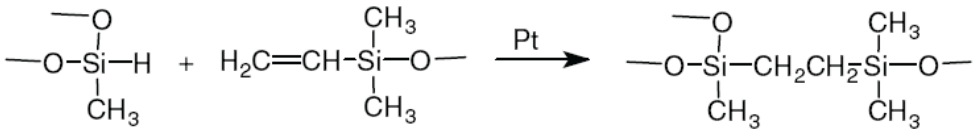

Figure 54. Addition cure chemistry of Pt catalyzed PDMS.

Preliminary coating experiments with a pre-crosslinked 20% (w/w) PDMS/hexane solution on Torlon® hollow fiber support showed that at a solution viscosity (≈ 50 cP), a defect-free coating was obtained with a CO_2 /N_2 selectivity = 8-10. The coating thickness obtained was roughly in the desired range of 1-5 µm with CO_2 permeance < 100 GPU. In contrast, a dilute 2% (w/w) PDMS/hexane solution, with low solution viscosity (≈1 cP), showed no CO_2 /N_2 selectivity, while also showing low CO_2 permeance < 100 GPU due to significant coating intrusion through the Torlon® hollow fiber support surface pores. It was hence desired to pre-crosslink the PDMS

to control the viscosity of the coating solution independent of the concentration. Sufficient solution viscosity prevented permeation of the coating solution, while high dilution ensured a sufficiently thin PDMS coating. We developed a PDMS pre-crosslinking procedure with gradual dilution enabling the preparation of carefully tailored PDMS solutions of various concentrations and of viscosity between 10 and 100 cP. Based on the studies at Georgia Tech the optimal solution properties were a pre-cross-linked 2% (w/w) PDMS/hexane solution with viscosity of about 50 cP .Using this solution to coat the Torlon® hollow fiber supports provided coatings exhibiting CO_2 /N_2 selectivity = 8-10, with high CO_2 permeance > 1000 GPU. The coating thickness was determined to be less than 1 μm.

The pre-crosslinking reaction was conducted in a 3 liter 3-neck round bottom flask. The target composition was a 20% (w/w) SYLGARD® 184/hexane solution with part A and part B mixed in a 10:1 (w/w) ratio. Initially the desired amount of Part-A was dissolved in hexane in the flask while heating to 80 °C, under reflux and stirring. When the desired temperature was reached, Part-B was added to achieve a total PDMS concentration of 20 % (w/w). After addition of the part-B component, the exact timing of the crosslinking reaction was started. Figure 55 shows the experimental setup for PDMS pre-crosslinking reaction scale-up.

The crosslinking reaction was carried out in three steps. The reaction was allowed to continue till the solution viscosity reached between 40-60 cP. The curing/cross-linking process was classified into three stages: liquid-gel-solid. At the start of the reaction the PDMS solution had low viscosity (liquid like), as the reaction progressed, the viscosity was found to increase exponentially. The solution had to be diluted once it reached the gel stage with a viscosity between 40-60 cP. Care was to be taken to ensure that the PDMS solution viscosity did not increase above 100-120 cP. Any increase beyond that viscosity could solidify the solution. In the following steps, the viscous solution was diluted with hexane to 10% (w/w), and then 5% (w/w) or alternatively to 2% (w/w), while the crosslinking reaction continued at 80 ◦C until the solution reached a viscosity of about 50 cP. Viscosity increase/molecular weight build-up took the most time in the initial 20% (w/w) step, with the following dilution/viscosity build-up steps taking significantly shorter time. 15 mL solutions were syringed / pipetted out in all the steps after every 30 minutes for viscosity measurement. Figure 56 shows the successful pre-crosslinking of PDMS coating solution showing the increase in viscosity over the course of the reaction at 80 °C, and the effect of dilution on viscosity of PDMS coating solution from: (a) 20 wt.%, (b) 10 wt.%, (c) 5 wt.%.

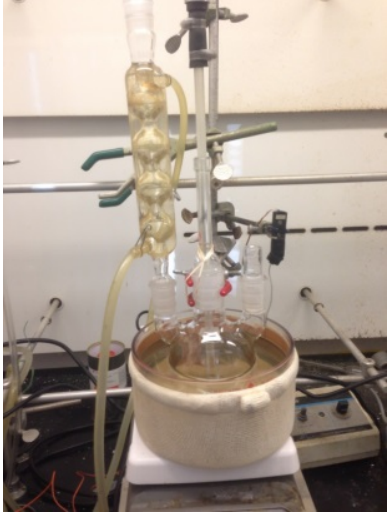

Figure 55. Experimental setup for PDMS pre-crosslinking reaction scale-up.

Viscosity measurements were conducted at 25 °C, using a Brookfield RVDV-II Pro viscometer. The solution of the pre-cross-linked PDMS was cooled down in an ice bath to stop the reaction. The PDMS solution was then stored in a refrigerator and was used for coating within 1-2 days. Solutions measured one week of making the solution showed roughly 10% increase in viscosity, however a detailed analysis of molecular weight increase was not conducted. The PDMS solution was used as an intermediate layer and for coating on continuous Torlon® hollow fiber support spools. By careful optimization, the process was scaled-up from 100 mL solution at Georgia Tech to 1L and eventually to 2L batches of 2 or 5 wt% PDMS/hexane solutions.

The viscosity build-up time increased to > 12 hours in cases when the SYLGARD® 184 batch was used repeatedly for the reaction. It was hypothesized that the delay in viscosity/molecular weight build-up could be due to deactivation of the Pt catalyst. The SYLGARD® 184 Part A/B batches once opened were stored in a glove box to prevent catalyst deactivation. It was also found that starting the reaction with a 40 wt.% PDMS/hexane solution led to faster increase in viscosity build as compared to starting with a 20 wt% PDMS/hexane solution.

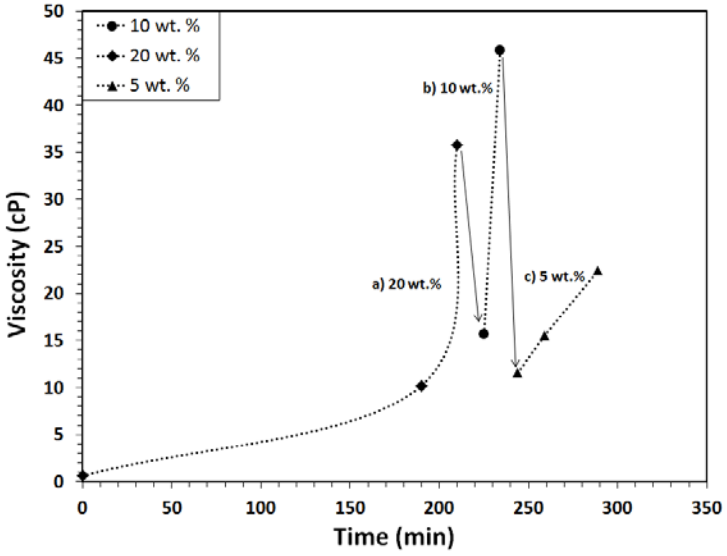

Figure 56. Crosslinking of PDMS coating solution showing the increase in viscosity over the course of the reaction at 80 °C, and the effect of dilution on viscosity of PDMS coating solution from: (1) 20 wt.%, (2) 10 wt.%,

(3) 5 wt

Additionally care was to be taken to ensure that the PDMS solution viscosity did not increase above 100-120 cP. Any increase beyond the viscosity could solidify the solution. To prevent the PDMS solution from solidifying it was critical to dilute with hexane at appropriate viscosity (typically, ≈50 cP). On the contrary, early dilution before appropriate molecular weight/viscosity buildup caused the crosslinking reaction to cease with no further build-up of viscosity as shown in Figure 57.

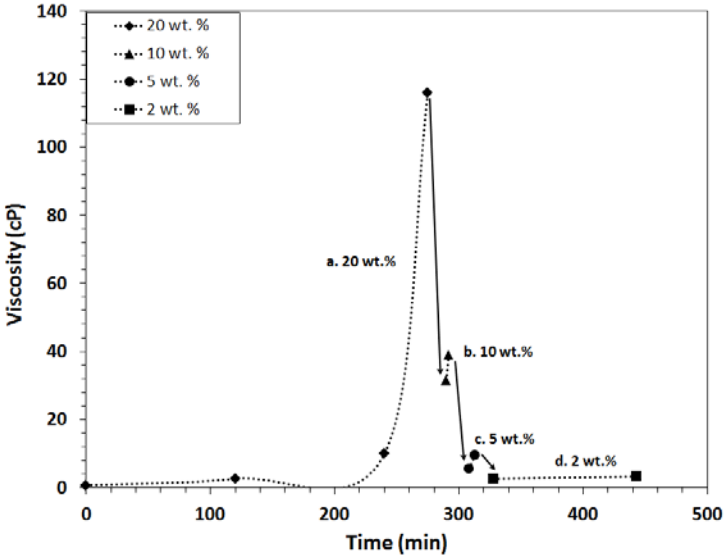

Figure 57. Crosslinking of PDMS coating solution showing the increase in viscosity over the course of the reaction at 80 °C, and the effect of dilution on viscosity of PDMS coating solution from: (a) 20 wt.%, (b) 10 wt.%, (c) 5 wt.%, and (d) 2 wt.%. Early dilution from 5 wt.% to 2 wt.% before appropriate molecular weight/viscosity buildup caused the crosslinking reaction to cease with no further build-up of viscosity

Torlon® continuous hollow fiber support spools were fabricated at GE utilizing the spin dope composition, fabrication and solvent exchange protocol described in the previous section. Gas performance testing of the HF supports, showed low permeance (<100 GPU) compared to a desired permeance of >20,000 GPU. While, the fiber permeance was low, it was still decided to coat a hollow fiber support spool with a PDMS intermediate layer to identify critical coating parameters and specific conditions. Coating quality and uniformity were characterized using SEM analysis. Gas permeation analysis was not performed since the permeance was expected to be quite low. To proceed further with coating of the polyphosphazene selective coating layer, the permeance of the Torlon® hollow fiber supports needed to be significantly improved.

Coating process parameters such as line speed, number of coating baths, drying time and drying temperature were varied. A 2 wt.% pre-crosslinked PDMS/hexane solution was utilized as the intermediate layer coating. The following parameters were varied in the coating run and are described in Table 28. The fiber drying temperature was set at 65 °C which is close to the boiling point of hexane (68 °C).

Table 28. PDMS intermediate layer coating conditions on Torlon® hollow fiber supports.

Coating line speed	0.1, 0.5, and 1 m/min
Number of PDMS coating baths	1 and 2
Number of turns in the oven	1 and 3

Torlon® hollow fibers were successfully strung through the system and coated without any fiber breakage under the various coating conditions. Coating line speed was found to be the most significant parameter affecting the coating quality. Low line speeds (0.1 m/min) showed poor coverage of coating with significant uncovered regions, while a high coating speed (1 m/min) was found to give a thick PDMS coating with some uncovered patches. Line speed affected the residence time of the fiber strand in the coating bath and also the residence time in the oven. While longer residence time in the oven was preferred (as described later), residence time in the coating bath had to be optimized. 0.5 m/min line speed was found to be adequate revealing a more uniform, thin coating. Figure 58shows the SEM images of the PDMS coated Torlon® hollow fiber supports with varying line speed.

The number of coating baths and the residence time in the oven were then varied while maintaining the coating speed at 0.5 m/min. Higher number of turns (3 vs. 1) provided a longer residence time in the drying oven (7 min vs. 3 min) providing a more uniform coating as shown in Figure 59 a and b vs. c and d. No significant difference was observed between 1 and 2 coating baths, Figure 59 a and c vs. b and d. Use of 1 coating bath was preferable since it allowed material saving. Based on SEM analysis of the PDMS coated hollow fibers, a coating line speed of 0.5 m/min, longer residence time in the drying oven and one PDMS coating bath was found to give the most uniform coating coverage on the fibers. Fiber support coated with a line speed of 0.1 m/min, 2 PDMS baths and three turns (residence time in the oven = 35 min) with significant uncoated regions is shown in Figure 60Figure 60 for comparison. These coating studies indicate a uniform intermediate layer coating could be applied on the bare Torlon® hollow fiber supports. Further development of the roll-to-roll coating process required improvements in the permeance of the continuous Torlon® hollow fiber supports.

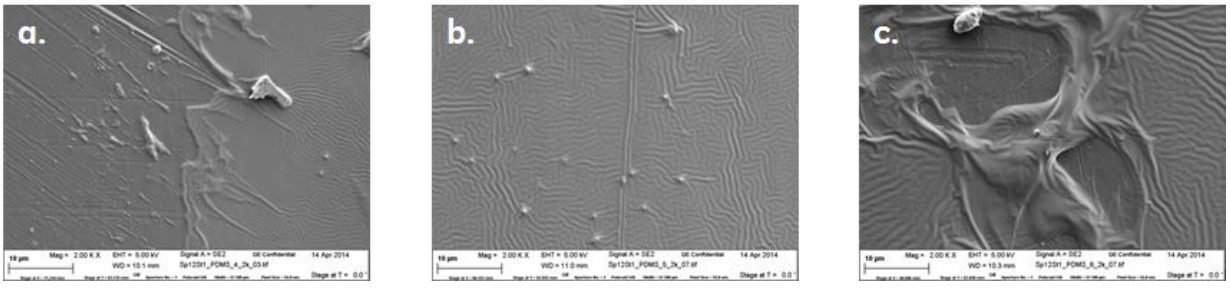

Figure 58. SEM images of PDMS coated Torlon® hollow fiber supports with varying line speed (left to right) a. 0.1 m/min, b. 0.5 m/min and c. 1 m/min. Other coating parameters, number of coating baths = 1, number of turns/winds = 3, drying temperature = 65 °C.

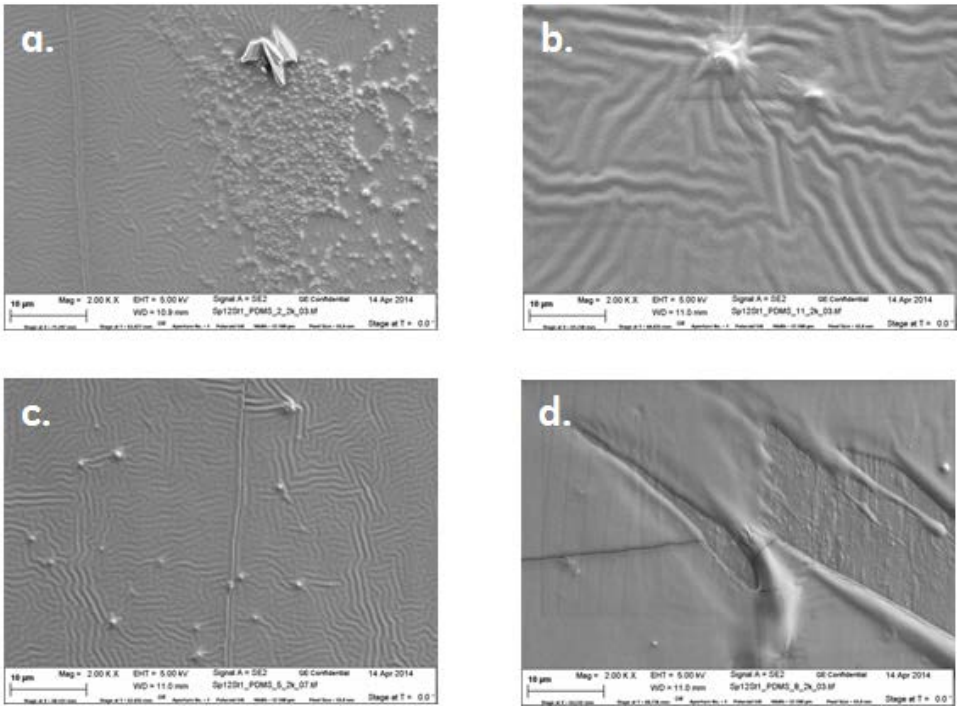

Figure 59. SEM images of PDMS coated Torlon® hollow fiber supports with varying number of baths and number of winds through the drying oven (left to right) a. 1 bath/1 wind, b. 2 bath/1 wind, c. 1 bath/3 winds, d. 2 baths/3 winds. Other coating parameters, coating line speed = 0.5 m/min, drying temperature = 65 °C.

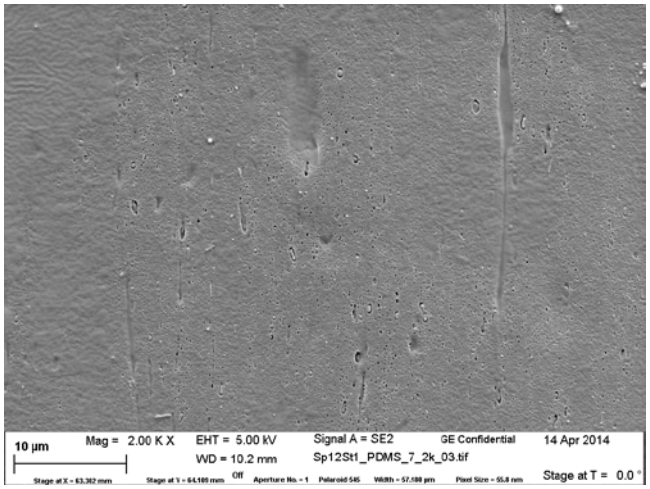

Figure 60. SEM image of PDMS coated Torlon® hollow fiber support showing negligible coating. Coating parameters, coating line speed = 0.1 m/min, number of PDMS baths=2, number of turns in the oven =3, drying temperature = 65 °C.

The Effect of Additional Solvent Exchange on Torlon® HF Gas Permeance

In order to evaluate the impact of re-wet post-treatment of hexane, and methanol on bare Torlon® HF characteristics (a totally dry fiber after the full standard solvent exchange and drying) with high gas permeances (around 16000 GPU to CO_2), three HF modules were formed with two fibers in each module and the following experimental steps were performed. This

study was intended to investigate the effect of solvent exposure that applied for fiber post-treatments (i.e., solution mixture of PDMS in hexane) on the robust Torlon® support. Sample 1 was made by soaking one HF module directly in methanol for 2 h leaving it out to dry in ambient air. Sample 2 was prepared by first soaking another dual fiber HF module in methanol for 2 h and then in hexane for two hours. Finally, sample 3 was a dual fiber HF module that was only soaked in hexane for two hours and left to dry. To completely remove any residual methanol and hexane liquids, all HF modules were heated at 120 °C for 1 hour under vacuum. This experimental procedure is illustrated in the flowchart shown below (Figure 61).

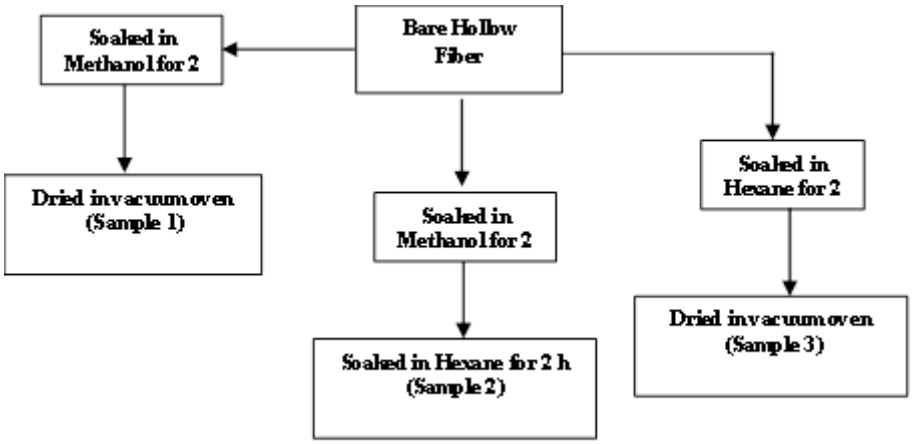

Figure 61. Flowchart of experimental procedure.

Figure 62 shows SEM images of the cross section (bore region, middle region and outer region) of a bare hollow fiber membrane prepared from PAI dope solution (25% Torlon®: 63% NMP: 5% water: 7% PVP) via phase separation techniques at variable quench bath temperature of 55°C. Figure 7a shows SEM images of the cross-section for bare PAI fibers that had been through complete standard solvent exchange procedure (water, methanol, and hexane exchanges) and dried in a vacuum oven at 180 °C for 72 h before re-wetting. The bare Torlon® hollow fibers exhibited permeances (GPU) for CO_2 , N_2 and He of about 16000, 17000 and 30000 GPU, respectively.

Figure 62 (b), (c) and (d) show SEM images for PAI fibers treated with methanol, methanol + hexane, and hexane, respectively. Even with the re-wetting and drying process used in this study, porosity is maintained in most of the fiber wall. It is easy to distinguish significant differences in the morphology of the outer dense skin and transition layers in the fibers. Pore sizes and characteristics on the bore side, middle and the core were similar to neat fibers without any changes after re-doing the solvent treatment and heat treating at 120 °C. However, the pore cell in the outer region of the fibers collapsed after exposure to solvent, thereby resulting in a dense outer region and the pores were invisible on the outside surface for the methanol and methanol+hexane treated fiber. Moreover, a re-wet hollow fiber with methanol and hexane, also reduces the pore density on the surface and leads to undesirable gas transport properties. The skin layer thicknesses of the fibers appear to be approximately 7 µm (methanol); < 4 µm (methanol+hexane) <<< 0.7 µm (hexane). The outer porous substructures of the Torlon® hollow fiber precursors are lost during post-treatment, resulting in a relatively thick

and dense layer of fiber. The total fluxes of different pure gases before and after solvent treatment and the skin layer thickness based on SEM imaging estimates are given in Table 29. Assessments of the skin layer thickness based on SEM imaging are reliable and in agreement with pure gas permeation measurements. Low fluxes were obtained for fibers exposed to methanol before drying (sample 2). It appears that methanol is more aggressive for post-treatment than hexane in this study.

The densification of the outer surface of the porous fiber is believed to take place during the solvent and thermal treatment of Torlon® fibers and is expected to decrease fiber productivity. Since additional solvent and heat-treatment of Torlon® hollow fibers resulted in significant effects on transport properties, the effects of the different solvents' solubility parameter and surface tension on the PAI polymer were investigated to try to understand the trends better. Table 30 shows the solubility parameters and surface tension for water, methanol, hexane and the PAI polymer. By comparing the results of gas transport properties, the SEM images, and the parameters in Table 30, we concluded that the effects of various solvents on Torlon® hollow fiber properties are related to their respective solubility parameters and surface tensions. Swelling of the polymer for cases with similar solubility parameters between the solvent and the Torlon® increases the probability of damaging effects on the fiber morphology and gas separation properties. Moreover, these effects are usually much more pronounced when the hollow fiber is exposed to solvent in the liquid state.

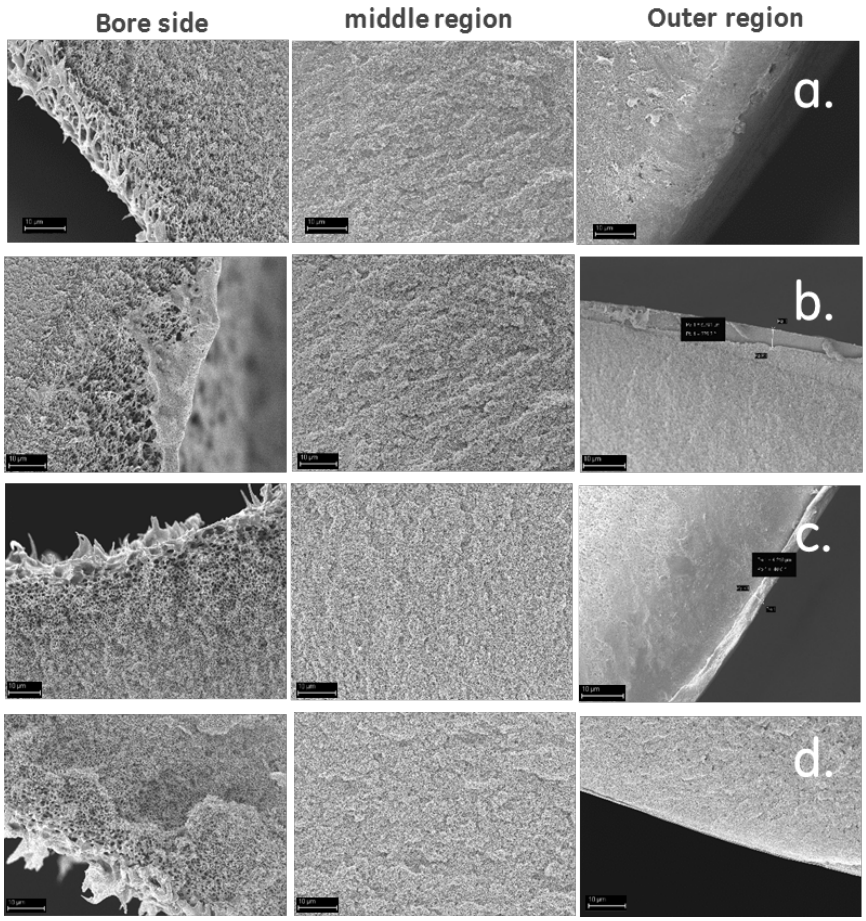

Figure 62. SEM images of the cross-section of bare Torlon® hollow fiber membrane (a); methanol-sample 1 (b); methanol and hexane-sample 2 (c); and hexane-sample 3 (d). (Scale bar is 10 m in all images).

Table 29. Total fluxes of different pure gases before and after solvent treatment.

Torlon® hollow fibers	Skin layer thickness (l_{SEM}) μm	$\alpha CO_2/N_2$	α_{He}/N_2	CO_2 (P/l) (GPU)	N_2 (P/l) (GPU)	He (P/l) (GPU)
Bare Torlon® hollow fibers	-	0.97	2.50	16915	17427	43590
Sample 1 (methanol)	7.0	1.09	6.23	178	163	1017
Sample 2 (methanol+hexane)	4.0	0.82	3.55	6547	7992	28344
Sample 3 (hexane)	0.7	0.90	2.68	11195	12370	33100
* Samples 1 to 3 were heat-treated at 120 °C for 1 h in preheated vacuum oven.						
[a] Obtained from cross-section of SEM images.						

Table 30. Solubility parameter and surface tension for water, methanol, hexane and the PAI polymer.

Polymer and solvents	Solubility parameter $J^{1/2}cm^{-3/2}$	Surface tension
		N/m
PAI[24]	33.7	-
Water[25]	47.7	0.073
Methanol[25]	29.6	0.023
Hexane[25]	14.9	0.018

To understand the above effects better, dynamic mechanical analysis (DMA) measurements were employed to investigate the presence of sub-Tg motions within the region of the β relaxation for pure Torlon®. Dynamic Mechanical Analysis (DMA) was utilized to investigate the presence of sub-Tg motions in pure Torlon® via location of the β relaxation peak. Mechanical measurements were performed on a TA Q800 DMA operated in tension mode using a Torlon® test strip with an average thickness of 89 microns. Measurements were recorded at 1 Hz while heating at 3 °C/min from 35 to 300 °C. Storage modulus (E'), loss modulus (E"), and tan δ (E"/E') data were recorded using a strain amplitude of 0.06%, thereby providing data within the linear viscoelastic regime for the polymer. Figure 63 illustrates the smoothed values for tan δ (E"/E') over the temperature interval of 35°C to 300°C, thereby revealing the presence of two relaxations. The first and most recognized relaxation, the alpha relaxation, corresponds with the presence of large-scale segmental motion associated with the glass transition. The onset of the alpha relaxation is observed in Figure 63(a) by the increase in tan δ as the temperature increases to the upper limit of the temperature interval. An additional relaxation observed in Figure 63(b) is seen by the broad peak in tan δ at ~94°C, corresponding to the β relaxation. Sub-Tg relaxations are generally associated with small, localized motions involving either individual functional groups or small segments of the polymer chain. (Burgess, Leisen et al. 2014) Consequently, the resulting magnitude of tan δ for the β relaxation is significantly smaller than that for the alpha relaxation due to the comparatively smaller scale of activated chain motion. Distinct segmental motions can be assigned to the β relaxations for simple polymers such as poly(ethylene terephthalate). (Light and Seymour 1982; Maxwell, Monnerie et al. 1998; Maxwell, Ward et al. 1998) However, the likely presence of complex and coordinated motions in bulky polymers such as Torlon® make assignment of specific motions to the β peak speculative. A similar assessment was made regarding the sub-Tg relaxations in Matrimid® reported by Comer et al., (Comer, Kalika et al. 2009)who also indicated that the β peak for Matrimid exhibited a fair degree of cooperativity. Following this notion for Torlon®, it was decided to dry the Torlon®-based hollow fibers at ambient temperature, which is significantly lower than the β peak shown in Figure 63 (b). It was hypothesized that drying the fibers above ambient temperature and at temperatures approaching the β peak of ~94°C will result in some degree of substructure collapse and loss of permeability.

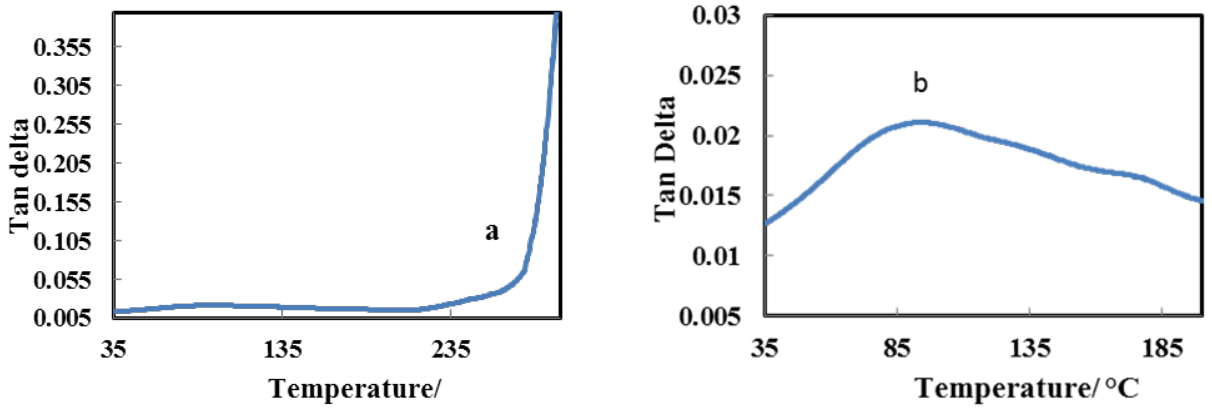

Figure 63. DMA of neat Torlon® film. (a) Focuses on α relaxation; (b) focuses on β relaxation.

Based on the above study, we concluded that additional solvent exchange steps and heat treatment can have negative effects on Torlon® hollow fibers performance. Such effects are particularly apparent when the solvent, like methanol, has a tendency to swell the polymer and possibly depress the β peak to considerably below 94°C. Moreover, water, with its high surface tension is particularly damaging to the pore structure, even for less depression of the β peak. This conclusion is validated by Table 29, which shows a drop in performance of all gases after the fibers have been re-wet and dried in air. Dramatic effects on gas permeation due to capillary force acting on the PAI HF membrane have been observed after re-wetting and heat treatment. The solvent effects were influenced by the drying temperature. A high boiling-point (bp) and high surface tension solvent, i.e., water (bp= 100 °C; surface tension = 0.073 N/m), is seen to be particularly damaging. However, even methanol with a low boiling point, low surface tension (bp = 64 °C; 0.023 N/m) can swell Torlon® and even the low sorbing, low surface tension hexane (bp = 68 °C; surface tension = 0.018 N/m), can induce some pore collapse in the important outer regime. In the higher bp solvents, Torlon® polymer chains in the outer regime may also have a longer time to solidify due to the slow evaporation rate of solvents, thereby forming a highly self-organized structure and resulting in a more non-porous top layer. Although differences in sorption of the various penetrations can complicate the above trends, the boiling point of the solvent does correlate with performances losses.

Preparation and characterization of composite membranes with PDMS and MEEP as the selective layer

MEEP/PDMS/PAI Batch In-situ Coating Process and Characterization

A two-step in-situ PDMS solution coating PDMS coating process was used in this work. The first step in our process defective fibers were contacted with the pre-polymerized 2 wt% PDMS solution in hexane in the module without vacuum, followed by decanting the solution quickly and drying the module in vacuum oven. The next step recovered the PDMS intrinsic selectivity because the small pores have not been coated completely. Subsequently, vacuum was applied to the bore side for a very short time as shown in Figure 64 in order to obtain a defect-free and thin coating layer. In this step, all the large pores can be covered by PDMS coating. No vacuum was applied, so minimal PDMS invasion into large pores occurs, and high

permeance was retained. In-situ coating of the PAI support membrane in PDMS solutions is followed by placing in a vacuum oven at 70 °C for 1-2 h to complete the cross-linking. After this step, CO_2 /N_2 selectivity would be slightly higher than the uncoated fiber but usually lower than the PDMS intrinsic selectivity, indicating that the coating was incomplete. The next step in the module was done by using the pre-polymerized 0.5 wt% PDMS solution in hexane with a vacuum finally applied to the bore side (760 torr) for a very short time (i.e., 2 min noted above) as shown in Figure 64 in order to obtain a defect-free and thin coating layer.

We used this set-up for coating both PDMS and MEEP solutions. The feedback from both the batch coating process and from membrane testing was used to further adjust and optimize both the hollow fiber support polymer dope formulation and the hollow fiber spinning process parameters.

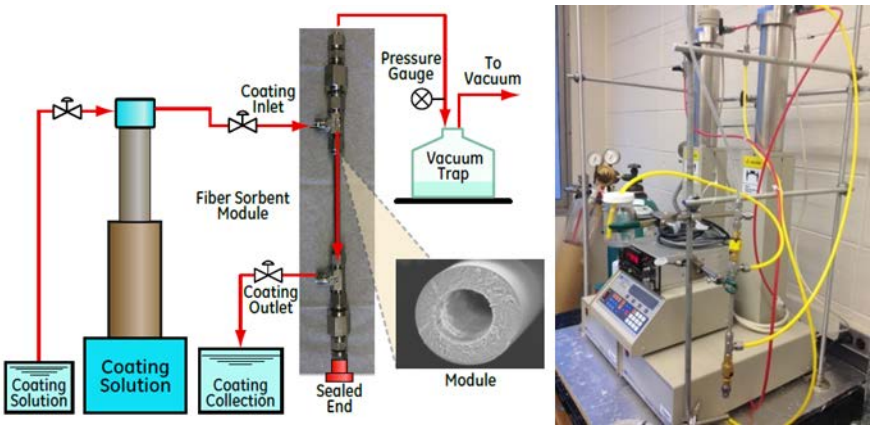

Figure 64. Developed batch coating setup at Georgia Tech.

Two PDMS cross-link approaches were employed in this study. In the first approach, PDMS/PAI HF modules were dried in a pre-heated vacuum oven at 70 °C for 3 h as has been done before. The second approach was developed in this study. Through this process, the PDMS/PAI hollow fibers were dried in the hood overnight at room temperature. Finally, the fibers were incorporated into modules, and the gas permeances were measured after post-treatment. Gas transport results for CO_2 were typically found to be around 1100 GPU with PDMS intrinsic selectivity for most of the fibers. Note that the intrinsic PDMS selectivity for CO_2 over N_2 is 11.6 at ambient temperature. For PDMS concentration in the range of 1-2 wt% solutions, slightly lower gas selectivity is obtained for roughly 20% of the fibers in comparison with the PDMS intrinsic selectivity (11.6), indicating that the coating layer has some minor defects. SEM images of the cross-section and the surface of PDMS/PAI composite hollow fibers are presented in Figure 65 a and b, respectively. The thickness of the PDMS on top of the 20-50 nm pore size Torlon® HF support layer (SEM) was about 2 µm. For all prepared membranes, we also calculated αCO_2 /N_2 in order to check the quality of the PDMS layer. For all composite PDMS/Torlon® HF membranes, the αCO_2 /N_2 was above 8 for 2 wt% PDMS in hexane (the ideal αCO_2 /N_2 is 11.3) showing a good quality of the PDMS coating.

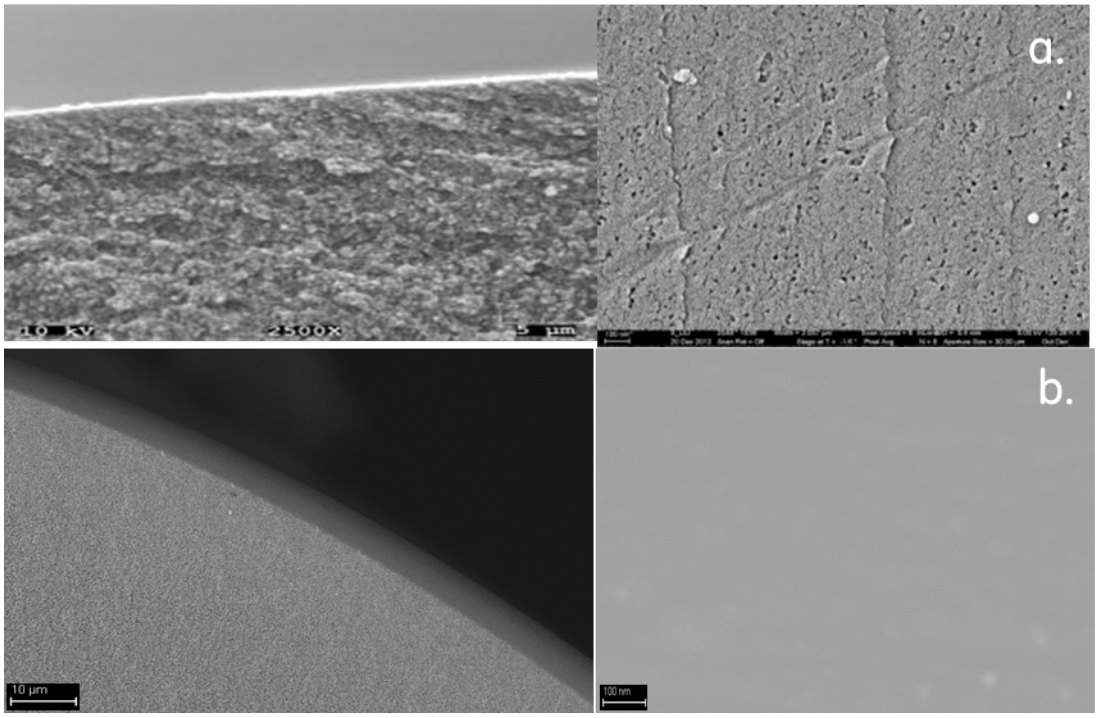

Figure 65. Scanning electron microscopy (SEM) images of outer layer cross-section and top-down (surface) of bare Torlon®® HF (a), PDMS/Torlon® composite HF membrane (b).

The gas transport properties of PDMS/PAI composite membranes were also affected by the crosslinking post-treatment temperature (Figure 66). We found that higher post treatment temperatures (> 70 C) of PDMS/ could lead to substructure collapse, which decreased both permeance and selectivity (Figure 66a). Crosslinking at a low temperature resulted in a higher CO_2 /N_2 selectivity and permeance (Figure 66b). The optimal crosslinking temperature for achieving an adequate permeance at intrinsic CO_2 /N_2 selectivity of PDMS solutions depended on the type of solvent applied for pre-crosslinking solutions. We found the suitable temperature for PDMS crosslinking was about 25 °C (ambient condition). A further increase in temperature yielded lower flux value as well as lower CO_2 /N_2 selectivities for the PDMS/PAI composite membranes (Figure 66a). In this research, the PDMS coating was conducted using a dip coating and ambient temperature crosslinking procedure to examine the skin integrity of fibers.

The skin integrity of PDMS deposited on bare hollow fibers, which had only Knudsen selectivity, was confirmed by comparison to the intrinsic selectivity of PDMS. The PDMS caulked fibers showed CO_2 /N_2 selectivity of 8.36, reflecting the porous nature of the bare fibers, and the efficacy of the PDMS coating. These results clearly show that the development of high flux support membranes with uniform surface porosity and the preparation and crosslinking of the PDMS selective layer for making composite membranes was achieved. Such PDMS/Torlon® composite membranes were used for the subsequent deposition of more selective layers on the intermediate PDMS layer.

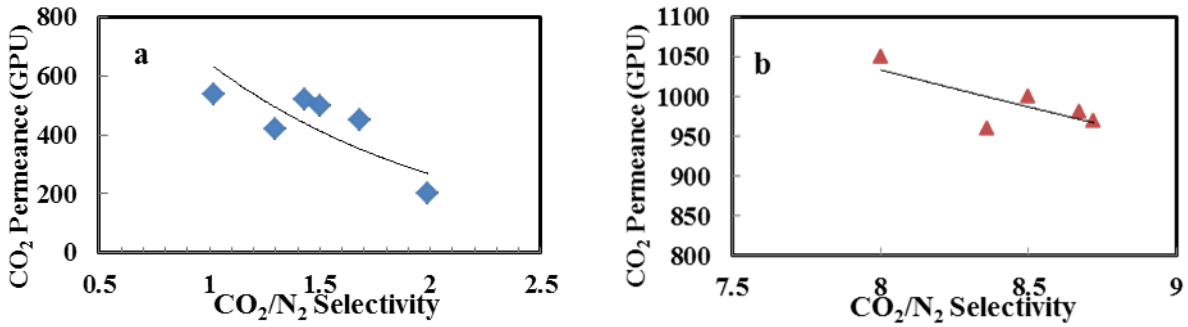

Figure 66. Transport properties of PDMS/Torlon® composite hollow fiber membranes: (a) Thermally cured at 70 °C under vacuum, and (b) crosslinked at ambient temperature and pressure. Tested at 35 psig and 35°C (Note that GPU refers to 1* 10-6 cc(STP)/(cm2 s cmHg). Lines are drawn to indicate the trend and are not model fits.

MEEP solution (5% in ethanol) preparation protocol

One gram of 80% Pure 2-(2-methoxyethoxy) ethanol phosphazene (MEEP; synthesized by INL) polymer was added to a 40 mL glass jar equipped with a stir bar, 19 grams of ethanol was added and the mixture was sealed and stirred overnight at room temperature to form a homogeneous solution mixture. Then 20 milligrams of initiator AIBN was added (2 wt% based on polymer) and allowed to dissolve overnight in ethanol to form the coating solution for preparation of MEEP/PDMS/PAI composite hollow fiber membranes.

Coating and ozone crosslinking of MEEP on the PDMS/PAI composite hollow fiber membrane

PDMS/PAI composite hollow fiber in the module was soaked in the 5 wt. % MEEP in ethanol solution. Subsequently, unlike the simple dip coating for the PDMS, vacuum is applied to the bore side (760 torr) for a very short time (1-2 min) in order to obtain a defect-free and thin coating layer. We found that higher crosslinking temperatures of MEEP/PDMS/PAI composite membranes developed defective skin and substructure collapse which tended to decrease both permeance and selectivity. On the basis of our experimental results, we found that the suitable temperature for PDMS and MEEP crosslinking is around ambient temperature. To avoid high temperature crosslinking, MEEP/PDMS/PAI composite hollow fiber modules were dried and crosslinked in the presence of 0.005-0.010 ppm ozone for 10-120 min in ambient temperature. After this step, CO_2 /N_2 selectivity was significantly higher than the PDMS/PAI composite hollow fiber. Table 31 compares the MEEP/PDMS thickness visualized by SEM and the CO_2 and N_2 permeance measurements, assuming that the gas transport is determined by the MEEP/PDMS coating layers. Clearly optimization of the above steps can allow creating thinner selective layers. In-situ coating with the 5 wt. % MEEP in ethanol solution has been carried out on different spin - states of Torlon® hollow fiber with different surface porosity and morphology by using a syringe pump and pulling vacuum from the bore side.

Fibers with MEEP coating showed higher selectivity than fibers coated with PDMS. MEEP/PDMS/PAI composite hollow fibers also showed higher flux than cases using only MEEP. The transport property of Torlon® fibers was confirmed by MEEP/PDMS coating and drying at ambient temperature in the presence of ozone (0.5-1 ppm for 10-120 min) and the caulked

fibers showed higher selectivities. Ozone is a powerful oxidizing agent, far stronger than O2. It is also unstable at high concentrations, decaying to ordinary diatomic oxygen. Ozone reacts directly with organic double bonds. Also, when ozone breaks down to dioxygen it gives rise to oxygen free radicals, which are highly reactive and possible sources for crosslinking initiators.

Table 31. Pure gas CO_2 and N_2 permeation results for Torlon® hollow fibers after MEEP/PDMS post-treating. Test at 35 psig used at 35°C.*

Module ID	Post-treatment processes	$\alpha CO_2/N_2$	CO_2 (P/l) (GPU)	N_2 (P/l) (GPU)
ARS12-562-St.1	Coated in 2 wt.% PDMS, crosslinked in the precent of O_3 at ambient temperature	8.19	69	8
ARS12-562-St.1	Coated in 5 wt.% MEEP in ethanol solution, dried at ambient temperature in the present of ozone for 1h	22.40	37	2
ARS2-577-St.4	Coated in 2 wt.% PDMS, crosslinked in the precent of O_3 at ambient temperature	3.32	21	6
ARS2-577-St.4	Coated in 5 wt.% MEEP in ethanol solution, dried at ambient temperature in the present of ozone for 1h	20.62	15	1
ARS2-543-St. 7	Coated in 2 wt.% PDMS, crosslinked in the precent of O3 at ambient temperature	7.38	1050	140
ARS2-543-St. 7	Coated in 5 wt.% MEEP in ethanol solution, dried at ambient temperature in the present of ozone for 1h	27.32	83	3
ARS2-546-St. 7	Coated in 2 wt.% PDMS, crosslinked in the precent of O3 at ambient temperature	7.72	970	130
ARS2-546-St. 7	Coated in 5 wt.% MEEP in ethanol solution, dried at ambient temperature in the present of ozone for 1h	21.55	960	45

Note that GPU refers to 1 10-6 cc(STP)/(cm2 s cmHg).

Typical SEM images of the cross-section of the MEEP/PDMS/PAI are shown in Figure 67. Re-measured values of the gas permeance are also shown and indicate CO_2 permeance of the MEEP/PDMS/PAI composite hollow fiber to be about 964 GPU with CO_2 /N_2 selectivity as high as 21.6, which is close to the MEEP intrinsic selectivity.

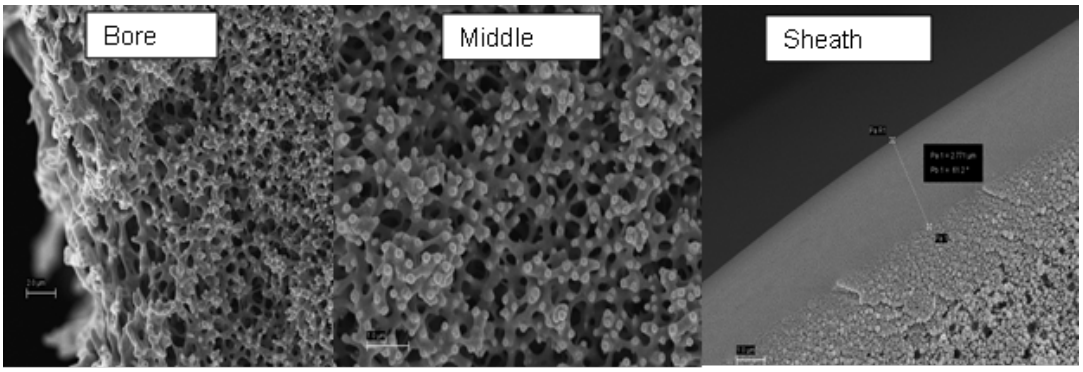

Figure 67. SEM images of MEEP/PDMS/PAI composite hollow fibers (sheath side).

Sequential coating and simultaneous crosslinking of the PDMS and MEEP on Torlon® hollow fiber membrane

We demonstrated a method of making composite hollow fiber membranes by forming an intermediate layer upon the engineered hollow fiber porous support and sequentially coupling a selective layer coating solution upon the intermediate layer. Both coating solutions were then crosslinked, respectively. We demonstrated a process for sequential coating of PDMS and MEEP on the highly porous hollow fiber support surface and simultaneous crosslinking of both rubbery polymers in the presence of 0.005-0.010 ppm ozone for 10-120 min in ambient temperature.

Through this process, first, bare Torlon® HF's were coated in 2 wt. % solution of PDMS in hexane. In the second step, PDMS/PAI HF modules were used for in-situ coating of 5 wt. % solution of MEEP in ethanol on top of the PDMS/Torlon® composite hollow fiber membrane. The MEEP/PDMS coated Torlon® HF's were then exposed to an ozone (0.005-0.01 ppm O3 for 10-120 min) treatment at ambient temperature to crosslink both polymers. Results from gas transport suggest that the MEEP/PDMS was successfully crosslinked on the porous Torlon® hollow fiber support with a 40 min ozone exposure (See Table 32). The new MEEP/PDMS/PAI composite hollow fiber membrane exhibited the intrinsic selectivity of phosphazene ($\alpha CO_2/N_2$= 20-28) and a permeate flux up to 1500 GPU, which is significantly higher selectity than that those obtained from PDMS membranes without the MEEP coating. In summary, we have described a novel technique that could lead to improved stability or crosslinking of two rubbery polymers simultaneously in the presence of ozone.

Table 32. Pure gas CO_2 and N_2 permeation results for Torlon® hollow fibers after MEEP coating and PDMS re-caulking with subsequent crosslinking of both MEEP & PDMS. Test at 35 psig used at 35°C.

Module ID	Post-treatment processes	$\alpha CO_2/N_2$	CO_2 (P/l) (GPU)	N_2 (P/l) (GPU)
ARS18-618-St.4	Dip coated in 2 wt.% PDMS in hexane, then in-situ coated in 5 wt.% MEEP in ethanol and finally crosslinked in the presence O_3 at ambient temperature	28.04	11.9	0.4
ARS18-620-St.3	Dip coated in 2 wt.% PDMS in hexane, then in-situ coated in 5 wt.% MEEP in ethanol and finally crosslinked in the presence O_3 at ambient temperature	24.40	23.2	0.9
ARS2-550-St.7	Dip coated in 2 wt.% PDMS in hexane, then in-situ coated in 5 wt.% MEEP in ethanol and finally crosslinked in the presence O_3 at ambient temperature	30.30	55.2	1.8
ARS18-630-St.2	Dip coated in 2 wt.% PDMS in hexane, then in-situ coated in 5 wt.% MEEP in ethanol and finally crosslinked in the presence O_3 at ambient temperature	28.52	37.0	1.3

The MEEP/PDMS/PAI composite hollow fiber membranes in Table 31 and Table 32 show attractive selectivity for post-combustion CO_2 capture. Through these new coating processes, different bare Torlon® HF's with various sheath porosities and gas permeances can be coated with CO_2 permeance up to 1000 GPU for CO_2 . An intermediate layer (PDMS) with a selective layer (MEEP) coating with crosslinking's at ambient temperature improved the selectivity with a higher flux over a MEEP-only coating solution. SEM images of the cross-section of the MEEP/PDMS/PAI composite membrane are shown in CλΞdzŴŜcy. On the basis of our experimental results, we found that ambient crosslinking temperature was best for the PDMS and MEEP in the presence of O3. Although defect-free MEEP/PDMS/PAI composite hollow fibers have yielded higher fluxes and selectivities to CO_2 , concerns about possible damage to the MEEP coating due to ozone exposure led us to terminate this approach to avoid possible long term stability issues.

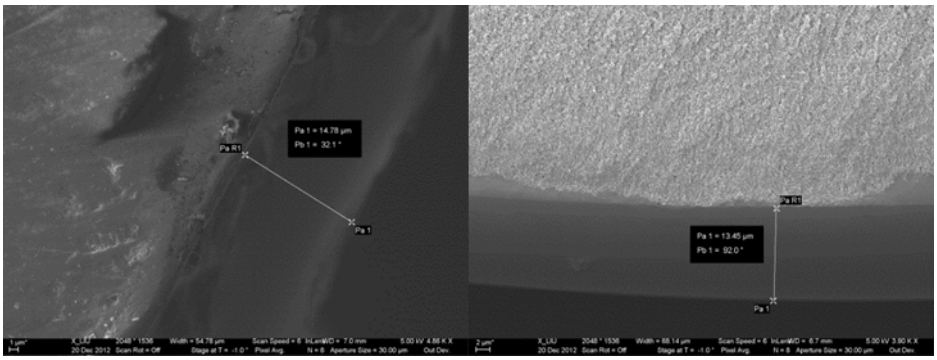

Figure 68. SEM images of MEEP/PDMS/PAI composite hollow fibers (sheath side).

Direct MEEP coating on a lower permeance and smaller pore size hollow fiber module

The aim of this part of the study was to prepare composite hollow fiber membranes to further tune the coating layer thickness to 0.1 µm, minimize defects in multi-fiber modules, and identify the path to defect-free coated hollow fibers using the in situ direct hollow fiber module coating process. We completed a systematic investigation of the parameters that are important to prepare a stable, defect-free MEEP/PAI composite membrane. The key process parameters explored included: fiber pre-wetting in ethanol, direct MEEP coating, circulating MEEP flow rate and coating time, drying process and the number of coating steps in combination with the support pore size in these steps. Based on these tests, correlation between the process variables and the membrane integrity were established. The optimum concentration of the MEEP coating (5 wt% solution) was flushed through the PAI-HF module for about 2 minute with 1 torr inside the module bores during the circulation of MEEP solution. The coated HF module was left at ambient temperature overnight then dried in the pre-heated conventional oven at 110 °C for 10 min and 3 h to complete the cross-linking process. After this step, the module displayed a slightly higher CO_2 /N_2 selectivity than the uncoated fiber module but still lower than the MEEP intrinsic selectivity, indicating that the coating is incomplete (See Table 33). The second round of the direct MEEP coating showed a significantly higher CO_2 /N_2 selectivity. The permeation results of 5%MEEP/PAI HF are listed in Table 33. However, as the results show, CO_2 selectivity decreased significantly due to physical aging after one month. In addition, the

MEEP/HF module dried at 110 °C for 10 min resulted in a significantly lower selectivity as compared with the same MEEP/HF module that was dried at 110 °C for 3 h. Pre-wetting of PAI-HF with ethanol and direct coating of MEEP on PAI-HF decreased the gas permeation dramatically and should be avoided.

Table 33. Effect of direct MEEP coating on the gas transport properties in MEEP/PAI material (5 wt. % 0082 solution).

Module	Selectivity CO_2 /N_2	CO_2 (P/l) (GPU)	N_2 (P/l) (GPU)
ARS10-367-St.4 (Dried at 110 °C for 3 h)			
Neat PAI fibers	0.97	8480	8708
First MEEP/PAI	0.94	4954	5250
Second MEEP/PAI	40.7	86	2
After 1 month	1.62	176	109
ARS2-384-St.1 (Dried at 110 °C for 3 h)			
Neat PAI fibers	0.9	5657	6281
First MEEP/PAI	0.93	174	187
First MEEP/PAI	22.35	17.21	0.77
After 1 month	4.82	2.28	0.47
ARS10-409-St.4 (Dried at 110 °C for 10 min)			
Neat PAI fibers	0.97	8480	8708
First MEEP/PAI	0.9	114	127
Second MEEP/PAI	1.62	2	1

Characterization of MEEP/PDMS/PAI hollow fiber (HF) composite membrane after long term testing at WRI:

Pure gas permeation was carried out and the results are shown in Table 34. The results from long term testing for flue gas post combustion CO_2 capture at WRI on this same module also verified low CO_2 permeance but no N_2 and O2 permeance at 35 °C and 60 °C at 30 psi for 320 h. In order to investigate the differences in fiber structure, SEM characterization was performed on the samples used for permeation results. Figure 69 shows SEM images of the cross section (sheath side, middle and bore side) of the hollow fiber membrane returned by WRI. Figure 15 compares the MEEP/PDMS thickness visualized by SEM of about 200 nm and the CO_2 and N_2 permeance measurements (Table 34), assuming that the gas transport is determined by the MEEP/PDMS coating layers with intrusion of MEEP/PDMS solution into hollow fiber support. Increasing the coating layer thickness caused the reduced permeance of the membrane. SEM images of top view confirmed that the all pores are well-coated in the

outer regime. Inspection of the module after its testing suggested that some fibers were "clumped" together (Figure 70), possibly during in-situ coating. Solution to this potential problem would require more investigation.

Table 34. Gas transport properties of module 230 (5 wt% MEEP/2 wt% PDMS/PAI composite HF membrane).

35 C, 30 psid pure gas	Number of fibers	$\alpha CO_2/N_2$	CO_2 (GPU)	N_2 (GPU)
ARS9-230-ST.5	3	37.41	2.21	0.1

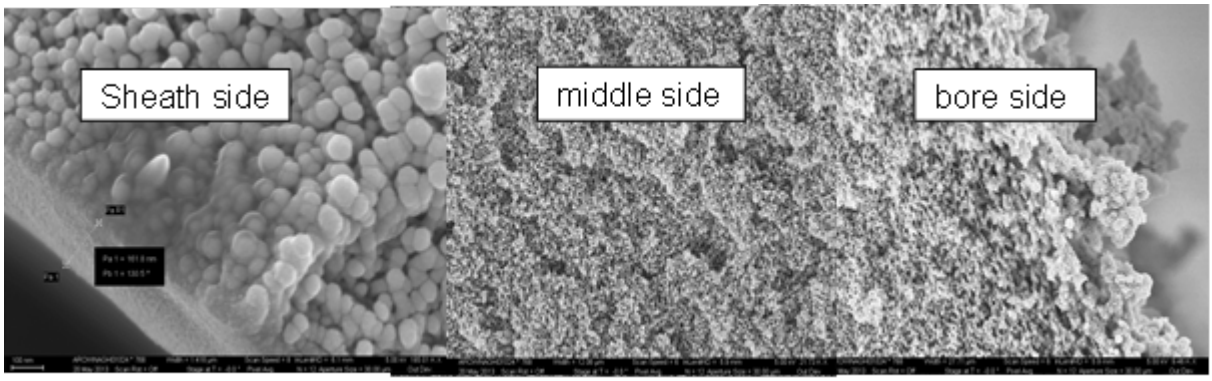

Figure 69. SEM images-cross section module 230 (5 wt%MEEP/2wt%PDMS Torlon® HF membrane).

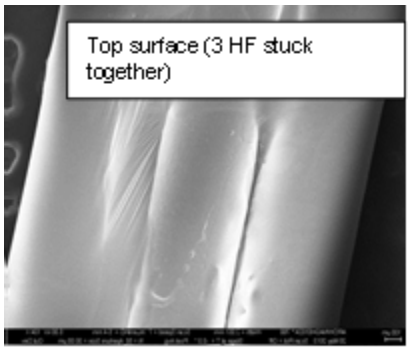

Figure 70. SEM images-top surface of module 230 (5 wt%MEEP/2wt%PDMS Torlon® HF membrane)

The effect of physical aging on the permeation of CO_2 through a MEEP/PAI HF membrane

The effect of physical aging on gas transport can be quite significant in asymmetric hollow fiber membranes compared to flat dense films. The primary objective of this study is to highlight the physical aging of MEEP/PAI HF composite membrane at ambient temperature. Single gas (N_2 and CO_2) permeation was carried out and the results are shown in Table 35. To the best of our knowledge, the work presented here is the first study on the effect of physical aging on the permeation of a plasticizing gas through MEEP/PAI HF composite membranes.

Table 35. Effect of physical aging on carbon dioxide permeation and selectivity through MEEP/PAI hollow fiber membranes at 30 psig and 35 °C (5 wt % 0082 solution).

Module ID	Coating process	α CO_2 /N_2	CO_2 (P/l) (GPU)	N_2 (P/l) (GPU)
ARS2-305-St.4	MEEP-00-82	51.39	149	3
ARS2-305-St.4	MEEP-00-82	1.43	132	92
ARS2-305-St.4	MEEP-00-82	1.35	12	9
ARS2-305-St.4	PDMS-30 PSI	1.96	6	3

The study of the gas transport properties in MEEP/PAI hollow fiber membrane has shown asymptotic reduction in both gas permeance and CO_2 selectivity with time. The time-dependent gas transport properties illustrated above are a result of some complex physical aging. Physical aging is a well-known phenomenon in glassy polymers that results from their nonequilibrium nature. However, such effects are not expected in rubbery polymers such as MEEP. The gas properties results show a slightly higher CO_2 /N_2 selectivity and a lower flux for an additional PDMS top coating on MEEP/PAI HF module. While not proven definitely, we suspect that the apparent physical aging reflects migration of some incompletely crosslinked MEEP chains into the PDMS and even the Torlon® support, thereby generating defects during long term exposure to feed gas. More effective crosslinking of the MEEP may solve this problem and should be pursued in the future.

The effect of pure ethanol on Torlon® HF gas permeance

Torlon® 4000T polyamide-imide was chosen as the substructure material because it brings together superior mechanical properties typically associated with polyamides, which are high thermal stability, solvent resistance and gas permeability. In order to evaluate the impact of pure ethanol on bare Torlon® HF characteristics, a couple of HF modules were constructed and the following experimental steps were carried out to verify this effect:

- Prepared 8 modules (2 fibers in each) with bare Torlon® fibers, with different permeance (4000-17000 GPU) and spin state
- Measured bare fiber performance
- Poured ethanol in the module and let it soak for 5 min
- Decanted the solution
- Left HF modules overnight at ambient conditions
- Dried the modules at different conditions (i) 110 °C for 3 h in conventional oven; (ii) 80 °C for 3 h in vacuum oven
- Measured the gas permeance after post-treatment.

Table 36. Effect of ethanol on Torlon® HF gas permeance.

Module ID	Post-treatment conditions	$\alpha CO_2/N_2$	CO_2 (P/l) (GPU)	N_2 (P/l) (GPU)
ARS2-417-St. 7	Bare HF (3 min epoxy; DP 100)	0.85	14333	16813
ARS2-417-St. 7	Soaked 5 min in ethanol, dry overnight then 3 h at 110 °C in conventional oven	0.82	6057	7407
ARS2-418-St. 7	Bare HF (high temperature epoxy; DURALCO 4540N)	0.86	12093	14115
ARS2-418-St. 7	Soaked 5 min in ethanol, dry overnight and then 3 h at 80 °C in vacuum oven	0.87	6863	7880
ARS2-419-St. 7	Bare HF (3 min epoxy; DP 100)	0.85	8496	10045
ARS2-419-St. 7	Soaked 5 min in ethanol, dry overnight then 3 h at 110 °C in conventional oven	0.93	3629	3885
ARS2-420-St. 7	Bare HF (high temperature epoxy; DURALCO 4540N)	0.85	12564	14752
ARS2-420-St. 7	Soaked 5 min in ethanol, dry overnight and then 3 h at 80 °C in vacuum oven	0.88	6030	6844
ARS2-421-St. 8	Bare HF (high temperature epoxy; DURALCO 4540N)	0.9	7171	7956
ARS2-421-St. 8	Soaked 5 min in ethanol, dry overnight then 3 h at 110 °C in conventional oven	0.97	286	296
ARS2-422-St. 8	Bare HF (high temperature epoxy; DURALCO 4540N)	0.8	4802	5974
ARS2-422-St. 8	Soaked 5 min in ethanol, dry overnight and then 3 h at 80 °C in vacuum oven	0.6	26	43
ARS14-423-St. 3	Bare HF (high temperature epoxy; DURALCO 4540N)	1.02	16531	5974
ARS14-423-St. 3	Soaked 5 min in ethanol, dry overnight then 3 h at 110 °C in conventional oven	1.01	8439	8387
ARS14-424-St. 3	Bare HF (high temperature epoxy; DURALCO 4540N)	1	20213	20304
ARS14-424-St. 3	Soaked 5 min in ethanol, dry overnight and then 3 h at 80 °C in vacuum oven	0.97	7014	7230

This study was intended to be a "control" experiment to show that exposure of the robust Torlon® would not be affected by the ethanol used for making MEEP solution and coating. The results were surprising and are not yet understood.

Pure gas permeation measurements were carried out before and after treatment and the results have been shown in Table 36. As can be seen, the PAI-HF modules soaked in ethanol for 5 min resulted in significantly lower gas permeation compared to the bare fiber module.

We found that (i) pre-wetting of PAI-HF with ethanol, and (ii) direct coating of MEEP on PAI-HF decreased the gas permeation dramatically. In addition, the study of the gas transport properties in MEEP/PAI hollow fiber membrane showed asymptotic reduction in CO_2 selectivity over a time period.

Task 5: Test Membranes at Bench-Scale in Coal Flue Gas

Georgia Tech testing

Georgia Tech designed and constructed a membrane fouling analysis set-up to investigate the fouling potential of phosphazene materials in a controlled environment. Figure 71 shows the developed membrane fouling analysis set-up process flow diagram. The unit was used to test the best performing membranes with a non-adhesive surface under dry and humid conditions to detect possible problems prior to actual coal flue gas testing. Aging of composite hollow fiber membranes should be small in the absence of the hypothesized diffusion of the partially uncrosslinked MEEP into the fiber support. Aging was assessed by characterizing the flux decline and changes in selectivity by exposure to the clean, dry pure CO_2 stream. Feedback on polymer material and coating solution properties was provided to INL for material improvements and feedback from both the membrane testing and actual coal flue gas testing will be used to further adjust and optimize coating solution properties.

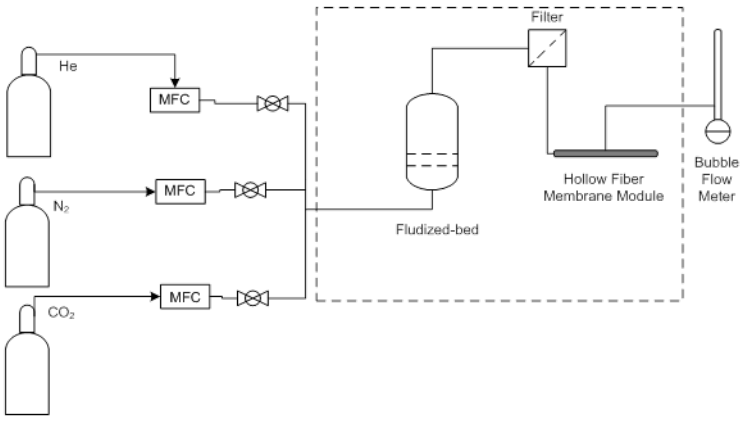

Figure 71 Process Flow Diagram of Membrane Fouling Analysis Set-up.

The membrane fouling analysis set-up test unit consists of a 1) fluidized bed of Bitumen fly ash (provided by WRI); 2) A cyclone (filter) separator which has been positioned after the

fluidized bed to cut-off fly ash particles larger than 10 µm (i.e., fractions between 0.5 and 10 µm).

The fouling potential of phosphazene materials in a controlled environment has been carried out by using bituminous fly ash on MEEP/PMS/PAI membrane. The effect of bituminous fly ash on the composite hollow fiber membrane performance was determined by pure N_2 and CO_2 feed gas streams at 35 °C and 35 psig pressure. Composite coated hollow fiber membranes have been used for the long term exposure tests. Therefore, the system was allowed to flow for 120 h on-stream for each gas. The CO_2 /N_2 selectivities and fluxes have been in-situ measured in the presence of Bitumen fly ash (Figure 72). It is clear that the presence of fly ash in the feed gas streams did not affect the membrane performance. The particular membrane tested was not as high as some of the more recent membranes that have been formed; however, it serves the purpose of showing the desired stability against fly ash. More studies regarding the fouling potential on new batches of phosphazene materials and their quality as membrane outer selective layers in direct contact with flue gas is required.

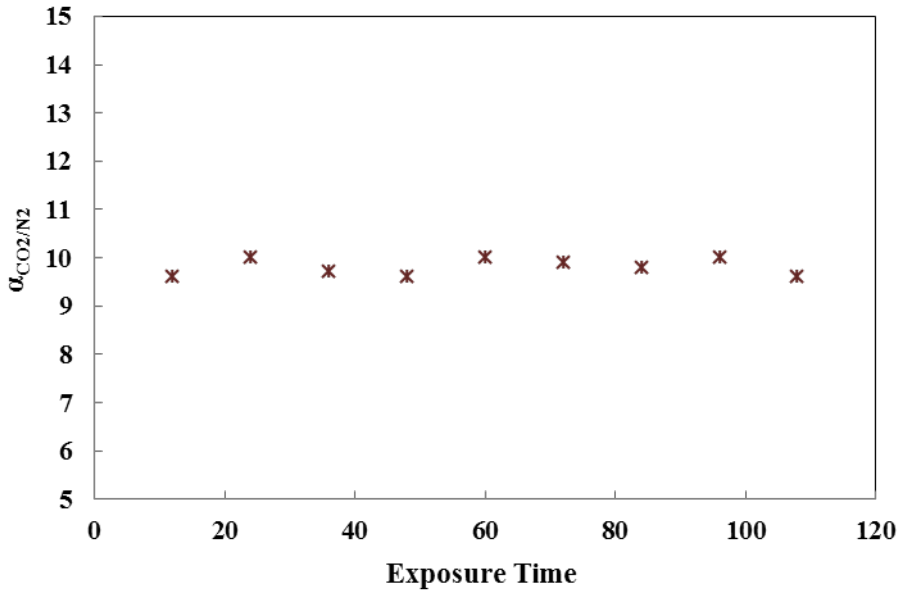

Figure 72 In-situ gas transport properties of composite MEEP/PDMS/PAI HF membrane with exposure to fly ash. Test at 35 psig used at 35°C (Note that GPU refers to 1* 10-6 cc(STP)/(cm2 s cmHg).

Effect of water/gas mixtures on gas transport properties of MEEP/PDMS/PAI composite HF (module 391)

As part of a mutual collaboration between Georgia Tech, GE and INL, the membrane unit developed by Georgia Tech was used for additional evaluation of the membrane system to remove carbon dioxide from simulated water saturated CO_2 . Georgia Tech progressed towards testing membrane aging in a water-saturated pure CO_2 stream. Feedback on polymer material and composite membrane performance was shared with GE Global Research and INL for material optimization.

Figure 73 shows the process flow diagram of the set-up that was constructed at Georgia Tech. Water-saturated pure CO_2 and N_2 streams pass through the membrane modules to

ascertain the performance of the system for separating carbon dioxide from water in the gaseous stream. This set-up was constructed and is being used to test the best performing membranes for potential fouling of the membrane surface to detect possible problems prior to actual coal flue gas testing. There is one main inlet valve for the gas feed and two main exit valves: one for the retentate and the other for the permeate stream. The permeate stream is operated under ambient pressure to facilitate the selective transport of carbon dioxide across the membrane interface. Gas isolation valves for the inlet and exit of membrane module allowed for the number of modules on-line to be varied. The module was un-insulated with no heat-tracing and therefore experiments were conducted at ambient temperature. A Panametric Moisture Image Series 1-humidity/temperature probe was used to monitor the moisture in the retentate stream. A single N_2 and CO_2 feed gas stream of about 27% relative humidity was supplied to the shell side of the hollow fiber membrane in a module at about 30 psig at ambient temperature, while the shell side was being evacuated. Higher % relative humidities could be investigated in future studies, but the stability shown in this study is encouraging. The permeate flow rate was measured with a soap bubble gas flow meter. The feedback from both the membrane testing and actual coal flue gas testing could be used to further adjust and optimize coating solution properties.

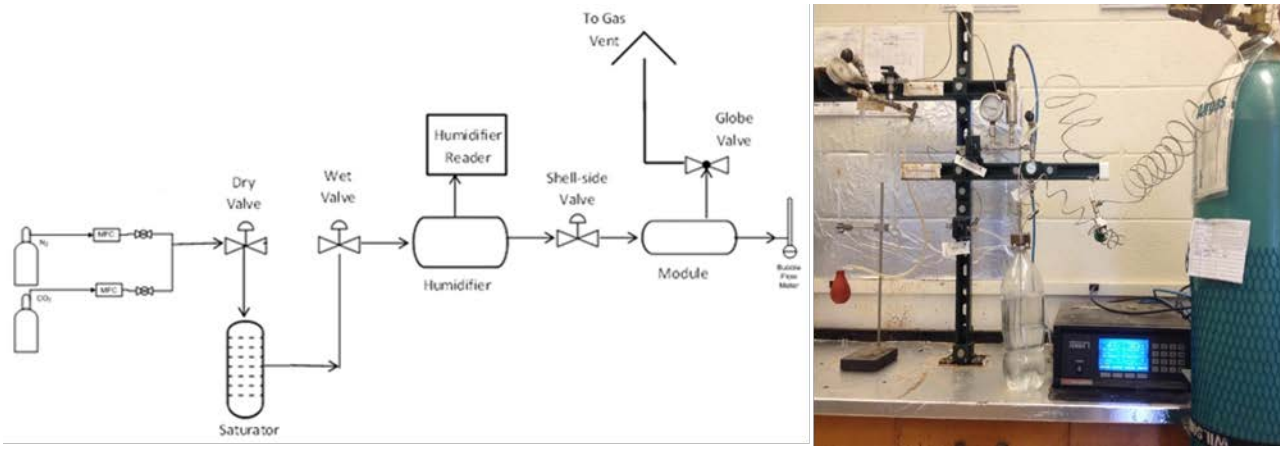

Figure 73. Process flow diagram and fouling membrane set-up for the measurement of gases vapor mixture in the pressure range 30- 60 psig at ambient temperature. The membrane fouling analysis set-up test unit consists of a 1) bubble column (saturator); 2) demister (humidifier); 3) HF module and 4) bubble flow meter.

To the best of our knowledge no study has been carried out on phosphazene hollow fiber membranes so far. A gas/vapor mixture is generated by flowing a gas stream through a bubble column and a demister. The latter separates the entrained liquid droplets from the gas stream. The wet gas stream is mixed with a dry gas stream to the desired humidity and is sent to the composite MEEP/PAI hollow fiber module. The water vapor concentration in this stream is controlled by adjusting the flow rates of the dry and wet stream with the respective mass flow controllers. This gas mixture flows over a polymeric hollow fiber membrane mounted in a membrane module and leaves the system via a back pressure regulator, which controls the total pressure in the system. The flow rate of the stream leaving the membrane hollow fiber module is measured with a soap bubble meter. The potential fouling of phosphazene materials

in a controlled environment has been evaluated in MEEP/ PAI membrane module. The effect of wet CO_2 on the 5%MEEP/PAI hollow fiber membrane was determined at ambient temperature during exposure tests at 30, 45 and 60 psig pressures. Before exposure, the membrane permeation performance was determined by pure CO_2 gas feed stream permeation rates. Module 391 has been used for the wet N_2/CO_2 exposure tests. Therefore, the module has been in-situ measured for gas permeance in the presence of water. The permeation results of module ARS9-391 membrane before and after exposure at different pressures (i.e., 30, 45, 60 psig) are listed in Table 37.

Table 37. Gas transport properties of 5%MEEP/PAI HF with dry and wet gases at different pressures exposure.

					Test conditions		
Module ID	Coating process	$\alpha CO_2/N_2$	CO_2 (P/l) (GPU)	N_2 (P/l) (GPU	Humidity (%)	T (°C)	P (psig)
ARS9-391-St.1	Bare HF	0.82	2682.7	3279.3	-	35	30
ARS9-391-St.1	First MEEP-0082	0.86	648.5	758.1	-	35	30
ARS9-391-St.1	Second MEEP-0082	10.73	43.1	4	-	35	30
ARS9-391-St.1	Third MEEP-0082	24.04	22.36	0. 93	-	35	30
ARS9-391-St.1	-	23.98	13.43	0.56	27.3	22.5	30
ARS9-391-St.1	-	24.27	14.81	0.61	27.2	22.5	45
ARS9-391-St.1	-	24.19	15.24	0.63	27.2	22.5	60

As the results show, CO_2 permeation and total permeate flow rate increase with greater CO_2 feed pressure. Moreover, higher relative humidity and lower temperature enhance separation efficiency. It must be noted that these findings are still preliminary in nature. Further refinement of the information should be detailed in a future study. The CO_2 permeance and CO_2/N_2 selectivity (initially 24.43) were maintained around 13.4 and 24, respectively after 24 h of exposure to gases containing water at different pressures at 22.5 °C. Similarly, the N_2 permeance of the 5%MEEP/PAI membrane decreased from 0.9 to 0.6 upon exposure to a pure gas containing water at 30 psig total pressure at 22.5 °C. More study however needs to be performed to evaluate the potential fouling of phosphazene materials and quality as a membrane outer selective layer in direct contact with flue gas.

MEEP/PDMS/PAI Composite Hollow Fiber Membrane Long-Term Stability

The long-term permeance and CO_2/N_2 selectivity stability of MEEP/PDMS/PAI composite membranes is important for integration in real-world industrial applications. Therefore, long-term stability evaluation was carried out by retesting composite membranes via permeation measurements with CO_2 and N_2. At 35 °C and 35 psig, CO_2 and N_2 permeating fluxes through MEEP/PDMS/PAI membranes are given as a function of process time (Table 38 and Figure 74). Unfortunately, it is evident that CO_2/N_2 selectivities and fluxes through all membranes are unstable for long-time operation under the same operating conditions. The CO_2/N_2 selectivity of the MEEP/PDMS/PAI membrane dropped from ~30 to less than 2 after 96 h of

retesting. As noted earlier in the discussion of the aging effects, we hypothesize that these instabilities reflect migration of insufficiently crosslinked MEEP chains that ultimately lead to defects in the composite coating.

Table 38. Transport properties of MEEP/PDMS/Torlon® composite hollow fiber membranes after 24, 48 and 72 h. Tested at 35 psig used at 35°C.

Module ID	$\alpha CO_2/N_2$	CO_2 (P/l) (GPU)[1]	N_2 (P/l) (GPU)[1]	Processing Time (h)
ARS8-724-St.7	20.92	159	7.6	24
ARS8-724-St.7	15.75	200	12.7	48
ARS8-724-St.7	1.22	256.3	210	96
ARS8-720-St.7	20.72	51.8	2.5	24
ARS8-720-St.7	13.89	100	7.2	48
ARS8-720-St.7	7.59	180	23.7	96
ARS8-719-St.7	22.53	72.1	3.2	24
ARS8-719-St.7	17.38	73	4.2	48
ARS8-719-St.7	5.71	120	21	96
ARS8-718-St.7	34.10	34.1	1	24
ARS8-718-St.7	20.63	66	3.2	48
ARS8-718-St.7	8.28	96	11.6	96
ARS3-691-St.1	33.33	130	3.9	24
ARS3-691-St.1	24.83	114.2	4.6	48
ARS3-691-St.1	1.19	248.1	208.8	96
1 Note that GPU refers to 1* 10-6 cc(STP)/(cm2 s cmHg				

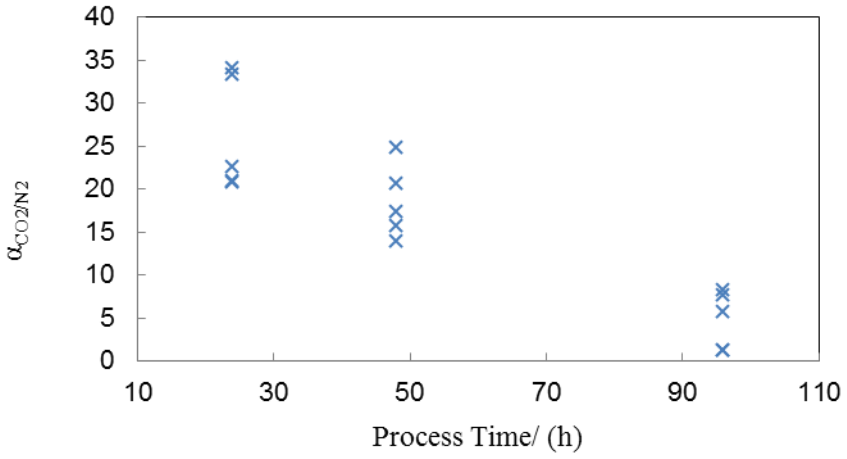

Figure 74. Transport properties of MEEP/PDMS/Torlon® composite hollow fiber membranes as a function of process time. Tested at 35 psig used at 35°C.

WRI Test setup and conditions

The carbon dioxide separation performance of three planar polymer membranes supported on 47 mm diameter porous steel disks coated with 0.1 mm titania was testing using simulated combustion gas mixtures. The membranes were exposed to a gas composition of 80% N_2, 15% CO_2 , 5% O2 and trace amounts of SOx and NOx at 60˚C with a minimum transmembrane pressure of 30 psid. Two membrane formulations were tested: 80% MEE cross-linked with 2% benzoyl peroxide for 10 min. at 130 ^{o}C and an interpenetrating network of Poly(bisphenoxy)phosphazene and 95 % MEE/ 5% 2-allylphenol phosphazene with no cross-linking. The goal for each test was 200 hours of continuous operation.

Two tanks of mixed gas were used to provide the correct composition. The first tank was 10% oxygen in nitrogen. The second tank was 30% carbon dioxide in nitrogen with 160 ppm of nitric oxide and 100 ppm of sulfur dioxide. The gas from the first tank was passed through a 50˚ C water bath to provide humidity just below the dew point for the 60˚ C membrane test. The second tank gas was not humidified as too much loss of the acidic gases would occur in the water bath. The net gas mixture at the inlet to the membrane was 80% nitrogen, 15% carbon dioxide, 5% oxygen, 80 ppm nitric oxide and 50 ppm sulfur dioxide. The sweep gas in all testing was argon at atmospheric pressure. Flux data for carbon dioxide, nitrogen and oxygen was provided by GC measurement where possible. Nitric oxide and sulfur dioxide values were determined by gas phase FTIR.

Data analysis

The first membrane tested was an 80% MEE membrane cross-linked at 130°C. The membrane surface was somewhat tacky before testing. The membrane was heated to 60°C and pressurized to 30 psid. The initial carbon dioxide flux was 75 sccpm/m2 with selectivity versus nitrogen about 12. Over time the carbon dioxide flux increased, while the selectivity decreased. After 138 hours the carbon dioxide flux had increased to 150 sccpm/m. The nitrogen flux also increased, resulting in a selectivity decrease to 2. The test was discontinued at this point. A plot of the data is shown below, along with an image of the membrane after testing (Figure 75). Any colors visible on the surface of the membrane are reflections.

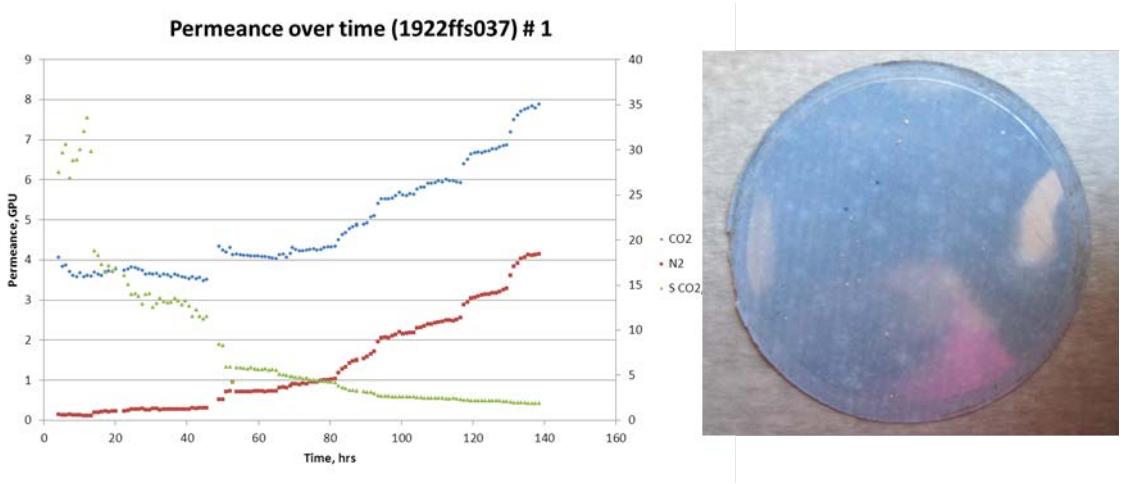

Figure 75.Permeance over time of 80% MEE membrane Photo to right is of the membrane after testing.

The second membrane tested was an interpenetrating network of Poly(bis-phenoxy)phosphazene and 95% MEE/ 5% 2-allylphenol phosphazene with no cross-linking. This membrane was not tacky before testing. Measurements for this membrane were initially taken at 30 psid and increased to 50 psid after 200 hours. The initial carbon dioxide flux was 350 sccpm/m2 and the selectivity versus nitrogen was about 9. Over time the carbon dioxide flux decreased as did the selectivity. At 200 hours the carbon dioxide flux was down to 170 sccpm/m2, and the selectivity versus nitrogen was down to 6. At this point the pressure was increased to 50 psid. The carbon dioxide flux was 240 sccpm/m2 and the selectivity versus nitrogen remained at 6. The oxygen selectivity versus nitrogen was consistent over the membrane test at between 1 and 2. Initial testing of oxygen using Draeger tubes indicated higher oxygen content, but Draeger tubes turned out to be unreliable in this gas mixture, possibly affected by humidity. A plot of the data is shown in Figure 76 below.

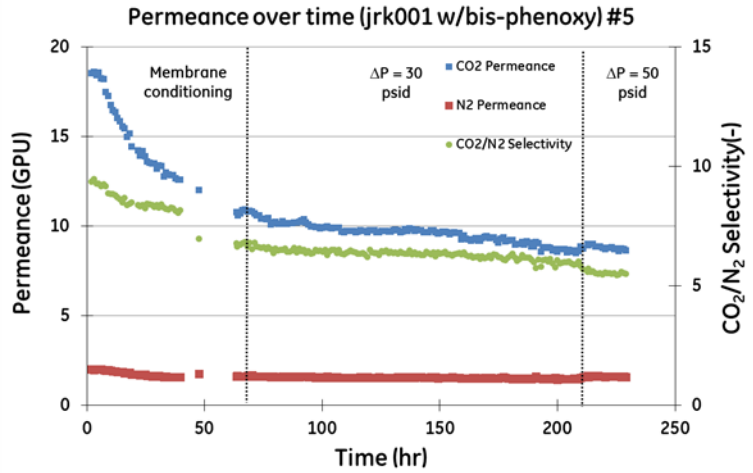

Figure 76. CO_2 and N_2 permeance and selectivity over time of IPN phosphazene membrane .

The third membrane tested was the same as membrane 6. This membrane was not tacky before testing. The test lasted for 180 hours. The pressure across the membrane was held at 30 psid for the first 140 hours. The pressure was then increased to 50 psid and held at that value from 140 to 160 hours. The pressure was then increased to 75 psid for the remainder of the test. The initial carbon dioxide flux was 350 sccpm/m2 and the selectivity versus nitrogen was about 10. Over time the carbon dioxide flux decreased somewhat as did the selectivity. At 140 hours the carbon dioxide flux was down to 325 sccpm/m2, and the selectivity versus nitrogen was down to 8. At this point the pressure was increased to 50 psid where the carbon dioxide flux was 490 sccpm/m2 and the selectivity versus nitrogen remained at 8. The increase to 75 psid increased the carbon dioxide flux to around 600 sccpm/m2, and the selectivity reduced to 6. The oxygen selectivity versus nitrogen was consistent over the membrane test at 1, or no significant selectivity. A plot of the data is shown in Figure 77 below, along with an image of the membrane after testing.

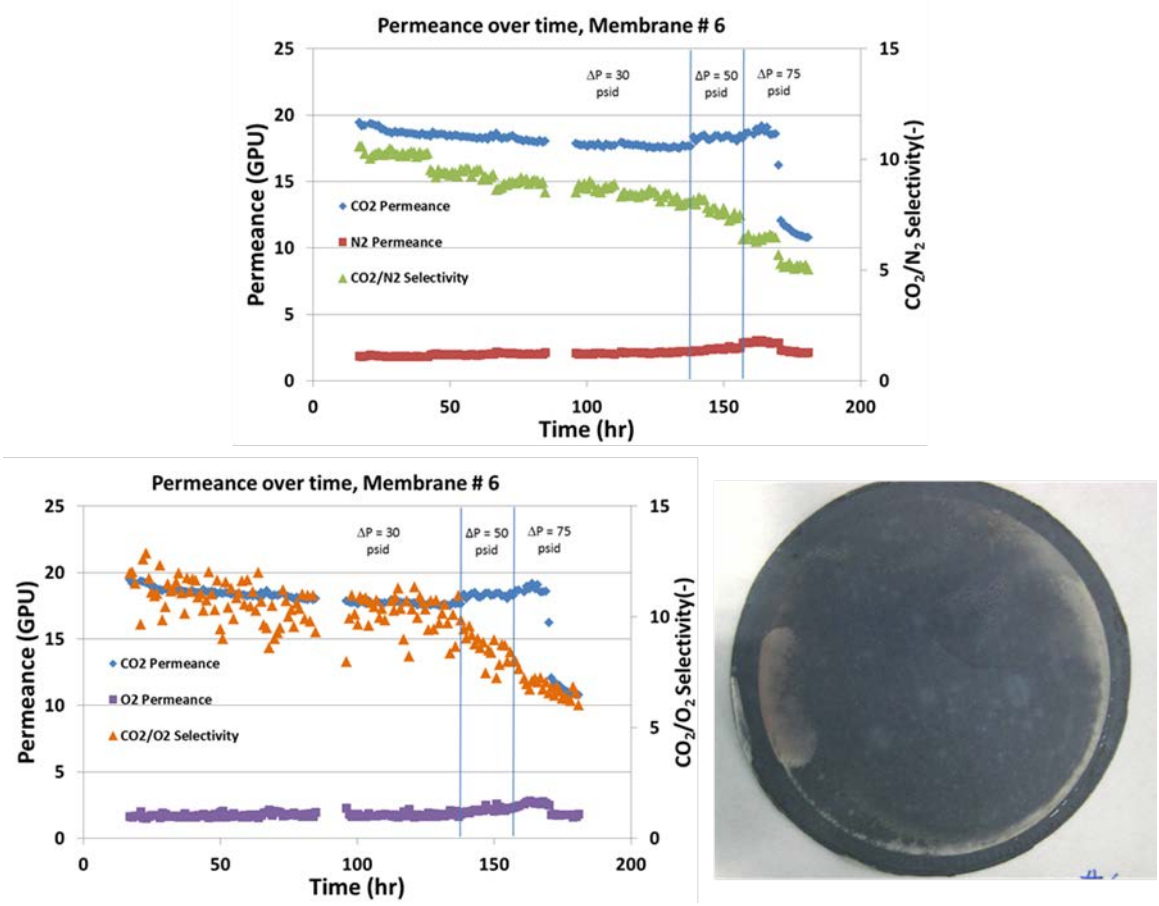

Figure 77. CO_2 , O_2, N_2 permeances and selectivities for membrane 6 Photo is for the membrane after testing.

Only one 80% MEE membrane was tested, and its properties began to degrade after 40 hours of testing, as demonstrated by the increase of both CO_2 and N_2 permeance and a corresponding decrease in CO_2 /N_2 selectivity. Both of the membranes with bis-phenoxy showed a CO_2 /N_2 selectivity from ~ 5 -10, with the selectivity decreasing over time.

In general, the phosphazene membranes showed CO_2 /N_2 selectivity from 5 – 20 prior to membrane degradation. The CO_2 permeance was between 4 and 20 GPU. As pressure across the membrane was increased to 50 psi and greater, membrane selectivity decreased. For membrane #6, O2 permeance was also measured, demonstrating a CO_2 /O2 selectivity of 5-10. It was also observed that small amounts of nitric oxide and sulfur dioxide passed through the membranes.

WRI Coal flue gas performance test composite hollow fiber membrane modules

Hollow fiber membrane modules were tested in a gas composition of 80% N_2, 15% CO_2 , 5% O_2 and trace amounts of SOx and NOx at 60˚C with a minimum pressure of 30 psid and a maximum pressure of 70 psid across the membrane.

Data analysis: 2013 Hollow Fiber Module Testing

Two hollow fiber modules 230 and 218 were sent for testing at WRI in April 2013 (Table 39). The modules each consisted of three Torlon® fibers, coated with 5 wt% PDMS solution

followed by 5 wt% MEEP solution. The MEEP polymer solution was from batch -77. The coating was thermally cross-linked at 100 ˚C for 3 hr under vacuum after application and drying.

The modules were initially tested at Ga Tech before sending. Module 230 had a low CO_2 flux but CO_2 /N_2 selectivity greater than 30. Module 218 had a lower selectivity but a higher CO_2 flux, with pure CO_2 permeance greater than 20 GPU at 350°C and 30 psig across the membrane.

Table 39.CO_2 and N_2 p permeance and selectivity for hollow fiber membranes.

Module ID	Notes	# fibers	Selectivity CO_2 /N_2	CO_2 (P/l) (GPU)	N_2 (P/l) (GPU)
ARS9-230-ST.5	5 wt% PDMS coating, 5 wt% MEEP coating on Torlon® support	3	37	2.2	0.1
ARS2-218-ST.4	5 wt% PDMS coating, 5 wt% MEEP coating on Torlon® support	3	10	23	2

Module 230 was tested with feed gas 80% N_2, 15% CO_2 , 5% O2 and trace amounts of SOx and NOx at 60 ˚C for greater than 300 hours (Figure 78 and Figure 79). For the first 160 hours, the pressure across the membrane was held at 30 psid. The membrane was started at 35 °C, then heated to 60 °C after the first 100 hours.

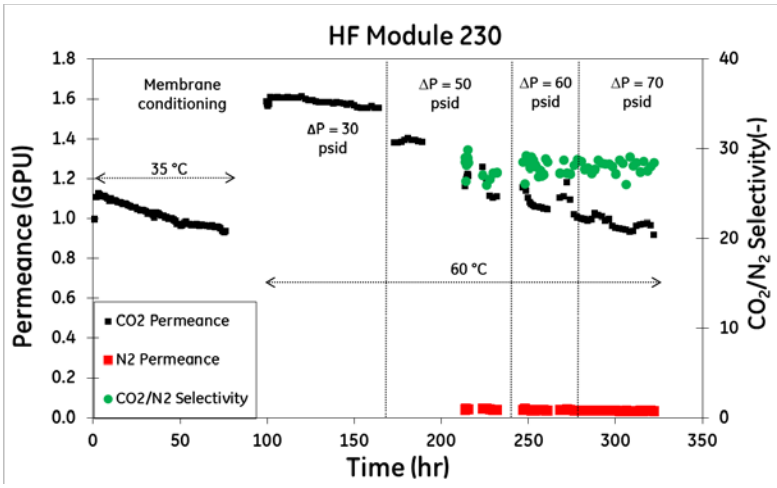

Figure 78. CO_2 and N_2 permeance and selectivity for HF module 230 in simulated flue gas.

After 160 hr, the pressure across the membrane was brought to 50 psid and held for 60 hours. The pressure was then increased to 60 psid and held for an additional 20 hrs. The pressure was then increased to 70 psid for the remainder of the test. The CO_2 /N_2 selectivity held stable throughout the test close to 30. CO_2 /O2 selectivity was stable close to 6. As measured in the pure gas testing, the permeance of this membrane was low, less than 2 GPU. Additionally, the permeance seemed to decline as the test progressed.

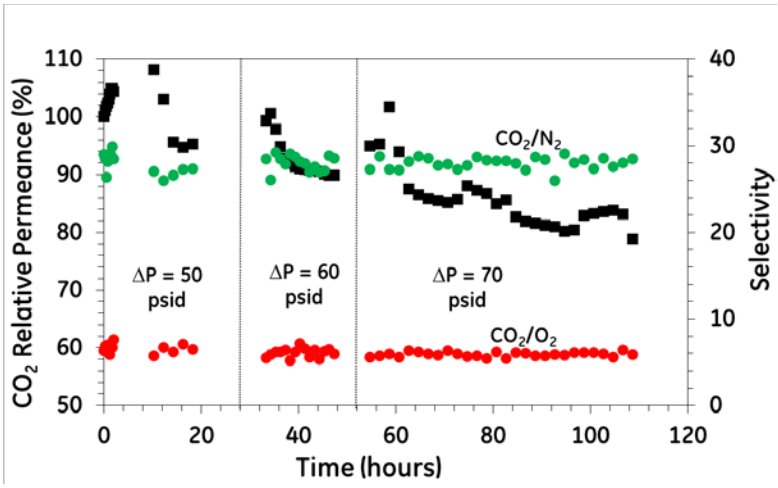

Figure 79. Relative CO_2 permeance and CO_2 /N_2 and CO_2 /O_2 selectivities for HF membrane with simulated flue gas at increasing pressures.

The next module tested had a higher CO_2 permeance but lower CO_2 /N_2 selectivity as fabricated. The same behavior was seen at WRI test conditions. This module was tested for approximately 24 hr, at 50 psid (Figure 80).

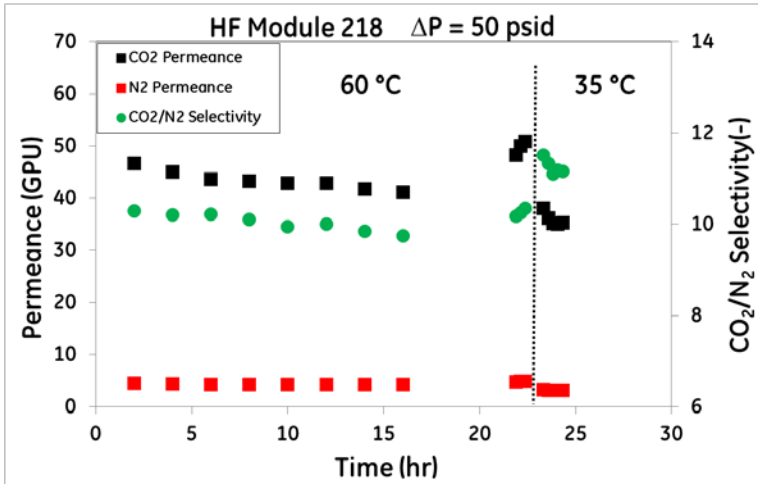

Figure 80. CO_2 and N_2 permeance and selectivity for HF Module 218 tested over 24 hr.

Data analysis: 2014 Hollow Fiber Module Testing

Module 691 was sent for testing in May 2014, and consisted of one Torlon® fiber, coated with 2% PDMS, 5% MEEP and a 0.5% PDMS guard layer. The MEEP polymer was from batch -77 and exposed to 4 ppm ozone for 40 min at ambient temperature after drying overnight.

The module performance, as tested at Georgia Tech is shown in Table 40. The module was tested at 35 ˚C with 30 psig pressure across the membrane in pure N_2 and pure CO_2 . The membrane performance was tested again 3 weeks after coating, and the selectivity was still above 20 and the CO_2 permeance was above 100 GPU.

Table 40. Module 691 performance at Georgia Tech.

Module ID	Notes	Selectivity CO_2 /N_2	CO_2 (P/l) (GPU)	N_2 (P/l) (GPU)
ARS3-691-St.1	Dip Coated in 2% PDMS, heated in oven at 60 °C for 3h	6.	929	146
ARS3-691-St.1	In-situ coated with 5 % MEEP-77, dried at ambient temperature overnight then exposed to 4 ppm ozone for 40 min at ambient temperature	27	174	6
ARS3-691-St.1	In-situ coated with 0.5% PDMS, dried at ambient temperature overnight	33	130	4
ARS3-691-St.1	Tested again before shipping to WRI, 3 weeks after coating	25	114	5

The module was shipped to WRI for testing. During the initial 13 hours of testing, the module showed CO_2 /N_2 selectivity ~ 20, as seen at Ga Tech, and a CO_2 permeance around 20 GPU (Figure 81). The lower permeance may be due to the differences between mixed feed gas and pure feed gas as well as different test set-up and instrumentation between Ga Tech and WRI. Additionally, based on the measurements at Ga Tech before shipping, there was a decline in module CO_2 permeance from 130 to 114 GPU. It is not clear whether this is an actual decline in membrane flux or if the difference of 16 GPU is within the system variation for repeat measurements on an identical sample.

After 13 hours of testing, the module failed, demonstrating evidence of a leak through the module seal or membrane. The CO_2 and N_2 permeance through the module both increased, and CO_2 /N_2 permeance dropped to 1, indicating non-selective flow through the membrane. At this point, testing was discontinued.

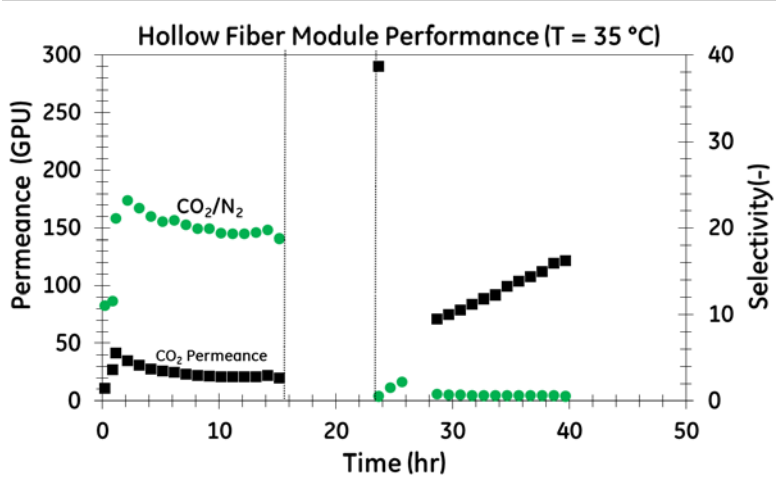

Figure 81. WRI performance for Module 690

The module was returned to Georgia Tech for post mortem analysis. A second coat of 5 wt% MEEP solution was found to restore selectivity to greater than 20, but CO_2 permeance was reduced to less than 100 GPU due to addition of another layer of coating. The module was retested 1 week after recoating, and the selectivity was found to have slightly decreased while both CO_2 and N_2 permeance slightly increased, indicating the possible beginning of membrane degradation (Table 41).

Table 41. Module 691 performance testing at Georgia Tech initial and after re-coating.

Module ID	Notes	αCO2/N2	CO2 (P/l) (GPU)	N2 (P/l) (GPU)
ARS3-691-St.1	Dip Coated in 2% PDMS, heated in oven at 60 °C for 3h	6.34	929.0	146.4
Tested 4/25/2014	In-situ coated with 5 % MEEP-77, dried at ambient temperature overnight then exposed to 4 ppm ozone for 40 min at ambient temperature	27.07	174.2	6.4
Tested 5/5/2014	In-situ coated with 0.5% PDMS, dried at ambient temperature overnight	32.98	130.0	3.94
Tested 6/9/2014	Sent back from WRI	1.19	248	209
Tested 6/17/2014	In-situ coated with 5 % MEEP-82, dried at ambient temperature overnight then heated in oven at 60 °C for 3h	21.03	43	2
Tested 6/19/2014	Tested after two days	16.03	52	3

Conclusions: Coated Hollow Fibers

These membranes we intended to operate at temperatures compatible with existing flue gas cleanup conditions. The polymer coating was intended to provide a separation layer with high selectivity, high permeability, ease of application and compatibility with the hollow fiber support layer. The hollow fiber supports need to provide high mechanical and chemical stability as well as high porosity while still having an asymmetric structure to minimize intrusion of polymer coating. The effects of polymer dope compositions, air gap conditions, coagulant bath temperature and spinning speed have been optimized in order to control the membrane morphology. As intended, the Torlon® hollow fiber support should be close to Knudsen type selectivity, and have a high permeance; thereby indicating low transport resistance.

Several states of Torlon® hollow fibers with various surface morphology and gas transport properties were developed. New processes and protocols for coating of both PDMS and MEEP were explored and developed. An intermediate layer PDMS coating and crosslinking at ambient temperature was explored as a way to enhance selectivity with a higher flux. Defect-free fibers showed intrinsic selectivity to CO_2 ; however, long term stability was not satisfactory. A hypothetical explanation of the instability relates to insufficient crosslinking of the MEEP selective layer. Crosslinking to achieve more complete crosslinking might be possible; however, higher temperature treatment of the composite damaged the skin and caused serious substructure collapse of these defect-free fibers. Different bare Torlon® HF's with various sheath porosities and gas permeances can be coated through this protocol to provide the gas permeance up to 1000 GPU for CO_2 and N_2 gases. An intermediate layer (PDMS) and selective layer (MEEP) coating and crosslinking at ambient temperature were explored as a way to enhance selectivity with a higher flux. Defect-free MEEP/PDMS/PAI composite hollow fibers yielded higher fluxes and selectivities to CO_2 . MEEP/PDMS/PAI composite membranes were characterized for the separation of CO_2 /N_2 separation at 30 psig and 35 °C. The separation performances with MEEP/PDMS coated PAI hollow fibers membrane were significantly higher than the uncoated PAI hollow fibers. CO_2 flux decreases linearly with the PDMS and MEEP coating. The effect of actual fly ash on flux and CO_2 /N_2 selectivity of composite MEEP/PMS/PAI hollow fiber membrane were studied. The gas permeation and CO_2 /N_2 selectivity was stable for over 120 h time-on-stream exposure to actual fly ash on MEEP/PMS/PAI hollow fiber membrane. In addition, the preliminary effects of humidity on gas permeation and CO_2 selectivity of MEEP/PAI hollow fiber membrane were studied. The results indicated that CO_2 gas permeation and selectivity of MEEP/PAI hollow fiber membrane were maintained under exposure to wet CO_2 . The effect of actual fly ash on flux and CO_2 /N_2 selectivity of composite MEEP/PMS/PAI hollow fiber membranes were also studied. The gas permeation and CO_2 /N_2 selectivity was stable for over 120 h time-on-stream of actual fly ash on MEEP/PMS/PAI hollow fiber membrane. Further work should also focus on controlling the coating layer thickness and the refining of MEEP/PAI-HF membrane models.

The experimental results illustrate that MEEP/PDMS/PAI HFs composite membranes yielded promising CO_2 /N_2 selectivity. If the instability observed in long-term stability testing can be overcome to avoid loss in CO_2 /N_2 selectivity as a function of time, the composite hollow fibers could be attractive options for CO_2 capture.

Task 6: Conduct Process Evaluation and Module Design

Technical and economic feasibility study

A preliminary technical and economic feasibility analysis was performed to evaluate the impact of integrating a membrane in a PC boiler. The energy penalty (EP) and increase in cost of electricity (COE) for 90% carbon capture is discussed. Different scenarios based on membrane properties are presented that impact both the EP and the COE.

Process description

The overall process flow is described in Case 9 and Case 10 of the Black's DOE/NETL report (Black 2010). The Case 9 is for a subcritical PC boiler without CO_2 capture and Case 10 is for a subcritical PC boiler with CO_2 capture unit using MEA system. The MEA separation units utilize four key processes: CO_2 Absorption, CO_2 Desorption, Sorbent Handling and CO_2 Compression. The flue gas from the power plant is processed in a direct contact cooler (DCC) to reduce the temperature to 40 C (104 F) and then enters the absorber.

The base case membrane process configuration with major process units is shown in Figure 82 in which the flue gas after the FGD and DCC is fed to the membrane system. This system is similar to that found to be optimal for membrane based CO_2 capture from pulverized coal power plant exhaust gases in the DOE-sponsored study (Merkel, Lin et al. 2010). In this process, the flue gas is subjected to particulate removal and desulfurization prior to CO_2 capture. The Membrane-I unit is operated at a pressure ratio of 5-10 with vacuum applied on the permeate side and compression on the feed side if necessary. The CO_2 lean retentate gas is fed to the Membrane II unit, where the gradient for CO_2 transport across the membrane is provided by counter-current air sweep at ambient conditions. The CO_2 enriched air stream is fed to the boiler while the retentate that contains low amounts of CO_2 (corresponding to >90% CO_2 capture) is vented.

The CO_2 enriched permeate from the Membrane-I unit is compressed to 25 bar and cooled to ambient temperature to condense out the water, and then cooled to -20°C when CO_2 condenses. The liquid CO_2 is separated to yield a high-purity CO_2 stream that is then pumped to 140 bar for sequestration. The uncondensed gas from the separator still has significant amounts of CO_2 and is recovered using another membrane unit (not shown) as permeate to the compressor and condenser. The retentate is recycled to the flue gas feed.

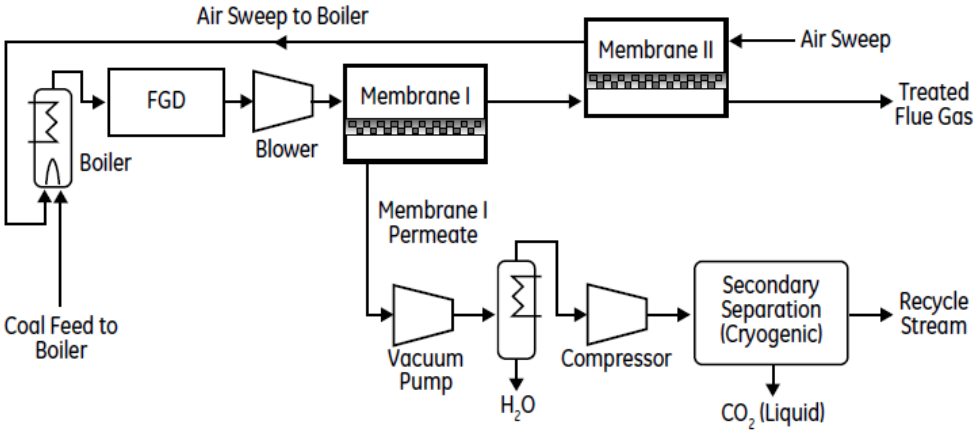

Figure 82. A block flow diagram for the base case membrane based process for flue gas CO_2 capture.

Membrane model development

In the first step to model this system individual membrane models were developed. The Membrane-I is a cross-flow vacuum sweep and Membrane-II is a counter-current air sweep. Aspen Custom Modeler® was used to model the membranes. It was later evaluated that if Membrane-I is operated in counter-current mode then additional reduction in total membrane area could be achieved. This analysis is covered in the subsequent sections.

Cross Flow Membrane Model

The cross flow vacuum sweep membrane modeling was initiated using an example from the Aspen library. The model was modified according to the initial estimates of membrane properties for the hollow fiber membranes being developed in this program. Figure 83 shows the cross flow model in the Aspen Custom Modeler.

Flue gas composition was obtained from the DOE-NETL report (Black 2010) . The flue gas compositions for Subcritical PC (Case 9 and Case 10) and Supercritical PC (Case 11 and Case 12) are shown in Table 42. The flue gas composition is an input to the model for Membrane-I in Aspen Custom Modeler®. Other inputs to the model are shown in Table 43.

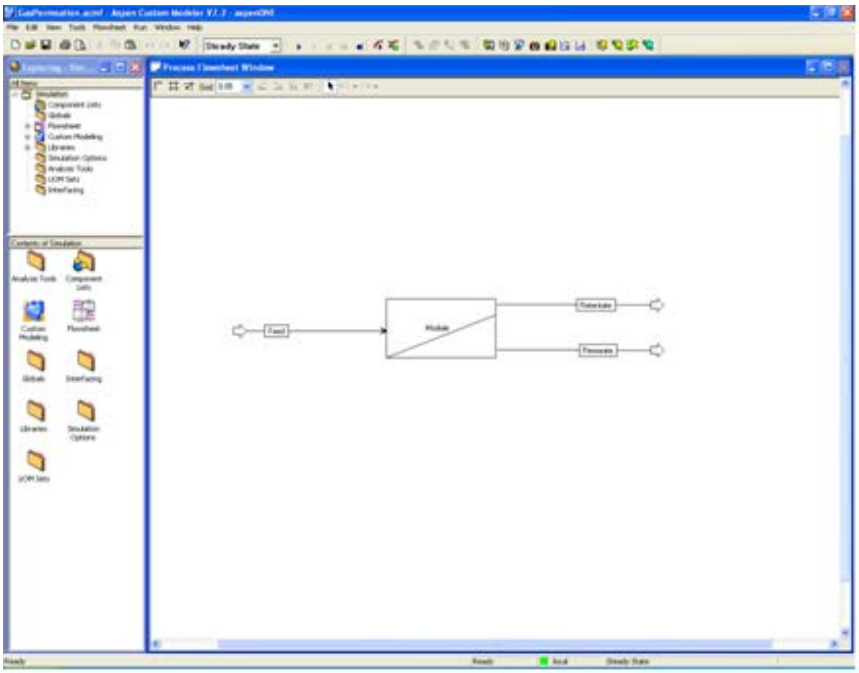

Figure 83. Cross flow membrane model for Membrane-I in Aspen Custom Modeler®.

Table 42. Flue gas composition from a PC boiler.(Black 2010)

	Subcritical PC Case 9	SCPC Case 11	Subcritical PC Case 10 (w/ CO_2 Capture)	SC PC Case 12 (w/ CO_2 Capture)
Ar (%v)	0.82%	0.82%	0.81%	0.81%
CO_2 (%v)	13.50%	13.53%	13.50%	13.50%
H_2O (%v)	15.17%	15.17%	15.37%	15.37%
N_2 (%v)	68.08%	68.08%	67.93%	67.93%
O_2 (%v)	2.43%	2.40%	2.38%	2.38%
FlowRate (m^3/s)	578	540	811	747
Mass Flow rate (kg/hr)	2,287,903	2,137,881	3,213,261	2,956,531

Table 43. Inputs to Membrane-I model.

Feed Flow	lb/hr	Refer Table 1
Feed Pressure	bar	Varied (Base Case: 2)

Feed Temperature	^{o}C	60
Feed Composition		Refer Table 1
CO_2 Permeance	GPU	Varied (Base Case 1000)
Selectivity	CO_2 /N_2	Varied (Base Case: 50)
Selectivity	CO_2 /H_2O	0.5
Selectivity	CO_2 /O_2	20
Carbon Capture	%	Base case 90%
Permeate Pressure	bar	0.2

Counter-current Membrane Model

In the second step a counter-current membrane model was developed. The counter-current membrane model was developed using knowledge gathered from other programs on membrane usage in hydrogen production and chemicals production utilizing water gas shift membrane reactors. In this project, the counter-current membrane does not involve any reactions taking place inside the membrane and hence the other models were modified to remove the kinetic reaction equations. The model is shown in Figure 84.

The mass balance of a counter-current membrane can be modeled as following:

$$dn_i/dz = -\pi d_i J_i \qquad (1)$$

where n_i is the molar flow rate of species i, z is the axial direction, di is the fiber internal diameter, and J_i is the permeation flux of species i across the membrane surface area. The permeation flux can be expressed as:

$$J_i = B_i * \Delta(P_i)/\theta \qquad (2)$$

where B_i is the permeability of component i, P_i is the partial pressure difference of the component across the membrane and θ is the thickness of the membrane functional layer.

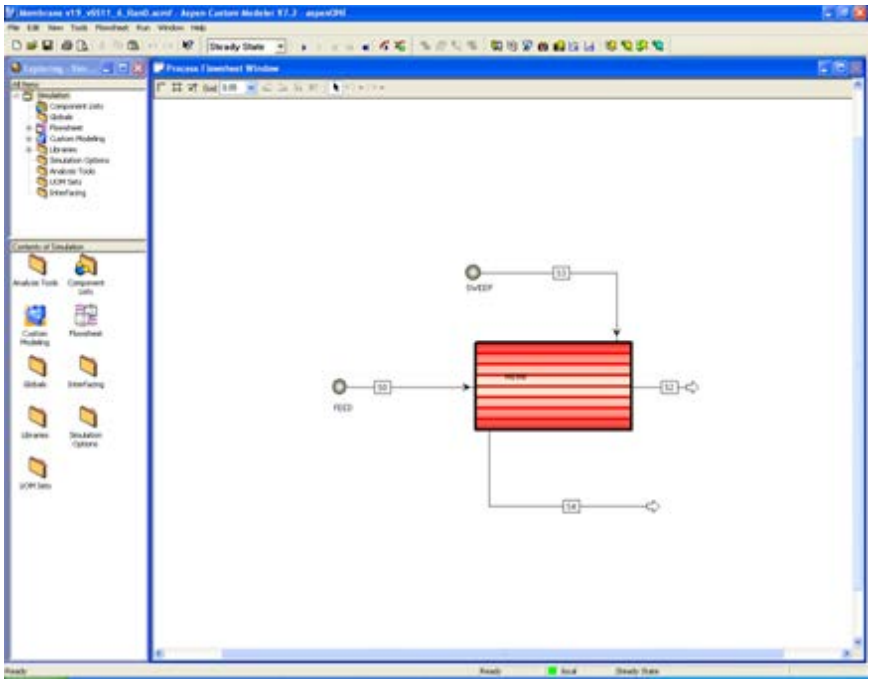

Figure 84. Counter-current membrane model for Membrane-II in Aspen Custom Modeler®.

Integrated Membrane Model

The next step involved combining the models developed for membrane-I and membrane-II into a single model with differential equations for each of the membranes being calculated separately in sub models. Figure 85 and Figure 86 show the combined models for membrane-1 and membrane-2 interacting with each other.

The combined model was built to complete the membrane portion of the configuration shown in Figure 82. Two cases were built to evaluate the possibility of reducing the membrane area further by using a counter-current membrane as membrane-I instead of a cross-current membrane. It is well known in the literature that counter-current membranes offer advantages vs. cross-current membranes. Lower membrane area is required for the same amount of gas separation if other factors are kept the same due to higher driving force achieved in counter-current mode. Case M1 and Case M2 are shown in Figure 85 and Figure 86 respectively.

Overall system model development

A block flow diagram of major unit operations for a carbon capture case is shown in Figure 6 as given in Case 10 of the DOE-NETL report (Black 2010). An Aspen Plus® model was built for the major unit operations up to FGD and then modified to add the membrane separation processes as shown in the membrane system block flow diagram in Figure 87 . The Aspen Plus® model is shown in Figure 88.

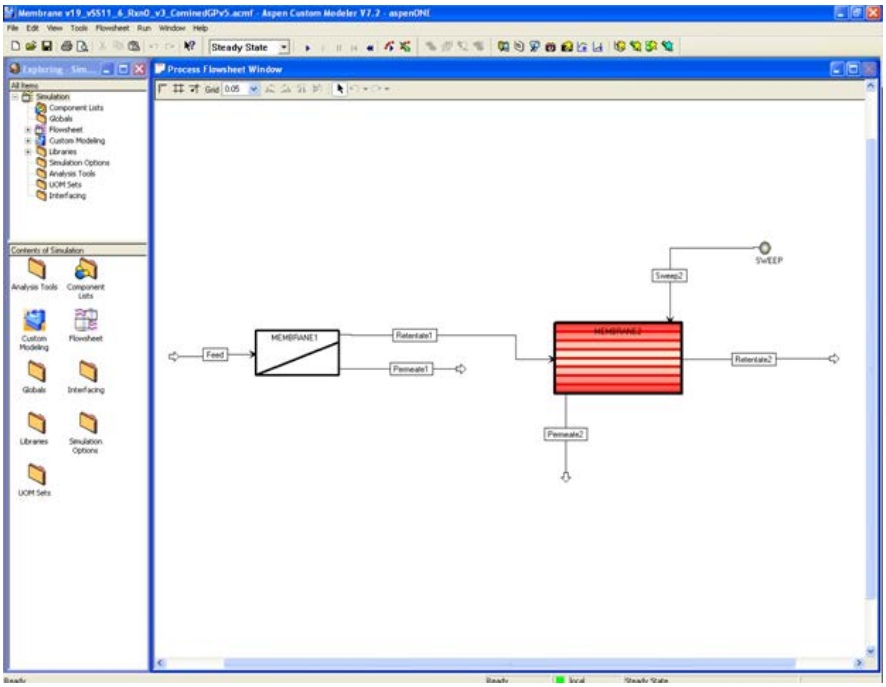

Figure 85. Combined model for Cross-flow membrane followed by counter-current membrane in Aspen Custom Modeler®- Case M1.

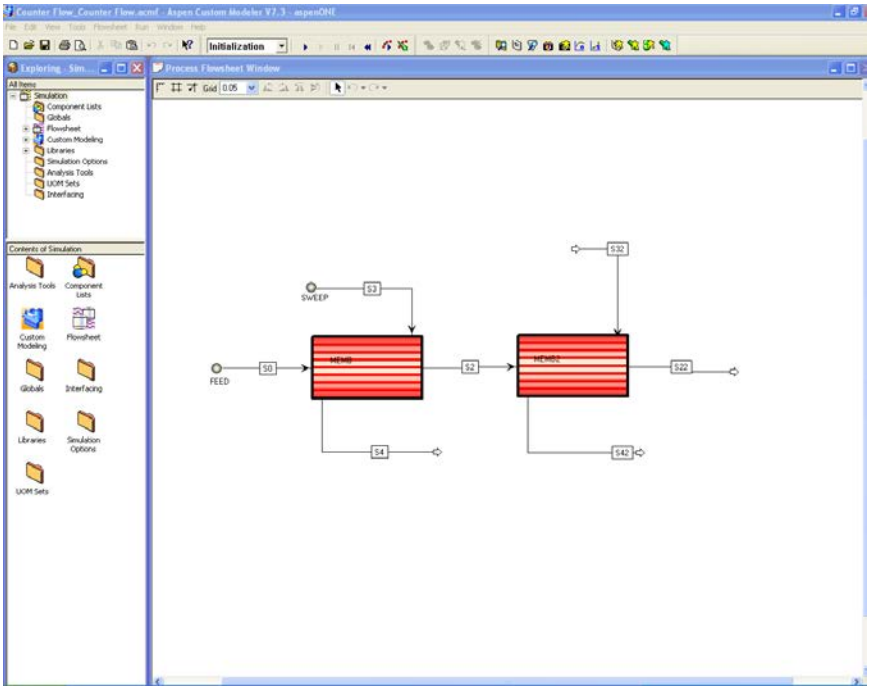

Figure 86. Combined model for counter-current membranes in series in Aspen Custom Modeler®-Case M2.

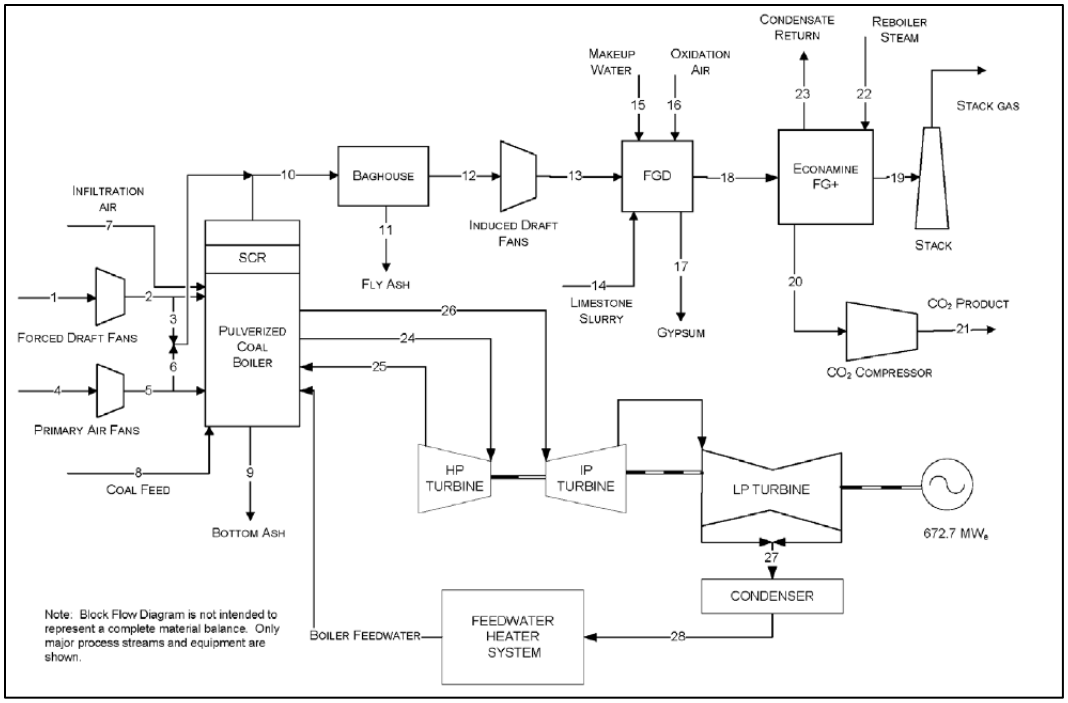

Figure 87. A block flow diagram for subcritical unit with CO_2 capture using solvents (Black 2010).

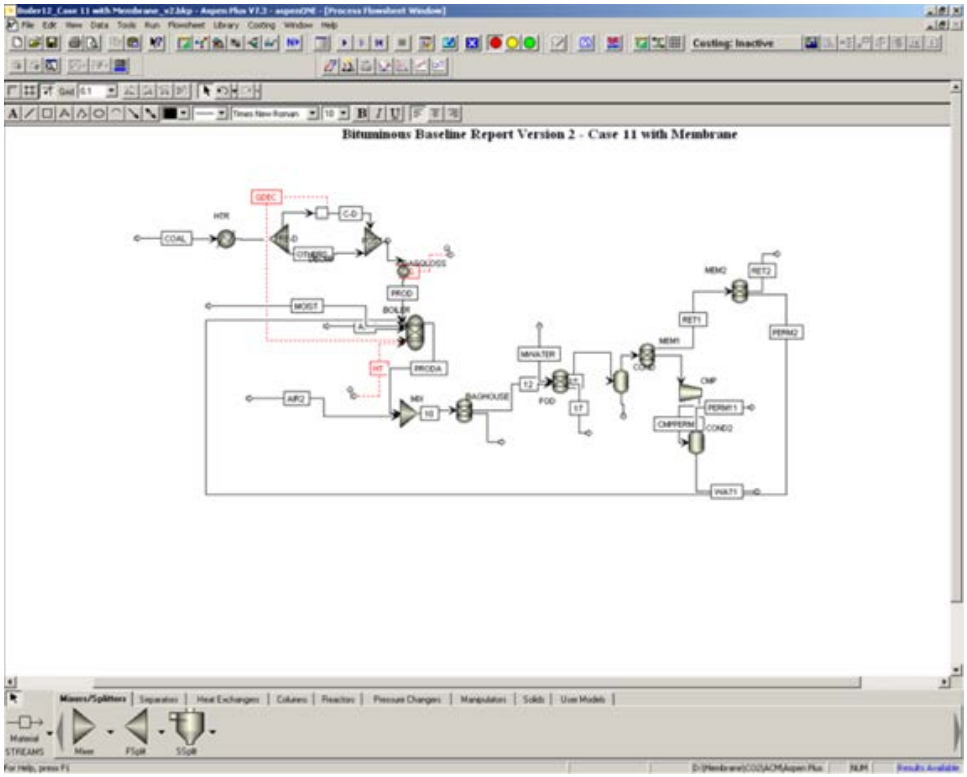

Figure 88. An example of Aspen Plus® model with major components for a PC boiler carbon capture case for membrane model integration.

Model Results and Sensitivity Analysis

The complete Aspen Plus® model and the membrane models in Aspen Custom Modeler® were used to evaluate the process shown in Figure 82. In the first case, the membrane-I was used in the cross-current mode (Case M1) and in the second case it was used in the counter-current mode (Case M2). The inputs to the models are shown in Table 42 and Table 43. Overall carbon capture percentage was assumed to be 90% to compare the two cases.

Results from Case M1 and Case M2 are shown in Figure 89. Comparing the membrane area required for the 2 cases it is seen that a reduction of 12% is achieved for membrane-I area by switching from cross-current mode to counter-current mode.

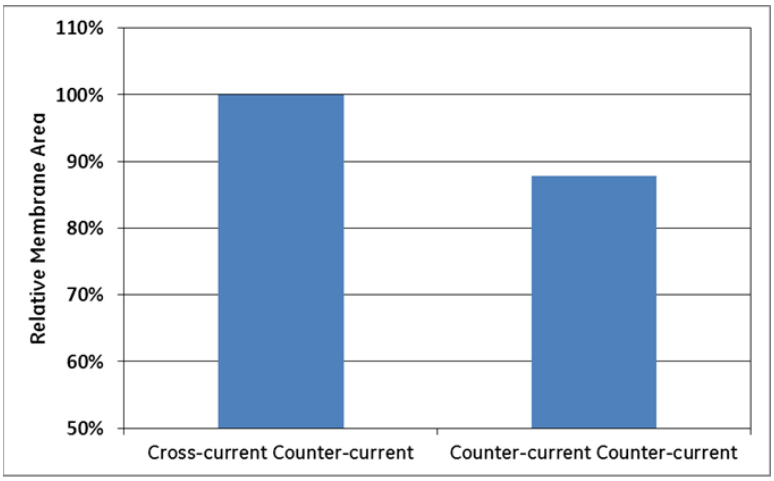

Figure 89. Comparison of two membrane configurations vs. membrane area required.

It is clear from the figure above that using the membrane-I in the counter-current mode **leads to a decrease in membrane area by 12%. Hence, the membrane-I and membrane-II are recommended to be used in the counter-current modes. In this case, the membrane area** required to separate 90% CO_2 is found to be the least between the two cases evaluated.

Further, a sensitivity analysis was carried out for total membrane area with respect to permeance and selectivity of the membrane. The results are shown in Figure 90.

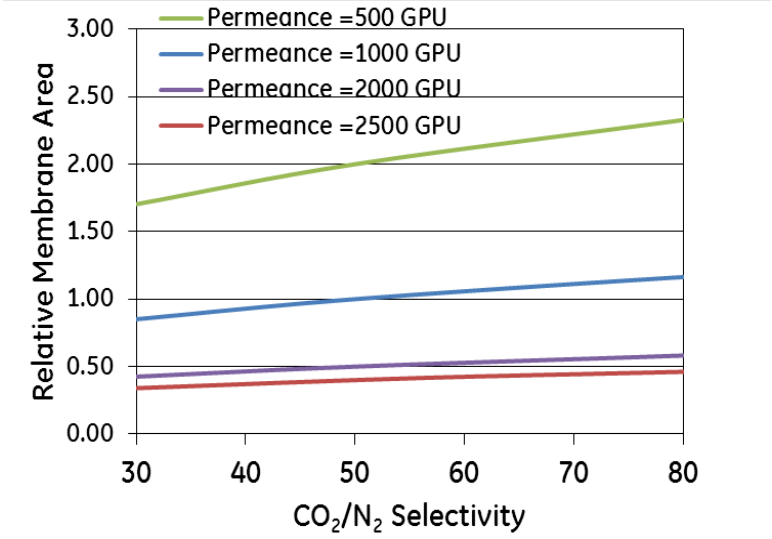

Figure 90. Sensitivity analysis for total membrane area vs. CO_2 /N_2 membrane selectivity.

It is clear from Figure 90 that increasing the permeance of the two membranes leads to a decrease in the total membrane area required for 90% carbon capture. The base case permeance is 1000 GPU. It is also clear from the figure above that increasing the selectivity while keeping the same permeance leads to a slightly higher membrane area required for 90% carbon capture. Increase in CO_2 /N_2 selectivity also has an effect on the purity of the CO_2 stream which is shown in Figure 91

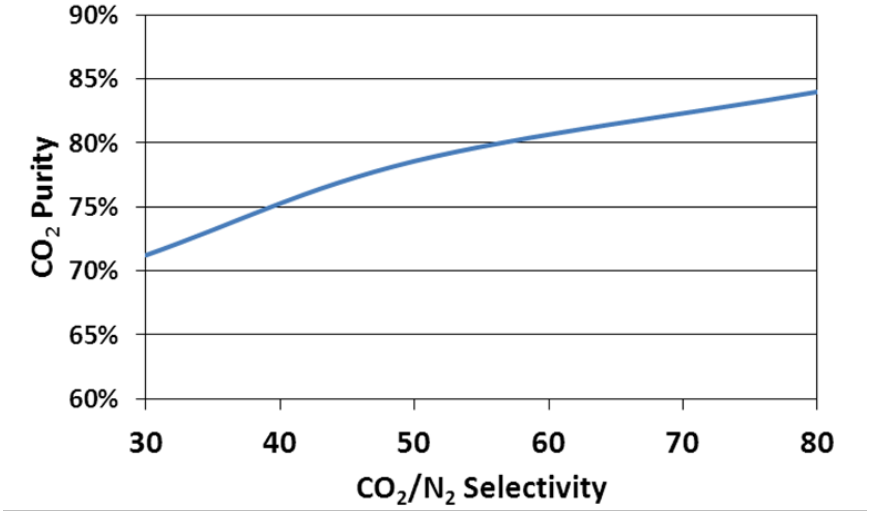

Figure 91. Sensitivity analysis for CO_2 purity vs. CO_2 /N_2 membrane selectivity.

It is clear from Figure 91 above that increasing the selectivity leads to an increase in the CO_2 purity of the stream that is sent to the cryogenic separation unit. The base case permeance used for the above figure is 1000 GPU.

Aspen Plus® simulation model was used to calculate the energy penalty for carbon capture on the overall system. Figure 92 shows the energy penalty for the membrane system as compared to the case 12 in the DOE-DOE-NETL report (Black 2010). The membrane case

assumptions are mentioned in this report earlier. In this base case, the feed pressure was increased to 2 bar and a vacuum sweep was used at 0.2 bar. A sensitivity analysis was carried out to calculate the increase in COE when different feed pressure was used as shown in Figure 93.

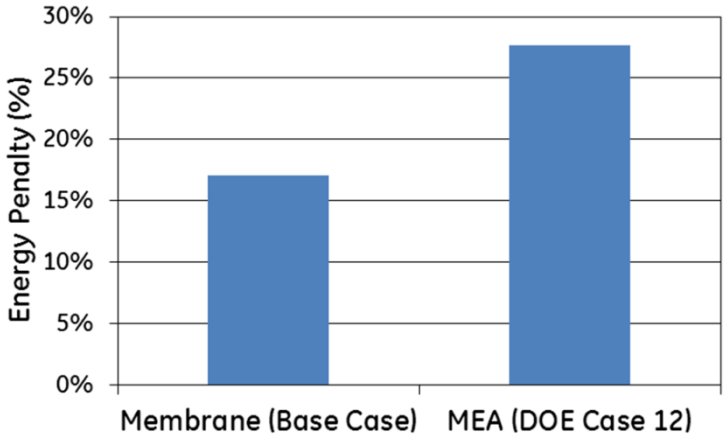

Figure 92. Energy penalty comparisons for carbon capture using membranes vs. DOE case 12.

It is clear from Figure 93 that increasing the permeance initially decreases the increase in COE significantly but after reaching a certain point the decrease becomes less prominent. Figure 93 also shows the effect of feed pressure on the increase in COE. Increasing the feed pressure to 2 bar as compared to 1.2 bar decreases the increase in COE. The sensitivity analysis with respect to feed pressure is more evident in Figure 94.

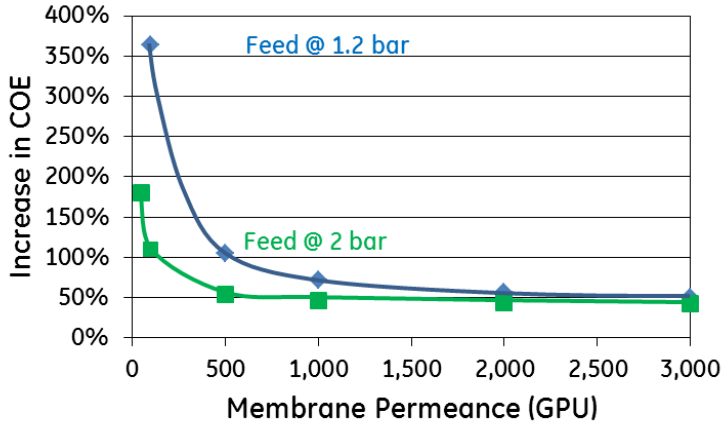

Figure 93. Sensitivity analysis of Increase in COE vs. feed pressure and membrane permeance.

It is clear from Figure 94 that increasing the feed pressure at first has a positive effect on decreasing the increase in COE but beyond 2 bar feed pressure the increase in COE starts rising. Hence, an optimum feed pressure is required for using membranes system for carbon capture.

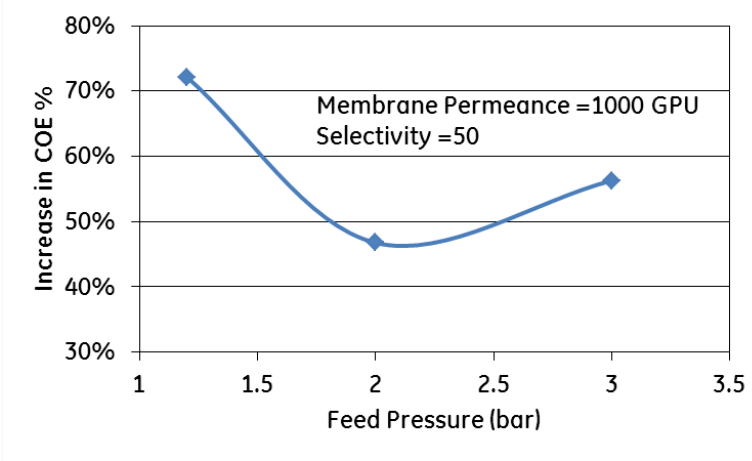

Figure 94. Sensitivity analysis of increase in COE vs. feed pressure.

Membrane cost is another parameter that has an effect on increase in COE. It is evident from Figure 95 that decreasing membrane cost decreases increase in COE. Hence, a smaller increase in COE can be observed if a combination of factors is used. Higher permeance, higher selectivity, lower membrane cost and optimum feed pressure are required to optimize the increase in COE.

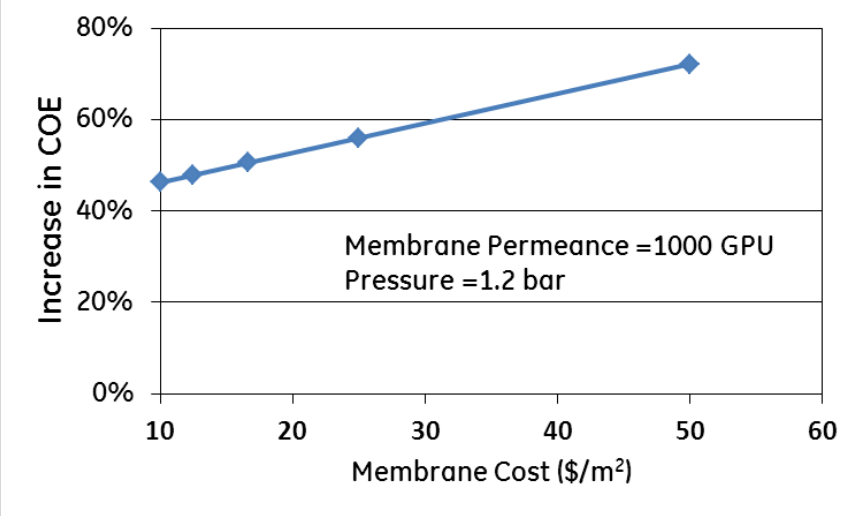

Figure 95. Sensitivity analysis of increase in COE vs. membrane cost.

Next Steps

Subsequent steps were planned to estimate the membrane cost via completing module design step. The module design task was to define the hollow fiber and module dimensions, flow configuration, and module geometry to enable modifications at the coal flue gas test rig at WRI. The experimentally determined permeance and selectivity performance of the hollow fiber membranes was to be used in conjunction with membrane module cost model developed in subsequent quarters to calculate the increase in COE at the completion of the project. These

next steps were not completed since the first review, the DoE requested we suspend this economic analysis.

Effect of Fly Ash

A preliminary estimate of effect of fly ash on the membrane was also carried out in this task. The percentage of membrane area covered is dependent on a number of variables such as amount of fly ash reaching the membrane, particle size of the fly ash and the thickness of the ash layer on the membrane. The DOE-NETL report gives the efficiency of removal of a bag house for the particulates as 99.8% with an inlet solids flow rate of 21,640 kg/hr for Case 10. Hence up to ~43 kg/hr of solids enter the FGD. The efficiency of particulate removal from the FGD can be in the range of 95%-99% depending on the particle size of the particulate matter giving a range of ~2-0.5kg/hr of solids that leave the FGD. Further, it was assumed that a single layer of particulates is formed on the membrane surface and that 1.3MM m2 of membrane area is required for carbon capture. Kim et.al. studied the particulate removal efficiency of a wet scrubber with respect to particle size as shown in Figure 96. A sensitivity analysis was carried out for the percentage of membrane area covered with fly ash with respect to particle size of particulate matter reaching the membrane. The results are shown in Figure 97. It is estimated with the previously mentioned assumptions that an area of about 3%-0.1% could be covered per day if the particle size reaching the membrane is between 1 and 10 microns.

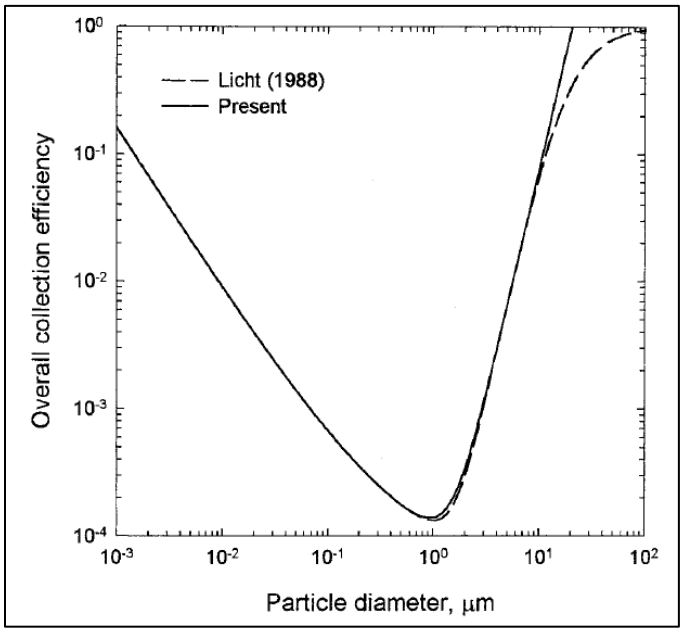

Figure 96. Overall removal efficiency with respect to particle diameter. (Kim, Jung et al. 2001)

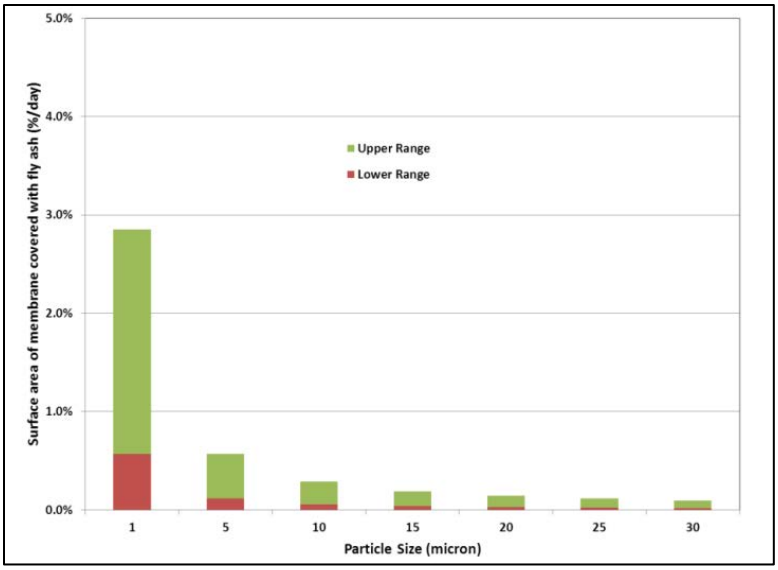

Figure 97. Percent of membrane area covered per day with fly ash.

Summary

In this task, cross flow and counter-current membrane models were developed in Aspen Custom Modeler® and then combined to generate an integrated model. This model was used to develop membrane performance targets such as selectivity and permeance. Also, an Aspen Plus® model was built with major components for a PC boiler case. The membrane mode developed in this task was used to calculate the membrane area required for 90% carbon capture and then a sensitivity analysis was carried out with respect to the critical parameters related to membrane performance. The Aspen Plus® model was used to calculate the energy penalty on the plant using membranes for carbon capture. The results from both models were used to calculate the increase in COE and then a sensitivity analysis was carried out against critical parameters.

Module designs and flow configuration trade-off analyses

Module design requirements and down selection

Different possible module designs for capture of CO_2 from flue gas on an industrial scale were explored with the following objectives:

- Large feed flow rate of the incoming flue gas (~ 500m3/s at ~60ºC, ~1 bar),
- Structural robustness/life
- Compactness of the CO_2 capture system and
- Capital and operating expenditures.

In the literature (Porter 1990; Koros and Fleming 1993; Baker 2000), there are four main designs used for similar applications such as heat exchangers, water purification units and fuel cells: (1) plate and frame design, (2) tubular design, (3) spiral-wound design, (4) hollow fiber designs.

In the plate and frame design, the selective membrane is coated on a planar substrate and housed in an assembly that provide flow paths for feed and sweep gases. These designs are usually used in solid oxide fuel cells (SOFC) and several such cells can be stacked in a compact fashion to maximize power. The disadvantages of this design for current application are low surface area/volume ratio leading to larger modules (See Table 44) excessive sealing areas (more prone to leakage/failure), and fouling (cleaning is difficult/expensive).

Table 44. Comparison of Area/Volume ratio of different designs (Koros and Fleming 1993; Li, Wang et al. 2004)

Module Design	Area/Volume ratio (ft^2/ft^3)
Plate & Frame	100 – 150
Tubular	200 – 250
Spiral Wound	200 – 250
Hollow Fiber	2000 – 4000

In a tubular design, the selective membrane is coated on a tubular substrate and housed in a shell. The feed gas usually flows inside the coated tube while the sweep gas flows outside of it. The main advantages are easily achievable high flow rates of feed gas, easy fabrication of module from off-the-shelf components and minimal sealing areas and operability under high temperature / pressure. The only disadvantage of this design is its low area /volume ratio.

In a spiral-wound design, the selective membrane is manufactured in the form of sheets, sandwiched between two spacers (feed and permeate) and wrapped around a perforated permeate collection tube. The permeate is collected at the center of the rolled membrane and hence achieves minimal pressure drop in the permeate side. However, its area/volume ratio is not high enough as shown in Table 44

In a hollow fibers design, the selective membrane is coated on a hollow polymeric fiber substrate (diameter ~ 300-500 microns for gas separation) and a bundle of these fibers are contained in a module tube with sealed ends. This sealing/potting prevents the mixing of permeate and feed gases. The area/volume ratio can be easily varied by varying the number of fibers in the module. Since for CO_2 separation from high flow rate flue gas requires high area/volume ratio (See Table 44), the hollow fiber design provides a lot of flexibility to increase this ratio without increasing the size of the module. Two critical factors for a successful design of a hollow fiber module are manufacturing defect free hollow fibers with coatings and the potting of the hollow fibers with high packing density.

Apart from achieving high area/volume ratio, hollow fiber module also provides a lot of flexibility with respect to different operating conditions/design considerations such as pressurized feed vs permeate vacuum, shell side feed vs bore side feed, and co-current vs counter current vs cross flow.

Based on the objectives for CO_2 separation from flue gas the hollow fiber module design looked most promising when compared to the other designs discussed above.

Hollow fiber module design considerations

A number of design considerations are available within the framework of hollow fiber module designs and depending on the application, different combinations can be chosen. They are:

Shell side feed vs. bore side feed:

In shell feed, the flue gas flows outside the hollow fiber, while in bore feed it flows inside the hollow fiber. Since the volumetric flow rate of flue gas is high (500m3/s) for the current application, it is better to have shell side feed due to the following:

a. bore side feed flow velocity is limited by its diameter due to the effect of "choking". When flow is choked, the gas velocity reaches a certain value and stays constant even when the driving potential (Δp) is increased. The pressure drop is also high along the length of the fiber which is undesirable for the recovery of CO_2 .

b. Mechanical stresses (hoop stress) on the fiber are tensile in bore feed while it is compressive in shell feed. It is well known that materials behave stronger in compression than in tension. In fact, Koros (Koros and Fleming 1993) mentions that the collapse pressure (compressive) is four times the tearing pressure (tensile) for hollow fiber.

c. small variations in the fiber diameter can significantly change the flow inside the fibers (flow is proportional to fourth power of diameter). A slightly large hollow fiber will have a significantly high flow rate than the others.

However, shell side feed also has some drawbacks. For long module, the permeate side pressure drop (lumen side) can be quite substantial. Creation of vacuum on the permeate side would alleviate this problem to some extent. Other potential problems for shell side feed mentioned in Liu et al. (Liu, Chakma et al. 2005)such as flow channeling/mal distribution only arises when the packing density of fibers is high.

Co-current vs counter-current vs cross flow configurations:

Depending on the path/stream line of the flow of the feed and the sweep gas, three different flow configurations are possible. In co-current flow, the path of the feed and sweep gas are parallel and gases flow in the same direction, while in counter current flow the paths are parallel and the flow is in the opposite directions. In the cross flow configuration, the path of feed and sweep gas are perpendicular to each other. With respect to hollow fibers, cross flow configurations can be either helically wound inside a cylindrical shell (Koch, Müller et al. 2008) or a radiator-type module (Li, Wang et al. 2004). Although, counter current flow configuration is reported to give the best CO_2 recovery compared to co-current and cross flow configurations from various mathematical models (Geankoplis 2003; Li, Wang et al. 2004; Khalilpour, Abbas et al. 2012), commercial membrane module designers such as MTR [2]use cross flow configurations in their spiral wound modules.

[2] Membrane Technology and Research, Menlo Park, CA. http://www.mtrinc.com/

Pressurized feed vs. vacuum permeate:

In order to achieve the necessary driving force for CO_2 separation to occur, a pressure differential must be created between the feed and the permeate side either by compressing the feed gas or by pulling a vacuum on the permeate side. In most industrial applications, the feed compression is preferred because the compression equipment is much cheaper than vacuum equipment and only a smaller membrane area is required for feed compression(Merkel, Lin et al. 2010). In the vacuum operation, a blower is still needed to push the flue gas through. However from an energy perspective, the vacuum permeate option is preferred because the energy required to create vacuum on the permeate side (small volume of gas) is much less than the energy required to compress the large volumes of feed gas(Khalilpour, Abbas et al. 2012). Although the initial cost (capital expenditure) is high for the vacuum permeate option, it is better with respect to energy efficiency.

Hollow Fiber Module Design Parameters

Having discussed the various designs and flow configurations of hollow fiber modules, the following design parameters are common to all the different configurations.

Permeate vacuum Level:

Increasing the level of vacuum in the permeate side increases the pressure ratio (feed pressure/permeate pressure) and hence the recovery of CO_2 . However, there are practical limitations in creating very low vacuum pressure because pressure drop inside the 300-micron diameter fiber is difficult to avoid even when large vacuum equipment is used. Hence a vacuum pressure of 0.2 bar is suggested for practical purposes(Merkel, Lin et al. 2010). Although increasing the fiber diameter would theoretically help in creating a uniform vacuum on the permeate surface, it is not practical because it would reduce the packing density of the module and increase the chance of the hollow fiber collapsing under external pressure.

Surface Area:

The surface area is one of the important factors in improving the overall efficiency of the module along with permeance and pressure ratio. There are a number of ways of increasing the surface area and each factor with its trade-offs is described below:

- Fiber length, diameter and number of fibers:

Although increasing the fiber length increases the surface area linearly, the pressure drop along the length could be high and hence the recovery of CO_2 does not improve with increase in length(Koch, Müller et al. 2008). An upper limit of 0.9m for the module length is suggested. An alternative to achieve the required surface area is to increase the number of fibers within the module of shorter length. However, increasing the packing density of fibers increases the risk of leakage near the potting/sealing arrangement. Several methods are reported in patents and papers that are focused on obtaining reliable potting methods(Azran and Dagan 2001; Li, Wang et al. 2004; Nakamatsu, Ohtani et al. 2007). In the invention, (Azran and Dagan 2001; Li, Wang et al. 2004) compressed air flows into the lumen of the fibers to prevent the flow of viscous epoxy while the syringe pushes the epoxy into the shell side. In the invention(Nakamatsu, Ohtani et al. 2007), they use baffled cylinder (helical slits on the inside face) made of polymer to divert the peeling force in the circumferential direction.

- Convoluted fibers:

Another possibility of increasing the surface area for the same length and nominal diameter of the fiber is to introduce a convoluted inner or outer surface (Azran and Dagan 2001). Figure 98 below shows a convoluted outer surface with a nominal radius R, amplitude of convolution A, number of cycles per circumference C. The radius, ρ, in polar coordinate can be written as:

$$\rho = R + A\sin C\theta \qquad (3)$$

and using the length of arc formula from integral calculus, $L = \int_0^{2\pi} \sqrt{\rho^2 + \left(\frac{d\rho}{d\theta}\right)^2}\, d\theta$ the percentage increase in surface area can be calculated as a function of $f\left(\frac{A}{R}, C\right)$. The increase in surface area for various C is plotted as a function of A/R ratio in Figure 98 (b). Although the results look promising as we can practically double the surface area by playing with the parameters, manufacturing of the fibers with the selective coating that are structurally robust can be quite a challenge. Even if manufactured successfully, due to the convoluted outer surface, fouling deposition rate can be quite high due to the topology and cleaning the fibers by water flushing would not be as successful as with a uniformly circular fiber.

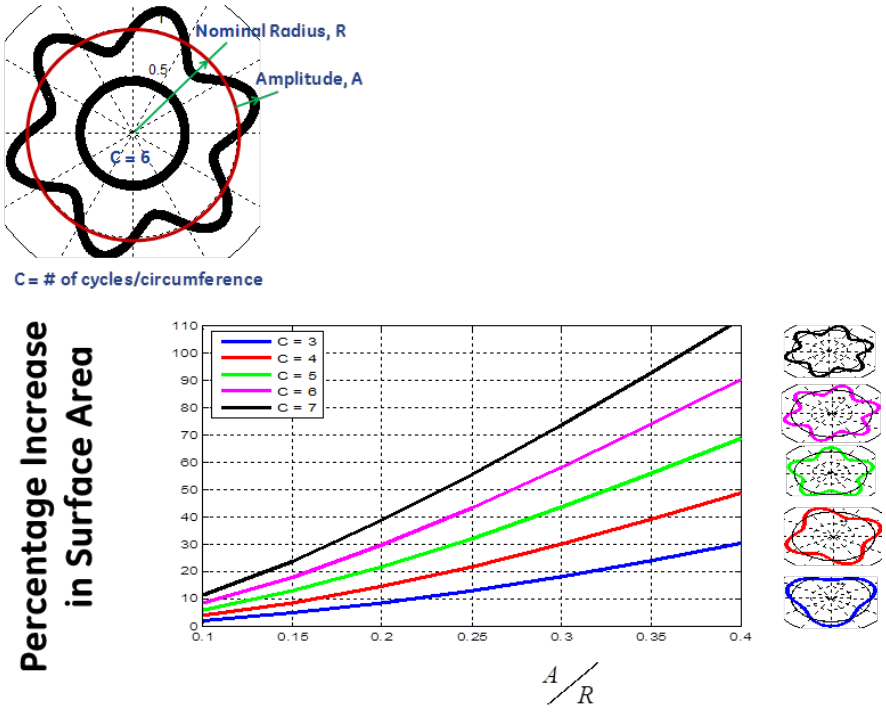

Figure 98. Convoluted surface hollow fiber and increase in surface area. (a) Convoluted Surface Hollow Fibers; (b) Percentage increase in Surface Area for different A/R, C values

Mechanical risks assessment

A risk review workshop was conducted within to methodically enumerate, rank, assess and mitigate risks related to mechanical failure of the hollow fiber membrane module. A

comprehensive list of risks was identified and ranked, at a component level (coating, substrate, potting etc.), module level (tube and shell design) and system level. A summarized version of this detailed risk analysis is given in Table 45 below. The list accounted for failures arising from various thermal, mechanical and environmental driving factors such as gas pressures, temperatures, residual stresses, chemical attacks, vibrations etc. The ranking methodologies are also described in Table 45. Based on the rankings, mechanical risks of the greatest and most immediate concern were identified as the risks related to the membrane failure and seals failure either during manufacturing or during operation. While some of the risks such as degradation due to SOX, NOX, fly ash and pin holes /leakage problems can only be mitigated experimentally, debonding/delamination of potting layer from casing and coating from substrate in HF can be mitigated/ avoided by design.

Table 45. Risk analysis summary.

Failure Mode	Risks								
	During Operation							During Manufacturing	
	Gas Pressure	CTE	High Temperature Degradation	SO_X, NO_X, fly ash degradation	Thermal cycling	Thermal Shock	Pressure Spikes	Residual Stresses	Leakage / Pinholes
Coating/Intermediate Layer									
Seals									
Substrate									
Pressure Vessel Housing / Flanges								N/A	N/A
Module Joints								N/A	N/A

Risk Probability

High

Medium

Low

Mitigation Plans:

1. Burst Tests / Porometry to estimate pore size and strength.
2. Simple FEA Analysis for estimation of stresses.
3. 200-hr SO_X, NO_X, Fly Ash exposure tests followed by selectivity measurement/ SEM observation.
4. Temperature and pressure exposure tests

Based on the ranking of the risks from Table 45, the following experiments and analyses were planned:

- 200-hour SOX, NOX, fly ash exposure tests followed by selectivity measurement/SEM observation.
- Temperature and Pressure exposure tests.
- Porometry / Burst tests to estimate pore size and strength.
- Simple FEA analysis to estimate stresses

Mechanical characterization of hollow fibers and evaluation of module stresses

Mechanical characterization of hollow fibers

The variation of mechanical properties of hollow fibers with changes in process parameters (state) such as flow rate, diameter of the nozzle, temperature of operation etc. were studied. Mechanical properties such as elastic modulus, yield point, failure stress and failure strain indicated in the stress-strain curve shown in Figure 99 are of interest from a mechanical design perspective. Another important objective was to evaluate if the mechanical properties changed appreciably for different state of the process settings.

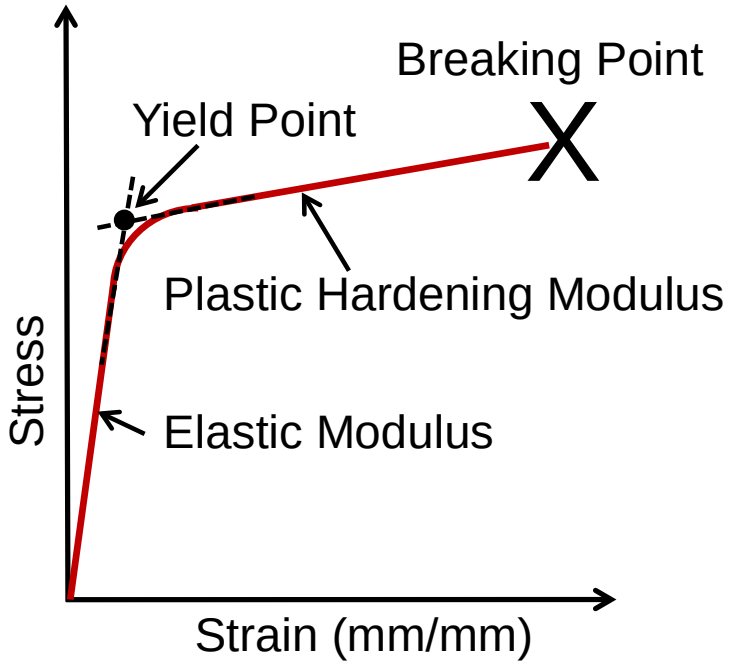

Figure 99. Illustration of stress-strain behavior of a Hollow Fiber specimen under uniaxial loading.

A magnified cut section view of a PES hollow fiber is shown in Figure 100. From the scaling in the figure the inner and outer diameter of the hollow fiber was calculated to be 300 and 550 microns respectively.

Stress-strain curves for PES hollow fibers were obtained (Figure 101). Comparing Figure 101 to Figure 99, the material behaves linearly elastic until 3N (40 MPa stress) and then hardens until the specimen breaks at approximately 5N (70 MPa). While the elastic portion and the plastic hardening portion of the curve is similar for all specimens, the breaking stress is lower for specimen #1. For all the other specimens the breaking stress is very close. The anomaly in the first specimen is attributed to the gripping mechanism used while conducting the experiment. Ignoring the first specimen data, the data from other specimens show consistent material properties (elastic modulus, yield point, hardening modulus, failure stress and failure strain) from the a particular state setting of the fiber spinning rig. The material properties extracted from the tests are tabulated in Table 46. The elastic modulus ~1500 MPa was used in the analysis of stress in the hollow fibers in the next section.

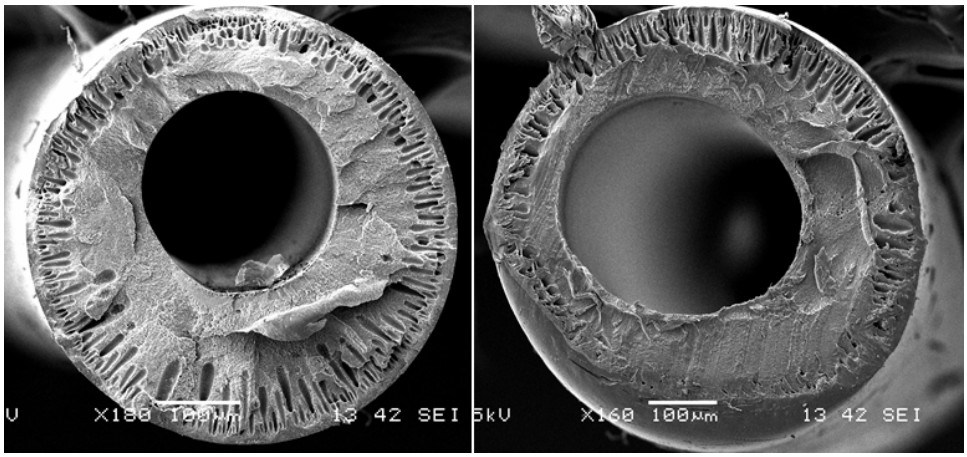

Figure 100. Magnified cut-section of a PES hollow fiber. Approximate outer diameter is 550 microns and inside diameter is 300 microns. The samples used in these uniaxial tests were taken from Spin #4 and state #1.

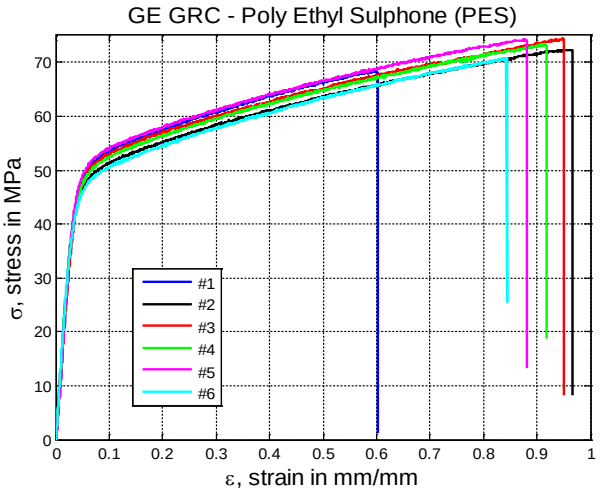

Figure 101. Stress-Strain curves for PES hollow fibers.

Table 46. Material properties of PES hollow fibers.

Specimen	Elastic Modulus (MPa)	Yield Stress (MPa)	Hardening Modulus (MPa)	Failure Stress (MPa)	Failure Strain
#1	1300	52.15	32	68.78	0.602
#2	1375	52.05	24	72.32	0.962
#3	1300	53.55	24	74.37	0.949
#4	1440	53.05	24	73.10	0.920
#5	1340	55.05	24	74.11	0.880
#6	1440	52.05	24	70.63	0.845

Module Thermal Stresses

Failure can occur if thermal stresses in the casing, epoxy or the hollow fibers in the hoop or circumferential direction due to CTE (thermal expansion) mismatch are high. The strategy was to model the casing and epoxy without hollow fibers (HF) first under a plane strain assumption and quantify the stresses. Different epoxy / casing materials were tried in the model and different designs were evaluated to reduce the stresses and hence the risk of failure. Then the HF was modeled with neighboring epoxy under plane strain conditions with initial far-field radial stresses arising from casing. In this step, the epoxy was modeled as an infinite medium and a separate model was created due to different length scales between HF and module dimensions. The stresses from the epoxy/casing model were used as an input into this HF/epoxy model.

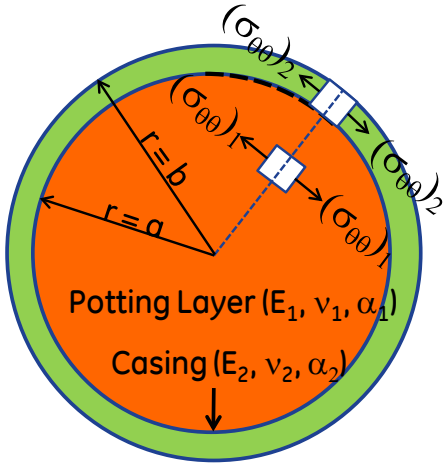

Figure 102. Model of Potting layer and casing with geometry and material property definitions.

The thermal stresses in a CO_2 module near the potting layer and casing is modeled here. A plane strain problem in polar coordinates is used in this analytical development to obtain the thermal stresses (Ugural and Fenster 2003). The casing is modeled as a hollow cylinder while the epoxy or the potting layer is modeled as a solid cylinder. Let the radius of the potting cylindrical material be 'a' and the radius of the casing be 'b'. An illustration is shown in Figure 102. The summary of the analytical results are given below. These derivations are done in a MAPLE worksheet version 12 (See Appendix I). The subscripts 'rr' and 'qq' denote the radial and tangential stresses respectively while the numbers '1' and '2' indicate potting layer and hollow fiber respectively.

$$\sigma_{rr(1)}(r,\theta) = \sigma_{\theta\theta(1)}(r,\theta) = -p \tag{4}$$

$$\sigma_{rr(2)}(r,\theta) = p\frac{a^2}{b^2-a^2}\left(1-\frac{b^2}{r^2}\right) \tag{5}$$

$$\sigma_{\theta\theta(2)}(r,\theta) = p\frac{a^2}{b^2-a^2}\left(1+\frac{b^2}{r^2}\right) \tag{6}$$

$$\text{where } p = \frac{\Delta T\left(a^2 - b^2\right)E_1E_2\left[\alpha_1\left(1+\upsilon_1\right) - \alpha_2\left(1+\upsilon_2\right)\right]}{\left(1+\upsilon_1\right)\left(1-2\upsilon_1\right)\left(a^2 - b^2\right)E_2 - \left(1+\upsilon_2\right)\left[a^2\left(1-2\upsilon_2\right) + b^2\right]E_1} \qquad (7)$$

Table 47. Mechanical properties of candidate material for the module. (Chung, Qin et al. 2000)

Material	Elastic Modulus, E (GPa)	CTE α (10-6/K)	Poisson Ratio
Steel	210	12	0.3
Epoxy	5 - 20	20 -100	0.4
PVC	3	50	0.3
HF (PES)*	0.5-2	100-200	0.3

Material property ranges for casing (steel and PVC), potting layer (epoxy), hollow fibers are given in Table 47. A design sensitivity study was conducted to identify the ideal choice of casing materials and epoxy by looking at the stress levels in respective materials. The first study used steel as the casing material with diameter of 8 inches with 0.5 inch thickness. The epoxy material property was varied and the circumferential stresses in both materials are shown in Figure. The stress in the steel casing is tensile while the stress in the epoxy potting layer is compressive and the stresses increase with an increase in the epoxy stiffness. A similar behavior was seen when the epoxy CTE was increased. The lowest yield stress of steel is 250 MPa. and the epoxy failure stress is not known. The stress levels are high in both materials due to the mismatch in both the elastic modulus and the CTE. Hence a proper combination of casing/epoxy should be chosen to reduce the stresses. A temperature rise of 60°C was used in this analysis similar to the flue gas temperature. For a temperature of 180°C (approximate temperature rise when the desulfurizer fails), the stresses become even higher in both the materials.

Next, the casing material was changed to PVC and the same sensitivity analysis was performed. Due to the similar mechanical properties of PVC and epoxy (elastic modulus and CTE), the stress levels are much lower in both materials as shown in Figure 104 and also are not sensitive to the epoxy elastic modulus changes. Since the stress levels are so low in this case, it was concluded that PVC/epoxy combination is a better choice for the module than the steel/epoxy combination. For a higher temperature rise of 82°C, the stresses in the PVC and epoxy are given in Table 48 and they are still lower than the steel/epoxy combination.

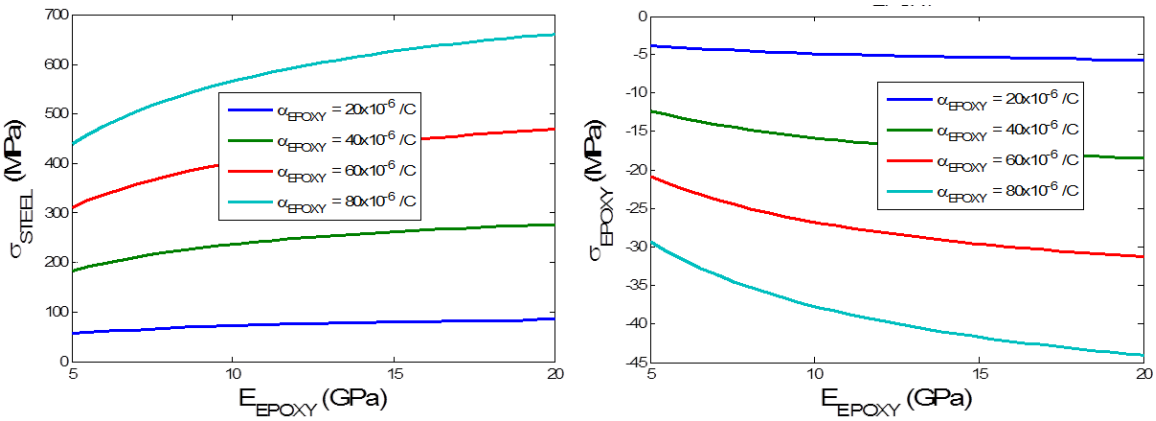

Figure 103. Hoop Stress in epoxy potting layer with a steel casing under thermal loading (60°C-22°C).

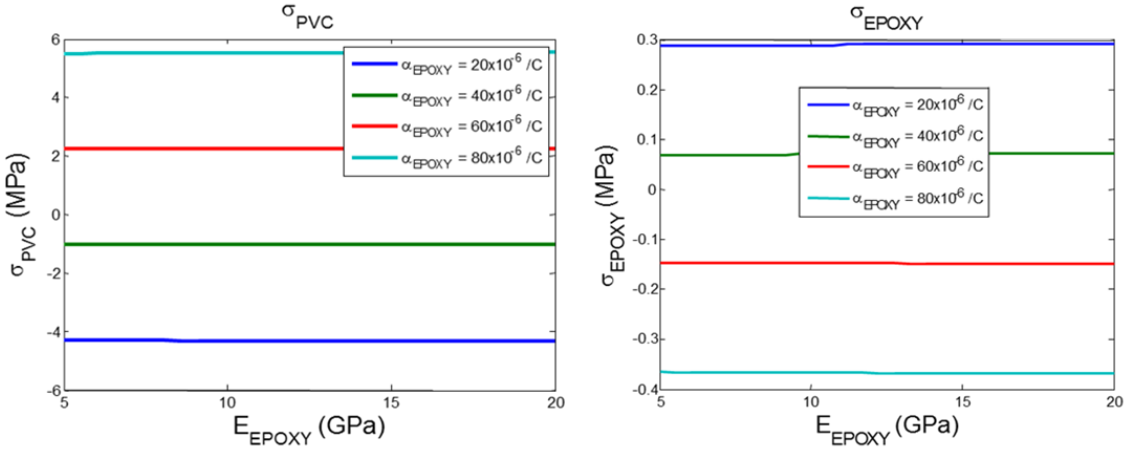

Figure 104. Hoop Stress in epoxy potting layer with a PVC casing under thermal loading (60°C-22°C).

Table 48. Hoop stress for a higher temperature rise (82°C-22°C) in the epoxy layer with a CPVC casing.

α_{epoxy} (10-6/K)	σ_{epoxy} (MPa)	σ_{CPVC} (MPa)
20	0.45	8.6
40	0.11	3.5
60	-0.23	-1.6
80	-0.58	-6.8

Model of Potting layer and Hollow Fiber with geometry and material property definitions

The thermal stresses in a CO_2 module near the hollow fiber were modeled. In the previous section, the bulk stresses in the potting layer and the casing were considered. In this

section, the stresses in the hollow fiber are considered. The stresses in the epoxy from the previous solution and the thermal loading were used to obtain HF stresses. This problem was solved separately because of the following:

1. Length scale difference between the casing and the hollow fiber is more than 1000

2. Hollow fiber need not be axi-symmetric with the casing axis.

A plane strain problem in polar coordinates was used in this analytical development to obtain the thermal stresses. The epoxy was modeled as an infinite medium in the polar coordinate with inner radius 'b0' and outer radius 'c0' that approaches infinity to simulate the infinite medium as shown in Figure 105. The hollow fiber was modeled as a hollow cylinder with inner radius 'a0'.

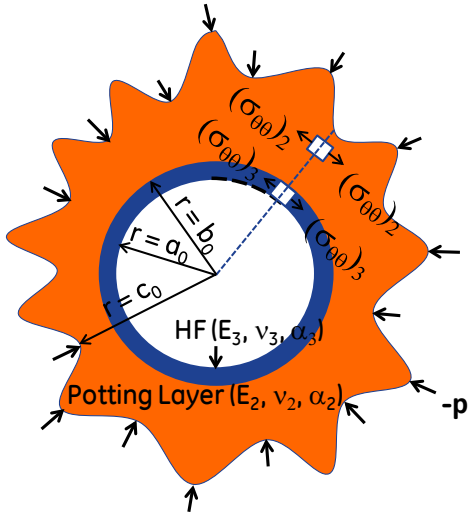

Figure 105. Thermal stresses in the hollow fiber and potting layer

The summary of the analytical results is given below. These derivations were done in a MAPLE worksheet version 12. (See Appendix J) The numbers '2' and '3' indicate potting layer and hollow fiber respectively.

$$\sigma_{rr(2)}(r,\theta) = -p + \frac{b_0^2}{r^2}(p - p_0) \tag{8}$$

$$\sigma_{\theta\theta(2)}(r,\theta) = -p - \frac{b_0^2}{r^2}(p - p_0) \tag{9}$$

$$\sigma_{rr(3)}(r,\theta) = p_0 \frac{b_0^2}{a_0^2 - b_0^2}\left(1 - \frac{a_0^2}{r^2}\right) \tag{10}$$

$$\sigma_{\theta\theta(3)}(r,\theta) = p_0 \frac{b_0^2}{a_0^2 - b_0^2}\left(1 + \frac{a_0^2}{r^2}\right) \tag{11}$$

$$\text{where} \quad p_0 = \frac{\left(a_0^2 - b_0^2\right)E_3\left\{E_2\Delta T\left[\alpha_2(1+\upsilon_2) - \alpha_3(1+\upsilon_3) - 2p(1-\upsilon_2^2)\right]\right\}}{(1+\upsilon_3)\left(a_0^2 + b_0^2(1-2\upsilon_3)\right)E_2 - (1+\upsilon_2)\left(a_0^2 - b_0^2\right)E_3} \tag{12}$$

is the interface radial stress between the hollow fiber and epoxy potting layer. The radius 'c0' does not appear in the solutions because it was eliminated by taking a limit as 'c0' approaches infinity.

Similar to the design study done in the previous section, the epoxy elastic modulus was varied and the stresses in the hollow fiber are plotted for different CTEs of epoxy material as shown in Figure. The stresses in the hollow fiber layer are much smaller than the failure stress and the yield point obtained from the tensile tests (See Table 46).

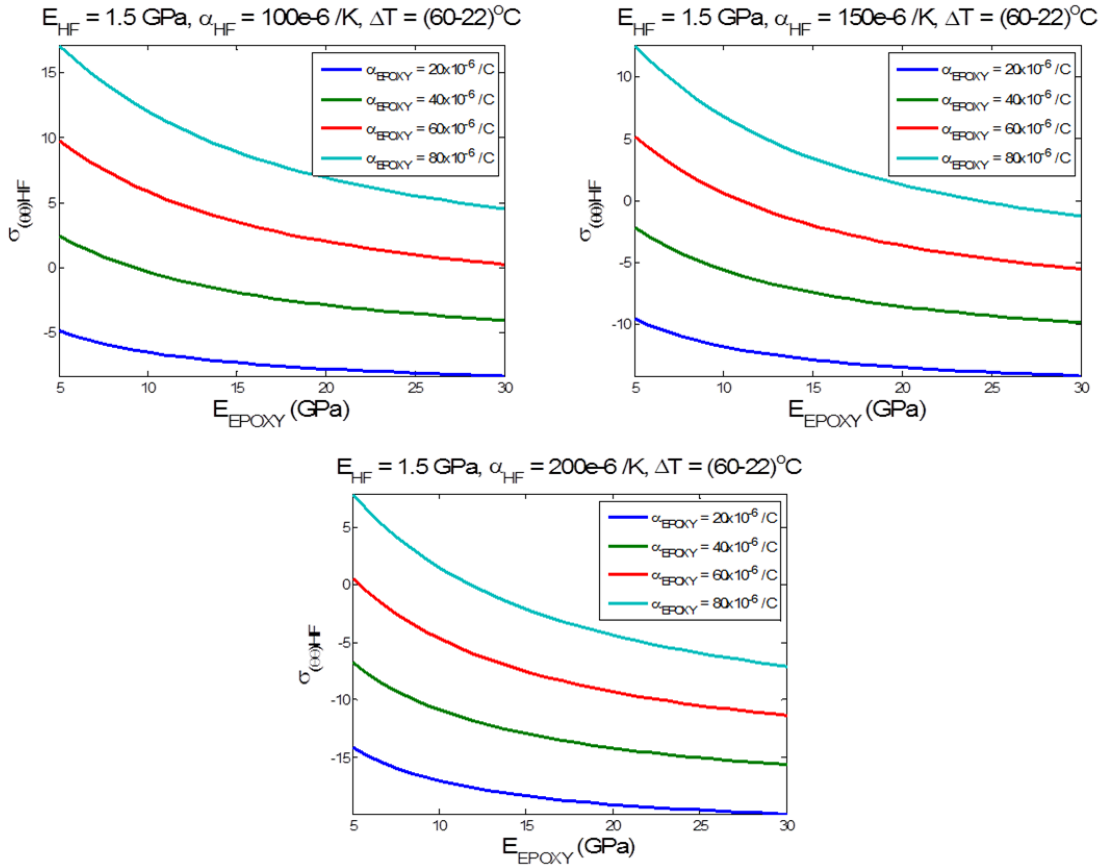

Figure 106. Sensitivity of Hoop stress in the Hollow Fiber for various Epoxy stiffness and thermal expansion.

The design sensitivity analysis for steel and PVC casing discussed above led to the conclusion that the PVC casing produced much less stress compared to the steel casing due to the smaller mismatch in mechanical properties between epoxy and PVC materials. The stress in the hollow fiber was found to be very small compared to the yield stress obtained from the tensile tests.

Hollow fiber stresses due to shell side and bore side pressures

The possibility of failure from stresses in the substrate due to the shell side and the bore side pressures were evaluated with the goal of optimizing hollow fiber dimensions.

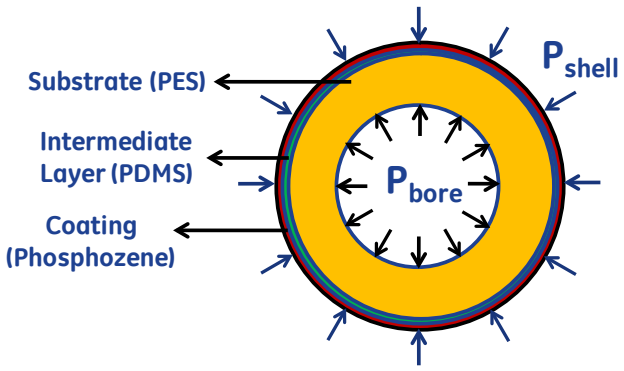

Figure 107. Hollow Fiber and coating stress analysis.

A cross-section of hollow fiber consisting of substrate, intermediate layer and coatings subjected to pressure loadings on the bore and shell side is shown in Figure 107. A thick cylinder solution subjected to internal and external pressure from Cook [1] was used in this study. The radial and hoop stresses in the hollow fiber substrate as a function of radius are given below:

$$\sigma_{rr}(r,\theta) = p_{bore}\frac{b^2}{b^2-a^2}\left(1-\frac{a^2}{r^2}\right) - p_{shell}\frac{a^2}{b^2-a^2}\left(1-\frac{b^2}{r^2}\right) \quad (13)$$

$$\sigma_{\theta\theta}(r,\theta) = p_{bore}\frac{b^2}{b^2-a^2}\left(1+\frac{a^2}{r^2}\right) - p_{shell}\frac{a^2}{b^2-a^2}\left(1+\frac{b^2}{r^2}\right) \quad (14)$$

In this study, four different flow configurations were used:

- Bore feed with vacuum on the permeate side
- Shell feed with vacuum on the permeate side
- Bore feed with atmospheric pressure on the permeate side
- Shell feed with atmospheric pressure on the permeate side

where p_{bore} is the pressure loading on the lumen side of the hollow fiber, p_{shell} is the pressure on the shell side, *'a'* is the inner radius of the substrate HF, *'b'* is the outer radius of the substrate HF and *'r'* is the radius.

For a hollow fiber with outer diameter of 550 microns, inner diameter of 300 microns and a pressure ratio (pfeed /ppermeate) of 6, the hoop stresses are plotted as a function of radius for the four different flow configurations in Figure 108. When permeate side is vacuum, the pressure applied is 0.2 bar. As expected bore feed gives tensile hoop stresses and shell flow gives compressive hoop stresses. Tensile failure pressure for a hollow fiber is much lower than its collapse pressure. Hence shell feed is preferred to bore feed from the mechanical stress point of view. The same trends are expected even when the pressure ratio is increased. Stresses are higher when the permeate side is at atmospheric pressure instead of vacuum. Tensile failure stresses in-house uniaxial tests is ~75 MPa (~10,000psi). Hence any of the flow configuration is far away from HF substrate failure.

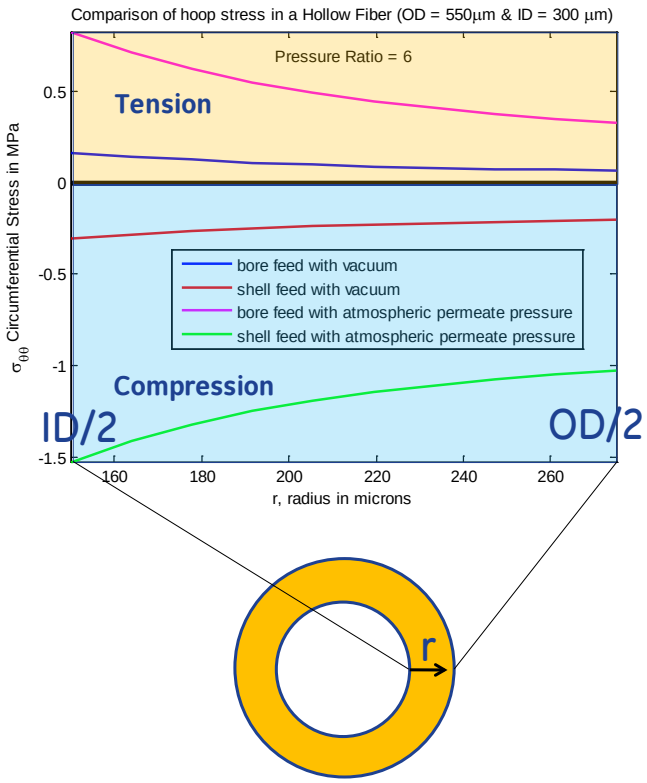

Figure 108. Hoop or circumferential stress in the Substrate of the Hollow Fiber for different flow configurations. The stress is plotted along the radius.

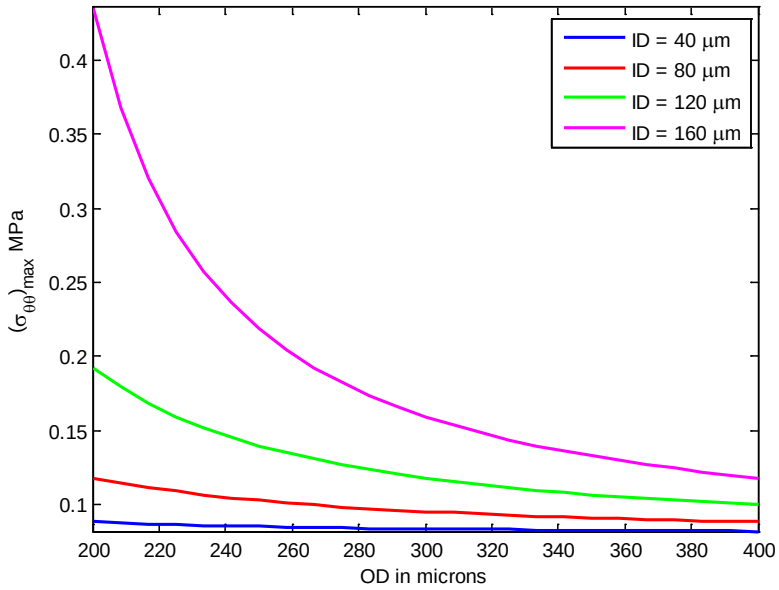

Figure 109. Maximum Hoop stress ($\sigma(\theta\theta,max) = \sigma(\theta\theta,r=ID/2)$) as a function of geometry of the hollow fiber.

Next, sensitivity of the maximum hoop stress on the hollow fiber geometry was studied. The hoop stress at the inner radius was used for this sensitivity because stress is highest at this location and fairly constant along the radius as shown in Figure 108. In Figure 109, the

maximum hoop stress is plotted against the outer diameter for various inner diameter values. As the OD increases for a constant ID, the thickness of the hollow fiber increases thereby reducing the stress. In Figure 3, bore feed with vacuum case is considered; however the same trends are seen even for other flow configurations.

In conclusion, structurally the hollow fibers are strong enough to withstand the loads during the membrane separation process.

Overall summary and conclusions

GE Global Research, Idaho National Laboratory (INL), Georgia Institute of Technology (Georgia Tech), and Western Research Institute (WRI) proposed to develop high performance thin film polymer composite hollow fiber membranes and advanced processes for economical post-combustion carbon dioxide (CO_2) capture from pulverized coal flue gas at temperatures typical of existing flue gas cleanup processes.

The project sought to develop and then optimize new gas separations membrane systems at the bench scale, including tuning the properties of a novel polyphosphazene polymer in a coating solution and fabricating highly engineered porous hollow fiber supports. The project also sought to define the processes needed to coat the fiber support to manufacture composite hollow fiber membranes with high performance, ultra-thin separation layers. Physical, chemical, and mechanical stability of the materials (individual and composite) towards coal flue gas components was considered via exposure and performance tests. Preliminary design, technoeconomic, and economic feasibility analyses were conducted to evaluate the overall performance and impact of the process on the cost of electricity (COE) for a coal-fired plant including capture technologies

At the onset of the project, Membranes based on coupling a novel selective material polyphosphazene with an engineered hollow fiber support was found to have the potential to capture greater than 90% of the CO_2 in flue gas with less than 35% increase in COE, which would achieve the DOE-targeted performance criteria.

While lab-scale results for the polyphosphazene materials were very promising, and the materials were incorporated into hollow-fiber modules, difficulties were encountered relating to the performance of these membrane systems over time. Performance, as measured by both flux of and selectivity for CO_2 over other flue gas constituents was found to deteriorate over time, suggesting a system that was more dynamic than initially hypothesized. These phenomena are believed to be associated with the *physical and mechanical* properties of the separation membrane - in this case MEEP poly(phosphazenes) - rather than chemical degradation by flue gas or one of its constituents.

The differences between the promising parameters measured for these materials on small scale and the observed challenges in implementing them in a Hollow-fiber form factor guide a few recommendations for future investigations in this area:

- In addition to the performance of separation material on idealized substrates (such as flat, porous ceramic discs), promising separation materials candidates should also

be tested for engineering properties (such as creep ,modulus, and tack) relevant to any final application

- Promising materials should be subjected to test-retest or extended duration testing to evaluate time-dependent behavior early in any experimental program.

Strategies to improve the composite systems via alternate chemistries and processing techniques were only partially successful in creating a more robust system, but the research provided critical insight into the barriers to engineering sophisticated composite systems for gas separation. Promising concepts to re-engineering the material systems were identified and may prove useful to future CO_2 separation material development programs. Recognizing the likelihood of material creep phenomena in the rubbery, low-modulus MEEP material, the Interpenetrating network (IPN) strategy was developed, and merits future study.

References

Allcock, H. R. (1994). "Crosslinking Reactions for the Conversion of Polyphosphazenes into Useful Materials." Chemistry of Materials **6**(9): 1476-1491.

Allcock, H. R. and G. K. Dudley (1996). "Lower Critical Solubility Temperature Study of Alkyl Ether Based Polyphosphazenes." Macromolecules **29**(4): 1313-1319.

Allcock, H. R., M. Gebura, et al. (1988). "Amphiphilic polyphosphazenes as membrane materials: influence of side group on radiation cross-linking." Biomaterials **9**(6): 500-508.

Allcock, H. R., C. J. Nelson, et al. (1993). "Gas permeation and selectivity of poly(organophosphazene) membranes." Macromolecules **26**(7): 1493-1502.

Azran, A. and G. Dagan (2001). Method for potting or casting inorganic hollow fiber membranes into tube sheets. US Patent 7,233,339, Toray Industries, Inc.

Baker, R. W. (2000). Membrane technology and Applications, John Wiley and Sons.

Baker, R. W. (2002). "Future directions of membrane gas separation technology." Industrial & Engineering Chemistry Research **41**(6): 1393-1411.

Beres, J. J., N. S. Schneider, et al. (1979). "Crystalline Poly(organophosphazene) Blends and Copolymers." Macromolecules **12**(4): 566-575.

Black, J. (2010). Cost and performance baseline for fossil energy plants. Bituminous coal and natural gas to electricity. RevisioN_2,, National Energy Technology Laboratory. **Volume1**.

Burgess, S. K., J. E. Leisen, et al. (2014). "Chain Mobility, Thermal, and Mechanical Properties of Poly (ethylene furanoate) Compared to Poly (ethylene terephthalate)." Macromolecules **47**(4): 1383-1391.

Cabasso, I. and K. A. Lundy (1986). Method of making membranes for gas spearation and the composite membranes. US, University of New York, Albany. **US Patent 4602922**.

Chung, T.-S., J.-J. Qin, et al. (2000). "Effect of shear rate within the spinneret on morphology, separation performance and mechanical properties of ultrafiltration polyethersulfone hollow fiber membranes." Chemical Engineering Science **55**(6): 1077-1091.

Comer, A. C., D. S. Kalika, et al. (2009). "Dynamic relaxation characteristics of Matrimid® polyimide." Polymer **50**(3): 891-897.

Favre, E. (2007). "Carbon dioxide recovery from post-combustion processes: Can gas permeation membranes compete with absorption?" Journal of Membrane Science **294**(1): 50-59.

Figueroa, J. D., T. Fout, et al. (2008). "Advances in CO_2 capture technology—The U.S. Department of Energy's Carbon Sequestration Program." International Journal of Greenhouse Gas Control **2**(1): 9-20.

Geankoplis, C. (2003). Transport Processes and Separation Process Principles. Englewood Cliffs, NJ, Prentice-Hall.

Gleria, M. and R. De Jaeger (2005). Polyphosphazenes: A Review. New Aspects in Phosphorus Chemistry V. J.-P. Majoral, Springer Berlin Heidelberg. **250:** 165-251.

Harrup, M. K. and F. F. Stewart (2000). "Improved method for the isolation and purification of water-soluble polyphosphazenes." Journal of Applied Polymer Science **78**(5): 1092-1099.

Jha, P., L. W. Mason, et al. (2006). "Characterization of Substituted Polyphosphazene Membranes − Pure and Mixed Gas Results." Industrial & Engineering Chemistry Research **45**(19): 6570-6577.

Khalilpour, R., A. Abbas, et al. (2012). "Modeling and parametric analysis of hollow fiber membrane system for carbon capture from multicomponent flue gas." AIChE Journal **58**(5): 1550-1561.

Kim, H., C. Jung, et al. (2001). "Particle removal efficiency of gravitational wet scrubber considering diffusion, interception, and impaction." Environmental Engineering Science **18**(2): 125-136.

Koch, B., M. Müller, et al. (2008). Hollow fiber module. US Patent 7,140,580, BEKO Technologies GmbH.

Koros, W. and G. Fleming (1993). "Membrane-based gas separation." Journal of Membrane Science **83**(1): 1-80.

Li, D., R. Wang, et al. (2004). "Fabrication of lab-scale hollow fiber membrane modules with high packing density." Separation and Purification Technology **40**(1): 15-30.

Light, R. and R. Seymour (1982). "Effect of sub-Tg relaxations on the gas transport properties of polyesters." Polymer Engineering & Science **22**(14): 857-864.

Liu, L., A. Chakma, et al. (2005). "CO_2 /N_2 separation by poly (ether block amide) thin film hollow fiber composite membranes." Industrial & Engineering Chemistry Research **44**(17): 6874-6882.

Maxwell, A., L. Monnerie, et al. (1998). "Secondary relaxation processes in polyethylene terephthalate–additive blends: 2. Dynamic mechanical and dielectric investigations." Polymer **39**(26): 6851-6859.

Maxwell, A., I. Ward, et al. (1998). "Secondary relaxation processes in polyethylene terephthalate-additive blends: 1. Nmr investigation." Polymer **39**(26): 6835-6849.

Merkel, T. C., H. Lin, et al. (2010). "Power plant post-combustion carbon dioxide capture: an opportunity for membranes." Journal of Membrane Science **359**(1): 126-139.

Murphy, M. K. (1988). Multicomponent gas separation membraes having polyphosphazene coatings. US, Mopnsanto Co. **US Patent 4728345**.

Nakamatsu, O., H. Ohtani, et al. (2007). Hollow-fiber membrane module. US Patent 7,233,339, Toray Industries, Inc.

Orme, C. J., M. K. Harrup, et al. (2001). "Characterization of gas transport in selected rubbery amorphous polyphosphazene membranes." Journal of Membrane Science **186**(2): 249-256.

Orme, C. J., J. R. Klaehn, et al. (2006). "Gas permeability in rubbery polyphosphazene membranes." Journal of Membrane Science **280**(1–2): 175-184.

Orme, C. J., J. R. Klaehn, et al. (2004). "Gas permeability and ideal selectivity of poly [bis-(phenoxy) phosphazene], poly [bis-(4-tert-butylphenoxy) phosphazene], and poly [bis-(3, 5-di-tert-butylphenoxy) 1.2 (chloro) 0.8 phosphazene]." Journal of Membrane Science **238**(1): 47-55.

Peterson, E. S., M. L. Stone, et al. (1993). "Mixed-Gas Separation Properties of Phosphazene Polymer Membranes." Separation Science and Technology **28**(1-3): 423-440.

Peterson, E. S., M. L. Stone, et al. (1995). "Chemical Separations Using Shell and Tube Composite Polyphosphazene Membranes." Separation Science and Technology **30**(7-9): 1573-1587.

Porter, M. C. (1990). Handbook of industrial membrane technology, William Andrew Publishing/Noyes.

Puri, P. S. (1989). Continuous process for making coated composite hollow fiber membranes. United States, Air Products and Chemicals, Inc. **US Patent 4863761**

Robeson, L. M. (2008). "The upper bound revisited." Journal of Membrane Science **320**(1): 390-400.

Stewart, F. F., M. K. Harrup, et al. (2000). "Synthesis, characterization and thermal stability of phosphazene terpolymers with 2-(2-methoxyethoxy)ethoxy and diacetone D-glucofuranosyl pendant groups." Polymer international **49**(1): 57-62.

Ugural, A. and S. Fenster (2003). Advanced strength and applied elasticity. , Elsevier Publishing Co.

Abbreviations

2-AP – 2-allylphenol

4-MEOP – 4-methoxyphenol

AIBN – 2,2’-azobis(2-methylpropionitrile)

BP – benzoyl peroxide

CA – cellulose acetate

DBU - 1,8-Diazabicyclo[5.4.0]undec-7-ene

DSC – differential scanning calorimetry

IPN – interpenetrating network

LCST – lower critical solution temperature

MEE – 2-(2-methoxyethoxy)ethanol

MEEP – poly[bis-2-(2-methoxyethoxy)ethoxyphosphazene]

NMP - N-Methyl-2-pyrrolidone

NMR – Nuclear Magnetic Resonance

PAI - polyamide-imide

PDMS – poly(dimethylsiloxane)

PEG-400 – 400 Dalton Poly[ethylene glycol]

PES - polyethersulfone

PEO – poly[ethylene oxide]

PPOP – poly[bis-phenoxyphosphazene] with 1 % 2-allylphenol

PVP – poly(vinylpyrrolidone)

Tg – glass transition temperature

TGA – Thermogravimetric analysis

THF – tetrahydrofuran

UV - ultraviolet

Appendices

Appendix A

Synthesis and purification procedures

Synthetic procedure for 80 % MEEP.

Poly(dichlorophosphazene) (~40 g) was dissolved in 600 mL anhydrous toluene under an argon atmosphere. Once dissolved, the polymer was precipitated by addition of 1.5 L hexanes and the supernatant was reduced to dryness to determine the mass of polymer by difference. The purified poly(dichlorophosphazene) (35.4 g) was re-dissolved in 600 mL anhydrous toluene under argon. In a separate flask, ¬4-methoxyphenol (10.8 g, 87.3 mmol) and 2-allylphenol (4.09, 30.5 mmol) were dissolved in ~1 L anhydrous THF under argon. NaH (60 %, 4.38 g, 110 mmol) was carefully added to the flask and the reaction was allowed to stir for 14 hrs. The polymer solution was poured into the phenoxide solution and the reaction stirred for 24 hrs. In a separate flask, 2-(2-methoxyethoxy)ethanol (120 g, 1.00 mol) was slowly added to a mixture of NaH (60 %, 34.7 g, 0.950 mol) in ~1 L anhydrous THF. The reaction was allowed to stir for 18 hrs. The alkoxide reaction solution was added to the polymer via cannula, and the reaction was allowed to stir at room temperature for 24 hrs.

80 % MEEP Purification Procedure

The crude polymer was precipitated with the addition of 4 L hexanes, and then re-dissolved in 1 L THF. The polymer was precipitated with 3 L hexanes and then dried in a vacuum oven at 50 °C overnight before being added to 1.5 L H2O. HCl (3 M) was used to neutralize, and then the mixture was heated to 70 °C. The polymer was collected by centrifugation and dissolved in 1 L THF. The solution was centrifuged and decanted into 4 L hexanes to precipitate the purified polymer, which was collected and dried in a vacuum oven at 50 °C (69.7 g, 79 % yield).

Appendix B

Yield and pendant group speciation data as determined by proton NMR spectroscopy.

Batch ID	Yield	Pendant group loading (NMR)		
	(%)	% MEE	% o-Allylphenol	% 4-Methoxyphenol
1922-FFS-001	48*	80	4	16
1922-FFS-029	42*	81	4	15
1922-FFS-037	59*	80	6	14
1922-FFS-055	73**	79	6	15
1922-FFS-060	63**	78	8	14
1922-FFS-066	57**	79	4	17
1922-FFS-073	45**	81	5	14
1922-JRK-077	69**	80	7	13
1922-FFS-082	70**	78	6	16
1922-FFS-086	66**	84	2	14
1922-FFS-090	61**	74	6	20
1922-JRK-094	48**	60	10	30
1922-JRK-097	93**	77	5	18
1922-JRK-099	62**	80	2	18
2309-JSM-001	80**	79	4	17
2309-JSM-005	71**	83	6	11
2309-JSM-008	79**	81	7	12
2309-JSM-018	77**	77	4	19

* Synthesis performed at the 0.25 mole scale.

** Synthesis performed at the 0.5 mole scale.

Appendix C

DSC and pure gas permeability data.

Batch ID	Tg (°C)	Flowing solid	CO_2 Permeability (Barrers)	CO_2 /N_2 Ideal Selectivity
1922-FFS-001	-67	No	~200*	29
1922-FFS-029	-68	No	69*	41
1922-FFS-037	-66	No	34*	38
1922-FFS-055	-69	Yes	NA	NA
1922-FFS-060	-68	Yes	78*	33
1922-FFS-066	-67	Yes	NA	NA
1922-FFS-073	-70	No	NA	NA
1922-JRK-077	-69	No	62*	27
1922-FFS-082	-69	No	437	32
1922-FFS-086	-71	No	418	35.8
1922-FFS-090	-70	No	473	29.2
1922-JRK-094	-69	Yes	370	30.1
1922-JRK-097	-73	Yes	532	33.2
1922-JRK-099	-74	No	531	34.6
2309-JSM-001	-75	No	550	37.9
2309-JSM-005	-75	No	477	39.1
2309-JSM-008	-75	No	481	39.1
2309-JSM-018	-77	No	591	36.6

Appendix D

45% and 95 % MEEP characterization data.

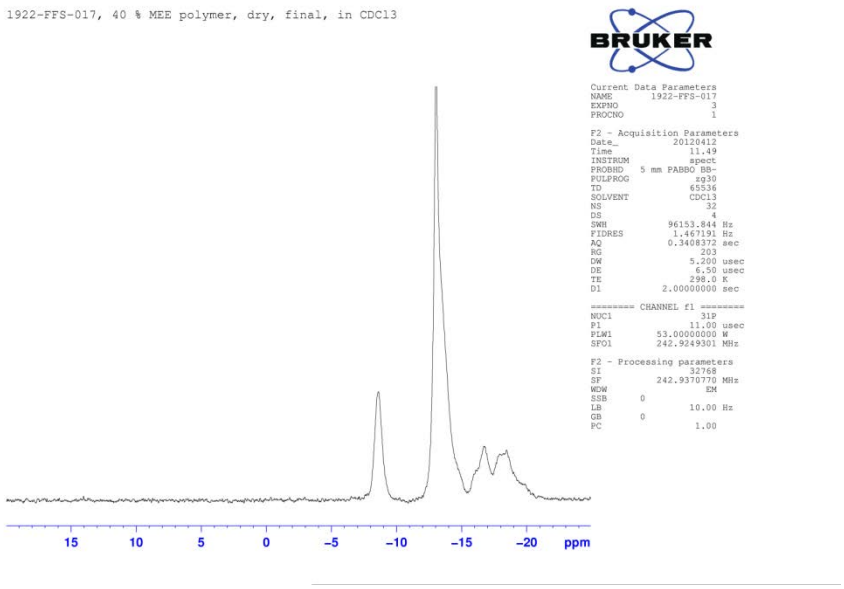

P-31 NMR spectrum of 45% MEEP

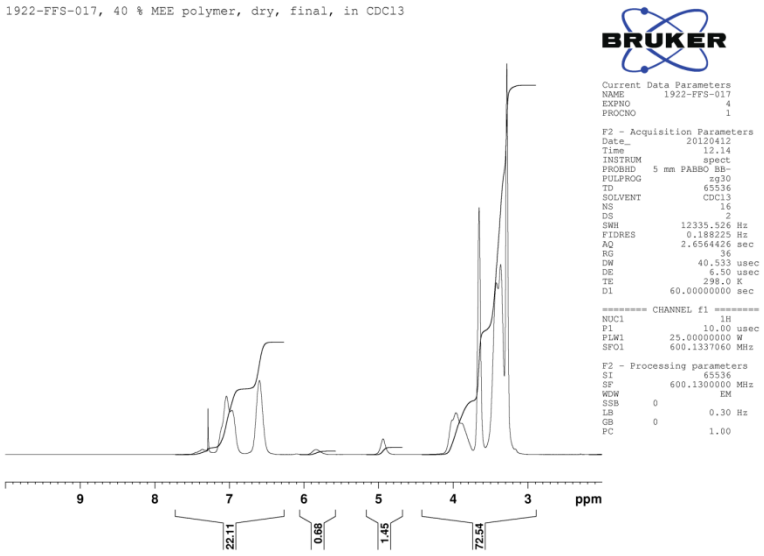

Proton NMR spectrum of 45% MEEP

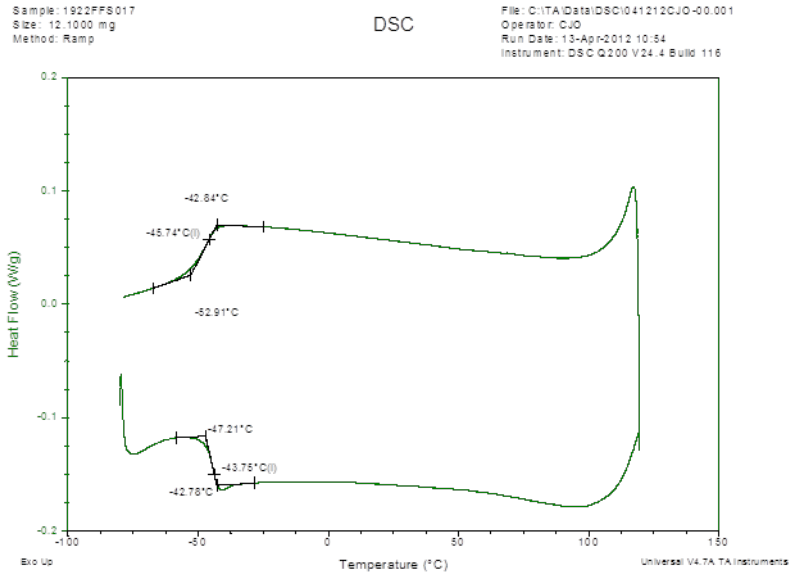

DSC data for 45% MEEP

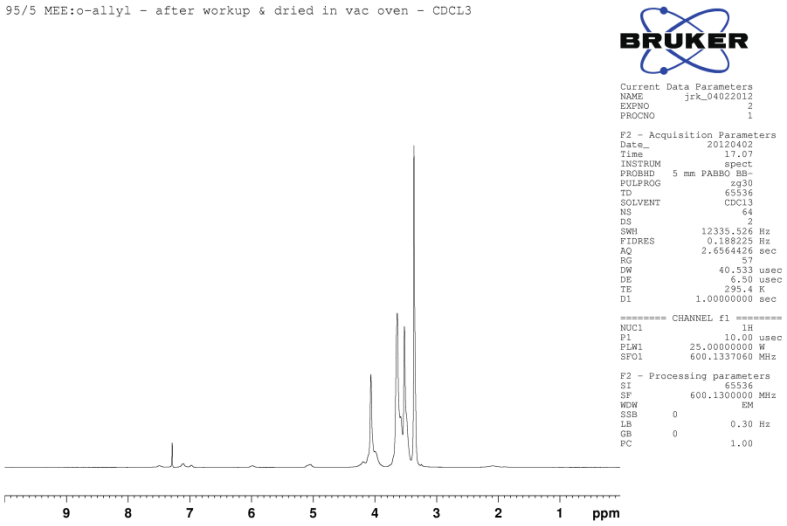

Proton NMR spectrum for 95% MEEP

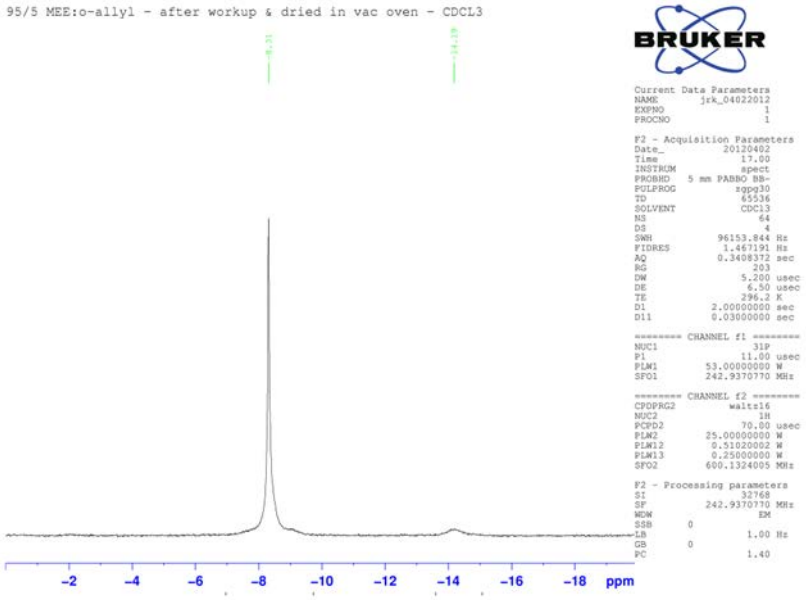

P-31 NMR spectrum of 95% MEEP

Appendix E

Cross-linking of 80% MEEP as a function of casting solution composition, temperature, and time.

Casting Solution	Cross-linking Temperature (˚C)	Cross-linking Time	CO_2 Permeability (Barrers)	N_2 Permeability (Barrers)	CO_2/N_2
5% Ethanol, 2 % AIBN	None	None	448.6	13.9	32.3
5% Ethanol, 2 % AIBN	130	10 minutes	523.1	15.17	34.5
5% Ethanol, 2 % AIBN	130	1 hour	301	10.43	28.9
5% Ethanol, 2 % AIBN	130	3 hours	189.4	6.7	28.3
5% Ethanol, 2 % AIBN	130	17 hours	128.9	4.12	31.3
Experiment #2					
5% Ethanol, 2 % AIBN	130	10 minutes	436.5	13.6	32.1
5% Ethanol, 2 % AIBN	130	1 hour	134.9	4.2	32.1
5% Ethanol, 2 % AIBN	130	2 hours	85	2.8	30.4
9% Ethanol, 2 % AIBN	130	10 minutes	475.3	14.3	33.2
9% Ethanol, 2 % AIBN	130	20 minutes	271.1	8	33.9
9% Ethanol, 2 % AIBN	130	1 hour	254.7	8.2	31.1
9% Ethanol, 2 % AIBN	130	2 hours	171.8	6.3	27.3
7% Ethanol, 2 % AIBN	none	none	446.5	14.07	31.7
7% Ethanol, 2 % AIBN	110	10 minutes	243.1	8.11	30.0
7% Ethanol, 2 % AIBN	110	1 hour	203.5	7.64	26.6
7% Ethanol, 2 % AIBN	110	18 hours	73.5	2.65	27.7
8% Ethanol	None	None	549.7	14.5	37.9
5% Ethanol, 2 % AIBN	70	30 minutes	307.9	9.62	32.0
5% Ethanol, 2 % AIBN	70	1 hour	226.7	6.53	34.7
5% Ethanol, 2 % AIBN	70	16 hours	82.5	3.15	26.2

Appendix F

TFE containing polymer characterization data.

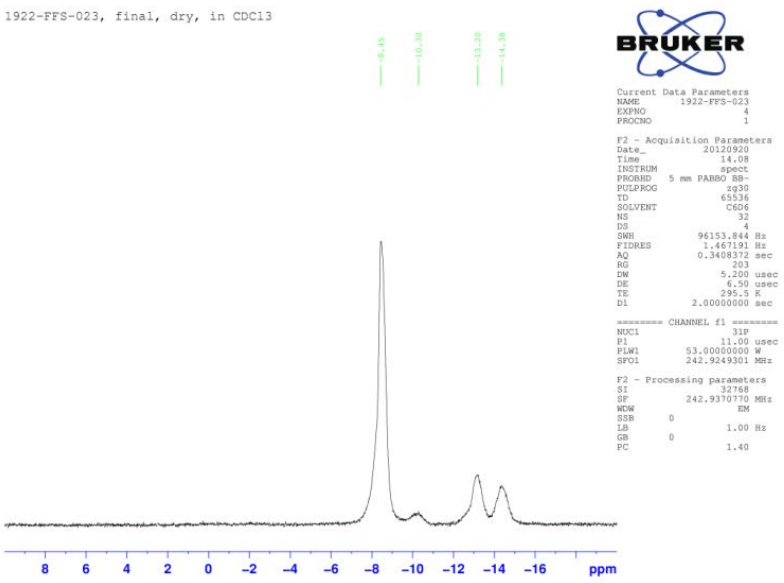

P-31 NMR spectrum of TFE polyphosphazene

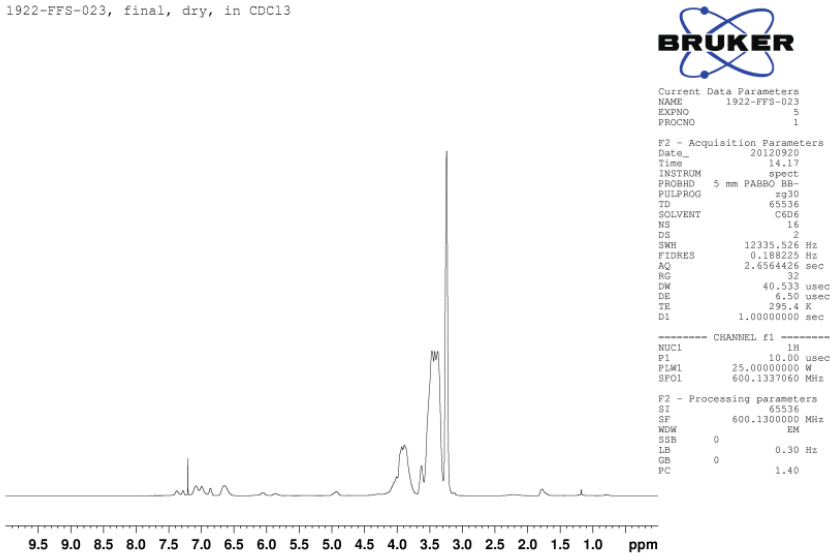

Proton NMR spectrum of TFE polyphosphazene

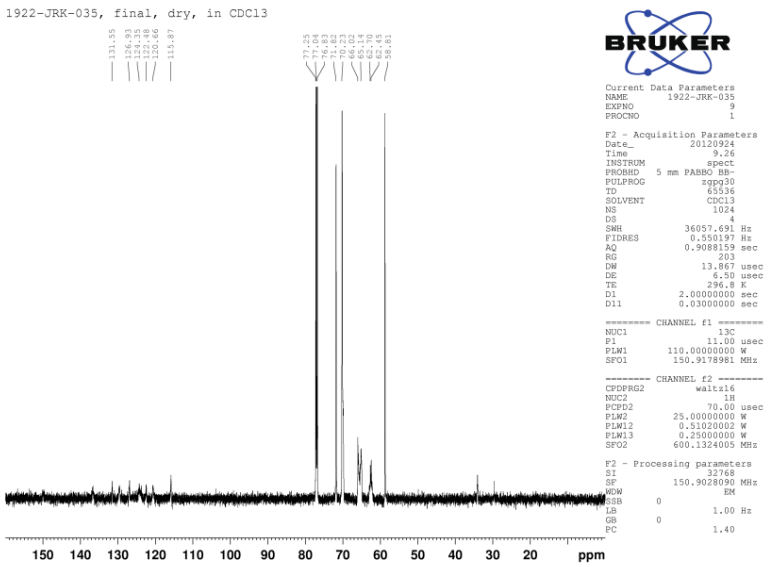

C-13 NMR spectrum of TFE polyphosphazene

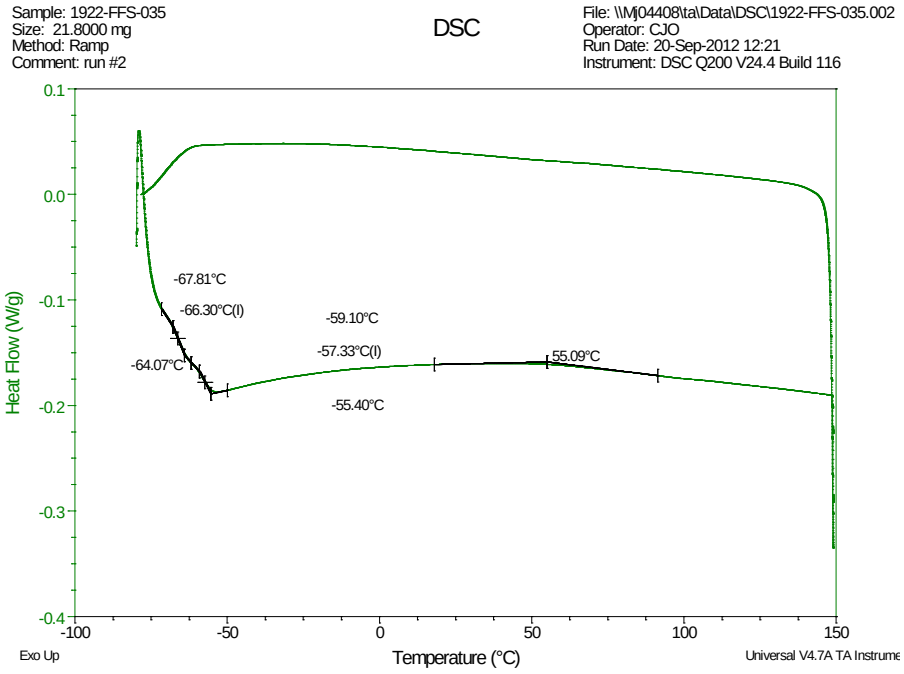

DSC plot of TFE polyphosphazene.

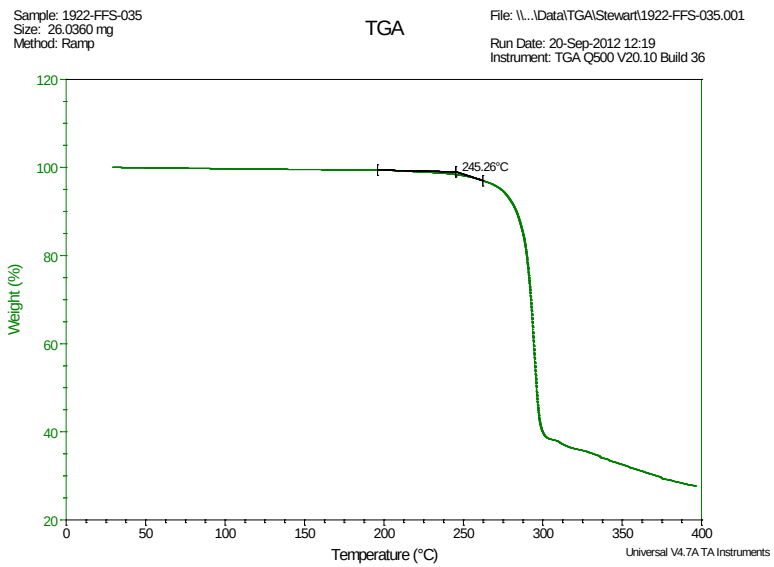

TGA plot for TFE polyphosphazene.

Appendix G

Characterization data for OPF phosphazene.

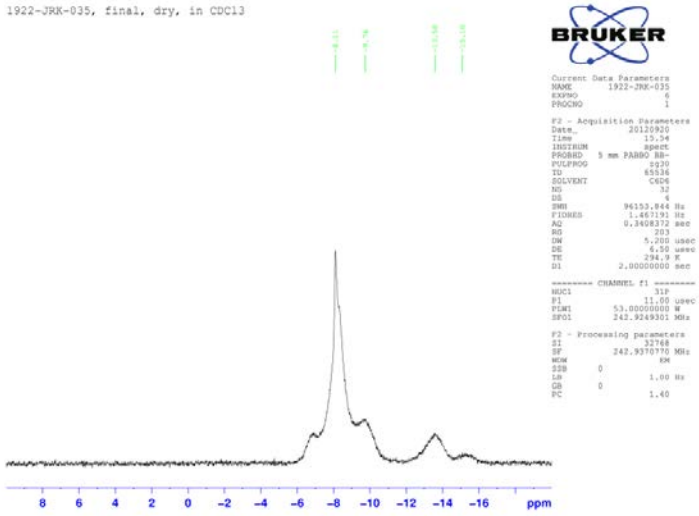

P-31 NMR spectrum of OFP phosphazene.

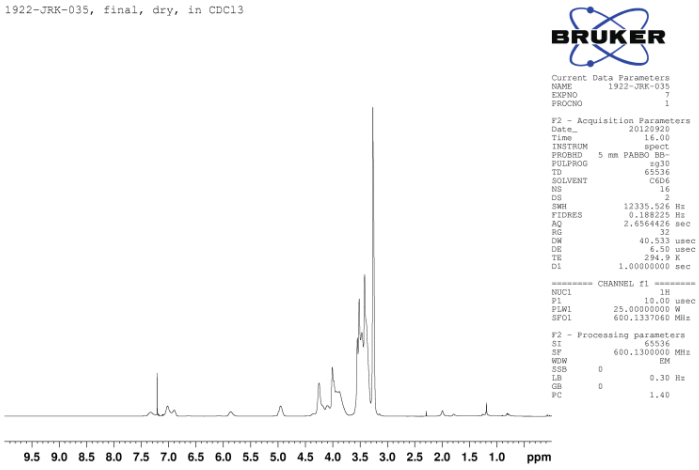

Proton NMR spectrum of OFP polyphosphazene.

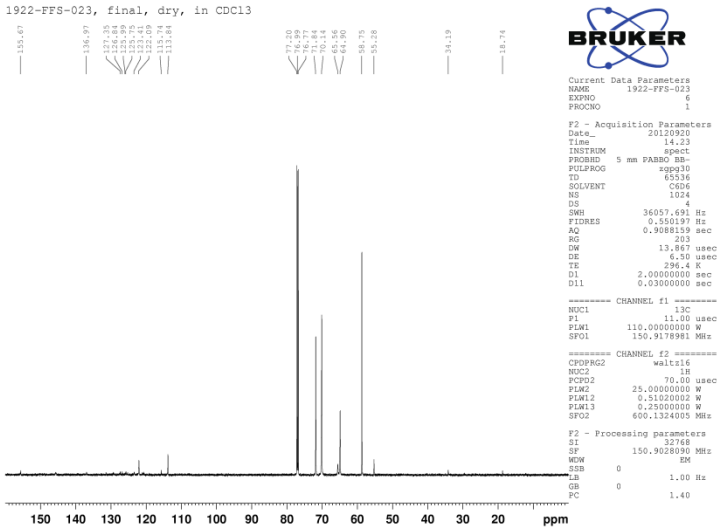

C-13 NMR spectrum of OFP polyphosphazene

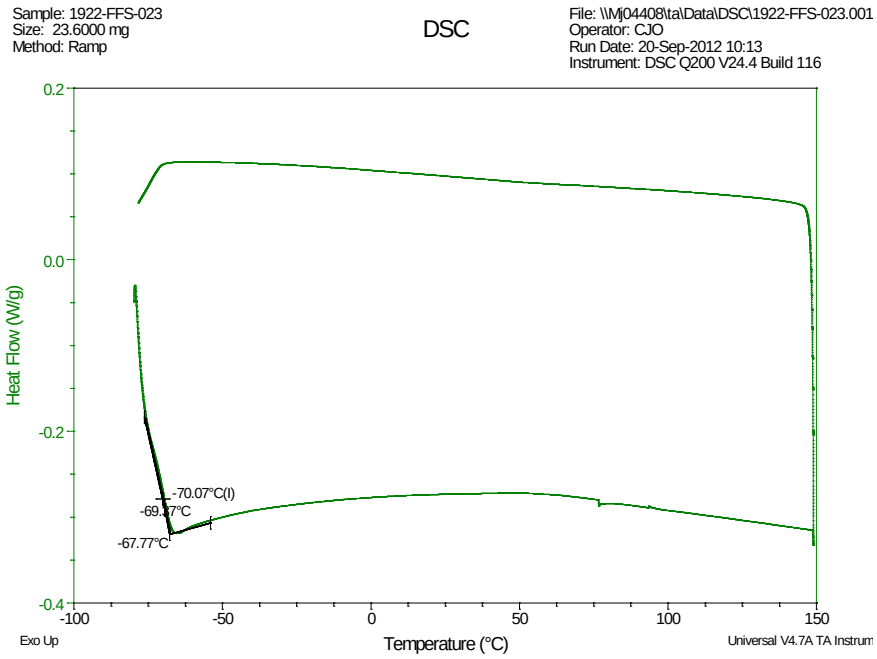

DSC plot of OFP phosphazene.

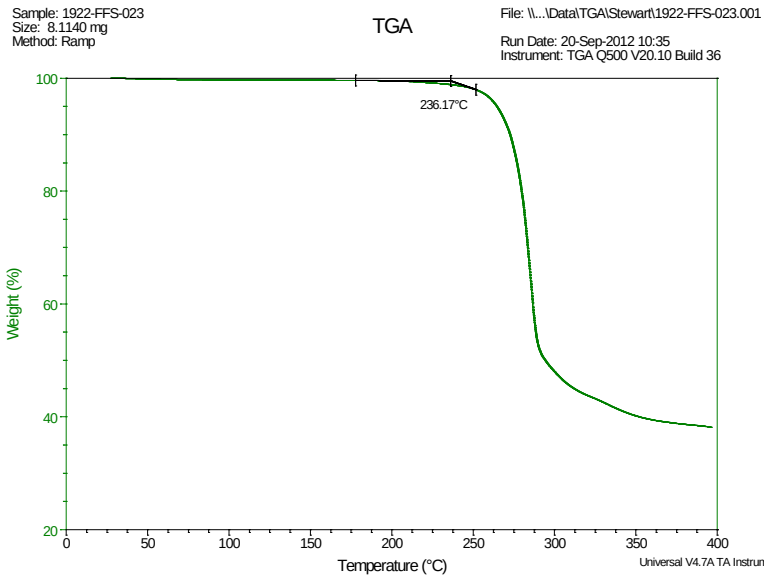

TGA plot of OFP phosphazene.

Appendix H

Raw data for IPN mixed gas performance as a function of temperature.

	Temp (°C)	1000/T (K)	P(N_2) (Barrers)	P(CO_2) (Barrers)	P(H_2O) (Barrers)	CO_2 /N_2
Day 1	30	3.299	12.6	349.3	2769.6	27.7
Day 2	35	3.245	8.5	267.8	1737.8	31.6
Day 2	45	3.143	16.2	338.0	1332.2	20.9
Day 2	50	3.095	20.3	365.6	1341.0	18.0
Day 2	55	3.047	24.9	395.7	2712.7	15.9
Day 2	63	2.975	31.4	427.5	1494.2	13.6
Day 2	67	2.940	32.6	423.9	1540.3	13.0
Day 3	25	3.354	7.2	240.3	1139.0	33.2
Day 3	35	3.245	13.2	329.0	1137.1	24.8
Day 3	45	3.143	16.2	338.7	1369.6	20.9
Day 3	55	3.047	20.7	359.4	1967.8	17.4
Day 3	65	2.957	32.4	391.4	1525.8	12.1
Day 3	75	2.872	38.0	421.4	1396.6	11.1
Day 3	85	2.792	41.7	439.0	2246.1	10.5
Day 3	95	2.716	46.5	426.3	1409.2	9.2
Day 3	105	2.644	47.4	431.2	1426.3	9.1
Day 4	27	3.332	5.1	157.5	943.8	31.1
Day 4	30	3.299	7.8	205.5	1263.9	26.5
Day 4	40	3.193	15.0	353.0	1388.1	23.6
Day 4	50	3.095	18.4	369.5	1357.3	20.1
Day 4	60	3.002	23.0	384.9	1949.4	16.7
Day 4	70	2.914	36.7	419.8	1566.6	11.4
Day 4	80	2.832	44.9	460.6	1630.3	10.3
Day 4	90	2.754	47.4	449.6	2633.2	9.5
Day 4	110	2.610	59.5	466.1	1932.7	7.8

Appendix I

(Double click the image below to open up the complete pdf file of Maple code)

```
> restart:
```

THERMAL STRESSES IN A CO_2 MODULE NEAR THE POTTING LAYER.

Reference: [1]. Advanced Strength and Applied Elasticity by AC. Ugural and SK. Fenster.

The thermal stresses in a CO_2 module near the potting layer is modeled here. A plane strain problem in polar corrdinates is used in this analytical development to obtain the thermal stresses. The casing is modeled as a hollow cylinder while the epoxy or the potting layer is modeled as a solid cylinder. Let the radius of the potting cylindrical material be 'a' and the radius of the casing be 'b'. An illustration is shown below.

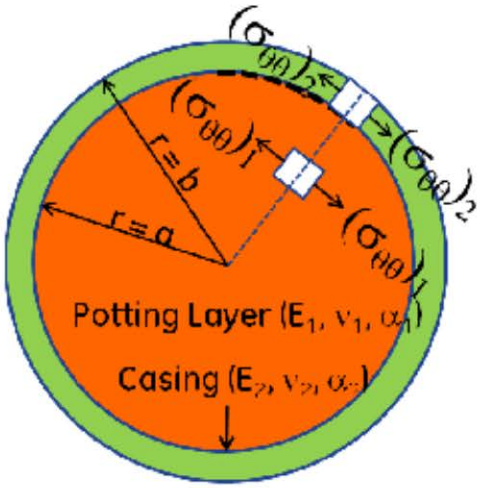

Figure 1: Model of Pollting layer and casing with geometry and material property definitions

```
> with(plots):
> with(linalg):
> with(student):
```

The equations for 'u' displacements, radial stress and hoop stress from the Ref. 1 in pages 288 are given below. A schematic of the stresses and displacements are given below in Figure 2:

Appendix J

(Double click the image below to open up the complete pdf file of Maple code)

```
> restart:
```

THERMAL STRESSES IN A CO_2 MODULE NEAR THE POTTING LAYER. Section II. EPOXY AND HOLLOW FIBER

Reference: [1]. Advanced Strength and Applied Elasticity by AC. Ugural and SK. Fenster.

The thermal stresses in a CO_2 module near the potting layer is modeled here. In the previous section, the bulk stresses in the potting layer and the casing was considered. In this section, the stresses in the hollow fiber is considered. The stresses in the epoxy from the previous solution will be used to obtain HF stresses. This problem is solved separately because of the following:
1. Length scale difference between the casing and the hollow fiber is more than 1000
2. Hollow fiber need not be axi-symmetric with the casing axis.

A plane strain problem in polar corrdinates is used in this analytical development to obtain the thermal stresses. The epoxy is modeled as a infinite medium in the polar coordinate with inner radius 'b0' and outer radius 'c0' that approaches infinity to simulate the infinite medium. The hollow fiber is modeled as a hollow cylinder with radius 'a0'. An illustration is shown below.

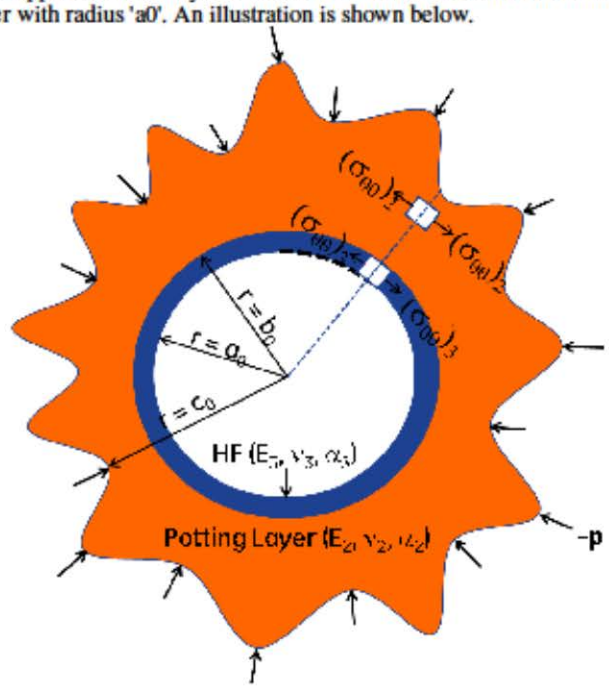

Figure 1: Model of Potting layer and Hollow Fiber with geometry and material property definitions

```
> with(plots):
```